THÈSE

En vue de l'obtention du

DOCTORAT DE L'UNIVERSITÉ DE TOULOUSE

Délivré par :

Institut National Polytechnique de Toulouse (Toulouse INP)

Discipline ou spécialité :

Génie des Procédés et de l'Environnement

Présentée et soutenue par :

M. PEDRO OLIVEIRA

le vendredi 6 juillet 2018

Titre :

Des propriétés morphologiques des flocs biologiques aux conditions de fonctionnement de systèmes à boues activées

---

Ecole doctorale :

Mécanique, Energétique, Génie civil, Procédés (MEGeP)

Unité de recherche :

Laboratoire de Génie Chimique (L.G.C.)

Directeur(s) de Thèse :

MME CHRISTINE FRANCES

MME MARION ALLIET

Rapporteurs :

Mme HÉLÈNE CARRERE, INRA NARBONNE

Mme SYLVIE GILLOT, IRSTEA

Membre(s) du jury :

M. LUC FILLAUDEAU, INRA TOULOUSE, Président

M. EUGENIO FERREIRA, UNIVERSITE DE MINHO BRAGA, Membre

Mme CAROLE COUFORT-SAUDEJAUD, INP TOULOUSE, Membre

Mme CHRISTINE FRANCES, CNRS TOULOUSE, Membre

Mme MARION ALLIET, INP TOULOUSE, Membre

M. PASCAL GINISTY, IFTS, Membre

Resumé

Parmi les différentes technologies pour produire un effluent conforme aux normes de rejet en vigueur, les Procédés par Boues Activées reste largement utilisés comme traitement biologique dû ses faibles coûts et sa faisabilité d'implémentation. Cette toute simple technique atteint une élimination adéquate de la matière organique en combinant de la biodégradation dans un bassin d'aération avec de la séparation solide-liquide travers d'un décanteur subséquent. Sachant que l'impact des paramètres opératoires sur l'efficacité du procédé est probablement corrélée aux propriétés de la boue, l'objectif de ce travail est de mettre en évidence des nouvelles perspectives sur cette association qui existe, en effet, parmi trois bases des Systèmes à Boues Activées : les conditions opératoires, les caractéristiques des flocs de boues et la performance du procédé.

Afin de atteindre cet objectif, une méthodologie pour la caractérisation des agrégats des boues activées a été établie dans un premier moment. Le développement de cette méthodologie a consisté en déterminer certains paramètres de mesure pour le microscope automatique Morphologi G3 : cellule d'analyse, facteur de dilution, grossissement, seuillage et nombre total de particules analysées. Les analyses ont été réalisées sur des différentes types de boues en permettant une évaluation de la robustesse de la méthodologie et en ressortant leurs différences en termes de propriétés de taille et forme – Diamètre équivalent (D_{eq}), Circularité (C), Convexité (C_x), Solidité (S) and Rapport d'Aspect (RA).

Avec le protocole d'analyse d'images bien défini, deux campagne expérimentales ont été mise en œuvre en utilisant un système à boues activées en échèle pilote alimenté avec de l'effluent synthétique. Tandis que les descripteurs morphologiques d'environ 100,000 flocs de boues par échantillon ont été analysée appliquant le protocole, la performance du procédé a été appréciée en parallèle en mesurant des indicateurs physicochimiques souvent associés aux traitements des eaux usées : Matières en Suspension (MES), Indice de Boue (IB), taux de abattement de la Demande Chimique d'Oxygène (DCO) et d'Azote (N), aussi bien que d'autres formes d'azote (ammonium et nitrate). Cette stratégie a principalement permis d'identifier des relations pertinentes entre les variables micro et macroscopiques.

Pendant la première campagne, trois valeurs différentes de l'âge de boue ont été imposées : 15, 20 et 30 jours. Concernant les paramètres morphologiques, lors d'un changement d'âge de boue, la taille et la circularité des flocs biologiques augmentent temporairement avant de se restabiliser à leurs valeurs initiales. En régime permanent, les distributions en taille et en circularité semblent indépendantes de l'âge de boue. Dans la deuxième campagne, plus d'une condition opératoire a été variée à chaque fois. La charge organique, le taux de recirculation et le rapport DCO:N ont été modifiés donc. Une forte charge organique a provoqué une augmentation de la taille des flocs et une diminution de la solidité. Ce résultat peut être expliqué par la croissance de bactéries filamenteuses qui impactent fortement la morphologie des f et par conséquence toute la performance du procédé. L'augmentation du taux de recirculation et la diminution du rapport DCO:N ont, tous les deux, induit une légère réduction de la taille de flocs et une évolution constante des valeurs de circularité et convexité. Au cours de cette campagne, l'analyse des distributions 3D en volume, lesquelles sont une importante outil pour croiser les données de taille et forme, et l'estimation de la dimension fractal 2D ont rendu la possibilité de mieux comprendre la dynamique de la structure des flocs soumis aux perturbations du procédé.

Abstract

Among the different technologies dealing with the strict regulations concerning wastewater treatment, the Activated Sludge Process remains extensively applied as a biological treatment because of its low cost and its convenience of implementation. This straightforward technique achieves good levels of organic matter removal combining biodegradation in an aerated tank with solid-liquid separation through a subsequent clarifier. The impact of the operational parameters on process efficiency is presumably correlated to the sludge properties. In this context, the aim of this work is to bring new insights into this association that, in fact, exists among three foundations of the Activated Sludge Systems: operating conditions, sludge floc characteristics and process performance.

In order to attain this objective, a methodology for morphological characterization of activated sludge aggregates was established in first moment. The steps involved in this methodology consisted in defining some analysis settings for the automated microscope Morphologi G3: sample carrier, dilution factor, magnification, threshold and total number of analysed particles. Analyses were performed on different types of sludge allowing an evaluation of the methodology robustness and putting in evidence their differences in terms of size and shape properties – Circular Equivalent Diameter (CED), Circularity (C), Convexity (C_x), Solidity (S), and Aspect Ratio (AR).

With the image analysis protocol well defined, two experimental campaigns were ran using a lab-scale activated sludge system fed with synthetic wastewater. While the morphological descriptors of about 100,000 sludge flocs per sample were analysed applying the protocol, process performance was assessed in parallel by measuring physicochemical parameters commonly associated with wastewater treatment: Total Suspended Solids (TSS), Sludge Volume Index (SVI), Chemical Oxygen Demand (COD) and Nitrogen (N) removal, as well as some nitrogen species (ammonium and nitrate). This strategy have mostly enabled to identify pertinent relationships between the micro and macroscopic variables.

Throughout the first campaign, three values of solids retention time (SRT) were tested: 15, 20 and 30 days. Increasing the SRT, the size and the circularity of the flocs increase temporarily before recovering their initial values. Under steady state conditions, the size and circularity distributions seem to be independent of the SRT. In the second campaign, more than one operating condition modification was carried out at time. Organic Load Rate (OLR), recycle and COD:N ration were varied then. A high OLR has promoted the increase of flocs size and the decrease of their solidity. This result can be explained by the development of filamentous bacteria that highly impacts on the aggregates morphology and consequently on the overall performance of the wastewater treatment. Recycle ratio increase and COD:N ratio decrease both promoted a slight reduction of floc sizes and a constant evolution of circularity and convexity values. During this campaign, the analysis of the volume-based 3D-distributions, which is a smart tool to cross size and shape data, and the estimation of the 2D fractal dimension enabled a deepest understanding of the dynamics of floc structure under process disturbances.

Remerciements

Cela me semble plus difficile que d'écrire toute la thèse, mais je le ferai quand même car je le dois à toutes les personnes que j'ai eu la chance de croiser pendant ces presque 4 années de thèse, et aussi aux personnes qui m'ont motivé depuis le début pour la réalisation de ce doctorat en France.

Je veux remercier tout d'abord mes trois directrices de thèse. Tels que les systèmes à boues activées, moi aussi j'ai eu trois piliers pour bien comprendre et pour bien appuyer mes travaux de recherche : Christine Frances, Marion Alliet et Carole Coufort-Saudejaud. Merci à vous de m'avoir fait confiance pour percer les mystères derrière les flocs de boues activées. Avec vous j'ai appris que je peux toujours regarder au-delà de ce que mes yeux peuvent voir, et je ne parle pas du « morpho », je parle de toutes les connaissances que vous m'avez gentiment transmises pour enrichir ma construction en tant que professionnel de la recherche.

J'ai besoin de remercier également les membres du jury. Ainsi, un grand merci aux rapportrices Hélène Carrère et Sylvie Gillot pour l'attention donnée à la lecture de ma thèse ainsi que pour les remarques faites, lesquelles ont apporté des améliorations à ce manuscrit, à Luc Fillaudeau pour avoir présider ce jury avec beaucoup d'humeur et de positivité, je n'aurais pas pu avoir un meilleur président de jury de soutenance de thèse, à Pascal Ginisty d'accepter de participer à la fin de ce travail, lequel il a pu apprécier lors d'autres présentations en congrès, et pour finir, « obrigado » à Eugénio Ferreira, j'ai été vraiment flatté avec la présence de quelqu'un que j'ai cité plus de 15 fois sur ce manuscrit, comme vous avez pu le remarquer.

Merci à Sylvie Schétrite et à Agathe pour leur apport sur le projet : démarrage de l'installation pilote, l'analytique et les conseils pour les bonnes pratiques en laboratoire. Egalement merci à Christine Rey-Rouch pour m'avoir formé sur le Morphologi G3. Comme disait Etienne Braak, lors de mon stage de master, je suis devenu le maître du « morpho ».

Je ne peux pas oublier de remercier à Marcia Duarte et à Gorete Ribeiro, mes professeures d'école d'ingénieur, grâce à elles j'ai pu me retrouver en France avec des personnes incroyables, dotées d'un haut niveau scientifique et de passion pour leur métier.

Le LGC a un personnel très sympathique, mais je dois particulièrement remercier Alain Philippe, Bernard et Dany pour tout le support administratif, technique et pourquoi pas amical ? Ils avaient toujours un bonjour avec plein de sourire et ils n'ont jamais refusé de m'aider quand j'en avais besoin.

Merci à CAPES pour le support financier au travers du programme Sciences sans Frontières, lequel a eu énormément de développement pendant le gouvernement Lula/Dilma.

Une deuxième partie de mes remerciements est dédiée aux amis et à la famille qui m'ont accompagné dans ce voyage appelé thèse de doctorat.

Merci à Jésus Villalobos et Mehran Abathi pour faire de l'ambiance du petit labo une ambiance très amicale, où on aide l'autre et où on découvre de la musique de qualité. Il faut me pardonner Jésus, je ne savais pas qui était Célia Cruz. Je tiens un grand merci à d'autres amis de la famille BioSym : Maria Beatriz, Sitha, Lauren, Manon, Paul Bro et Silvia. Ces deux derniers toujours avec pleine d'énergie pour une petite soirée. Merci aussi à Marco et Jésus (Chucho) d'avoir intégré des moments avec cette famille.

Merci à Léa Guérin et à Lucas Ruffel d'être des super collègues de bureau. Léa toujours souriante et ajoutant la touche féminine au bureau et Lucas avec tous les compliments qui ont gonflé mon ego : « ouh là, il est beau comme tout aujourd'hui ».

Je dois remercier les amis du couloir IRPI : Margot, Pei San, Sandy, Sébastien Wahl, Sid-Ahmed, Thibault, Vincent, Yandi et particulièrement merci à Sébastien Pecate et Imane. Vous tous avez fait de mes deux dernières années thèse, deux années de grande joie, arrosés des cafés, repas, des glaces « mcdo » (pour faire la digestion) et de bars à cocktail. Désolé Séb Pecate pour le cocktail au lait, je dois avouer qu'il était horrible.

Merci aux amis du Brésil, les « Pitxulas » et les « Amor Philieo » qui ont toujours su m'envoyer de l'énergie positive et de la motivation pour continuer la thèse et qui ont été très contents de voir le résultat final. Obrigado!

Maintenant je dois faire un grand merci à une des meilleures familles qui m'a accueilli ici en France, Clément, Xavier et Nout des Apollons de la Salud, on s'est connu il y a tout juste 1 an, mais c'est une durée suffisante pour que vous devenez des grands amis pour moi. Les randonnées dans les Pyrénées, les soirées cinés, les repas du mercredi et parfois du weekend, les pizzas du vendredi et les conseils pour la vie. Vous m'avez présenté des souvenirs d'une France très belle et aussi gourmande. Je vais toujours vous garder dans le cœur en espérant vos vacances à Natal et d'autres moments si agréables avec vous dans un autre coin du monde, pourquoi pas à Minorque? Je sais… Clément, tu ne supportes plus, mais il faut faire une exception pour moi.

Merci aux deux anges de gardes qui ont bien fait leur boulot de me garder avec eux. Germán, tu as été le début de thèse que je n'attendais pas. Tu m'as montré que la thèse peut avoir ces moments de difficultés mais qu'à la fin on peut toujours trouver une solution si on essaye de faire tout le possible. Tu m'as prouvé que malgré le temps et la distance certains « paramètres » peuvent rester constants et que le hasard est aussi un facteur qu'il faut prendre en compte dans le bilan global, merci Germán. Letícia (ou Leti), mon morceau brésilien, une sœur que le doctorat m'a offerte comme cadeau, merci pour tous les moments de discussion, pour tous les pauses cafés et aussi thérapies, pour toutes les gourmandises (chocolat, gâteux…) pour donner du moral et pour les déjeuners au « showroom » avec toi, ce dernier me va beaucoup manquer. Comme dit la chanson, la bonne chanson brésilienne : « O nosso santo bateu! ».

Avant de remercier les prochaines personnes, je dois m'excuser d'abord, car je dois écrire en portugais.

Obrigado aos meus pais, Silvana e Junior, a minha irmã, Sâmara e a minha avó, Maria das Graças (Boló) por todo o apoio nesses 4 anos de tese. Sem o suporte de vocês essa caminhada seria sem sombra de dúvidas mais difícil. Graças a todo o amor e todo aprendizado passados para mim, por vocês, percorrer todo esse tempo em outro país, tornou tudo mais fácil. É verdade que a tecnologia ajudou bastante, viabilizando nosso contato, mas se não fosse a certeza que sempre posso contar com vocês para todos os momentos, de nada valeria esse desafio. Um dia conversando com minha avó via Skype no terceiro ano de tese, ela me falou: "Amanhã quando você acordar, você será um novo homem. É assim a vida...". E vejam só, hoje eu acordei, e sou um Doutor, ela sempre teve razão.

Table of Contents

List of Figures

List of Tables

Nomenclature

[ ]*Terme en français

A	Actual area (μm^2)
A_C	Convex hull area (μm^2)
a_p	Pixel area (μm^2)
AR	Aspect Ratio (-)
[RA]	***[Rapport d'Aspect]***
b_f	Form factor for fractal dimension calculation (-)
BOD_5	Biochemical Oxygen Demand on five days
C	Circularity (-)
C_x	Convexity (-)
CED ou D_{eq}	Circle Equivalent Diameter (μm)
COD	Chemical Oxygen Demand ($mg.L^{-1}$)
[DCO]	***[Demande Chimique d'Oxygène]***
COD_{IN}	Chemical Oxygen Demand in the feed stream ($mg.L^{-1}$)
COD_{OUT}	Chemical Oxygen Demand at the clarifier outlet ($mg.L^{-1}$)
C:N	Carbon/Nitrogen ratio (-)
D_2	Fractal dimension from Area and Maximum length relationship (-)
D_f	Fractal Dimension (-)
d_p	Diameter of primary particles (μm)
D_{pf}	Fractal dimension from Area and Perimeter relationship (-)
DO	Dissolved Oxygen ($mg.L^{-1}$)
[OD]	***[Oxygène Dissous]***
F/M	Food-to-Microorganism ratio ($kgBOD_5.kgVSS^{-1}.d^{-1}$)
[C_m]	***[Charge massique]***
FF	Form Factor (-)

HRT	Hydraulic Retention Time (h^{-1})
[TSH]	***[Temps de Séjour Hydraulique]***
L	Length (µm)
N_f	Filament Number
*N*p	Number of primary particles
OLR	Organic Load Rate ($kg_{COD}.m^{-3}d^{-1}$)
[C_v]	***[Charge volumique]***
P	Actual perimeter (µm)
P_C	Convex hull perimeter (µm)
P_E	Equivalent perimeter (µm)
Q_E	Drained volume of excess sludge ($m^3.d^{-1}$)
Q_f	Feed flow rate ($m^3.h^{-1}$)
Q_R	recycle rate flow ($m^3.d^{-1}$)
RR	Recycle Ratio (-)
S	Solidity (-)
SE	Spherical Equivalent Volume (μm^3)
SRT	Solids Retention Time (d)
SVI	Sludge Volume Index ($mL.g^{-1}$)
[IB]	***[Indice de Boue]***
TN	Total Nitrogen ($mg.L^{-1}$)
TN_{IN}	Total Nitrogen in the feed stream ($mg.L^{-1}$)
TN_{OUT}	Total Nitrogen at the clarifier outlet ($mg.L^{-1}$)
TSS	Total Suspended Solids ($mg.L^{-1}$)
[MES]	***[Matières en Suspension]***
V	Aerated tank volume (m^3)
V_{sample}	Sample volume (mL)

V_{30}	Settled sludge volume after 30 min ($mL.L^{-1}$)
VSS	Volatile Suspended Solids ($mg.L^{-1}$)
X	Solids concentration in the aerated tank ($kg.m^{-3}$)
X_E	Solids concentration in the waste sludge ($kg.\ m^{-3}$)
W	Width (µm)

Abbreviations

APHA	American Public Health Association
AS	Activated Sludge
ASP	Activated Sludge Process
[PBA]	***[Procédés par Boues Activées]***
EPS	Extracellular Polymeric Substances
[SPE]	***[Substances Polymériques Extracellular]***
G	Greywater
I	Industrial effluent
IA	Image Analysis
[AI]	***[Analyse d'Images]***
M	Municipal effluent
M.A.	Micronutrients Addition
M1	Modification 1
M2	Modification 2
M3	Modification 3
M4	Modification 4
MBR	Membrane Bioreactor
[BàM]	***[Bioreactor à Membrane]***
MF	Microfiltration
SRT-15	Solids Retention Time at 15 days
SRT-20	Solids Retention Time at 20 days
SRT-30	Solids Retention Time at 30 days
UF	Ultrafiltration
WWTP	WasteWater Treatment Plant

Introduction générale

La probable carence en eau propre au cours des prochaines décennies conduit actuellement à un effort de recherche soutenu sur les procédés de traitement des eaux usées. Parmi ceux déjà existants, les systèmes à boues activées sont tout particulièrement mis en œuvre en tant que traitement secondaire. Ainsi, selon un bilan sur les différents systèmes d'assainissement réalisé en 2008 par « eaufrance », cette filière de traitement reste celle utilisée par 90% des stations d'épuration françaises avec une capacité de plus de 10 000 EH.

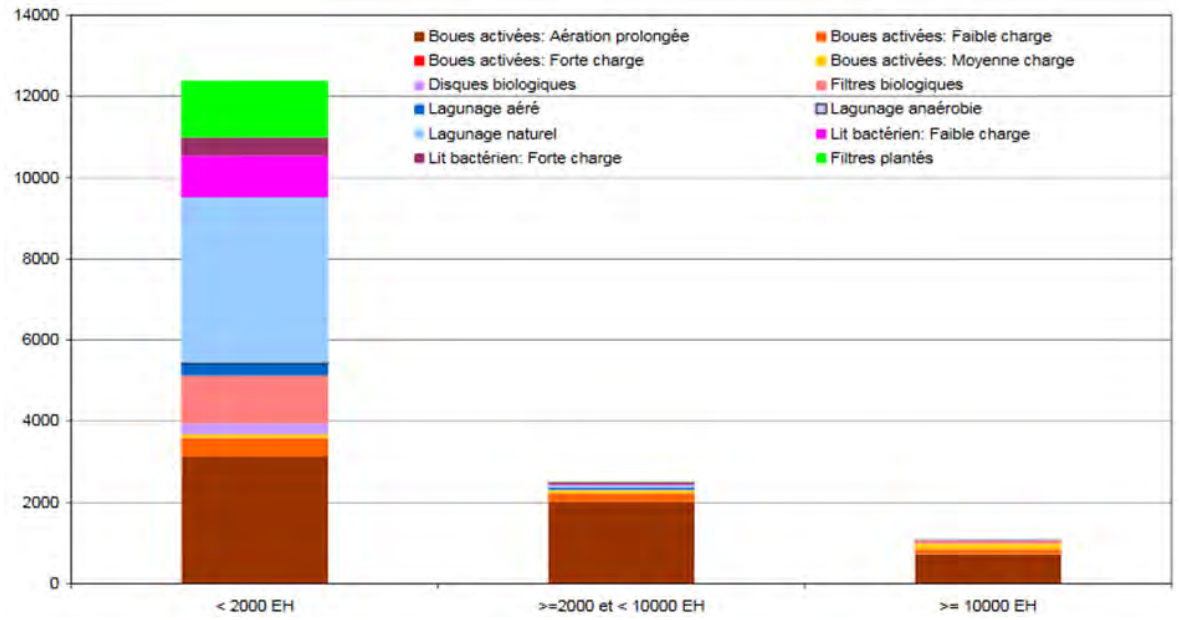

Figure 0-1. Nombre de stations de traitement des eaux usées par type de filière et par capacité nominale (Bilan d'assainissement 2008 « eaufrance », publié en 2010).

De façon simple, les procédés de traitement par boues activées consistent en un bassin d'aération dans lequel les microorganismes agglomérés sous forme de flocs sont mis en contact avec l'eau à épurer, et un clarificateur où l'eau épurée est séparée de la biomasse. La phase de traitement biologique réalisée au sein du bassin d'aération représente la phase clé de dégradation de la pollution et donc plus globalement de la chaîne du traitement des eaux. Cependant, le procédé étant soumis à des variations extérieures difficilement maitrisables comme le débit et la composition du flux d'entrée ou encore la température, son fonctionnement peut en être fortement perturbé. En effet, ce dernier repose sur le développement de différentes populations bactériennes qui vont réagir à ces perturbations dans leur capacités épuratrices mais aussi dans leurs interactions entre-elles, avec les particules et avec les produits solubles du milieu avec lesquels elles forment les flocs, et ainsi dans le fonctionnement hydrodynamique du procédé.

Les flocs biologiques jouent un rôle majeur dans un procédé de traitement par boues activées. La structure, la taille et la forme de ces agrégats biologiques sont des caractéristiques importantes vis-à-vis du procédé. En effet, si les flocs ne sont pas trop gros, compacts et denses, leur vitesse de sédimentation sera grande et la décantation se fera bien, Au contraire, si les flocs présentent une forme très irrégulière, ou une structure plutôt poreuse, la vitesse de

sédimentation peut être réduite, induisant des dysfonctionnements allant de la recirculation plus faible à un lessivage de la biomasse. Actuellement, avec l'évolution des outils numériques, il est possible d'analyser ces flocs de boues activées au travers d'images 2D, afin de caractériser leurs propriétés morphologiques (taille et forme). La morphologie des agrégats est intimement liée aux conditions opératoires, et ces deux éléments peuvent agir sur l'efficacité du procédé. L'objectif de ce travail est d'apporter un nouvel éclairage sur cette relation triangulaire, en se centrant sur les propriétés de taille et de forme des flocs de boues. Pour atteindre l'objectif visé les étapes suivantes ont été envisagées :

- L'établissement d'un protocole de mesure des paramètres morphologiques. Pour cela des boues réelles de stations d'épuration seront analysées à l'aide du Morphologi G3^{TM}, appareil combinant un microscope optique avec une platine automatisée et un logiciel supervisant l'acquisition et le traitement des images d'agrégats.

- Une fois le protocole établi, il sera alors possible de l'appliquer à des boues issues d'une installation pilote. Cette dernière permettra de faire varier les paramètres du procédé, par exemple, l'âge de boue, la charge volumique ou le taux de recirculation et d'analyser leur impact sur la morphologie des flocs biologiques et l'efficacité du procédé.

- Enfin, une analyse des dynamiques des distributions ainsi que de la dimension fractale est envisagée. Cela devrait permettre de mieux comprendre le phénomène de structuration des agrégats de boues activées en réponse à des modifications des conditions opératoires, sachant qu'un tel phénomène est important pour assurer une bonne sédimentation des flocs au niveau du décanteur dans les systèmes à boues activées

Le parcours pour réaliser ces étapes a été divisé en 5 chapitres qui constituent ce mémoire de thèse :

Le Chapitre I condense en trois parties l'intégralité de l'étude bibliographique qui a servi de support au travail expérimental développé. La première partie présente les grands principes du fonctionnement des procédés par boues activées ainsi que les paramètres d'évaluation de la performance du traitement. Dans une deuxième partie, sont abordées les études les plus pertinentes relatives au développement de protocoles d'analyse d'images et des outils qui sont utilisés pour décrire la forme, la compacité, la rugosité de surface et la structure plus ou moins ouverte des particules ou agrégats complexes tels que les flocs biologiques. Nous verrons comment ces travaux ont mis en relation les paramètres morphologiques avec les conditions opératoires. Enfin, la troisième partie est consacrée à la présentation du concept de la dimension fractale.

Le Chapitre II présente les moyens et les outils qui ont été nécessaires pour réaliser cette étude : installation pilote, microscope, méthodes d'analyses chimiques et physiques etc… Les définitions mathématiques des paramètres de fonctionnement du procédé ainsi que les descripteurs morphologiques pour caractériser les flocs des boues sont également présentés. Quelques concepts sur la statistique descriptive pour l'analyse de distributions de fréquence sont également rappelés dans ce chapitre.

Le Chapitre III introduit les premiers résultats expérimentaux associés à la définition d'un protocole d'analyse d'images robuste pour analyser les flocs de boues activées. Les étapes pour déterminer les paramètres tels que : le facteur de dilution, le grossissement, le critère d'arrêt d'analyse, le nombre de particules à analyser, le contraste, le niveau de seuillage… sont détaillées dans ce chapitre. La définition du protocole d'analyse d'image a été réalisée sur la base de mesures effectuées sur différentes boues issues de stations de traitement d'eaux résiduaires industrielles et municipales.

Le Chapitre IV présente les résultats de la première campagne expérimentale réalisée avec l'installation pilote et en appliquant le protocole d'analyse d'images précédemment défini. Pour cette campagne, la performance du procédé a été évaluée, de même que les caractéristiques morphologiques des flocs de boues pour trois conditions différentes d'âge des boues, à savoir 15, 20 et 30 jours.

Le Chapitre V aborde la seconde campagne expérimentale avec l'installation pilote, au cours de laquelle d'autres conditions opératoires classiques pour le procédé ont été modifiées. Ainsi, le système a été soumis à des modifications de la charge volumique, du taux de recirculation et du rapport COD:N. Les variations de la performance du procédé ainsi que les propriétés de taille et de forme des flocs des boues activées ont été analysées en parallèle de façon à appréhender l'effet de ces perturbations sur les propriétés des flocs et les performances du procédé. Pour terminer, un couplage des données relatives à la taille et à la forme des agrégats sous la forme de distributions tridimensionnelles est proposé et l'évolution de deux dimensions fractales au cours de la campagne est discutée.

Enfin, les conclusions de ce travail et les perspectives générales seront dégagées.

Chapter I. Synthèse de la littérature

Ce premier chapitre présente, dans un premier temps, les fondements théoriques associés aux procédés de traitement des effluents par boues activées : y seront rappelés successivement le principe de fonctionnement des réacteurs à boues activées, les conditions opératoires et les critères utilisés pour évaluer l'efficacité de ces procédés. Ceci permettra d'exposer dans la suite du chapitre, les principaux travaux de la littérature concernant la caractérisation des boues activées et leurs relations avec les paramètres opératoires.

I.1 Principes et mécanismes de traitement des eaux usées par boues activées

Le procédé par boues activées (PBAs), largement employé pour le traitement des eaux usées, est généralement l'étape secondaire dans une station d'épuration biologique. Dans ce procédé, la biomasse, présente au sein de flocs qui constituent la boue activée, dégrade la pollution purifiant ainsi l'effluent. Pour ce faire, l'effluent chargé en polluants est mélangé aux boues dans un bassin d'aération agité et aéré. L'effluent traité est ensuite séparé de la boue grâce à un décanteur (**Figure I-1**). Les boues concentrées dans le décanteur sont renvoyées au bassin d'aération pour conserver la biomasse.

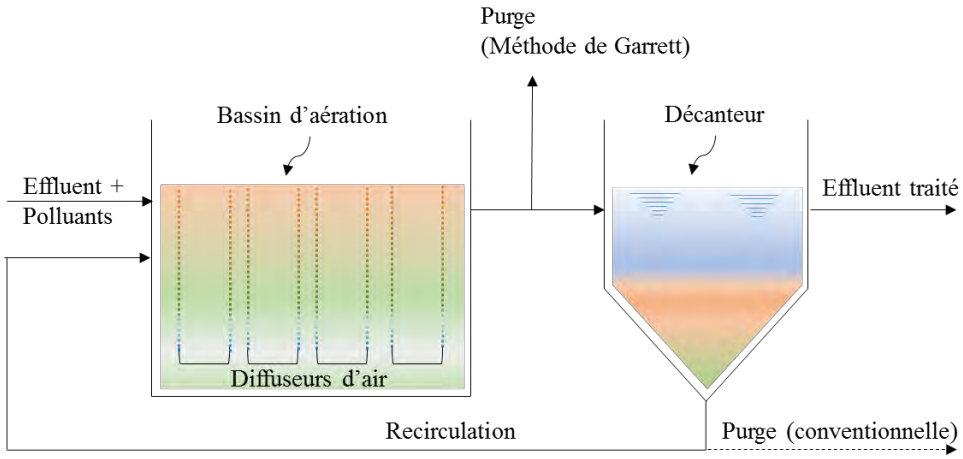

Figure I-1. Schéma d'un procédé par boues activées typique (Grady et al., 2011).

Afin de mieux décrire le procédé, ces opérations seront détaillées par la suite.

Bassin d'aération

C'est dans cette unité du système qu'ont lieu les réactions biochimiques de dégradation des polluants. Les microorganismes consomment le substrat présent dans l'effluent pour assurer leur développement. Pour cela, les bactéries, organisées en floc de boue, ont besoin d'oxygène qui est généralement fourni au système par injection d'air. Afin d'assurer une bonne performance du procédé et de travailler avec une concentration importante de biomasse dans le bassin d'aération, un recyclage des boues du décanteur vers le bassin d'aération est mis en place.

Dans ce cadre, les bactéries hétérotrophes aérobies sont les principaux agents responsables de l'élimination de la matière organique présente dans les polluants. L'équation d'oxydation du

glucose ci-dessous permet de représenter de façon globale la dégradation métabolique de ces composants.

$$C_6H_{12}O_6 + 6\ O_2 \rightarrow 6\ CO_2 + 6\ H_2O \quad \textbf{(I-1)}$$

Cette réaction est exothermique, libérant ainsi 2826 kJ par mole de glucose oxydé à la température de 298K. Normalement, 40% de l'énergie produite par cette réaction est utilisée par les bactéries pour assurer la maintenance de leurs activités (Wiesmann et al., 2007; Henze, 2008).

Décanteur

Cette unité a pour objectif de favoriser la séparation solide-liquide dans le procédé et de faire floculer et sédimenter les boues. L'effluent traité est évacué du système par surverse en partie supérieure du décanteur, tandis que les flocs, plus denses, sédimentent au fond du décanteur. La capacité de floculation est directement liée à la production d'une matrice colloïdale permettant l'agglomération de bactéries, de protozoaires, et de matière organique en flocs macroscopiques. Les flocs biologiques ainsi crées ont des dimensions supérieures aux microorganismes isolés, ce qui augmente la capacité de sédimentation.

Selon Von Sperling (2017), un décanteur fonctionnant en conditions normales doit pouvoir :

- Séparer efficacement des solides qui viennent du bassin d'aération, et donc produire un effluent final clarifié, de faible turbidité et de faible concentration en matières en suspension, dans une gamme inférieure ou égale à 20 à 30 mg/L.
- Concentrer de manière satisfaisante la boue sédimentée, laquelle composera la boue qui reviendra au bassin d'aération.

En raison de cette première caractéristique, les décanteurs secondaires sont communément aussi appelés clarificateurs.

Aération intermittente

Suivant le mode opératoire mis en œuvre, différentes variantes de PBAs existent. Parmi les plus utilisés, il est possible de trouver les PBAs qui fonctionnent avec une aération intermittente, c'est-à-dire que le procédé est soumis à des cycles aérobies et anoxies alternées pour réaliser l'élimination de l'azote conjointement à celle de la matière carbonée. En d'autres termes, cette stratégie permet l'abattement de l'azote au sein du bassin d'aération au travers de deux mécanismes qui sont respectivement la nitrification et la dénitrification.

Le processus de nitrification se déroule surtout pendant le cycle aérobie. Notamment, en présence d'oxygène, les bactéries *Nitrosomonas* et *Nitrococcus* sont responsables, tout d'abord, de l'oxydation de l'ammonium en nitrite selon la réaction suivante :

$$NH_4^+ + {}^3/_2\,O_2 \rightarrow NO_2^- + 2H^+ + H_2O \quad \textbf{(I-2)}$$

Ensuite les *Nitrobacters* réalisent l'oxydation de nitrites en nitrates en complétant cette première étape pour éliminer l'azote.

$$NO_2^- + ½\ O_2 \rightarrow NO_3^- \quad \textbf{(I-3)}$$

Les bactéries impliquées dans cette première étape sont également appelées autotrophes, vu leur capacité à synthétiser la matière organique à partir de substances minérales. Leur taux de croissance est plus faible que celui des bactéries dégradant la pollution carbonée, rendant ainsi fondamentale la détermination de la durée de chaque cycle (Fulazzaky et al., 2015).

Une fois que l'ammonium est transformé en nitrates, le processus de dénitrification est alors mis en place. La dénitrification consiste en la réduction biologique des nitrates en nitrites, suivie par une réduction des nitrites en oxyde nitrique, puis en oxyde nitreux et finalement en azote gazeux, lequel est libéré vers l'atmosphère. Le processus global de dénitrification peut être représenté par la réaction ci-dessous :

$$NO_3^- \rightarrow NO_2^- \rightarrow NO \rightarrow N_2O \rightarrow N_2^{\uparrow} \qquad \textbf{(I-4)}$$

Les transformations comprises dans cette étape sont effectuées par un groupe de bactéries hétérotrophes qui, en l'absence d'oxygène, sont capables d'utiliser les nitrates pour réaliser leur respiration. Pour que la dénitrification se passe correctement, le procédé doit donc inclure un fonctionnement anoxique (Rodríguez et al., 2011).

I.1.1 Composition et paramètres de description des boues activées

Les boues activées sont des suspensions, *i. e.* elles sont composées à la fois d'une phase solide et d'une phase liquide aqueuse. La phase solide est constituée principalement par les flocs. Ceux-ci sont formés par différents types de microorganismes comme des bactéries (*Nitrosomonas, Nitrococcus, Nitrobacters, Zoogleas*….), des protozoaires, métazoaires et, dans certains cas, on trouve aussi quelques espèces de champignons mais dont la présence n'est pas souhaitée parce qu'ils sont défavorables à la bonne structuration des flocs. Il est possible de trouver aussi dans la phase solide des particules inorganiques et organiques, telles que, des silicates, des phosphates de calcium, des oxydes de fer, des métaux alcalins et de la cellulose. D'autre part, la phase liquide, ou le surnageant des boues, est un mélange de minéraux et de substances organiques appelées Substances Polymériques Extracellulaires (SPE) issues de l'activité des microorganismes ou de la lyse celulaire (Wilén et al., 2008; Dai et al., 2018).

Les SPE sont généralement produites par l'activité microbienne ou libérées par lyse cellulaire et peuvent, également, être transportées par les eaux usées admises au traitement. Il s'agit de plusieurs familles biochimiques de molécules organiques telles que les polysaccharides (les plus connus étant des sucres) et les protéines, en quantité assez importante, ainsi que des substances humiques, des acides uroniques, nucléiques et des phospholipides en quantité moindre (Sobeck et Higgins, 2002).

Ces SPE jouent un rôle très important de liant dans la formation des flocs de boues assurant la cohésion entre les différents composants des agrégats microbiens. De plus, ils maintiennent la stabilité mécanique des flocs biologiques (Wang et al., 2014). Ces substances peuvent interagir par voie électrochimique et de cette façon connecter un microfloc à un autre en créant une sorte de pont, pour former un gros floc (macrofloc). Keiding et Nielsen (1997) ont rapporté que le floc est composé de micro colonies et de bactéries libres qui sont intégrées dans un « nuage » de SPE floculées. En outre, Eriksson et Alm (1991) soutiennent l'idée qu'à l'extérieur du floc

les cellules sont floculées grâce à quelques ponts polymériques dans une structure complexe, tandis qu'au sein du floc les cellules sont fortement liées par les matrices de SPE (**Figure I-2**).

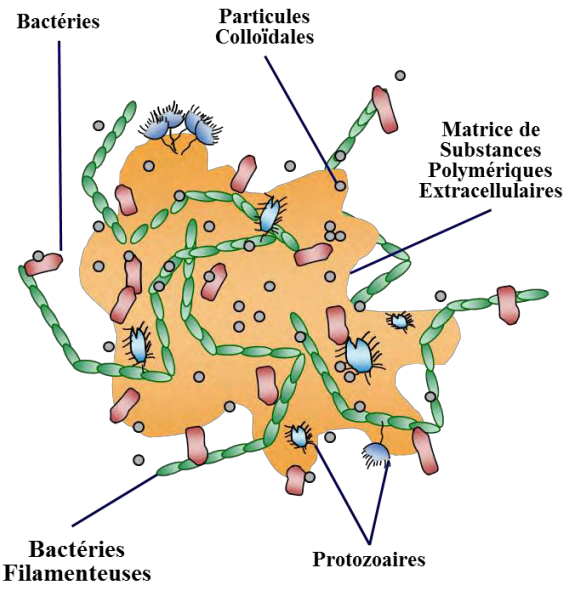

Figure I-2. Représentation d'un floc de boue activée (adaptée de Von Sperling, 2017).

Comme le montre la **Figure I-2**, les flocs contiennent aussi des bactéries que l'on nommera « floculantes » et des bactéries filamenteuses. Tandis que les bactéries « floculantes » aident au rassemblement d'autres microorganismes grâce à leur structure gélatineuse, les bactéries filamenteuses sont capables d'adsorber des matières colloïdales, des macromolécules, différents ions et des substances biologiquement actives, agissant comme une colonne vertébrale où les flocs de boues activées s'accrochent. Usuellement, les boues activées qui contiennent un excès de bactéries filamenteuses présentent une structure avec un aspect assez dispersé. Ainsi, un équilibre entre ces deux types de bactéries est généralement recherché afin d'assurer la formation des flocs ayant bonne capacité de décantation et par conséquent de garantir le succès opérationnel du procédé (Meng et al., 2006; Guo et al., 2014; Burger et al, 2017).

En fonction de la diversité des constituants des boues activées – microorganismes, particules inorganiques et substances polymériques extracellulaires – et de l'influence des conditions environnementales, les flocs typiques ont une forme assez irrégulière, une grande porosité, une masse hétérogène et forment des structures interconnectées (Chu et Lee, 2004). La stabilité de ces flocs est également régie par les lois de la chimie des colloïdes. Aussi, des changements relatifs à conditions physicochimiques comme la composition ionique, le pH ou les forces de tension superficielle peuvent également influencer la structuration de ces agrégats (Keiding et Nielsen, 1997).

I.1.2 Qualité de l'effluent (Entrée et Sortie)

Les eaux usées sont des milieux complexes. Afin de caractériser la qualité de l'effluent, il est nécessaire de quantifier la présence des différents constituants. La présence de telles substances est généralement exprimée par des concentrations équivalentes, en mg/L.

I.1.2.1 Demande Chimique d'Oxygène (DCO)

La Demande Chimique en Oxygène (DCO) est définie comme la masse d'oxygène nécessaire pour réaliser l'oxydation complète d'un composant organique présent dans l'eau. Si la DCO théorique d'une substance est souhaitée, alors il est nécessaire de développer son équation d'oxydation. Par exemple, la DCO théorique pour l'éthanol peut être estimée d'après l'équation suivante :

$$C_2H_6O + 3\ O_2 \rightarrow 2\ CO_2 + 3\ H_2O \qquad \textbf{(I-5)}$$

C'est-à-dire que pour une dégradation complète de 46 mg d'éthanol (1 mole) en dioxyde de carbone et d'eau, 96 mg d'O_2 (3 moles) sont nécessaires. D'un point de vue pratique, on a donc un facteur de 2,09 (ou 96/46) mg de DCO (ou O_2) pour calculer la DCO théorique.

La matière organique utilise l'oxygène disponible dans le milieu lors de sa dégradation ; la matière organique résiduelle privant le milieu de l'oxygène nécessaire à son bon fonctionnement est ainsi une source de pollution. La DCO est donc parfaitement adaptée pour évaluer l'efficacité d'élimination de la matière organique du procédé. Pour cela, des mesures sont effectuées sur le courant d'entrée et le courant de sortie, et la comparaison de ces deux valeurs permet d'obtenir un taux d'élimination global représentatif du fonctionnement du procédé (Wiesmann et al., 2007).

I.1.2.2 Azote Total

L'azote intervenant dans la formation d'acides aminés et de protéines, est un composé favorisant le développement des organismes vivants : sa présence en forte quantité induit principalement de l'eutrophisation et donc une déstabilisation du milieu. L'abattement de l'azote présent dans les effluents d'entrée est par conséquent une cible des systèmes à boues activées. Il est important de quantifier les concentrations d'azote total en sortie et en entrée afin de réaliser un bilan de l'efficacité du procédé vis-à-vis de cet élément.

L'azote total comprend toutes les formes d'azote existant dans le milieu : inorganique et organique. La première source est principalement due à la présence d'ammonium, ionisée (NH_4^+) ou non (NH_3), résultant de réactions d'hydrolyse et d'ammonification, ou encore, due à la présence de nitrites (NO_2^-) et nitrates (NO_3^-). La deuxième source, organique, est constituée par une fraction d'azote qui comme la matière carbonée est divisible en fraction inerte et biodegradable (Von Sperling, 2017). La fraction biodegradable de cette source organique est composée marjoritairement d'urée ($(NH_2)_2CO$), d'acides amines et proteins.

I.1.2.3 Phosphore

Présentant des inconvénients similaires à l'azote, le phosphore peut également se trouver sous forme minérale ou organique dans les boues activées.

Son élimination est souvent réalisée par voie chimique, grâce à l'ajout de sels de fer ou d'aluminium qui sont capables de se combiner avec les ions phosphate pour former un précipité de phosphate de fer ou d'aluminium ($FePO_4$ ou $AlPO_4$). La précipitation chimique peut être réalisée à plusieurs étapes dans la filière de traitement (Gaïd, 1999):

- au niveau de la décantation primaire ;
- dans le bassin d'aération de boues activées, le précipité décante alors dans le clarificateur ;
- enfin, sur l'eau épurée biologiquement avec un dispositif spécifique pour le faire décanter.

Le phosphore peut également être éliminé par voie biologique. Bien que cela soit plus complexe à faire, l'utilisation des microorganismes déjà présents dans les boues activées peut réduire les coûts du procédé de traitement par rapport aux produits ajoutés pour la précipitation. L'épuration biologique du phosphore est basée sur les principes suivants :

- Certaines bactéries *(Acinetobacter* par exemple) sont capables d'accumuler des quantités en excès de phosphore sous la forme de polyphosphates ;
- Ces bactéries doivent être, tout d'abord, placées dans une zone anaérobie, où elles réalisent la fermentation de substrats phosphatés en les assimilant comme produits de stockage dans leur cellule ;
- Après, au sein d'une zone aérobie, l'énergie fournie pour l'activité de ces bactéries s'accompagne de l'oxydation des produits stockés, ce qui donne de la place pour le stockage de plus de polyphosphates dans leur cellule.

Comme il est nécessaire d'alterner entre conditions aérobies et anaérobies, l'abattement de phosphore est normalement envisagé à côté de celui de l'azote.

I.1.2.4 *Effluent synthétique à traiter et besoins nutritionnels*

Pour alimenter les systèmes par boues activées, de nombreux travaux de recherche dans la littérature utilisent un effluent synthétique (Yoo et al., 1999; Hong et al., 2002; Yang et al., 2003; Ji et Zhou, 2006; Jamal Khan et al., 2011; Mesquita et al., 2011). Cela permet, à la fois, de simuler la nature d'un effluent réel et d'éviter les variations dans l'alimentation du procédé qui pourraient déstabiliser ce dernier.

Pour préparer un effluent synthétique, il est conseillé de respecter le ratio DBO:N:P de 100:5:1 afin de privilégier une croissance efficace des bactéries aérobies dans le bassin d'aération. De plus, des traces de minéraux doivent aussi être présentes dans l'effluent de façon à assurer un développement propre de la biomasse. Le **Tableau I-1** montre les substances et leurs concentrations, en mg/L, précédemment utilisées pour la préparation des effluents synthétiques lors de différents travaux de la littérature.

Les critères choisis pour déterminer la concentration de chaque composant restent néanmoins peu spécifiés. De manière générale, les auteurs essaient de reproduire les caractéristiques des eaux usées locales. Dans le cas de Jamal Khan et al. (2011), ils ont explicité que leur effluent représente ceux à forte charge organique. Mesquita et al. (2011) ont quant à eux cherché à simuler un effluent capable d'augmenter la croissance de bactéries filamenteuses dans la biomasse, avec le but d'identifier des anomalies de fonctionnement dans les procédés à boues activées.

Tableau I-1. Effluents synthétiques trouvés dans la littérature.

Type de Source	Substance	Composition en mg/L par Référence					
		Yoo et al. (1999)	Hong et al. (2002)	Yong et al. (2003)	Ji et Zhou (2006)	Jamal Khan et al. (2011)	Mesquita et al. (2011)
Carbone	CH_3COONa	256,41	-	-	-	-	2073,00
	Extrait de levure	50,00	-	-	-	-	-
	Glucose	-	470,00	-	278,00	1031,00	-
	Sucrose	-	-	390,00	-	-	-
Azote	CH_3COONH_3	240,88	-	-	-	-	-
	$(NH_4)_2SO_4$	230,00	125,00	-	-	-	140,00
	Urée	-	-	-	32	-	-
	NH_4Cl	-	-	-	-	191	-
Phosphore	KH_2PO_4	43,94	70	131,75	-	-	44,00
	K_2HPO_4	-	-	267,50	13,20	87,00	59,00
Sodium	$NaHCO_3$	125,00	200,00	106,00	-	200,00	100,00
Calcium	$CaCl_2$	10,00	-	1,87	6	10	-
	$CaCl_2$	-	140,00	-	-	-	30
Fer	$FeCl_2$	0,375	-	-	-	-	-
	$FeCl_3.6H_2O$	-	8,00	0,125	-	-	18,80
	$FeCl_3$	-	-	-	-	3,00	-
	$FeSO_4$	-	-	-	-	0,30	-
Manganèse	$MnSO_4$	0,038	-	-	-	-	-
	$MnSO_4.H_2O$	-	-	2,50	3,00	-	-
	$MnCl.H_2O$	-	-	-	-	2,00	-
Magnésium	$MgSO_4$	25,00	-	-	-	-	-
	$MgSO_4.7H_2O$	-	100,00	20,00	66,00	10,00	25,00
Zinc	$ZnSO_4$	0,035	-	-	-	-	-

I.1.3 Variables techniques (ou d'opération)

Afin que le procédé de traitement des eaux usées puisse fonctionner avec une efficacité maximale, il est nécessaire de déterminer les paramètres opératoires jouant un rôle important sur la performance du procédé. Les sections suivantes ont pour but d'exposer la dynamique de certains des paramètres habituellement considérés.

Sachant que les paramètres tels que l'âge de boue, le temps de séjour hydraulique et le taux de recirculation reposent sur des définitions mathématiques, ils ont été rapportés, au chapitre II, lequel est dédié à la description du matériel et des méthodes mis en œuvre au cours de la thèse.

I.1.3.1 Charges massique et volumique

Différents paramètres permettent de caractériser l'effluent qui rentre dans un système à boues activées, dont la charge massique (C_m) et la charge volumique (C_v), *i.e.* la quantité journalière de la pollution arrivant au procédé, respectivement, par unité de masse de microorganismes et par volume du bassin d'aération. Il est alors possible de définir un classement selon la concentration de matière organique. Le **Tableau I-2** distingue 5 classes de charge :

Tableau I-2. Classification de l'effluent qui rentre dans le système selon sa concentration en matière organique (Canler et al., 2011).

Classification	C_m (Kg DCO.Kg $MVS^{-1}.j^{-1}$)	C_v (Kg DCO.$m^{-3}.j^{-1}$)
Très faible charge	< 0,20	< 0,72
Faible charge	0,20 à 0,40	0,72 à 1,40
Moyenne charge	0,40 à 1,00	1,40 à 3,40
Forte charge	1,00 à 2,00	3,40 à 6,00
Très forte charge	> 2,00	> 6,00

Le terme MVS ou Matière Volatile en Suspension est souvent utilisé pour exprimer une concentration de biomasse plus précise dans le bassin d'aération. Une description mathématique de ces deux paramètres est également prévue lors du Chapitre II.

I.1.3.2 Oxygène dissous

Dans les procédés à boue activée, il est indispensable de fournir une certaine quantité d'oxygène dissous (OD) au milieu aqueux. Malgré le coût que cela représente, le niveau d'oxygène dissous est généralement maintenu entre 4 et 6 $mgO_2.L^{-1}$ (Knudson et al., 1982). Ces quantités d'oxygène sont nécessaires pour assurer l'activité des microorganismes aérobies ou facultatifs particulièrement ceux qui se trouvent au sein de flocs de boue activée et qui ont, donc, plus de difficulté pour accéder à l'OD, du fait des résistances à son transport et à son transfert par diffusion (Yadav et al., 2014).

Dans l'eau claire la valeur de l'OD à saturation est fonction de paramètres thermodynamiques, comme la température et la pression atmosphérique (Wells et al., 2009). Dans les boues, ces paramètres ont une influence similaire.

L'OD est un paramètre opératoire qui influe sur les performances du procédé :

- sur la croissance des microorganismes et par suite notamment sur le taux de dégradation des composés organiques,
- sur la biofloculation, laquelle est déterminante particulièrement lors de la décantation (Faust et al., 2014).

I.1.3.3 pH

Le pH est un paramètre chimique pertinent pour surveiller le bon développement de la biomasse. Les bactéries hétérotrophes, d'une façon générale, ont de meilleures performances lorsque l'environnement a une valeur de pH entre 6,5 et 8,5. Une croissance optimale est observée quand le système atteint un pH proche de 7,0 (Schmidell, 2007).

Dans les procédés aérobies de traitement d'effluents, les variations de pH observées influencent l'efficacité du procédé. Dans le cas du procédé à boues activées, la plage d'opération considérée comme adéquate est entre 7,0 et 8,0. Si la nitrification est recherchée, la gamme de pH optimale doit être légèrement au-dessus de la valeur de neutralité, soit entre 7,5 et 8,5 (Sant'Anna, 2010).

I.1.3.4 Température

La température est un paramètre qui affecte principalement l'action des microorganismes qui composent le système de boues activées (Schmidell, 2007). Le traitement aérobie d'effluents peut être opéré dans une large gamme de températures, de 10 à 40 ºC approximativement. La température de 35 ºC étant celle où l'activité microbienne atteint son point optimal, c'est par conséquent, la température à laquelle le procédé voit sa vitesse d'activité metabolique augmenter. Par contre, à une température voisine de 5ºC, par exemple, il est possible d'observer une réduction de la consommation de substrat. De même, dans le cas où la température est supérieure à 40 ºC, on observe une diminution de l'élimination de la matière organique, à cause de la mort de bactéries (Roques, 1980).

Liao et al. (2011) ont développé des réacteurs fonctionnant sous conditions thermophiles, i.e. avec des températures supérieures à 45 ºC. Cette stratégie est recommandée pour le traitement d'effluents avec des concentrations élevées en charge organique ; par exemple pour le traitement de pulpes de papier et de cellulose.

Koivuranta et al., (2017) ont pu aussi constater que les variations des temperatures dans l'effluent d'entrée, causées par les changements de saisons, peuvent affecter la formation des flocs de boues activées. Par exemple, lors de la période de l'hiver rigoreux, une abondance des bacteries filamenteuses a été observées pour un système à boues activées à grande echelle. Par conséquent, la forte concentration de ce type de bacterie a provoqué une perturbation dans la performance du procédé.

I.1.4 Perturbations opératoires dans les systèmes à boues activées

Comme mentionné précédemment, afin de garantir le bon fonctionnement d'un système à boues activées, il est nécessaire de trouver un juste équilibre entre bactéries « floculantes » et bactéries filamenteuses. Les principales perturbations de fonctionnement observées sont le moussage et le foisonnement des boues. Ces perturbations sont soit identifiées par l'observation directe du phénomène, soit quantifiées par la mesure de l'Indice de Boue (IB). La méthode standard pour déterminer l'IB sera détaillée dans le Chapitre II. Ce paramètre caractérise la capacité à sédimenter des boues. Il s'exprime en « mL » par « g » de matière en suspension (MES). Les boues montrant une mauvaise performance de décantation ont des IBs inférieurs à 50 $mL.g^{-1}$ ou supérieurs à 150 $mL.g^{-1}$ (Von Sperling, 2017).

Le moussage consiste en la formation d'une couche épaisse de mousse en surface de l'ensemble du système, bassin d'aération et décanteur. Ces mousses peuvent apparaître : (1) lors du démarrage du traitement dû à des charges massiques élevées et, dans ce cas, la situation se normalise rapidement lorsque la boue atteint sa maturation ou bien (2) lors l'arrivée d'effluents industriels chargés en agents tensioactifs.

Par ailleurs, le foisonnement (ou *bulking* en anglais) de boues est le terme utilisé pour décrire la perturbation qui est produite lorsqu'il y a un amoindrissement de la capacité de floculation, et par conséquent, de décantation des boues, dans le procédé. La littérature met en évidence deux catégories de foisonnement : le filamenteux et le dispersé.

- Le foisonnement filamenteux : il est directement lié à un important développement de bactéries filamenteuses. Ces filaments vont ensuite se répandre hors des limites des flocs en adhérant à d'autres flocs du même type, ce qui crée de nouvelles sur-structures extrêmement poreuses. La boue commence à occuper un grand volume dans le décanteur (représentée par des valeurs d'IB très élevées), pouvant conduire à une perte de biomasse par débordement du décanteur compromettant ainsi la qualité de l'effluent de sortie.

- Le foisonnement dispersé : dans ce cas on note une prédominance des bactéries « floculantes », lesquelles vont être liées plutôt par une mucilage d'exopolysaccharides que par des filaments. Les liaisons qui assurent alors la structuration de la boue sont insuffisamment rigides, ce qui génère des flocs biologiques fragiles, avec une faible compaction et assez dispersés les uns par rapport aux autres.

La **Figure I-3** synthétise l'effet de la prédominance d'un type de bactérie sur un autre, aussi bien que les deux types de foisonnements.

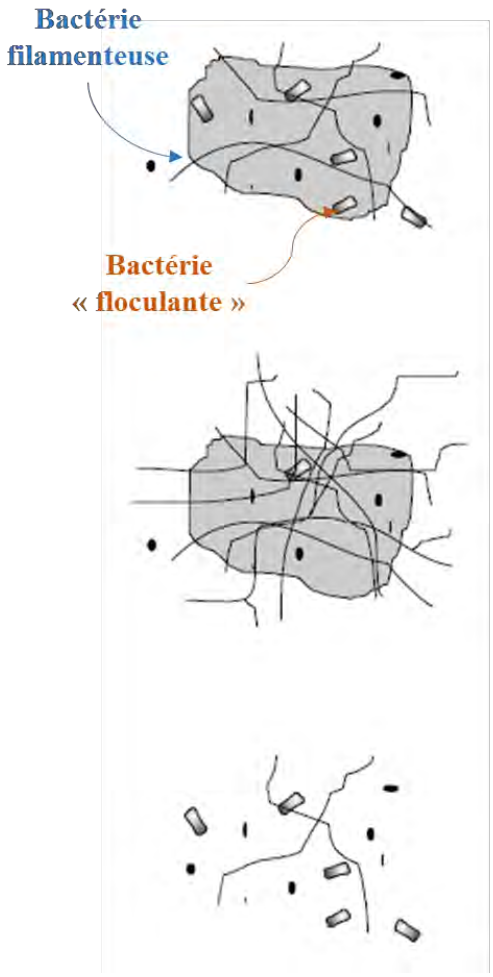

FLOC IDEAL

1. Bactéries filamenteuses et « floculante » en équilibre
2. Flocs grands et forts → flocs de taille importante et très résistants ou solides
3. Filaments ne dépassent pas trop les limites du floc
4. Bonne qualité de l'effluent de sortie
5. 50 mL.g^{-1} < IB ≤ 150 mL.g^{-1}

FLOC FILAMENTEUX

1. Bactéries filamenteuses en larges quantités
2. Flocs de très grande taille
3. Filaments dépassent trop les limites du floc affectant le compactage de la boue
4. Possible présence de la biomasse dans l'effluent de sortie.
5. IB > 150 mL.g^{-1}

FLOC DISPERSÉ

1. Bactéries « floculante » en larges quantités
2. Flocs petits et peu résistants
3. Sans interférence des filaments
4. Effluent de sortie turbide
5. IB ≤ 50 mL.g^{-1}

Figure I-3. Type de flocs selon la prédominance d'un certain type de bactéries (adaptée de Sezgin et al., 1978).

Plusieurs facteurs peuvent jouer sur l'équilibre entre ces deux communautés de bactéries, lesquels sont souvent associés aux variables techniques ou d'opération (Tandoi et al., 2017). Parmi eux, il est possible de mettre en avant :

- La concentration d'oxygène dissous ;
- La charge massique ou la quantité de nourriture apportée aux microorganismes ;
- La carence en nutriments ;
- Le pH très acide ;
- La présence d'un effluent septique.

Jusqu'à récemment, on connaissait assez peu comment ces paramètres pouvaient influencer sur la dynamique de l'équilibre de bactéries filamenteuses et floculantes. Cependant avec les progrès de l'analyse d'images issues d'observations microscopiques, les phénomènes biologiques au sein des boues activées ont pu être mieux appréhendés.

I.2 Caractérisation des flocs de boues activées par analyse d'images

L'analyse d'image est une technique qui a été utilisée à différentes fins dans le cadre d'études concernant les systèmes à boues activées : étudier le processus de biofloculation (Wilén et al., 2003a), analyser l'aspect morphologique des flocs (Perez et al., 2006; Ginoris et al., 2007; Liwarska-Bizukojc et al., 2015), identifier des problèmes de *bulking* filamenteux (Jenné et al., 2007; Amaral et al., 2013). Mesquita et al. (2009b) l'ont utilisée quant à eux afin de relier les caractéristiques morphologiques des flocs biologiques à leurs propriétés de sédimentation.

Dans la suite de ce travail, les différents points relatifs à l'Analyse d'Images (AI), de la conception du protocole d'AI à sa mise en œuvre, seront présentés.

I.2.1 Mise au point d'un protocole d'analyse d'images

Lors du développement d'un protocole d'analyse d'images, quelques étapes doivent être respectées afin de réussir une caractérisation appropriée de n'importe quel type de particules ou flocs. Ces étapes peuvent être séparées et ordonnées comme l'illustre le schéma de la **Figure I-4**.

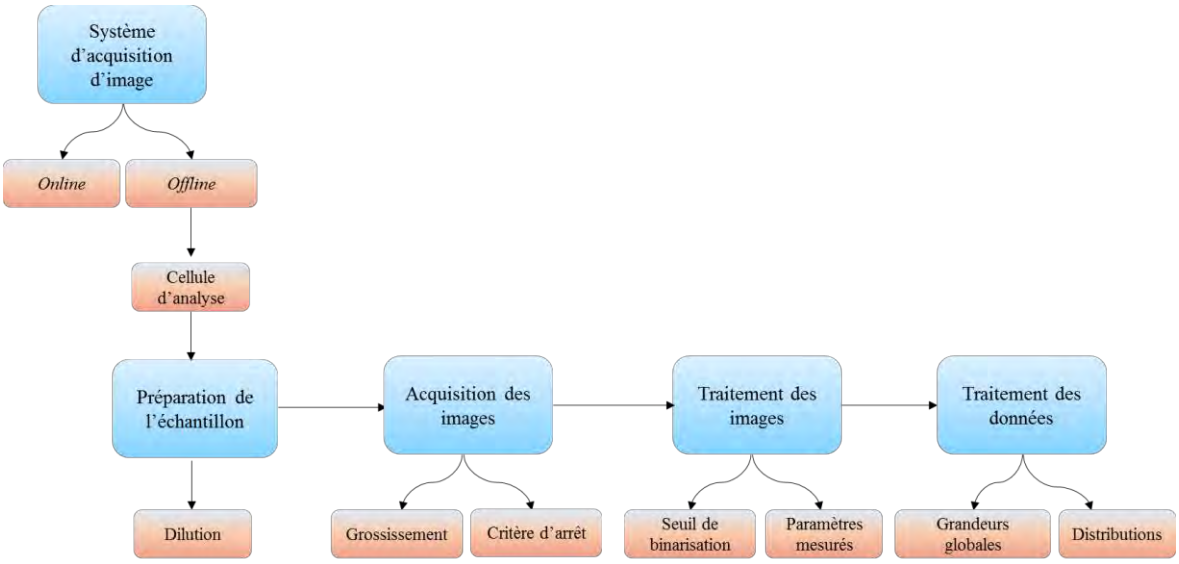

Figure I-4. Principales étapes pour la conception d'un protocole d'analyse d'images.

Ces différentes étapes ont été détaillées sur les prochaines sections en tenant compte des travaux déjà développés principalement pour la caractérisation des flocs de boues activées.

I.2.1.1 Préparation de l'échantillon

Puisque les boues activées contiennent en grand partie des constituants biologiques, leurs caractéristiques sont susceptibles d'évoluer assez rapidement lors d'une opération d'échantillonnage. En conséquence, les échantillons de boues doivent être analysés dans un intervalle de temps le plus court possible après leur prélèvement. Malgré l'importance de ce point, le temps entre l'échantillonnage et l'analyse par microscope est peu mentionné dans les travaux de la littérature. Amaral et al. (2013) rapportent dans leur étude un temps de 3 heures entre la collecte des échantillons et la préparation des dilutions pour les observations

microscopiques, tandis que Motta et al. (2002a) ont réalisé cette tâche dans les 8 heures suivant le prélèvement. Cela peut constituer une première estimation de la plage de temps conseillée à ne pas dépasser.

Pour les protocoles d'AI *offline*, avant même de parler de dilution, il est toujours nécessaire de s'assurer de l'intégrité de l'échantillon et de ne pas endommager la structure des flocs des boues en choisissant une cellule d'analyse compatible avec les matériaux liquides. Le choix du bon dispositif pour déposer les échantillons ayant été fait, il est alors souvent nécessaire d'effectuer une dilution de l'échantillon.

En effet, les matériaux, tels que les boues activées, ont besoin d'être dilués lors des analyses microscopiques afin de permettre une caractérisation morphologique représentative (Costa et al., 2013). Néanmoins, il est conseillé de ne pas diluer ces échantillons de façon aléatoire, un facteur de dilution optimal devant ainsi être déterminé. Quand la dilution est excessive, il y a le risque d'une déstructuration des flocs de boues. Sans oublier que le fait que la mesure des paramètres morphologiques des flocs soit mal estimée est possible lors de l'augmentation du facteur de dilution. En effet, augmenter le facteur de dilution est problématique car la quantité de biomasse par surface analysée sera à chaque fois plus réduite. D'autre part, si la dilution est insuffisante, il est fort probable que les flocs, filaments et autres types de particules, soient empilés les uns sur les autres, conduisant à une mauvaise estimation des paramètres morphologiques. Ainsi la valeur optimale du facteur de dilution doit permettre d'isoler les flocs de façon individuelle sur l'image, sans les déstructurer et d'obtenir assez d'agrégats pour que la statistique soit fiable.

Concernant les boues activées, il est possible d'indiquer quelques études qui ont été menées envisageant la définition d'un facteur de dilution optimal. Le **Tableau I-3** expose le type de boue utilisé dans les études ainsi que la gamme de concentration de biomasse (MES) observée pour chacun des échantillons. La plupart des auteurs estiment que la gamme de dilution doit être testée en se basant sur les valeurs de MES et aussi sur la taille attendue pour ces agrégats.

D'après Costa et al. (2013), le type de boue joue également un rôle très important dans le choix du facteur de dilution. Sachant que les boues anaérobies sont beaucoup plus concentrées que les boues aérobies, une classification différenciée est opérée par rapport à la taille de leurs flocs. Comme ils présentent une vaste plage de taille, les flocs anaérobies peuvent ainsi être classés en micro-agrégats et macro-agrégats.

Bien que la déstructuration des flocs soit un fait confirmé par ces études comme principal effet de l'augmentation de la dilution, une valeur optimale n'est pas vraiment définie dans ces travaux. En revanche, il est indiqué que la bonne dilution est possiblement comprise entre un facteur de 1:5 et 1:10 pour les deux types de boues.

Tableau I-3. Études déjà réalisées afin de trouver un facteur de dilution optimal pour les échantillons de boues activées.

Référence	Type de boue	MES ($g.L^{-1}$)	Dilutions testées
Barbusiński et Kościelniak (1995)	Aérobie	Maintenu à 3,0	1:5 à 1:10
Motta et al. (2002a)	Aérobie	1,2 à 3,0	1:2 à 1:20
Perez et al. (2006)	Aérobie-Anaérobie	3,0 à 4,7	1 :1 à 1:4
Costa et al. (2007)	Anaérobie	20,0 à 30,0	1:5 à 1:10
Mesquita et al. (2010a)	Aérobie	2,3 à 4,7	1:2 à 1:10

I.2.1.2 Système d'acquisition d'images

Les principaux composants d'un système d'acquisition d'images *offline* sont : un microscope automatique ou semi-automatique, une caméra haute résolution couplée à ce microscope et un logiciel qui permet d'acquérir et ensuite d'analyser les images enregistrées.

Deux types de microscopes sont largement utilisés pour la conception d'un système d'acquisition d'images : le microscope en champ clair et celui à contraste de phase.

- Microscope en champ clair : sur ce type de microscope, il est possible d'avoir une image assez nette des flocs de boues activées. Comme ils apparaissent en noir sur un fond brillant, cela permet de bien isoler les flocs. Toutefois, les objets avec un aspect transparent comme les filaments et les cellules libres sont dans ce cas peu visibles (Khan et al., 2018). Une solution trouvée (Wagner et al., 1993; Mesquita et al., 2010b) pour contourner ce problème est d'augmenter le contraste de tels objets par l'application de techniques de coloration.

- Microscope à contraste de phase : sur cette variante, l'objectif du microscope est capable de visualiser des objets avec des contours beaucoup plus brillants, ce qui peut être la source de certains problèmes lors du calcul des propriétés morphologiques (Pons et Vivier, 1999). Par contre, cela permet une bonne identification des bactéries filamenteuses (Araya-Kroff et al., 2004).

Récemment, Mesquita et al. (2010b) ont comparé la performance de ces deux types de microscopes et ils ont pu bien identifier simultanément les flocs et les filaments en utilisant uniquement le microscope en champ clair. Cela permet d'optimiser le temps d'observation microscopique contrairement à l'option qui consistait à utiliser un microscope différent pour quantifier chaque type d'objets.

Un autre point très important est le choix d'un grossissement pour visualiser les échantillons de boues activées. Bien que la plupart des études (da Motta et al., 2001; Costa et al., 2007; Mesquita et al., 2009b) soient réalisées avec des protocoles d'AI en utilisant un grossissement x100, Mesquita et al. (2010a) ont eu pour but d'examiner un grossissement plus petit et plus représentatif comme le x20 et de comparer sa performance avec celui de x100. Finalement, ils ont trouvé que l'utilisation d'un grossissement x100 engendrait moins de pertes de précision et de représentativité de la biomasse par rapport au grossissement x20.

La majorité des protocoles d'AI sont développés pour réaliser des caractérisations morphologiques *offline*. Cependant quelques méthodes *online* ont été rapportées dans la littérature (Koivuranta et al., 2013; Tomperi et al., 2016). Cela donne la possibilité de suivre la morphologie des flocs de boues en temps réel et de raccourcir le temps passé avec les préparations de dilutions. En revanche, ces systèmes « *online* » impliquent souvent des boucles de circulation pour amener l'échantillon jusqu'au microscope. Le fait de soumettre les flocs biologiques à des conditions de cisaillement différentes de celles de l'environnement du bassin d'aération peut mettre en cause une des règles fondamentales de la caractérisation morphologique des boues qui est de maintenir l'intégrité de l'échantillon. En outre, il semble y avoir une limitation au niveau de la distance focale, ce qui parfois nécessite le passage des flocs dans des capillaires ayant un diamètre interne inférieur à leur diamètre équivalent, induisant des contraintes de cisaillement suffisamment fortes pour modifier les propriétés observées.

La **Figure I-5** illustre un des systèmes d'acquisition *online* déjà développés pour l'indentification des boues en conditions normales et aussi filamenteuses. Dans le cas de cette étude (Koivuranta et al., 2013), les échantillons sont préalablement dilués dans un réservoir de mélange et sont ensuite renvoyées vers le dispositif qui capture les images des flocs sous un flux laminaire permettant de limiter l'endommagement des flocs.

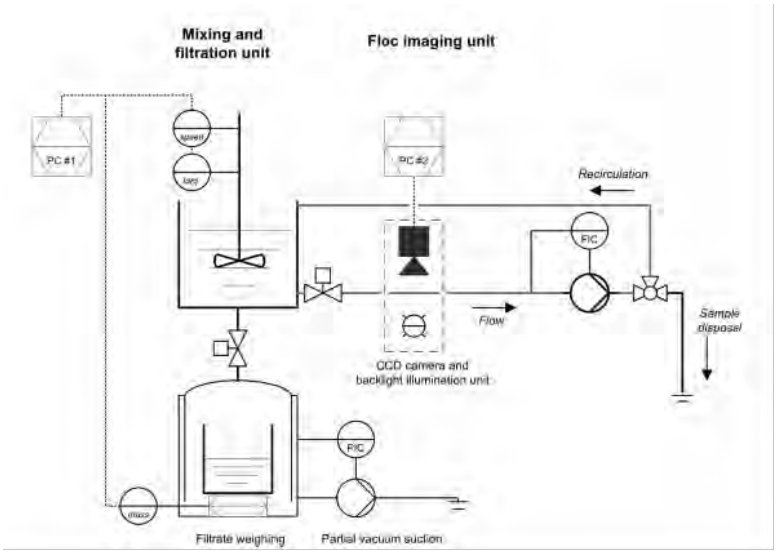

Figure I-5. Schéma du système d'acquisition d'images *online* (Koivuranta et al., 2013).

I.2.1.3 Traitement d'images

Une fois les images des flocs enregistrées, l'étape suivante consiste à les traiter, principalement, par l'application d'une procédure de seuillage pour isoler chaque floc et ainsi extraire les informations qui permettent la détermination des propriétés morphologiques de chaque objet isolé.

Le seuillage a pour but d'appliquer une procédure automatique pour distinguer, tout d'abord, les objets de l'arrière-plan de l'image. Dans les cas des boues activées, ces objets peuvent être des flocs, des filaments ainsi que d'autres organismes vivants dans le milieu, comme des protozoaires. Après cette étape d'identification, les objets sont séparés de l'arrière-plan par une méthode de segmentation, aussi connue sous le terme de binarisation. Pour ce faire, une valeur contenue dans une échelle de gris va être attribuée à ce qui est objet et à ce qui est arrière-plan. L'attribution d'un seuillage est généralement fonction de la subjectivité de l'opérateur, afin de limiter cette subjectivité, cette opération doit être automatisée le plus possible (Pons and Vivier, 1999).

L'isolement des objets est souvent suivi d'un post-traitement qui a pour but d'éliminer des parties qui ne sont pas représentatives de l'échantillon ou pour l'analyse de données réalisée ensuite. Dans les boues, on peut trouver des particules grossières qui n'ont pas été filtrées lors d'une filière de traitement primaire et qui ne sont pas la cible de l'analyse d'images.

De nombreux logiciels décrits dans la littérature envisagent l'automatisation du seuillage des images de boues activées (da Motta et al., 2001; Jenné et al., 2002; Mesquita, 2011). Parfois ils sont même très ciblés sur un constituant spécifique comme ceux développés par Amaral, (2003) et par Ginoris et al., (2007), qui se sont intéressés à la quantification des protozoaires et métazoaires présents dans les boues.

I.2.1.4 Traitement de données

Cette étape est réalisée après le traitement d'images lorsque les objets ont été bien identifiés. Sachant que les images ont été binarisées, il est alors possible de calculer plusieurs propriétés qui décrivent la taille et la forme des agrégats de boues activées. Parmi ces propriétés, certaines sont listées dans le **Tableau I-4** et seront mieux détaillées dans le **Chapitre II**.

Afin que le calcul de propriétés morphologiques puisse représenter la réalité d'un échantillon, un nombre suffisamment important d'objets, entre flocs et filaments, doit être analysé. Grijspeerdt et Verstraete (1997) ont utilisé une base de 150 objets pour la détermination des paramètres morphologiques de leurs échantillons tandis que Amaral et al., (2013) ont mesuré aux alentours de 3000 objets pour garantir la précision et par conséquent la fiabilité de leurs résultats. D'un autre côté, Koivuranta et al., (2013) ont mené leurs caractérisations morphologiques sur plus de 20.000 objets en affirmant que les données exposées dans leur étude pouvaient être plus pertinentes d'un point de vue statistique en comparaison à celles produites par leurs prédécesseurs.

Tableau I-4. Propriétés de taille et forme déterminées sur la base des images binarisées.

Propriétés	Notation	Définition
Surface	A	Surface cumulée de pixels
Périmètre	P	Distance cumulée entre les contours de pixels
Diamètre équivalent	D_{eq} (ou CED)	Diamètre d'un cercle avec la même surface que l'objet
Surface et périmètre convexe	A_C, P_C	Propriétés correspondant à la plus petite région convexe qui entoure la surface projetée par la particule.
Circularité	C	Similarité de l'objet avec un cercle parfait.
Convexité	C_x	Rend compte de la rugosité de l'objet.
Solidité	S	Rend compte des concavités de l'objet.
Elongation	E	L'allongement de l'objet défini depuis son rapport d'aspect (RA)

Compte tenu de la quantité considérable de données, comme celles présentées dans la littérature, il est nécessaire d'appliquer des approches statistiques pour extraire le maximum d'informations possible qui puisse être utile à la compréhension du fonctionnement du procédé.

Parmi les méthodes statistiques multi-variables utilisées pour traiter les jeux de données, l'ACPs (Analyse en Composantes Principales) et PLS (de l'anglais *Partial Least Squares*) sont mentionnées par Mesquita et al. (2013). La première explore principalement les combinaisons linéaires entre variables, bien que d'autres types de combinaisons puissent exister. Cette méthode permet de traiter simultanément un nombre quelconque de variables, toutes quantitatives, de manière à condenser les informations pour les interpréter plus facilement. La deuxième méthode est également linéaire, mais, celle-ci permet la construction d'un modèle qui peut être utilisé pour la prédiction de certains comportements du procédé.

Une autre manière d'analyser ces données est de mettre en place la statistique descriptive. L'analyse de distributions ainsi que l'accès aux paramètres issus de ces distributions (moyenne, mode, médiane, écart-type entre autres) peuvent rendre utile l'interprétation des résultats si elles sont mises en perspectives du fonctionnement du procédé. Les distributions de taille de particules sont souvent déterminées pour vérifier si la population des flocs suit une loi normale, log-normale ou Gaussienne (Liao et al., 2006; Liwarska-Bizukojc et al., 2015), ou encore pour estimer la taille moyenne des particules, laquelle joue un rôle très important sur la décantation des flocs de boues et sur la filtration dans le cas des bioréacteurs à membrane (Çiçek et al., 1999; Meng et al., 2006).

Bien que la même approche soit possible pour les paramètres morphologiques comme la circularité, la convexité, la solidité etc., la détermination des distributions pour ces paramètres restent encore peu explorée dans les travaux réalisés sur les flocs de boues activées.

La méthode statistique de traitement des données étant posée, le protocole d'analyse d'images dans son ensemble est alors établi et il peut être mis en œuvre pour aider à l'identification des comportements opérationnels et aussi des perturbations du procédé.

I.2.2 Mise en relation des paramètres du procédé avec les paramètres morphologiques

Les PBAs sont très sensibles aux modifications des conditions opératoires qui affectent directement l'équilibre entre les différents types de bactéries qui cohabitent dans l'environnement de la boue modifiant ainsi la structure des flocs. Inversement, les changements de structure des flocs impactent notamment l'efficacité de séparation solide-liquide qui a lieu dans le décanteur. Selon Amaral et Ferreira (2005), la caractérisation morphologique des flocs de boues est une piste pour relier la performance du procédé aux variations des paramètres opératoires.

Les études les plus pertinentes de la littérature par rapport à ce travail sont rapportées dans les sections suivantes.

I.2.2.1 Indice de boue (IB), Matières en Suspension (MES), paramètres de taille et de forme

L'indice de boue (IB) exprime la qualité de la décantation de la boue et les Matières en Suspension (MES) donnent une information concernant la concentration de biomasse. IB et MES constituent les mesures de routine dans une station d'épuration. En raison de la fréquence avec laquelle ils sont mesurés, et dû à leur importance technique, ces paramètres sont parmi les plus étudiés afin d'établir une relation avec les paramètres morphologiques.

Grijspeerdt et Verstraete (1997) ont été parmi les pionniers à suivre les descripteurs morphologiques des flocs de boues en établissant, par analyse d'image, un rapport avec les propriétés de sédimentation et le contenu des boues. Ils ont pu noter que les propriétés de taille et de forme étaient plus rapidement sensibles aux modifications opératoires que l'Indice de Boue. Ainsi, le diamètre équivalent et le facteur de forme (paramètre similaire à la circularité) ont commencé à changer 5 jours avant l'IB. Ceci suggère que toute évolution de la morphologie des agrégats peut être utilisée comme un critère d'intervention précoce sur le procédé dans le cas de perturbations. D'autre part, ils ont pu trouver une première relation linéaire entre la surface totale des flocs dans une image et la quantité de MES dans le système. La **Figure I-6** montre que la quantité de MES (X) augmente avec l'augmentation de surface projetée (A) des flocs. Cependant, l'applicabilité de cette corrélation est limitée car elle n'est valable que pour une concentration maximale de MES de 4 $g.L^{-1}$ et varie avec le type de boue.

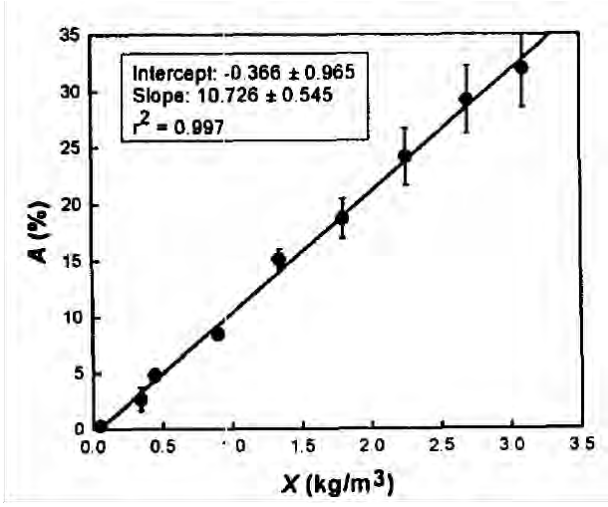

Figure I-6. Relation entre la surface totale de flocs dans une image avec la concentration de MES dans le système (Grijspeerdt et Verstraete, 1997)

D'autres travaux ont succédé à cette étude. Ils ont essayé principalement de prédire le comportement de ces deux paramètres classiques à partir de données issues de la caractérisation morphologique. Mesurer les MES et l'IB au moyen de méthodes classiques prend souvent beaucoup de temps, donc, toute stratégie qui peut optimiser le temps passé à l'obtention de ces données est recherchée. Le **Tableau I-5** liste les principaux travaux développées afin de prédire ces deux paramètres.

Tableau I-5. Liste de travaux réalisés sur la prédiction de l'IB et de MES.

Reference	Paramètres de taille et forme examinés*	Prédiction	
		IB	MES
Jenné et al. (2003)	A, P, C, N_f	×	
Casellas et al. (2004)	A, N_f	×	
Amaral et Ferreira (2005)	A, C_x, S, N_f	×	×
Jenné et al. (2005, 2006)	D_{eq}, DF, FF, C, C_x, RA, S, N_f	×	×
Liwarska-Bizukojc et Bizukojc (2005)	A moyenne		×
Mesquita et al. (2009a, 2009b)	Plus de 38 paramètres dont la morphologie et la physiologie de la boue sont comprises	×	

*Propriétés définies dans le Tableau I-4. Pour DF – Dimension Fractale, FF – Facteur de Forme et N_f – propriétés liées à la quantification de filaments.

Les études conduites par Mesquita et al. (2009a, 2009b) sont venues compléter celle de Amaral et Ferreira (2005). Ces différents travaux utilisent des méthodes statistiques (PLS et ACPs) pour condenser un large jeu de données déterminé en classant les flocs selon leurs tailles en trois catégories : grands (CED > 250 µm), intermédiaires (25 µm < CED ≤ 250) et petits (CED ≤ 25 µm). Leur approche met en évidence des paramètres clés pour l'estimation de l'IB, tels que le diamètre équivalent et la quantification de filaments (que ce soit leur nombre ou leur longueur).

Vu que le foisonnement (*bulking*) filamenteux est directement associé à une détérioration des capacités de sédimentation du floc et que l'IB est l'indicateur de cette capacité, des études relatives à des problèmes de sédimentation (Jenné et al., 2002; Motta et al., 2002b; Mesquita et al., 2011; Koivuranta et al., 2013; Amaral et al., 2013) mesurent la morphologie des filaments en parallèle de l'IB afin de trouver des moyens de détecter à l'avance ces perturbations.

I.2.2.2 Influence de l'âge de boue

L'impact de l'âge de boue, aussi décrit comme le temps de séjour des flocs dans le bassin d'aération, sur la morphologie des agrégats a été largement étudié, principalement, parce qu'il est un des paramètres opératoires qui peut jouer sur la dynamique de la structuration des flocs. Li et al. (2018) ont montré dans leur étude avec des réacteurs à l'échelle du laboratoire que ce paramétre du procédé affecte principalment les profiles des distributions de taille de particules, lequels ont un resultát sur la décantation des flocs de boues activées.

Bisogni et Lawrence (1971) ont réalisé un des premiers travaux sur l'étude de l'influence de l'âge de boue sur les caractéristiques des flocs. Ils ont travaillé sur des réacteurs à l'échelle du laboratoire, où ils ont fait varier l'âge de boue dans une plage comprise entre 0,25 à 12 jours. Leurs observations microscopiques ont permis de conclure que les flocs avec un âge de boue de 0,25 à 2 jours présentaient une croissance dispersée, tandis que ceux entre 2 et 9 jours avaient une taille moyenne et une densité adéquate. En revanche, ceux entre 9 et 12 jours avaient des formes très irrégulières et lâchées, présentant une tendance à la défloculation.

Dans une autre étude, Lovett et al. (1983) ont fait varier l'âge de boue de leur système entre 4 et 20 jours. Ils ont trouvé un résultat similaire à celui de Bisogni et Lawrence (1971) lorsque l'âge de boue reste inférieur à 8 jours. Par contre, ils n'ont pas pu vérifier une tendance à la défloculation quand l'âge de boue était d'environ 20 jours, mais ont noté une diminution de la quantité de matériaux dispersés.

Liao et al. (2000) ont également réalisé une étude où l'âge de boue a varié entre 4 et 20 jours. Leur étude a spécifiquement cherché à voir comment l'âge de boue pouvait impacter la quantité de l'eau liée (*bound water*) existant dans les flocs de boues. Pour ce faire, ils ont mesuré la taille des flocs afin de la corréler avec le contenu de l'eau liée. Finalement, ils ont trouvé des concentrations plus importantes d'eau liée pour les âges de boues compris entre 9 et 20 jours pour des agrégats dont la taille moyenne est d'environ 100 µm.

En complément des études précédemment citées, Liss et al. (2002) ont étudié l'effet de l'âge de boue sur la concentration de substances polymériques extracellulaires (SPEs) dans le milieu ainsi que l'influence de ces composants sur la structuration des flocs de boues. Dans ce but, ils ont utilisé la microscopie électronique à balayage pour observer les agrégats. Ils ont observé que les flocs pour un âge de boue entre 16 et 20 jours ont présenté une structure plus compacte

et plus sphérique que les flocs provenant d'un réacteur d'un âge de boue entre 4 et 9 jours. De plus, une concentration plus élevée de SPEs a été mesurée pour des âges de boues plus importants.

Avec l'utilisation croissante des Bioréacteurs à Membrane (BàM) comme procédé de traitement secondaire au XXI siècle, l'influence de l'âge de boue sur la performance de ces systèmes a commencé aussi à être étudiée. Massé et al. (2006), par exemple, ont effectué une comparaison entre un PBA et un BàM qui ont fonctionné dans une même plage d'âge de boue, de 10 à 30 jours. Lorsque l'âge de boue a augmenté, la taille moyenne en volume de la population des flocs a diminué pour les deux procédés. Tandis qu'à 10 jours, la gamme de variation était entre 120 et 200 µm, à 30 jours elle est passée de 70 à 100 µm dans les deux cas. La seule différence était la présence d'une sous-population avec une taille moyenne de 10 µm pour les BàM avec un âge de boue de 30 jours.

Dans une autre étude, Liao et al. (2006) ont cherché à approfondir l'effet de l'âge de boue sur les caractéristiques et la structure des boues activées. Ils ont analysé la taille mais également la forme des flocs. Lors d'un suivi de la taille médiane (d_{50}) des flocs en fonction de l'âge de boue, ils ont pu vérifier que les distributions de taille des flocs étaient plus stables pour des âges de boues (*SRT*) entre 9 et 20 jours, avec des écart-types plus faibles (**Figure I-7**).

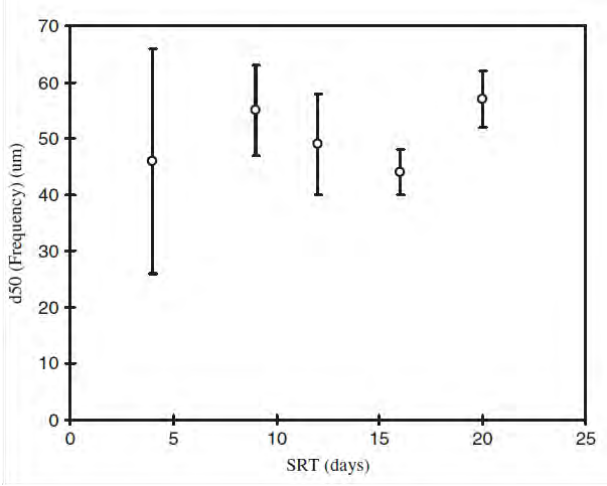

Figure I-7.Effet de l'âge de boue sur la taille médiane des flocs (Liao et al., 2006).

En outre, les flocs issus des âges de 4 et 6 jours ont présenté des facteurs de forme inférieurs à 0,20, ce qui indique un degré élevé d'irrégularité du contour des flocs. Il faut souligner aussi que pour ces deux âges un foisonnement filamenteux modeste a été identifié. Pour les âges de 9, 12, 16 et 20 jours, par contre, des flocs plus sphériques et compacts ont été observés.

Ahmed et al. (2007) ont, quant à eux, étudié l'effet de l'augmentation de l'âge de boue sur la pression transmembranaire nécessaire pour le fonctionnement des BàM. Ils ont pu identifier qu'il y avait une augmentation de la taille moyenne des flocs, calculée en nombre, lorsque l'âge de boue est augmenté. Cela peut être visualisé par le déplacement des distributions vers la droite (âges des boues de 10, 40 et 100 jours).

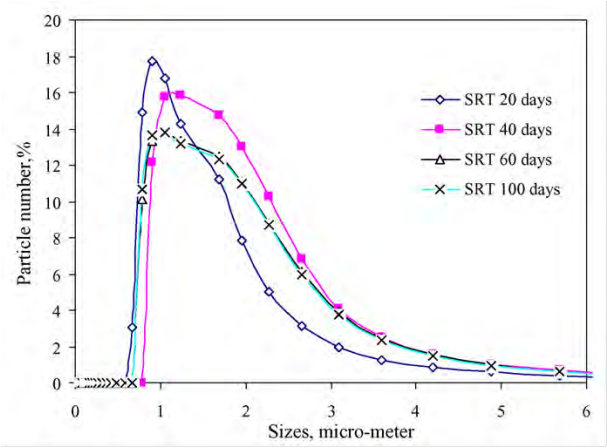

Figure I-8. Distribution en nombre des particules pour différents âges de boues dans un BàM (Ahmed et al., 2007).

En conséquence, l'augmentation de l'âge de boue a été associée à une diminution du taux de colmatage de la membrane ainsi qu'à une diminution de la résistance spécifique du gâteau qui se forme sur la surface de la membrane.

Plus récemment, Van den Broeck et al. (2012) ont développé leur propre technique d'analyse d'images pour examiner l'effet de l'âge de boue sur le colmatage des membranes, qui constitue encore le principal inconvénient lors de l'opération des BàM. Ils ont trouvé un résultat similaire à celui de Ahmed et al. (2007), quand leur bioréacteur a fonctionné avec des âges de boues de 30 et 50 jours, le taux de colmatage a été réduit. L'observation de la surface totale des flocs dans une image, pour les âges de boues les plus importants a montré une diminution de la fraction de petits fragments mesurée, pouvant expliquer ainsi une moindre participation au colmatage de la membrane.

I.2.2.3 Influence de la charge organique

La charge organique détermine « le régime » des microorganismes dans les PBAs. Elle va interférer directement dans la croissance de la biomasse, laquelle est responsable de la formation des flocs. Si la charge organique est faible, le développement de certaines bactéries, principalement du type « floculant », est limité. Par contre, si la charge est très forte, la croissance des bactéries est accélérée, surtout celle des bactéries filamenteuses, et des cas de foisonnement peuvent survenir (Sezgin et al., 1978). Comme cette condition joue évidement sur l'équilibre de ces deux types de bactéries, elle a aussi été la cible de plusieurs études qui impliquent la caractérisation morphologique de la boue.

Par exemple, Palm et al. (1980) ont étudié l'impact de l'augmentation de la charge organique lorsque leur système a fonctionné sur deux plages d'oxygène dissous : de 3,0 à 3,5 et de 3,5 à 4,0 mg O_2. L^{-1}. En parallèle, ils ont mesuré l'indice de boue, la vitesse de sédimentation des flocs, et comme descripteur morphologique, l'extension de filaments. La variation de la charge et l'évolution de ces grandeurs mesurées sont rapportées de haut en bas sur la **Figure I-9**.

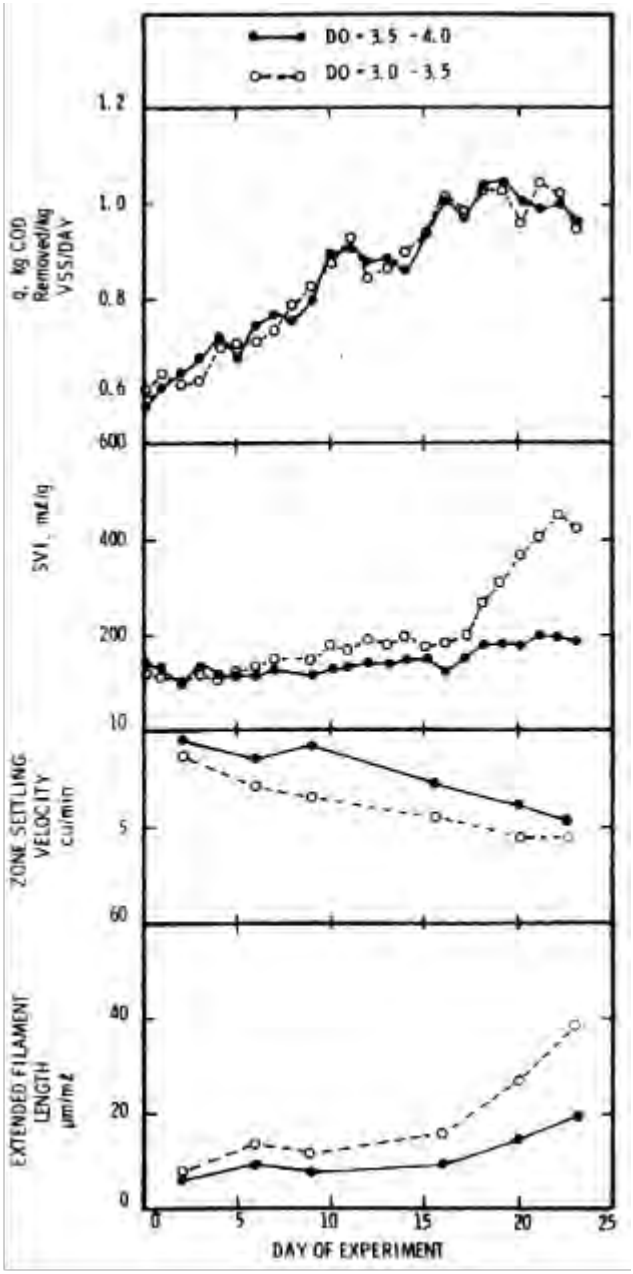

Figure I-9. Variation de la charge organique (*q*), IB (*SVI*), vitesse de sédimentation (*ZSV*) et extension des filaments pour deux plages d'OD (*DO*) (Palm et al., 1980).

Comme il est clairement exposé sur la **Figure I-9**, une augmentation de la charge organique a été accompagnée d'une diminution de la capacité de décantation des flocs, comme indiqué par une élévation de l'IB et une réduction de la vitesse de sédimentation. De l'augmentation de l'extension de filaments, il est possible de déduire qu'un foisonnement filamenteux a eu lieu dans le système, et que celui-ci est encore aggravé lorsque les concentrations d'OD sont plus faibles.

D'autre part, Barbusiński et Kościelniak (1995) ont regardé l'influence de la charge organique sur la taille moyenne des flocs de boues activées. A cette fin, ils ont imposé un cycle de variation dans leur système : ils ont augmenté la charge massique de 0,18 à 0,81 $Kg_{COD}.Kg_{MES}^{-1}.j^{-1}$ puis

baissé la charge brusquement à 0,58 $Kg_{COD}.Kg_{MES}^{-1}.j^{-1}$ et diminué encore la charge jusqu'à 0,22 $Kg_{COD}.Kg_{MES}^{-1}.j^{-1}$. Comme il est possible de le vérifier sur la **Figure I-10**, la taille moyenne de flocs de boues activées a augmenté avec l'augmentation de la charge organique et a diminué avec la diminution lente, sans que le chemin soit le même.

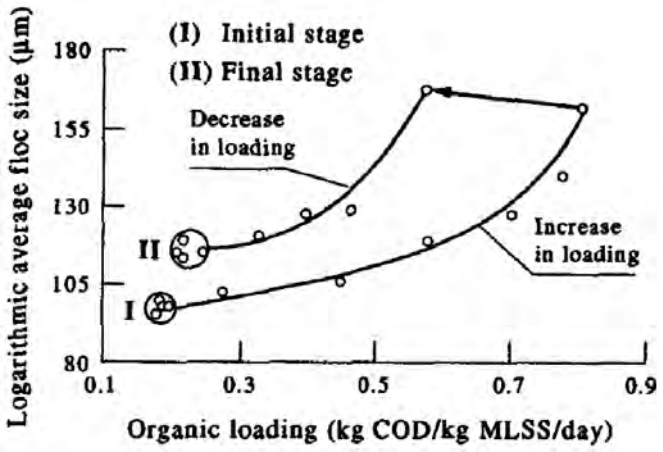

Figure I-10. Effet d'un changement cyclique de charge organique sur la taille moyenne des flocs (Barbusiński and Kościelniak, 1995).

Par rapport à leurs observations microscopiques, ils ont pu confirmer des perturbations sur la taille des flocs, comme la croissance dispersée et même la rupture des flocs lors des changements de charges organiques à long terme.

Wilén et al. (2008) ont mentionné qu'ils ont obtenu un résultat similaire à celui de Barbusiński et Kościelniak (1995) : lorsqu'ils ont augmenté la charge organique, des flocs considérablement plus grands et aussi plus instables ont été observés. Comme ils ont également étudié l'effet de la composition de la boue parallèlement à l'effet de la charge organique, le résultat observé a été attribué à une augmentation de carbohydrates dans le milieu, lesquels facilitent la cohésion des flocs mais sont aussi facilement hydrolysés.

L'effet de la variation de la charge organique a été aussi exploré lors des travaux avec des BàMs qui utilisent la micro et l'ultrafiltration. Domínguez et al. (2012) ont soumis deux BàM à l'échelle du laboratoire, l'un avec une microfiltration (MF) et l'autre avec une ultrafiltration (UF), à une même variation de charge organique : de 0,4 à 1,2 $Kg_{COD}.m^{-3}.j^{-1}$. L'augmentation de la charge a provoqué une élévation de concentrations en MES suivie par une perte de perméabilité des membranes dans les deux réacteurs. La perte étant encore plus importante pour le bioréacteur utilisant l'ultrafiltration. Au moyen de l'analyse des distributions de tailles de flocs dans les deux cas, ils ont pu identifier que les tailles moyennes ont évolué de 31,5 µm à 42 et 66 µm respectivement pour les bioréacteurs MF et UF (**Figure I-11**).

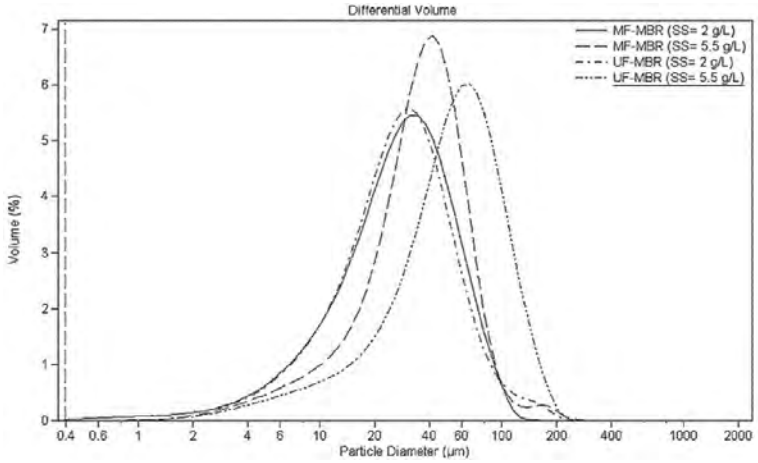

Figure I-11. Distribution de particules dans le BàM – MF et UF à une concentration de MES de 2 et 5.5 g.L^{-1} (Domínguez et al., 2012).

Plus récemment, Amanatidou et al. (2016) ont appliqué l'analyse d'images pour étudier la croissance de microorganismes et leurs caractéristiques sous des charges organiques très fortes issues d'effluents d'abattoirs. Dans ce cas, ils ont montré que la croissance de bactéries filamenteuses n'était pas uniquement limitée aux charges organiques fortes, mais qu'elle pouvait aussi se produire avec des charges moyennes.

I.2.2.4 Influence du taux de recirculation et du rapport DCO:N

Bien que l'aptitude de ces deux conditions opératoires à modifier la morphologie des flocs de boues soit une réalité, l'étude de l'impact de ces deux paramètres reste encore limitée pour établir une relation directe avec la performance des PBAs.

Tout d'abord, le taux de recirculation est considérablement plus étudié avec les BàMs en prenant en compte la quantité d'énergie qui est dépensée pour réaliser la filtration dans le module membranaire. Kim et al. (2001), par exemple, ont vérifié l'effet du type de pompe utilisé pour réaliser la recirculation sur la taille moyenne des flocs en fonction du temps d'opération du BàM. Comme le montre la **Figure I-12**, la comparaison a été effectuée entre une pompe rotative et une pompe centrifuge.

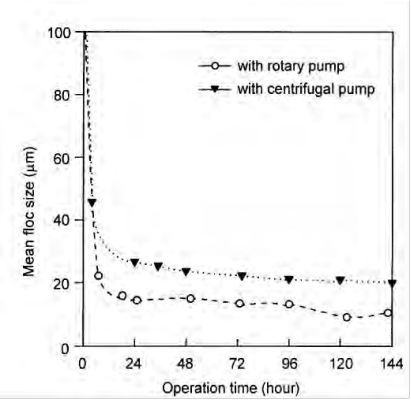

Figure I-12. Variation de la taille moyenne des flocs selon le type de pompe utilisé pour la recirculation dans les BàMs (Kim et al., 2001).

Comment on peut le voir, dans les premières 24h d'opération, pour les deux pompes, il y a une chute de la taille moyenne de flocs ; avec un effet plus prononcé pour la pompe rotative. Ce résultat indique que le cisaillement imposé aux flocs par la pompe rotative est plus grand que celui qui est imposé par la pompe centrifuge. Après 24h, la taille moyenne semble se stabiliser pour les deux pompes.

Stricot et al. (2010), de leur côté, ont évalué la taille de flocs et la concentration de matière soluble (SPE) selon la contrainte hydrodynamique imposée par la recirculation dans les BàMs : soit une recirculation à basse vitesse, soit une recirculation à haute vitesse. Pour le BàM qui a fonctionné avec une recirculation à basse vitesse, aucun changement significatif n'a été identifié au niveau des caractéristiques des flocs ou de la concentration de substances polymériques. En revanche, pour le BàM qui a fonctionné avec une recirculation à plus grande vitesse, une rupture des flocs ainsi qu'une augmentation de la concentration de SPE dans le milieu ont été observées.

L'effet du rapport DCO:N sur les propriétés de taille est souvent relié aussi aux concentrations de SPE. Ye et al. (2011) ont étudié l'effet du rapport DCO:N en passant de 20 à 100 et de 20 à 4, respectivement, dans un procédé à l'échelle du laboratoire. Comme le montre la **Figure I-13**, quand leur système a été alimenté avec un rapport DCO:N de 20, les tailles de flocs ont oscillé entre 180 et 210 µm. Par ailleurs, la taille a diminué jusqu'à 60 et 85 µm lorsque les rapports ont été passés à 4 et 100, chacun. Aux alentours du jour 40, les rapports ont été rétablis à 20 dans les deux cas. Une récupération complète de la taille pour le réacteur qui avait un rapport de 100 est observée, tandis que celui pour lequel le rapport avait diminué jusqu'à 4 présente, à la fin, une taille inférieure à la valeur initiale.

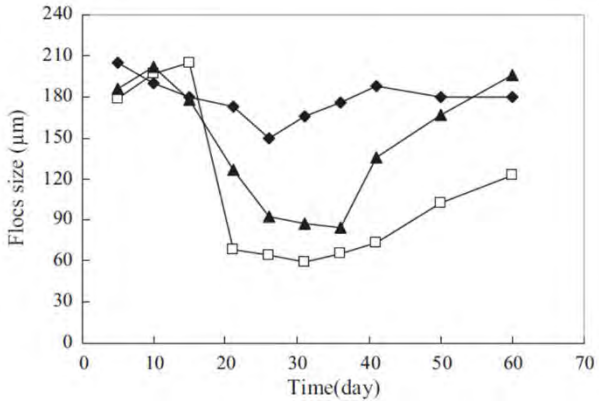

Figure I-13. Effet du rapport DCO:N sur la taille des flocs.
Rapport DCO:N : (♦) 20; (▲) 100 ; (□) 4 (Ye et al., 2011).

L'étude explique que pour le rapport DCO:N de 4, la taille des flocs n'a pas pu revenir à son niveau précédent en raison d'une importante baisse de la production de SPE, du type carbohydrate.

Enfin, Amanatidou et al. (2015) ont rapporté qu'avec un rapport COD:N faible, les bactéries qui constituent le milieu se trouvent dans une situation où la quantité de carbone est limitée. Ainsi elles vont prioritairement utiliser le carbone pour la production d'énergie et limiter la consommation de carbone destiné à la production de SPE. Puisque les SPE contribuent favorablement à la formation de flocs, une carence de ces substances peut induire une prédominance de flocs plus fragiles et donc plus petits. Une tendence similaire a été également

remarquée plus tard par Nguyen et al. (2017) qui ont observé des flocs avec des petites dimensions (35 – 40 µm) lors de faibles ratios (2,5) entre la matière carbonée et la matèire azotée.

I.2.2.5 Influence de l'oxygène dissous (OD)

Dans les PBAs, l'aptitude à la sédimentation des agrégats biologiques dépend principalement de leurs caractéristiques morphologiques. Parmi les différents paramètres opératoires, la concentration d'oxygène dissous (OD) est connue pour influencer la structure et la taille des flocs de boues activées non-filamenteux (Wilén et Balmér, 1999).

Jusqu'à la fin du XX^{e} siècle, il y a eu peu d'études concernant l'effet de la concentration d'OD sur les propriétés de sédimentation des boues activées. Knudson et al. (1982) ont remarqué que les flocs ont de grandes dimensions lors d'une augmentation des niveaux de la concentration d'OD. Starkey et Karr (1984), quant à eux, ont montré que de faibles concentrations d'OD sont défavorables à une floculation efficace des agrégats biologiques. Li and Ganczarczyk (1993), enfin, ont constaté que la charge massique et la disponibilité d'oxygène dissous sont des facteurs qui peuvent avoir une influence sur les distributions de tailles des flocs de boues activées.

Suite à ces résultats, Wilén et Balmér (1999) ont étudié l'effet de la concentration d'oxygène dissous, pour une gamme de 0,5 à 5 mgO_2/L, sur la structure, la taille et la distribution de taille des flocs de boues activées, et pour ce faire un granulomètre laser a été utilisé. Dans une première étape de leurs travaux, les concentrations d'OD, pour deux réacteurs chargés avec des boues activées, ont été de 0,5 et 2 mgO_2/L. Le système qui avait la concentration autour de 2 mgO_2/L a présenté des flocs de dimension supérieure et une forme légèrement plus régulière. Pour le système où la concentration d'OD a varié entre 0,5 et 1 mgO_2/L, les flocs ont eu approximativement la même taille que ceux produits à 2 mgO_2/L, par contre, leur structure est devenue très irrégulière et poreuse. De plus, les microorganismes *Zoogloeal* et filamenteux ont commencé à se développer dans le milieu. Par analyse microscopique, les genres fréquents identifiés ont été *Sphaerotilus natans*, suivi par *Thiotrix I* et *II*. Lors d'une autre étape de ces travaux, le réacteur réglé à 2 mgO_2/L a été comparé avec un autre à 5 mgO_2/L. Dans les deux cas, les tailles moyennes des flocs de boues activées ont généralement été supérieures à 300 µm. Le système à la concentration de 5 mgO_2/L a présenté des flocs biologiques encore plus grands, avec une prolifération excessive de bactéries filamenteuses, fait qui attribue à l'agrégat une haute porosité et une faible densité ; conduisant ainsi à une diminution de la capacité de sédimentation. Selon Wilén and Balmér (1999), aucune relation n'a été établie entre la concentration d'OD et la taille moyenne (diamètre équivalent) des flocs. Ils ont seulement constaté, en effet, qu'il y avait une tendance à la formation de flocs de grandes tailles lorsque la concentration d'OD était élevée.

Dans le même contexte, Faust et al. (2014) ont réalisé une recherche similaire à celle conduite par Wilén et Balmér (1999). Ils ont évalué la capacité de floculation des boues activées pour deux concentrations différentes d'OD : 1 et 4 mgO_2/L. D'abord, ils ont remarqué la même tendance : des flocs de grandes tailles ont été observés pour la plus importante concentration d'OD. En outre, Faust et al. (2014), se sont intéressés à l'efficacité de floculation des boues activées définie par le rapport entre les valeurs de DCO soluble à l'entrée et à la sortie du

système pour les différentes concentrations d'OD considérées. Lorsque la DO était de 4 mgO_2/L l'efficacité (91 %) a été considérablement supérieure à celle obtenue pour 1 mgO_2/L (65%).

Oxygène dissous à micro-échelle

Actuellement, avec l'avènement des micros et nanotechnologies, il est possible de progresser sur les analyses au niveau microscopique, notamment en ce qui concerne la relation entre la concentration d'OD et la taille moyenne des flocs biologiques. Par exemple, grâce à une technique à microélectrodes, Han et al. (2012) ont été capables de tracer le profil d'oxygène dissous à l'intérieur d'un floc de boue activée (Figure I-14).

Ces études employant des microélectrodes ont montré que les concentrations d'OD au sein du floc biologique sont généralement inférieures à celles à la surface externe du floc. De plus, des changements sur les profils de concentration d'OD ont été observés suivant la variation de la taille des agrégats. La **Figure I-14** illustre comment la concentration d'OD (*DO concentration*) varie selon la distance à l'intérieur du floc (*profondeur du floc* ou *depth of floc*), pour six flocs de taille différente. L'illustration suggère qu'une chute de la concentration d'OD peut être facilement observée au sein des flocs de grandes dimensions (« C » et « D »).

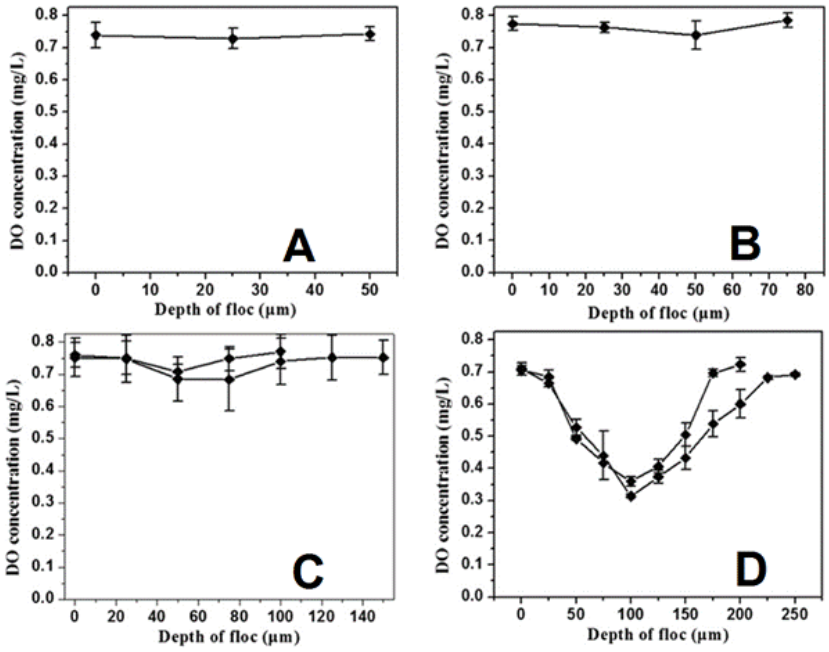

Figure I-14. Profils de concentration d'OD dans les flocs de diamètres A : 50 µm – B : 75 µm – C : 100 et 140 µm – D : 200 et 250 µm (Han et al., 2012).

Certaines hypothèses ont été formulées pour mieux expliquer les chutes d'OD au sein du floc biologique. La première hypothèse porte sur l'efficacité du transport de masse. Les caractéristiques comme la dimension et la forme sont importantes pour la diffusion efficace de substances chimiques. En considérant la diffusion comme le principal mécanisme de transport de soluté, à travers le floc de boue activée, il est possible de dire que la résistance au transport d'oxygène augmente au fur et à mesure que la taille du floc augmente, cette resistance étant presque négligeable pour les flocs d'un diamétre inferieur à 50 µm (Fan et al., 2017). La deuxième hypothèse est basée sur la consommation d'oxygène par les micro-organismes qui

sont présents dans le floc : les agrégats de grande taille contiennent un nombre plus important de microorganismes, et présentent donc, une consommation plus élevée d'oxygène. Une dernière hypothèse pour cela, et la plus probable, est que le résultat obtenu soit le résultat d'une combinaison des deux mécanismes mentionnés précédemment. Il existe donc une compétition entre les phénomènes de diffusion et de consommation de l'OD à l'intérieur des agrégats.

I.2.2.6 Corrélation entre les propriétés morphologiques

A ce jour, peu de relations entre les différentes propriétés morphologiques des agrégats biologiques ont été établies. Une relation entre circularité et convexité a néanmoins été mise en évidence. Les travaux réalisés de Perez et al., 2006 ou Oliveira et al., 2012 montrent qu'il y a une corrélation entre ces deux paramètres de forme. Perez et al. (2006) ont considéré ces deux paramètres, ainsi que la dimension fractale des flocs biologiques. Ils ont pu constater que ces caractéristiques, permettaient de renseigner sur l'irrégularité des agrégats de boue activée. Dans cette étude, la circularité est bien corrélée avec la convexité et à un degré moindre avec la dimension fractale. A partir de ces résultats, il est possible de suggérer que plus les flocs sont circulaires et réguliers, plus ils ont une surface lisse.

Dans le cadre d'une recherche ayant pour objectif de caractériser les boues activées, en fonction des paramètres morphologiques, Oliveira et al. (2012) ont remarqué une dépendance linéaire entre les valeurs moyennes de circularité et convexité (**Figure I-15**), avec un facteur de corrélation de 0,96. C'est-à-dire un résultat similaire à celui trouvé par Perez et al. (2006), qui ont trouvé avec la matrice de Pearson une bonne corrélation entre les valeurs de circularité et de convexité de leurs flocs, indiquée par un coefficient de régression de 0,75.

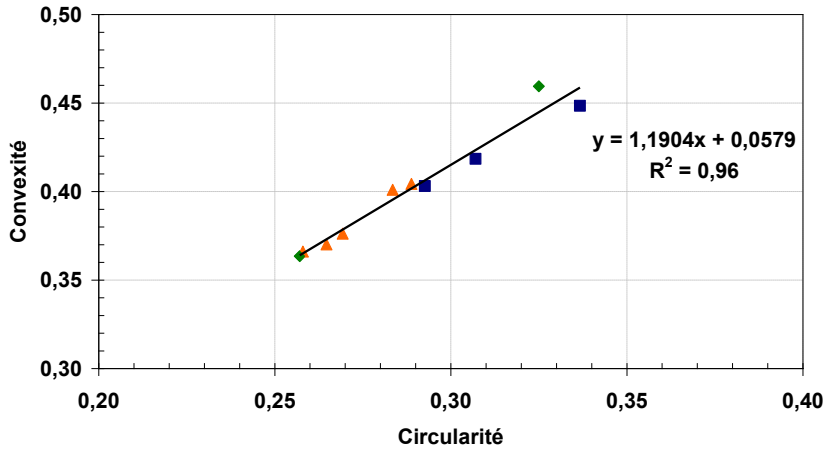

Figure I-15. Convexité moyenne fonction de la circularité moyenne pour toute la durée de l'expérience ayant 3 conditions d'aération différentes (■, ◆, ▲).

I.3 Dimension Fractale par analyse d'images

I.3.1 Le concept de dimension fractale introduit par Mandelbrot

En 1982, Mandelbrot a introduit le concept de 'fractale' pour décrire les objets qui présentent un contour rugueux ou irrégulier, tels que les paysages de montagne ou bien les côtes du littoral. Mandelbrot a observé que souvent, les objets présents dans la nature, ne sont pas composés de formes élémentaires pouvant être ajustées aux standards de la géométrie Euclidienne (**Figure I-16b**).

Afin de décrire les propriétés scalaires de ces objets, il a créé la géométrie fractale. Lorsque les agrégats fractals sont regardés par rapport à leurs surfaces A_a, il est possible de trouver une relation entre A_a et d_a^n, où d_a est le diamètre d'un agrégat et le n un exposant qui peut être, dans ce cas, inférieur à 2 (Meakin, 1988). Similairement, une relation a été trouvée par rapport aux masses des agrégats, $M_a \alpha d_a^n$ et $n < 3$. Ce genre de relations est nécessaire pour mieux comprendre les propriétés et formes des particules, principalement quand ces particules sont des agrégats composés par un arrangement de particules primaires ou d'agrégats déjà existants. (Logan, 2012).

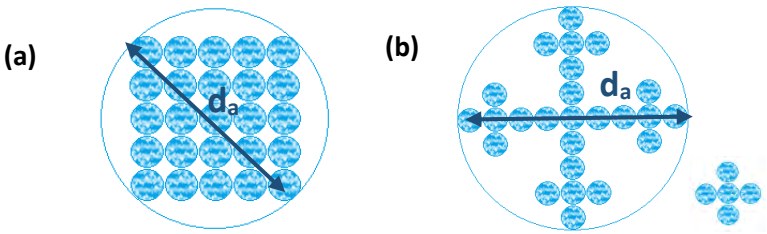

Figure I-16. Deux agrégats composés par 25 particules ; (a) Non fractal (b) Fractal (Logan, 2012).

Sur l'objet **(a)** de la **Figure I-16,** on a premièrement un agrégat bidimensionnel carré, formé par des particules primaires sphériques de diamètre d_p qui obéissent aux relations de la géométrie Euclidienne. Etudiant cet objet sur différentes échelles, il est possible de vérifier qu'à mesure que cet objet grandit, le nombre de particules primaires qu'il inclut, Np, augmente avec sa longueur au carré. Par exemple, l'agrégat **(a)** de diamètre $d_a = 5\ d_p$, contient 25 particules primaires (Np = 25). Si cet agrégat avait eu un diamètre $d_a = 2\ d_p$, il aurait contenu 4 particules primaires (Np = 4). Une relation peut alors être établie entre le diamètre de l'agrégat d_a et le nombre de particules primaires qu'il contient (Np). En effet :

$\ln(N_p)/\ln(d_a) = \ln(4)/\ln(2) = \ln(25)/\ln(5) = 2.$

Il est donc possible de voir que $N\text{p}\ \alpha\ d_a{}^2$.

Pour un objet fractal, le nombre de particules primaires suit une loi de puissance selon (Bushell et al., 2002):

$$N_p = b_f d_a^{D_f} \qquad \textbf{(I-6)}$$

Où D_f est la dimension fractale, qui peut varier entre 1 (celle d'un assemblage linéaire de particules primaires) et 3 (celle d'une sphère), et b_f est un facteur de forme qui dépend du choix de la taille utilisée pour définir la dimension fractale de l'ordre d'unité. Quand D_f est égale à une valeur entière, l'objet suit la géométrie Euclidienne. Par contre, si D_f est une valeur inférieure à la dimension analysée, cet objet sera fractal si l'invariance par changement d'échelle (répétition d'un motif) est maintenue. Par exemple, dans l'agrégat **(b)** de la **Figure I-16** où le motif primaire est en forme de croix, le nombre total de particules suit une même relation sur différentes échelles de longueur : ln(5)/ln(3) = ln(25)/ln(9) = 1,465 ou D_f = 1,465.

La notion d'objet fractal est donc ainsi basée sur une invariance d'échelle c'est-à-dire sur la répétition d'un même motif au sein d'un agrégat.

I.3.2 Mesure de la dimension fractale

Si la définition de la dimension fractale proposée par Mandelbrot (1982) est relativement simple, sa mise en œuvre expérimentale peut revêtir un certain niveau de complexité. De ce fait, différentes méthodes permettent de mesurer une dimension fractale (**Tableau I-6**). Toutefois, il est important de souligner que toutes ces dimensions fractales ne sont pas équivalentes et ne peuvent donc pas être directement comparées.

I.3.2.1 Diffraction de la lumière et Box counting

Dans leur étude sur la stabilité des flocs de boues activées, la corrélation utilisée par Wilén et al. (2003b) détermine la dimension fractale d'une population d'agrégats au moyen d'une analyse par diffusion de la lumière. Cette technique avait déjà été utilisée par Spicer et al. (1998) et Guan et al. (1998) pour caractériser respectivement la morphologie de flocs minéraux et bactériens. Elle consiste à relier l'intensité diffusée et l'angle de diffusion. Ce genre d'analyse est réalisé dans un granulomètre, le Mastersizer/E de Malvern Instruments. Wilén et al. (2003b) ont montré que la dimension fractale, ainsi que la taille des flocs et le nombre de filaments, sont des paramètres qui peuvent bien décrire la stabilité des agrégats soumis à des contraintes de cisaillement dans un PBA.

Dans une autre étude, Perez et al. (2006) ont évalué la dimension fractale de flocs de boue activée à l'aide de la méthode de quantification de carrés (ou Box-counting Method). Cette méthode est connue pour être une technique exhaustive de détermination de la dimension fractale. Selon cette méthode de mesure de la dimension fractale, la gamme de D_f est comprise entre 1 et 2. Quand D_f est équivalente à 1, les objets ont un contour irrégulier, tandis que $D_f = 2$ est la valeur attribuée aux objets assez irréguliers. A partir de l'acquisition de plusieurs données relatives aux descripteurs morphologiques de flocs de boues activées, Perez et al. ont établi une matrice de Pearson qui permet de trouver les corrélations possibles entre les paramètres collectés. Comme résultat, ils ont trouvé un bon degré de corrélation entre dimension fractale et convexité qui peut être expliqué par le fait que la régularité des flocs augmente au fur et à mesure que la convexité se rapproche de 1.

I.3.2.2 Détermination de la dimension fractale par analyse d'image

Les méthodes basées sur l'analyse d'images permettent de mesurer des propriétés d'une population d'agrégats et tout particulièrement la dimension fractale. Dans la littérature, on retrouve différentes méthodes de mesure de la dimension fractale : au sein d'une population d'agrégats, les paramètres : périmètre (P), surface (A), et masse d'agrégat (*M*) sont généralement reliés à une taille caractéristique *l* – rayon de giration (Rg), diamètre équivalent ou longueur maximale – (Logan, 2012).

La dimension fractale basée sur le périmètre D_{pf} est définie par :

$$A \propto P^{2/D_{pf}} \quad \textbf{(I-7)}$$

Elle caractérise la régularité du contour de l'agrégat, c'est-à-dire l'aspect de surface de l'objet. D_{pf} vaut 1 si le contour de l'objet est assez lisse, par exemple le cas d'un cercle ou d'un carré. Une valeur D_{pf} >1 caractérise un contour irrégulier présentant une rugosité de surface.

La dimension fractale bidimensionnelle D_2 est définie par :

$$A \propto l^{D_2} \quad \textbf{(I-8)}$$

D_2 est l'équivalent en deux dimensions de la dimension fractale massique. Elle varie entre 2 (celle d'un disque) et 1 (celle d'un assemblage linéaire). Dans les deux cas, les dimensions fractales morphologiques sont obtenues à partir de régressions linéaires en log-log des **Équations-(**I-7) et **I-8.**

Enfin, la dimension fractale tridimensionnelle D_3 correspond à :

$$M \propto l^{D_3} \quad \textbf{(I-9)}$$

D_3 est l'équivalent de la dimension fractale massique, laquelle peut varier entre 3 (celle d'une sphère) et 1 (celle d'une conformation linéaire). Pour déterminer D_3 il est donc nécessaire de connaître des propriétés tridimensionnelles telles que le volume ou le nombre de particules primaires contenues dans l'agrégat. Cette dimension fractale D_3 ne peut donc pas être déterminée à partir d'analyse d'images car les informations natives dans ce cas sont seulement bidimensionnelles (Lee et Kramer, 2004).

La notion de dimension fractale est couramment mise en œuvre pour analyser la morphologie de flocs minéraux (Nan et al., 2009; Oliveira et al., 2010) ou biologiques (Wilén et al., 2003b; Chu and Lee, 2004; Perez et al., 2006; Zhao et al., 2013). Elle permet ainsi de quantifier les irrégularités de surface ou la forme générale des agrégats. La dimension fractale peut aussi dans

certains cas donner une information concernant la capacité des flocs à sédimenter ou permettre de mieux comprendre certains mécanismes de colmatage en BàMs.

Chu and Lee (2004b) ont choisi une relation de dimension fractale entre surface projetée et périmètre analogue à la relation **(I-7)** pour analyser le comportement des pores de flocs de boues activées : après un processus de floculation en utilisant un floculant commercial, puis suite à des étapes de congélation et décongélation. L'analyse de la dimension fractale a révélé que les agrégats ayant floculé en employant uniquement le floculant ont présenté une surface plus rugueuse que ceux qui ont été congelés et décongelés ensuite.

D'autre part, Meng et al. (2006) ont aussi utilisé une relation basée sur le périmètre, $P \propto A^{Dpf/2}$ permettant d'après eux de mieux évaluer les irrégularités de contour des flocs, afin de différencier les flocs de boues activées normaux de flocs filamenteux. Meng et al. ont montré que la dimension fractale est plus élevée pour les flocs de boues filamenteuses et relient ce résultat à la très grande irrégularité de surface des agrégats filamenteux.

Pour évaluer la dimension fractale et mieux comprendre la structure des flocs, Aouabed et al. (2008) et Oliveira et al. (2010) ont appliqué une relation entre les surfaces projetées de flocs et leurs tailles caractéristiques (diamètre équivalent et rayon de giration, respectivement) $A \propto d_p^{Df}$. D'après l'analyse de la dimension fractale faite par Aouabed et al., qui ont comparé les flocs des acides fluviques sous deux conditions de pH : 5 et 7, une structure plus fragile pour les flocs exposés à un pH proche de la neutralité a été observée. Similairement, Oliveira et al. ont observé une structure plus « ouverte » pour les flocs de kaolin et charbon actif, laquelle est tout à fait en accord avec les faibles valeurs de dimension fractale obtenues.

L'analyse de la dimension fractale dans les travaux de Nan et al. (2009) a eu pour objectif de mieux comprendre le processus de floculation de particules minérales de kaolin. Pour ce faire, ils ont choisi une corrélation entre surface et périmètre. Pour le calcul de la dimension fractale, les valeurs moyennes de surface et périmètre à chaque minute du temps expérimental (20 min, au total) ont été prises en compte. Ils ont ainsi pu confirmer que la conformation des flocs de kaolin est de type fractal et évolue au cours du temps.

Suivant le même ordre d'idées, Zhao et al. (2013) ont utilisé deux dimensions fractales pour évaluer la capacité de déshydratation de flocs de boues : une première (variant entre 1 et 2) reliant la surface projetée et la longueur maximale du floc, et une seconde (qui peut être égale ou supérieure à 1) reliant le périmètre et la longueur maximale du floc. Sur la base de leurs résultats, coupler les deux dimensions fractales a permis d'identifier l'augmentation de la porosité des flocs de boues activées au cours du temps, cela a aussi pu expliquer la plus grande difficulté à déshydrater des agrégats qui avaient probablement gardé plus d'eau dans leurs interstices.

Tableau I-6. Données bibliographiques sur l'utilisation de la dimension fractale comme indicateur de la régularité morphologique des flocs. (M : masse du floc, A : Surface projetée, P : Périmètre, D_f : Dimension fractale 2-3D et D_{pf} : Dimension fractale basée sur le périmètre).

Référence	Type de floc	Rapport de Dim. Fractale	Plage (cercle ou sphère)	Résultats
Wilén *et al*. (2003b)	flocs de boues activées	$M(R) \propto R^{Df}$	1 – 3 (3)	gros flocs plus irréguliers (D_f= 1,96) que petits (D_f = 2,48)
Chu et Lee (2004b)	flocs de boues activées	$A \propto P^{2/Dpf}$	> 1 (1)	pores de flocs ont été plus irréguliers (D_{pf} = 1,31) que ceux qui ont passés par les étapes de congélation et décongélation (D_{pf}= 1,25)
Meng *et al.* (2006)	flocs de boues activées normales et filamenteuses	$P \propto A^{Dpf/2}$	> 1 (1)	flocs de boues normales sont plus réguliers (D_{pf} = 1,12) que ceux provenant de boues filamenteuses (D_{pf} = 1,53)
Perez *et al.* (2006)	flocs de boues activées	*Box-Couting Method*	1 – 2 (1)	une corrélation raisonnable entre la dimension fractale et convexité a été observée.
Aouabed *et al*. (2008)	flocs de matière organique (acide fulvique commercial)	$A \propto d_p^{Df}$	1 – 2 (2)	flocs d'acide fulvique à un pH = 5 plus réguliers (D_f = 1,48) que à un pH= 7 (D_f = 1,33)
Nan *et al*. (2009)	flocs minéraux (kaolin)	$A \propto P^{Dpf}$	> 1 (1)	les flocs ont maintenu leur similarité au cours du temps (D_{pf} = 1,92)
Oliveira *et al*. (2010)	flocs minéraux (carbone activé et kaolin)	$A \propto r^{Df}$	1 – 2 (2)	flocs de carbone activé et kaolin ont présenté une structure ouverte et de moyenne compaction (D_f = 1,2 et 1,0, respectivement)
Zhao *et al*. (2013)	flocs de boues activées (purge)	$A \propto L_{max}^{Df}$ $P \propto L_{max}^{Dpf}$	1 – 2 (2) > 1 (1)	au cours de temps : l'augmentation de la porosité de flocs a induit une difficulté accrue de déshydratation (D_f = 1,95 à 1,86 et D_{pf}= 1,18 à 1,19)

I.4 Bilan de la littérature

Parmi les différentes technologies pour produire un effluent conforme aux normes de rejet en vigueur, les Procédés par Boues Activées sont largement utilisés en tant que traitement biologique du fait de leur faible coût et de leur facilité d'implémentation. Ces procédés réalisent l'abattement des polluants en deux étapes : (1) la biodégradation par des microorganismes dans un bassin d'aération et (2) la séparation de la biomasse par décantation.

La biomasse est formée par des agrégats couramment appelées flocs biologiques qui contiennent principalement des bactéries (filamenteuses ou floculantes), des particules colloïdales et des SPE. Au vue de la variété des espèces, les agrégats peuvent ainsi être structurés de différentes manières et présenter des propriétés morphologiques très variées selon les conditions opératoires (pH, Température, Oxygène dissous….). De plus, la littérature montre que les propriétés morphologiques jouent aussi un rôle majeur sur l'efficacité du procédé.

Dans le contexte d'une relation triangulaire impliquant, (1) les conditions opératoires, (2) les propriétés de taille et de forme des flocs de boues et (3) les performances du procédé de traitement (**Figure I-17**), plusieurs équipes ont choisi d'étudier l'évolution de la morphologie des boues lors de perturbations classiques qui peuvent survenir dans les stations d'épuration mettant en œuvre les PBAs comme traitement secondaire. Pour évaluer la morphologie des agrégats, des techniques reposant sur l'analyse d'images ou la granulométrie laser sont généralement mises en œuvre.

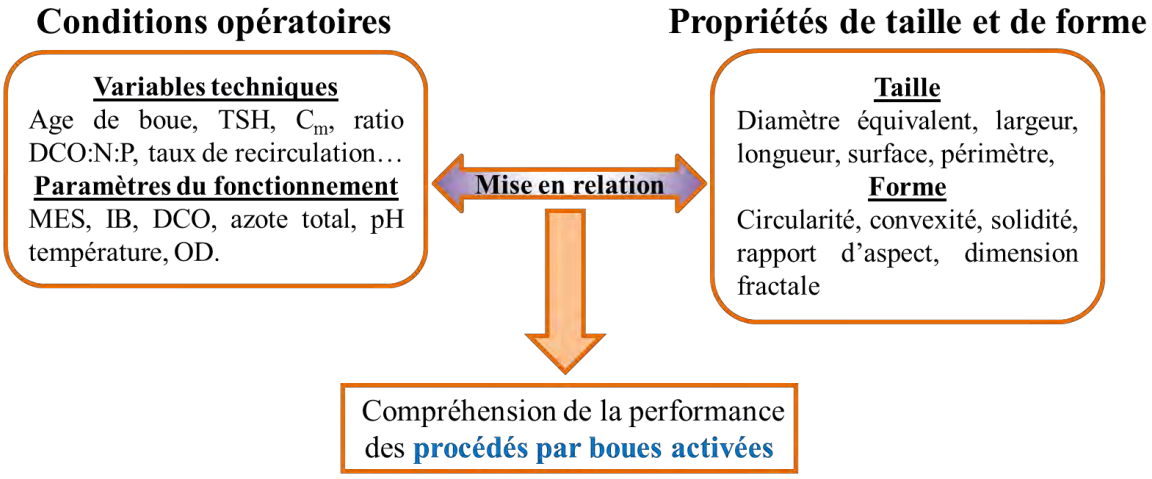

Figure I-17. Schéma de la relation triangulaire impliquant les conditions opératoires, les propriétés de taille et de forme des flocs de boues et les performances du procédé de traitement.

L'étape préalable à toute analyse d'image (AI) consiste à développer une méthodologie pour acquérir les images des flocs. Pour cela, différentes méthodologies existent : *en ligne (Online)* (Koivuranta et al., 2013) ou *hors ligne (Offline)* à l'aide d'outils tels que des microscopes. Le travail d'analyse est ensuite généralement effectué sur des images qui ont été binarisées. Des

descripteurs morphologiques, issus de la géométrie euclidienne, tels que le diamètre équivalent, surface, périmètre, longueur, largeur, circularité, convexité, solidité ou rapport d'aspect sont mesurés ou calculés (Amaral, 2003). Parfois, d'autres paramètres, comme la dimension fractale, sont aussi pris en compte lorsque les objets analysés présentent des formes géométriques très irrégulières (Snidaro et al., 1997; Jenné et al., 2002). Ces paramètres-ci reflètent la complexité d'une structure, telle que celle des flocs biologiques qui sont présents dans les boues activées. Bien que la nature de ces paramètres puisse varier considérablement d'une application à l'autre, ils fournissent des informations globales concernant la structure et la morphologie des flocs biologiques.

I.5 Références

Ahmed, Z., Cho, J., Lim, B.-R., Song, K.-G., and Ahn, K.-H. (2007). Effects of sludge retention time on membrane fouling and microbial community structure in a membrane bioreactor. J. Membr. Sci. *287*, 211–218.

Amanatidou, E., Samiotis, G., Trikoilidou, E., Pekridis, G., and Taousanidis, N. (2015). Evaluating sedimentation problems in activated sludge treatment plants operating at complete sludge retention time. Water Res. *69*, 20–29.

Amanatidou, E., Samiotis, G., Trikoilidou, E., Tzelios, D., and Michailidis, A. (2016). Influence of wastewater treatment plants' operational conditions on activated sludge microbiological and morphological characteristics. Environ. Technol. *37*, 265–278.

Amaral, A.L. (2003). Image analysis in biotechnological processes : applications to wastewater treatment. PhD thesis, University of Minho.

Amaral, A.L., and Ferreira, E.C. (2005). Activated sludge monitoring of a wastewater treatment plant using image analysis and partial least squares regression. Anal. Chim. Acta *544*, 246–253.

Amaral, A.L., Mesquita, D.P., and Ferreira, E.C. (2013). Automatic identification of activated sludge disturbances and assessment of operational parameters. Chemosphere *91*, 705–710.

Aouabed, A., Hadj Boussaad, D.E., and Ben Aim, R. (2008). Morphological characteristics and fractal approach of the flocs obtained from the natural organic matter extracts of water of the Keddara dam (Algeria). Desalination *231*, 314–322.

Araya-Kroff, P., Amaral, A. l., Neves, L., Ferreira, E. c., Pons, M.-N., Mota, M., and Alves, M. m. (2004). Development of image analysis techniques as a tool to detect and quantify morphological changes in anaerobic sludge: I. Application to a granulation process. Biotechnol. Bioeng. *87*, 184–193.

Barbusiński, K., and Kościelniak, H. (1995). Influence of substrate loading intensity on floc size in activated sludge process. Water Res. *29*, 1703–1710.

Bisogni, J., and Lawrence, A.W. (1971). Relationships between biological solids retention time and settling characteristics of activated sludge. Water Res. *5*, 753–763.

Bushell, G.C., Yan, Y.D., Woodfield, D., Raper, J., and Amal, R. (2002). On techniques for the measurement of the mass fractal dimension of aggregates. Adv. Colloid Interface Sci. *95*, 1–50.

Burger, W., Krysiak-Baltyn, K., Scales, P.J., Martin, G.J.O., Stickland, A.D., and Gras, S.L. (2017). The influence of protruding filamentous bacteria on floc stability and solid-liquid separation in the activated sludge process. Water Res. *123*, 578–585.

Canler, J.-P., Perret, J.-M., Duchène, P., and Cotteux, E. (2011). Aide au diagnostic des stations d'épuration par l'observation microscopique des boues activées (Editions Quae).

Casellas, M., Dagot, C., Pons, M.-N., Guibaud, G., Tixier, N., and Baudu, M. (2004). Characterisation of the structural state of flocculent microorganisms in relation to the purificatory performances of sequencing batch reactors. Biochem. Eng. J. *21*, 171–181.

Chu, C.P., and Lee, D.J. (2004). Multiscale structures of biological flocs. Chem. Eng. Sci. *59*, 1875–1883.

Çiçek, N., Franco, J.P., Suidan, M.T., Urbain, V., and Manem, J. (1999). Characterization and Comparison of a Membrane Bioreactor and a Conventional Activated-Sludge System in the Treatment of Wastewater Containing High-Molecular-Weight Compounds. Water Environ. Res. *71*, 64–70.

Costa J.C., Abreu A.A., Ferreira E.C., and Alves M.M. (2007). Quantitative image analysis as a diagnostic tool for monitoring structural changes of anaerobic granular sludge during detergent shock loads. Biotechnol. Bioeng. *98*, 60–68.

Costa, J.C., Mesquita, D.P., Amaral, A.L., Alves, M.M., and Ferreira, E.C. (2013). Quantitative image analysis for the characterization of microbial aggregates in biological wastewater treatment: a review. Environ. Sci. Pollut. Res. *20*, 5887–5912.

Dai, Q., Ma, L., Ren, N., Ning, P., Guo, Z., Xie, L., and Gao, H. (2018). Investigation on extracellular polymeric substances, sludge flocs morphology, bound water release and dewatering performance of sewage sludge under pretreatment with modified phosphogypsum. Water Research *142*, 337–346.

Domínguez, L., Cases, V., Birek, C., Rodríguez, M., and Prats, D. (2012). Influence of organic loading rate on the performance of ultrafiltration and microfiltration membrane bioreactors at high sludge retention time. Chem. Eng. J. *181–182*, 132–143.

Eriksson, L., and Alm, B. (1991). Study of Flocculation Mechanisms by Observing Effects of a Complexing Agent on Activated Sludge Properties. Water Sci. Technol. *24*, 21–28.

Fan, H., Liu, X., Wang, H., Han, Y., Qi, L., and Wang, H. (2017). Oxygen transfer dynamics and activated sludge floc structure under different sludge retention times at low dissolved oxygen concentrations. Chemosphere *169*, 586–595.

Faust, L., Temmink, H., Zwijnenburg, A., Kemperman, A.J.B., and Rijnaarts, H.H.M. (2014). Effect of dissolved oxygen concentration on the bioflocculation process in high loaded MBRs. Water Res. *66*, 199–207.

Fulazzaky, M.A., Abdullah, N.H., Mohd Yusoff, A.R., and Paul, E. (2015). Conditioning the alternating aerobic–anoxic process to enhance the removal of inorganic nitrogen pollution from a municipal wastewater in France. J. Clean. Prod. *100*, 195–201.

Ginoris, Y.P., Amaral, A.L., Nicolau, A., Coelho, M.A.Z., and Ferreira, E.C. (2007). Development of an image analysis procedure for identifying protozoa and metazoa typical of activated sludge system. Water Res. *41*, 2581–2589.

Grady, C.P.L., Daigger, G.T., Love, N.G., and Filipe, C.D.M. (2011). Biological Wastewater Treatment (IWA Publishing - Co-Publication).

Grijspeerdt, K., and Verstraete, W. (1997). Image analysis to estimate the settleability and concentration of activated sludge. Water Res. *31*, 1126–1134.

Guan, J., Waite, T.D., and Amal, R. (1998). Rapid Structure Characterization of Bacterial Aggregates. Environ. Sci. Technol. *32*, 3735–3742.

Guo, J., Wang, S., Wang, Z., and Peng, Y. (2014). Effects of feeding pattern and dissolved oxygen concentration on microbial morphology and community structure: The competition between floc-forming bacteria and filamentous bacteria. J. Water Process Eng. *1*, 108–114.

Han, Y., Liu, J., Guo, X., and Li, L. (2012). Micro-environment characteristics and microbial communities in activated sludge flocs of different particle size. Bioresour. Technol. *124*, 252–258.

Henze, M. (2008). Biological wastewater treatment : principles, modelling and design (London: IWA Pub).

Hong, S.P., Bae, T.H., Tak, T.M., Hong, S., and Randall, A. (2002). Fouling control in activated sludge submerged hollow fiber membrane bioreactors. Desalination *143*, 219–228.

Jamal Khan, S., Ilyas, S., Javid, S., Visvanathan, C., and Jegatheesan, V. (2011). Performance of suspended and attached growth MBR systems in treating high strength synthetic wastewater. Bioresour. Technol. *102*, 5331–5336.

Jenné, R., Cenens, C., Geeraerd, A.H., and Impe, J.F.V. (2002). Towards on-line quantification of flocs and filaments by image analysis. Biotechnol. Lett. *24*, 931–935.

Jenné, R., Banadda, E.N., Philips, N., and Impe, J.F.V. (2003). Image Analysis as a Monitoring Tool for Activated Sludge Properties in Lab-Scale Installations. J. Environ. Sci. Health Part A *38*, 2009–2018.

Jenné, R., Banadda, E.N., Smets, I.Y., Bamelis, A., Verdickt, L., and Impe, J.F.V. (2005). Activated sludge image analysis system: monitoring settleability and effluent clarity. Water Sci. Technol. *52*, 193–199.

Jenné, R., Banadda, E.N., Gins, G., Deurinck, J., Smets, I.Y., Geeraerd, A.H., and Impe, J.F.V. (2006). Use of image analysis for sludge characterisation: studying the relation between floc shape and sludge settleability. Water Sci. Technol. *54*, 167–174.

Jenné, R., Banadda, E.N., Smets, I., Deurinck, J., and Van Impe, J. (2007). Detection of Filamentous Bulking Problems: Developing an Image Analysis System for Sludge Composition Monitoring. Microsc. Microanal. *13*, 36–41.

Ji, L., and Zhou, J. (2006). Influence of aeration on microbial polymers and membrane fouling in submerged membrane bioreactors. J. Membr. Sci. *276*, 168–177.

Keiding, K., and Nielsen, P.H. (1997). Desorption of organic macromolecules from activated sludge: Effect of ionic composition. Water Res. *31*, 1665–1672.

Khan, M.B., Nisar, H., and Ng, C.A. (2018). Image Processing and Analysis of Phase-Contrast Microscopic Images of Activated Sludge to Monitor the Wastewater Treatment Plants. IEEE Access 6, 1778–1791.

Kim, J.-S., Lee, C.-H., and Chang, I.-S. (2001). Effect of pump shear on the performance of a crossflow membrane bioreactor. Water Res. *35*, 2137–2144.

Knudson, M.K., Williamson, K.J., and Nelson, P.O. (1982). Influence of Dissolved Oxygen on Substrate Utilization Kinetics of Activated Sludge. J. Water Pollut. Control Fed. *54*, 52–60.

Koivuranta, E., Suopajärvi, T., Hattuniemi, J., Stoor, T., and Illikainen, M. (2017). The effect of seasonal variations on floc morphology in the activated sludge process. Environ.Technol. *38*, 3209–3215.

Koivuranta, E., Keskitalo, J., Haapala, A., Stoor, T., Sarén, M., and Niinimäki, J. (2013). Optical monitoring of activated sludge flocs in bulking and non-bulking conditions. Environ. Technol. *34*, 679–686.

Lee, C., and Kramer, T.A. (2004). Prediction of three-dimensional fractal dimensions using the two-dimensional properties of fractal aggregates. Adv. Colloid Interface Sci. *112*, 49–57.

Li, D., and Ganczarczyk, J.J. (1993). Factors affecting dispersion of activated sludge flocs. Water Environ. Res. *65*, 258–263.

Li, Z. and Stenstrom M. K. (2018). Impacts of SRT on Particle Size Distribution and Reactor Performance in Activated Sludge Processes. Water Environ. Res. *90(1)*, 48-56.

Liao, B.Q., Allen, D.G., Droppo, I.G., Leppard, G.G., and Liss, S.N. (2000). Bound Water Content of Activated Sludge and Its Relationship to Solids Retention Time, Floc Structure, and Surface Properties. Water Environ. Res. *72*, 722–730.

Liao, B.Q., Droppo, I.G., Leppard, G.G., and Liss, S.N. (2006). Effect of solids retention time on structure and characteristics of sludge flocs in sequencing batch reactors. Water Res. *40*, 2583–2591.

Liao, B.Q., Lin, H.J., Langevin, S.P., Gao, W.J., and Leppard, G.G. (2011). Effects of temperature and dissolved oxygen on sludge properties and their role in bioflocculation and settling. Water Res. *45*, 509–520.

Liss, S.N., Liao, B.Q., Droppo, I.G., Allen, D.G., and Leppard, G.G. (2002). Effect of solids retention time on floc structure. Water Sci. Technol. *46*, 431–438.

Liwarska-Bizukojc, E., and Bizukojc, M. (2005). Digital image analysis to estimate the influence of sodium dodecyl sulphate on activated sludge flocs. Process Biochem. *40*, 2067–2072.

Liwarska-Bizukojc, E., Klepacz-Smółka, A., and Andrzejczak, O. (2015). Variations of morphology of activated sludge flocs studied at full-scale wastewater treatment plants. Environ. Technol. *36*, 1123–1131.

Logan, B.E. (2012). Environmental Transport Processes (John Wiley & Sons).

Lovett, D.A., Kavanagh, B.V., and Herbert, L.S. (1983). Effect of sludge age and substrate composition on the settling and dewatering characteristics of activated sludge. Water Res. *17*, 1511–1515.

Mandelbrot, B.B. (1982). The Fractal Geometry of Nature.San Francisco

Massé, A., Spérandio, M., and Cabassud, C. (2006). Comparison of sludge characteristics and performance of a submerged membrane bioreactor and an activated sludge process at high solids retention time. Water Res. *40*, 2405–2415.

Meakin, P. (1988). Fractal aggregates. Adv. Colloid Interface Sci. *28*, 249–331.

Meng, F., Yang, F., Xiao, J., Zhang, H., and Gong, Z. (2006). A new insight into membrane fouling mechanism during membrane filtration of bulking and normal sludge suspension. J. Membr. Sci. *285*, 159–165.

Mesquita, D.P. (2011). Image analysis and chemometric techniques as monitoring tools to characterize aggregated and filamentous organisms in activated sludge processes.

Mesquita, D.P., Dias, O., Dias, A.M.A., Amaral, A.L., and Ferreira, E.C. (2009a). Correlation between sludge settling ability and image analysis information using partial least squares. Anal. Chim. Acta *642*, 94–101.

Mesquita, D.P., Dias, O., Amaral, A.L., and Ferreira, E.C. (2009b). Monitoring of activated sludge settling ability through image analysis: validation on full-scale wastewater treatment plants. Bioprocess Biosyst. Eng. *32*, 361–367.

Mesquita, D.P., Dias, O., Elias, R. a. V., Amaral, A.L., and Ferreira, E.C. (2010a). Dilution and Magnification Effects on Image Analysis Applications in Activated Sludge Characterization. Microsc. Microanal. *16*, 561–568.

Mesquita, D.P., Dias, O., Amaral, A.L., and Ferreira, E.C. (2010b). A Comparison between Bright Field and Phase-Contrast Image Analysis Techniques in Activated Sludge Morphological Characterization. Microsc. Microanal. *16*, 166–174.

Mesquita, D.P., Amaral, A.L., and Ferreira, E.C. (2011). Characterization of activated sludge abnormalities by image analysis and chemometric techniques. Anal. Chim. Acta *705*, 235–242.

Mesquita, D.P., Amaral, A.L., and Ferreira, E.C. (2013). Activated sludge characterization through microscopy: A review on quantitative image analysis and chemometric techniques. Anal. Chim. Acta *802*, 14–28.

Motta, M. da, Amaral, A.L., Neves, L., Araya-Kroff, P., Ferreira, E.C., Alves, M.M., Mota, M., Roche, N., Vivier, H., and Pons, M.N. (2002a). Efeito da diluição na caracterização da biomassa de sistemas de tratamentos de efluentes por análise de imagem. In Proceedings of the 14th Brazilian Congress of Chemical Engineering, Natal, Brazil, p.9, CD-ROM

Motta, M. da, Pons, M.N., and Roche, N. (2002b). Study of filamentous bacteria by image analysis and relation with settleability. Water Sci. Technol. *46*, 363–369.

da Motta, M., Pons, M.-N., Roche, N., and Vivier, H. (2001). Characterisation of activated sludge by automated image analysis. Biochem. Eng. J. *9*, 165–173.

Nan, J., He, W., Song, J., and Song, X. (2009). Fractal Growth Characteristics of Flocs in Flocculation Process in Water Treatment. In International Conference on Energy and Environment Technology, 2009. ICEET '09, pp. 582–588.

Nguyen, T.N.P., Chao, S.-J., Chen, P.-C., and Huang, C. (2017). Effects of C/N ratio on nitrate removal and floc morphology of autohydrogenotrophic bacteria in a nitrate-containing wastewater treatment process. J. Environ. Sci.

Oliveira, C., Rodrigues, R.T., and Rubio, J. (2010). A new technique for characterizing aerated flocs in a flocculation–microbubble flotation system. Int. J. Miner. Process. *96*, 36–44.

Oliveira P. H. S., Schetrite S., Alliet M., Braak E., Coufort-Saudejaud C., Tourbin M., Frances C. (2012). Caractérisation morphologique des flocs issus des boues de bioréacteurs à membranes immergées pour le traitement des eaux usées : influence des contraintes de cisaillement liées aux aérations. In: JOURNEÉS INFORMATION EUAX, 20, Poitiers/France. *Présentation Orale***.** APTEN: Poitiers.

Palm, J.C., Jenkins, D., and Parker, D.S. (1980). Relationship between Organic Loading, Dissolved Oxygen Concentration and Sludge Settleability in the Completely-Mixed Activated Sludge Process. J. Water Pollut. Control Fed. *52*, 2484–2506.

Perez, Y.G., Leite, S.G.F., and Coelho, M. a. Z. (2006). Activated sludge morphology characterization through an image analysis procedure. Braz. J. Chem. Eng. *23*, 319–330.

Pons, M.-N., and Vivier, H. (1999). Biomass Quantification by Image Analysis. In Bioanalysis and Biosensors for Bioprocess Monitoring, (Springer, Berlin, Heidelberg), pp. 133–184.

Rodríguez, D.C., Pino, N., and Peñuela, G. (2011). Monitoring the removal of nitrogen by applying a nitrification–denitrification process in a Sequencing Batch Reactor (SBR). Bioresour. Technol. *102*, 2316–2321.

Roques, H. (1980). Fondements théoriques du traitement biologique des eaux. Volume 2 (Paris, France: Technique et Documentation).

Sant'Anna, G.L. (2010). Tratamento biológico de efluentes: fundamentos e aplicações (Interciência).

Schmidell, W. (2007). Tratamento biológico de águas residuárias (Tribo da Ilha).

Sezgin, M., Jenkins, D., and Parker, D.S. (1978). A Unified Theory of Filamentous Activated Sludge Bulking. J. Water Pollut. Control Fed. *50*, 362–381.

Snidaro, D., Zartarian, F., Jorand, F., Bottero, J.-Y., Block, J.-C., and Manem, J. (1997). Characterization of activated sludge flocs structure. Water Sci. Technol. *36*, 313–320.

Sobeck, D.C., and Higgins, M.J. (2002). Examination of three theories for mechanisms of cation-induced bioflocculation. Water Res. *36*, 527–538.

Spicer, P.T., Pratsinis, S.E., Raper, J., Amal, R., Bushell, G., and Meesters, G. (1998). Effect of shear schedule on particle size, density, and structure during flocculation in stirred tanks. Powder Technol. *97*, 26–34.

Starkey, J.E., and Karr, P.R. (1984). Effect of Low Dissolved Oxygen Concentration on Effluent Turbidity. J. Water Pollut. Control Fed. *56*, 837–843.

Stricot, M., Filali, A., Lesage, N., Spérandio, M., and Cabassud, C. (2010). Side-stream membrane bioreactors: Influence of stress generated by hydrodynamics on floc structure, supernatant quality and fouling propensity. Water Res. *44*, 2113–2124.

Tandoi, V., Rossetti, S., and Wanner, J. (2017). Activated Sludge Separation Problems: Theory, Control Measures, Practical Experiences (IWA Publishing), London UK, 320 p.

Tomperi, J., Koivuranta, E., Kuokkanen, A., Juuso, E., and Leiviskä, K. (2016). Real-time optical monitoring of the wastewater treatment process. Environ. Technol. *37*, 344–351.

Van den Broeck, R., Van Dierdonck, J., Nijskens, P., Dotremont, C., Krzeminski, P., van der Graaf, J.H.J.M., van Lier, J.B., Van Impe, J.F.M., and Smets, I.Y. (2012). The influence of solids retention time on activated sludge bioflocculation and membrane fouling in a membrane bioreactor (MBR). J. Membr. Sci. *401–402*, 48–55.

Von Sperling, M. (2017). Activated Sludge and Aerobic Biofilm Reactors (IWA Publishing).

Wagner, M., Amann, R., Lemmer, H., and Schleifer, K.H. (1993). Probing activated sludge with oligonucleotides specific for proteobacteria: inadequacy of culture-dependent methods for describing microbial community structure. Appl. Environ. Microbiol. *59*, 1520–1525.

Wang, B.-B., Chang, Q., Peng, D.-C., Hou, Y.-P., Li, H.-J., and Pei, L.-Y. (2014). A new classification paradigm of extracellular polymeric substances (EPS) in activated sludge: Separation and characterization of exopolymers between floc level and microcolony level. Water Res. *64*, 53–60.

Wells, G.F., Park, H.-D., Yeung, C.-H., Eggleston, B., Francis, C.A., and Criddle, C.S. (2009). Ammonia-oxidizing communities in a highly aerated full-scale activated sludge bioreactor: betaproteobacterial dynamics and low relative abundance of Crenarchaea. Environ. Microbiol. *11*, 2310–2328.

Wiesmann, U., Choi, I.S., and Dombrowski, E.-M. (2007). Fundamentals of biological wastewater treatment (Weinheim: Wiley-VCH Verlag).

Wilén, B.-M., and Balmér, P. (1999). The effect of dissolved oxygen concentration on the structure, size and size distribution of activated sludge flocs. Water Res. *33*, 391–400.

Wilén, B.-M., Jin, B., and Lant, P. (2003a). The influence of key chemical constituents in activated sludge on surface and flocculating properties. Water Res. *37*, 2127–2139.

Wilén, B.-M., Jin, B., and Lant, P. (2003b). Impacts of structural characteristics on activated sludge floc stability. Water Res. *37*, 3632–3645.

Wilén, B.-M., Lumley, D., Mattsson, A., and Mino, T. (2008). Relationship between floc composition and flocculation and settling properties studied at a full scale activated sludge plant. Water Res. *42*, 4404–4418.

Yadav, T.C., Khardenavis, A.A., and Kapley, A. (2014). Shifts in microbial community in response to dissolved oxygen levels in activated sludge. Bioresour. Technol. *165*, 257–264.

Yang, P.Y., Su, R., and Kim, S.J. (2003). EMMC process for combined removal of organics, nitrogen and an odor producing substance. J. Environ. Manage. *69*, 381–389.

Ye, F., Ye, Y., and Li, Y. (2011). Effect of C/N ratio on extracellular polymeric substances (EPS) and physicochemical properties of activated sludge flocs. J. Hazard. Mater. *188*, 37–43.

Yoo, H., Ahn, K.-H., Lee, H.-J., Lee, K.-H., Kwak, Y.-J., and Song, K.-G. (1999). Nitrogen removal from synthetic wastewater by simultaneous nitrification and denitrification (SND) via nitrite in an intermittently-aerated reactor. Water Res. *33*, 145–154.

Zhao, P., Ge, S., Chen, Z., and Li, X. (2013). Study on pore characteristics of flocs and sludge dewaterability based on fractal methods (pore characteristics of flocs and sludge dewatering). Appl. Therm. Eng. *58*, 217–223.

Chapter II. Materials and Methods

This chapter describes the means, the tools and the techniques employed to develop all the experiences as well as the image analysis procedure for characterizing the activated sludge flocs. The fundaments of descriptive statistics for the treatment of the datasets are also reminded in the following paragraphs.

II.1 Experimental setup: description and operation

II.1.1 Pilot set-up

One of the central objectives of this study is to verify how the variations of the operating conditions in activated sludge systems can impact the bioflocs size and shape in relation to the overall process performance. To that end, a pilot system (**Figure II-1**) was designed.

This pilot is based on a typical activated sludge system, it means a cylindrical aerated tank (total and working volume of 0.03 and 0.02 m^3, respectively) connected to a clarifier (with a capacity of 0.006 m^3). The system was continuously fed through two peristaltic pumps (Masterflex®): one for the concentrated synthetic wastewater that comes out from a storage tank (0.005 m^3) and also for the pH buffer solution ($NaHCO_3$); and the other one for tap water addition to dilute the synthetic feed solution. Such dilution was indispensable to reproduce an effluent with the characteristics close to those ones of a secondary wastewater treatment. A third pump (Masterflex®) was placed to perform sludge recirculation from the clarifier to the aerated tank.

II.1.2 Temperature, Dissolved Oxygen (OD) and pH

The characteristics of the liquid phase have been monitored *in situ* by probes, Mettler Toledo. Those probes were properly calibrated before the initiation of any experiment. The values of temperature, dissolved oxygen (DO) and pH, inside the aerated tank, were recorded by a computer using the software DasyLab® at a frequency of 1 Hz. Following these parameters in real time made it possible to quickly interfere in case of an unusual profile, generally, associated with technical failures.

Temperature

Experiments were performed at room temperature as it is done in full-scale units. Anyway, the temperature was recorded in order to detect potential issues.

pH control

Microorganisms are strictly dependent on an optimal pH range to efficiently eliminate pollutants, thereby a buffer solution of sodium bicarbonate ($NaHCO_3$) with a concentration of 35 $g.L^{-1}$ was continuously injected in the aerated tank. The pH was thus maintained between 7.0 and 8.0.

Oxygen supply

The oxygen necessary to maintain the metabolic activity of the microorganisms was introduced by compressed air insufflation. The air was diffused from the bottom of the vessel thanks to a perforated membrane (Flygt®) promoting, at the same time, biomass homogenization. The volumetric flowrate of air was set at 0.3 $m^3.h^{-1}$. The pilot worked under intermittent aeration in order to enable a nitrification-denitrification process. Then a programmer allowed imposing the aerobic and anaerobic sequencing intervals which were set at 1.5 hour each.

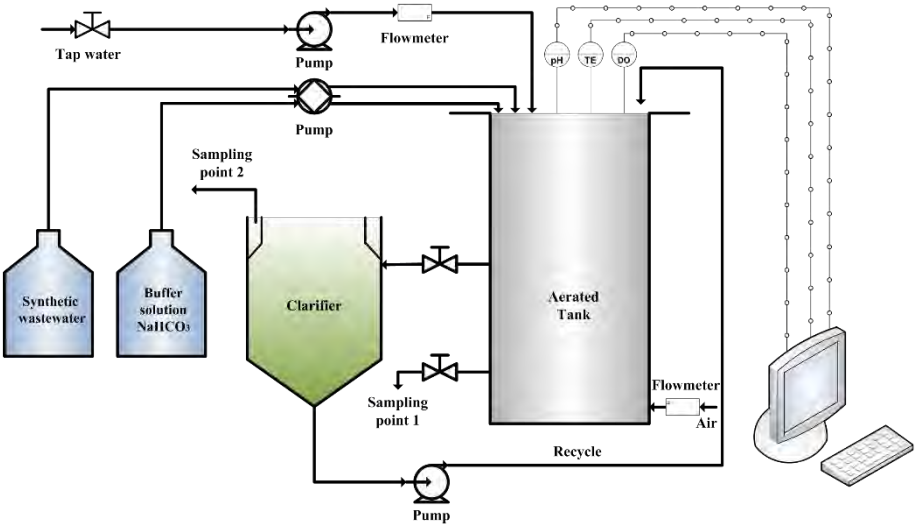

(a) Representative diagram of the lab-scale pilot.

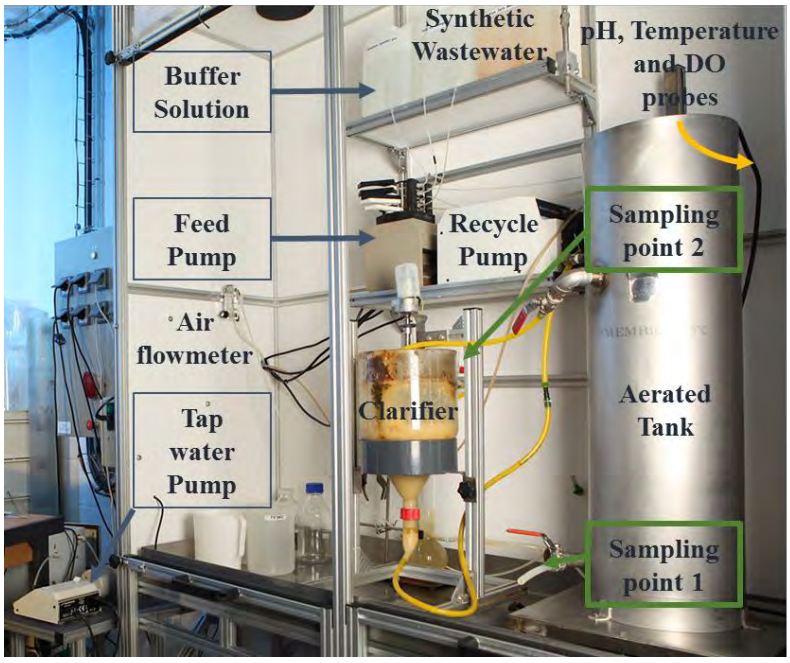

(b) The real lab-scale pilot.

Figure II-1. Description of lab-scale pilot components.

II.1.3 Sampling points

Samples were withdrawn from two different points in the pilot system (**Figure II-1**). The first one which was also used to waste the exceed sludge, was at the bottom of the aerated tank; samples were used for image analyses, TSS and SVI measurements. The second point was located at the clarifier outlet to assess the process efficiency regarding the organic matter removal and nitrogen contents.

II.1.4 Pilot system start-up

II.1.4.1 Activated sludge inoculum

Most of the experiments, especially those reported in the **Chapters IV** and **V**, were carried out with activated sludge provided by the WWTP of Nailloux, located in the southwest of France. This plant treats about 900 m^3 per day of domestic wastewater and it has a Population Equivalent (PE) number of 4500, with the possibility of extending to 6000. In this unit, the biological treatment consists of passing the pre-treated effluent through three sequential tanks: pre-anoxic, anaerobic and aerobic-anoxic tanks.

Inoculation was made by introducing 25 L of the effluent freshly collected from the aerobic-anoxic tank, which is also equipped with submerged membrane modules. In this tank, biomass can reach concentrations from 8 up to 12 $g_{TSS}.L^{-1}$. The duration of time between the sludge sampling and the bioreactor inoculation never exceeded 2 hours.

II.1.4.2 Composition of the synthetic wastewater

In order to have a better control of the feeding properties, a synthetic effluent has been used.

A concentrated synthetic wastewater that is diluted afterward by the tap water stream was used. Not only, it allowed a good preservation of the nutritive solution, but it also made easy to modify the organic loading rate. Thereby, both feeding flow rates were calibrated to reach a 1:100 dilution ratio. The effect of the buffer solution flow rate on dilution could be neglected since it was quite small.

This solution was mainly composed by substrates easily biodegradable, whose composition was chosen in accordance with previous works as reported in the **Chapter I**. The necessary amounts of carbon (COD), nitrogen and phosphorus were provided by glucose ($C_6H_{12}O_6$), ammonium chloride (NH_4Cl) and monobasic potassium phosphate (KH_2PO_4), respectively. The trace elements, for biomass maintenance, were ensured by the addition of the following compounds: iron (III), chloride ($FeCl_3$), calcium chloride ($CaCl_2$) and magnesium sulphate heptahydrate ($MgSO_4.7H_2O$). In start-up conditions, this wastewater was prepared to supply the system with a COD:N:P ratio of 100:7:1. The concentration of each substance is listed in the **Table II-1**.

Table II-1. Composition of the synthetic wastewater stream in normal conditions.

Composition	Concentration ($mg.L^{-1}$)
$C_6H_{12}O_6$ (*COD*)	750 (*800*)
NH_4Cl	214
$FeCl_3$	0.03
$CaCl_2$	10
$MgSO_4.7H_2O$	25
KH_2PO_4	51

The synthetic wastewater pH was always adjusted to 7.0 with a sodium hydroxide (NaOH) solution (10N).

II.2 Operating variables and assessment of the pilot performance

It is very important to correctly define some operational parameters regarding wastewater treatment by activated sludge systems. Such parameters are well consolidated in the field and they play a great role on the process efficiency. A detailed description of each one and the techniques used to evaluate the pilot performance can be seen on the next sections.

II.2.1 Food-to-Microorganism ratio (F/M) and Organic Loading Rate (ORL)

The Food-to-Microorganism ratio (F/M) normally characterizes the biological balance in the treatment. It is defined as the substrate concentration to the total mass of suspended solids inside the aerated tank. However, in some cases, the actual mass of microorganisms represented by the volatile suspended solids is used instead of the total mass of suspended solids. So, the (F/M) ratio can be expressed as:

$$F/M = \frac{F}{M} \qquad \textbf{(II-1)}$$

F/M	Food-to-Microorganism ratio	$[kgBOD_5.kgVSS^{-1}.d^{-1}]$
F	substrate received per day	$[kgBOD_5.d^{-1}]$
M	mass of microorganism in aerated tank	[kgVSS]

On the other hand, the Organic Loading Rate (OLR) must be interpreted as the aerated tank capacity in treating a volume of organic matter coming into the system per day:

$$OLR = \frac{F}{V} \quad \textbf{(II-2)}$$

OLR	Organic Loading Rate	[$kgBOD_5.m^{-3}.d^{-1}$]
V	aerated tank volume	[m^3]

Regularly, the F/M ratio and the ORL are estimated in terms of COD. A conversion to DBO_5 can be easily obtained by the standard COD/DBO_5 ratio for each type of effluent (about 2.5 or 3 for effluents classified as municipal). Such estimation was used in this study.

II.2.2 Hydraulic Retention Time (HRT)

In activated sludge systems, the Hydraulic Retention Time (HRT) is calculated as the relationship between the operating volume of the aerated tank and the feed flow rate.

$$HRT = \frac{V}{Q_f} \quad \textbf{(II-3)}$$

HRT	hydraulic retention time	[h]
V	volume of the aerated tank	[m^3]
Q_f	feed flow rate	[$m^3.h^{-1}$]

The above expression gives the average duration in which the liquid effluent remains in the aerated tank. This parameter is mostly fixed in function of the organic load (COD) in the feed flow rate. In general, it usually takes values between 10 and 24 hours (Wiesmann et al., 2007; Henze et al., 2008).

II.2.3 Solids Retention Time (SRT)

As reported by Wilén and Balmér (1999), the Solids Retention Time (SRT) is a process parameter that must be carefully chosen, since it may affect significantly bioflocs morphology. Moreover, it is already known that aggregates morphology is a key-factor on clarifier performance and, consequently, on the overall process performance (Wilén et al., 2003b; Perez et al., 2006; Koivuranta et al., 2014; Mesquita et al., 2016).

The SRT is defined as the mean time spent by the activated sludge in the aerated tank. Mathematically, this parameter is a relation of the mass of solids contained in the aerated tank to the mass of solids that is daily wasted, as it can be observed in the equation below (Wiesmann et al., 2007; Henze et al., 2008):

$$SRT = \frac{VX}{Q_E X_E} \quad \textbf{(II-4)}$$

SRT	solids retention time	[d]
V	aerated tank volume	[m^3]
Q_E	drained volume of excess sludge	[$m^3.d^{-1}$]
X	solids concentration in the aerated tank	[kg. m^{-3}]
X_E	solids concentration in the waste sludge	[kg. m^{-3}]

Generally, SRTs are specified throughout treatment conception according to the project requirements. Once determined, the SRT is maintained by the removal of the excess sludge. Such removal occurs daily when the treatment is stabilized. In this study, as it was previously mentioned, the removal was made directly from the aerated tank. This modification is increasingly applied to simplify the previous equation, since X and X_E would be the same. Then the volume that needed to be wasted is basically the ratio of the aerated tank volume to the fixed SRT.

$$Q_E = \frac{V}{SRT} \quad \textbf{(II-5)}$$

The SRT selection carries several side-effects: sludge conditioning, final disposal of the wasted sludge, floc settleability, and the most important of them, the quality of the treated water, in order words, it has an important role on COD, nitrogen and even phosphorus biological elimination (Wiesmann et al., 2007).

II.2.4 Recycle Ratio

The sludge recirculation from the clarifier towards the aerated tank is indispensable for keeping constant the biomass concentration in the aerated tank and an efficient organic matter removal. In most of the cases, the settled sludge should not stay more than 2 hours inside the clarifier. Therefore, it is advisable to adopt at least a 1:1 recycle ratio for recycle and feed flow rates (Q_R/Q_f) respectively.

$$RR = \frac{Q_R}{Q_f} \quad \textbf{(II-6)}$$

Q_R	recycle rate flow	[$m^3.d^{-1}$]

II.2.5 Pilot performance monitoring

The treated effluent was assessed by measuring chemical oxygen demand (COD), total nitrogen (TN), ammonium ($N\text{-}NH_4^+$) and nitrate ($N\text{-}NO_3^-$) concentrations. The activated sludge

performance was evaluated by the total suspended solids (TSS) and the sludge volume index (SVI) measurements. All analytical methods applied to quantify these parameters are indicated as follows.

II.2.5.1 COD, TN, NH_4^+, NO_3^- quantification

Samples of about 40 mL of the treated effluent were collected at the clarifier outlet (sampling port 2 - **Figure II-1**). This sampling was always performed at the end of the aerobic period to avoid as much as possible microbial activity cycle variations that are related to aeration sequencing. After, those samples were filtered with a glass fibre prefilter (Minisart®), which has a pore size of 1.2 µm. COD, TN, $N\text{-}NH_4^+$ and $N\text{-}NO_3^-$ contents were analysed in triplicate, once a week, using Hach-Lange cell tests, which are easily readable on the Hach-Lange spectrophotometer (DR3900) as well. In the **Table II-2**, the test kits references are gathered with their respective ranges and confidence interval of the measures.

Table II-2. Cell test corresponding to each analysis.

Analysis	Cell test reference	Range of measure ($mg.L^{-1}$)	Confidence interval (95%)
Chemical oxygen demand (COD)	LCI 500	0 – 150.0	± 2.0 $mg.L^{-1}$
Total nitrogen (TN)	LCK 338	20.0 – 100.0	± 2.1 $mg.L^{-1}$
Ammonium ($N\text{-}NH_4^+$)	LCK 339	0.23 – 13.5	± 0.45 $mg.L^{-1}$
Nitrate ($N\text{-}NO_3^-$)	LCK 303	2.0 – 47.0	± 0.80 $mg.L^{-1}$

The cell tests are based on a fully automatic spectrophotometry. The user only needs to insert the cell inside the spectrophotometer. The cell test is detected from its barcode (IBR+). As presented in the **Figure II-2**, a rotation of the cell takes place and 10 measurements are executed eliminating any possible interference of scratches, soil or flaws. Thereafter, the result is immediately displayed in $mg.L^{-1}$.

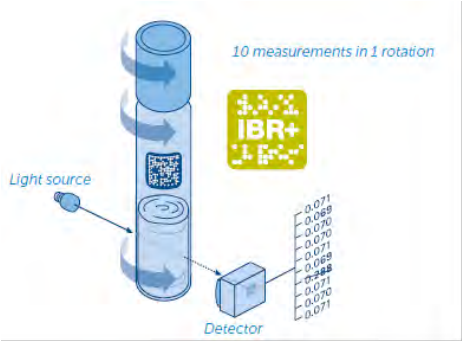

Figure II-2. Schematic representation of cell tests principle (Hach-Lange® Brochure for cuvette tests).

At the beginning, COD and TN concentrations in the synthetic wastewater were respectively measured by the LCK 514 (range of measure: 100 – 800 $mg.L^{-1}$; confidence interval: ± 8.3 $mg.L^{-1}$) and LCK 338 cell tests. This procedure allowed to validate the spectrophotometer measurements accuracy and the synthetic wastewater preparation, since those amounts were predefined by stoichiometric calculations.

The COD and TN removal efficiencies were calculated in accordance with the equations **(II-7)** and **(II-8)**. Both equations are a comparison of the concentrations found in the feed flow rate with the ones observed in the treated effluent.

$$\%\ \text{COD Removal} = \frac{COD_{IN} - COD_{OUT}}{COD_{IN}} \times 100\% \qquad \textbf{(II-7)}$$

COD_{IN}	COD concentration in the feed stream	$[mg.L^{-1}]$
COD_{OUT}	COD concentration in the treated effluent	$[mg.L^{-1}]$

$$\%\ \text{TN Removal} = \frac{TN_{IN} - TN_{OUT}}{TN_{IN}} \times 100\% \qquad \textbf{(II-8)}$$

TN_{IN}	TN concentration in the feed stream	$[mg.L^{-1}]$
TN_{OUT}	TN concentration in the treated effluent	$[mg.L^{-1}]$

II.2.5.2 Total suspended solids (TSS) determination

TSS determination was carried out through a gravimetric technique adapted from the Standard Methods (Eaton and Franson, 2005). A well-mixed sample (50 mL) was collected from the aerated tank (sampling point 1 - **Figure II-1**). The sample was then deposed in an aluminium plate previously weighted. The sample was dried in an oven at 103 to 105°C until a constant weight was reached. According to this method, 24 hours was enough to obtain no more variation on the weight measurements. After 24 hours, the aluminium plate was weighted again. The

difference between the increase in the weight and the weight of the plate, or the dried residue, represents the total suspended solids.

$$TSS = \frac{\Delta m}{V_{sample}} \times 1000 \quad \textbf{(II-9)}$$

TSS	total suspended solids	[g.L^{-1}]
Δm	weight of the dried residue	[g]
V_{sample}	Sample volume	[mL]

Measurements of TSS were accomplished in duplicate and three times a week.

II.2.5.3 Sludge volume index (SVI)

In activated sludge systems, the settling characteristics of the suspension are described by the sludge volume index (SVI). It corresponds to the volume occupied by 1 g of suspension after 30 minutes of sedimentation in a 1L graduated cylinder (Eaton and Franson, 2005). SVI determination is directly dependent on total suspended solids measurements, as it can be observed in the equation **(II-10)**.

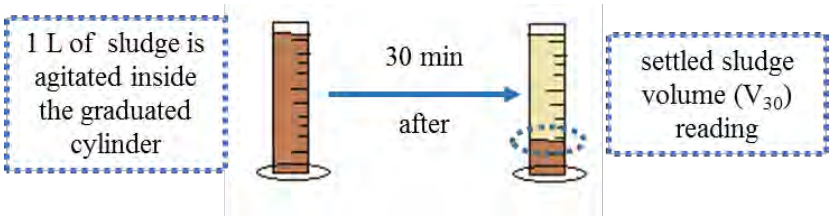

Figure II-3. Protocol for SVI determination.

$$SVI = \frac{V_{30}}{TSS\ (g.L^{-1})} \quad \textbf{(II-10)}$$

SVI	sludge volume index	[mL.g^{-1}]
V_{30}	settled sludge volume after 30 min	[mL.L^{-1}]

Quantifying SVI is effortless and not time-consuming. In addition, the practice has shown that is extremely helpful in routine process control since it can give considerable information about the sludge quality (**Chapter I.1.4**).

II.2.6 Summary of operating parameters in the pilot system

Some operating parameters of the pilot were preserved constant, others were maintained in a given values or ranges and others were modified as the objective of this work. The parameters that were preserved constant or maintained have received this status because they were considered by experienced work (Seviour and Blackall, 2012; Spellman, 2013) as the suitable conditions to lead this research with activated sludge systems. **Table II-3** summarizes these key parameters showing their respective values or ranges and the status that they have assumed during the experimental campaigns as well.

Table II-3. Summary of key operating parameters of the lab-scale pilot.

Operating parameters	Value	Status
Aerobic-anoxic periods (h)	1.5 – 1.5	Constant
Air flow rate ($m^3.h^{-1}$)	0.3	Constant
DO in aerobic cycles ($mg.L^{-1}$)	> 4	Maintained
OLR ($kg_{COD}.m^{-3}.d^{-1}$)	1.00 – 3.75	Varied
C:N Ratio (-)	100:7 – 100:28	Varied
Recycle Ratio (-)	1:1 – 3:1	Varied
HRT (h)	20h	Constant
SRT (days)	15 – 20 – 30	Varied
pH range (-)	7.0 – 8.0	Maintained
Temperature (°C)	17.8 – 23.5	Maintained

II.3 Morphological characterization of the activated sludge flocs

For activated sludge flocs, a single information about the size is insufficient to be able to properly characterize their behaviour in the process. Generally, information about the shape must be also included in order to obtain a complete morphological characterization. The size and shape descriptors for these particles is known as morphological parameters. This section, in particular, will present the apparatus used to acquire the morphological parameters of the activated sludge flocs.

II.3.1 Morphologi G3

The Morphologi G3™ (Malvern®) is an instrument that executes an advanced characterization of the size and shape of particles or aggregates in powders or suspensions (**Figure II-4**). For that purpose, it applies a technology which combines an optical microscope (coupled with a

CDD camera) and a software that conducts the automatic progress of the analysis, besides treating all collected data.

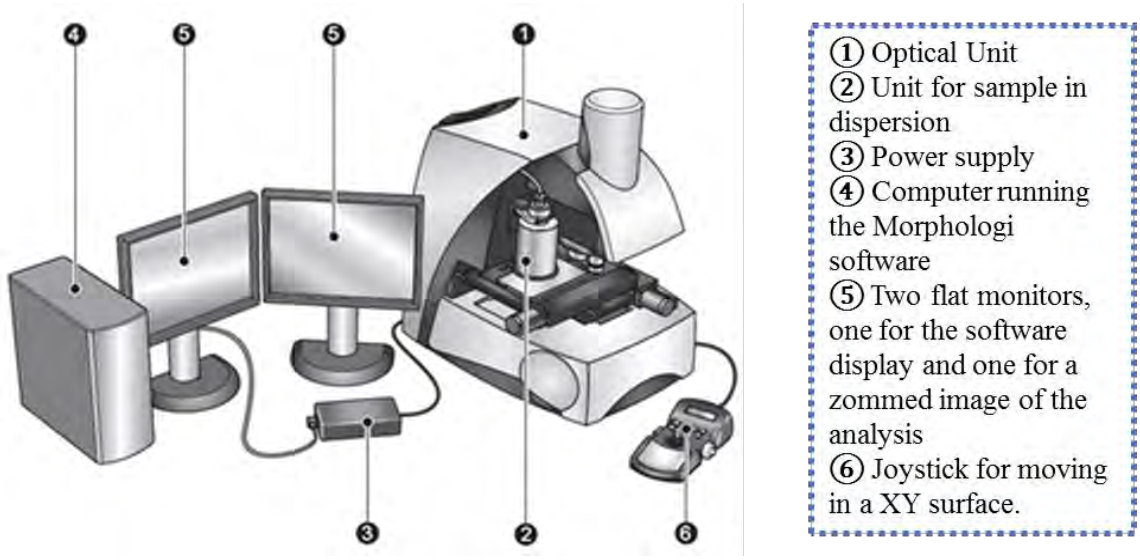

Figure II-4. Morphologie G3 arrangement.

Measurements carried out with this device can be separated in three essential steps: sample preparation, image acquisition and dataset treatment. These steps are detailed below.

Sample preparation

This step is fundamental to improve accuracy and reproducibility of the results. During the measurement, the aggregates must have a satisfactory spatial distribution; any overlap between flocs should thus be avoided. Consequently, it is always imperative to perform a sample dilution for concentrated suspensions (as activated sludge). Moreover, samples can be analysed with the unit for dispersion, in the case of free-flowing powders, or through a wet cell, or even a 4 slides plate in the case of evaporative or oil suspensions.

Image acquisition and treatment

For the image acquisition, the magnification and the stop criterion, either the number of recorded particles or the scanned area must be defined.

Thereafter, a binarization of the acquired images is handled to isolate each aggregate. The threshold of the grey level is fixed by the user (256 grey levels are available).

Dataset treatment

Morphologi G3^{TM} software is responsible for calculating each morphological parameter for all isolated elements found on the captured images. For each parameter, statistical properties such as: mean values, standard deviations, distribution or moments can be further calculated. The usual ones are described in the section **II.3.3**.

II.3.2 Morphological parameters

As an image of the projection of a particle or an aggregate has been obtained and digitized, it is thus possible to explore their morphological descriptors (parameters). There are many ways to subcategorize these descriptors and such terms will depend on the research field. One common way to subdivided them is based on size and shape definition. The size descriptors regularly denote dimension and are extensive, which reflects the proportions of the particle. In contrast, the shape descriptors are mostly referred to as form aspects, they are ratio of size descriptors and are intensive.

II.3.2.1 Size descriptors

Conventionally, the area, the perimeter, and equivalent dimensions are classified as size descriptors. From the area, several results as the circular equivalent diameter and spherical equivalent volume are calculated.

Area

The area of an aggregate A (**Figure II-5)** is calculated as the sum of the areas of each individual pixel, a_p within the borders of the projected image of this aggregate.

$$\boldsymbol{A} = \sum \boldsymbol{a_p} \qquad \textbf{(II-11)}$$

At this point, the unit of A is pixel^2, however Morphologi^{TM} software is calibrated in order to convert this measurement into µm^2.

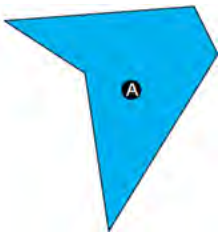

Figure II-5. Object with an area already converted.

Perimeter

The perimeter of the aggregate, P, measures the total length of the edges of the aggregate projection. This value is obtained summing the length of the boundary pixels and it must include a correction that considers direction changes. The perimeter of the **Figure II-6**, for example, is the sum of the edges **(A)** + **(B)** + **(C)** + **(D)** + **(E)**.

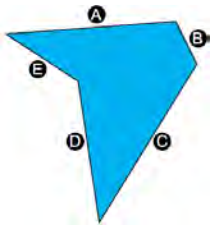

Figure II-6. The total length of the edges of an object – perimeter definition.

Convex hull perimeter

For understanding about the convex hull perimeter concept, one can imagine a particle surrounded by a rubber band. It is sometimes called as convex envelope or only envelope. **Figure II-7** illustrates the difference between a perimeter, P (on the left side) and a convex hull perimeter, P_C (on the right side). The convex perimeter is expressed in µm as well.

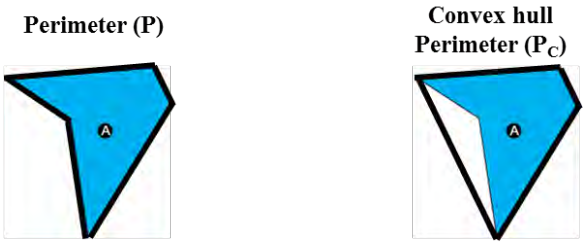

Figure II-7. Perimeter (left) and convex hull perimeter (right) of the object.

Convex hull area

The convex hull envelope can also be applied to determine the respective convex hull area, A_C as it is demonstrated in **Figure II-8**. As the actual area, the convex hull area is also represented in μm^2.

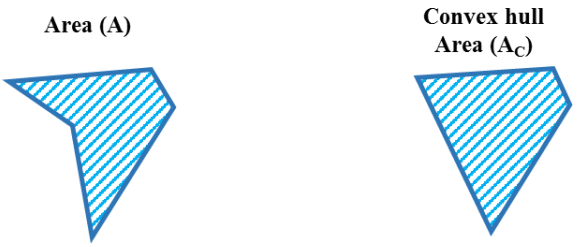

Figure II-8. Area (left) and convex hull area (right) of the object.

Circle Equivalent Diameter

The circle equivalent diameter (*CED*), or area-equivalent diameter, is defined as the diameter of a circle with the same area as the one of the analysed particle (**Figure II-9**). Thus, supposing that a particle has been measured with area, *A*, the *CED* can be estimated by the following equation:

$$CED = \sqrt{\frac{4A}{\pi}} \qquad \textbf{(II-12)}$$

CED is a measure of length, thereby reported in µm.

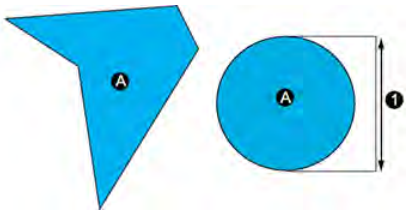

Figure II-9. CED of a particle (1): the area of the object and area of the circle are equal (A).

Spherical Equivalent volume

Similarly to the *CED*, the spherical equivalent volume, *SE*, is defined as the volume of a sphere whose diameter is a function of the measured area.

$$SE = \frac{1}{6}\pi(CED)^3 \qquad \textbf{(II-13)}$$

Length and Width

In order to measure the length and the width of a particle, it is necessary to define before the major and minor axes.

Each particle matter has major and minor axes (**Figure II-10**). The major axis (**1**) passes through the centre of mass of the object at an orientation corresponding to the minimum rotational energy of the shape. The minor axis (**1'**) also passes through the centre of mass of the object and it is perpendicular to the major axis. As both are termed as an orientation, they are expressed in degrees and can take values from 0° to 180°.

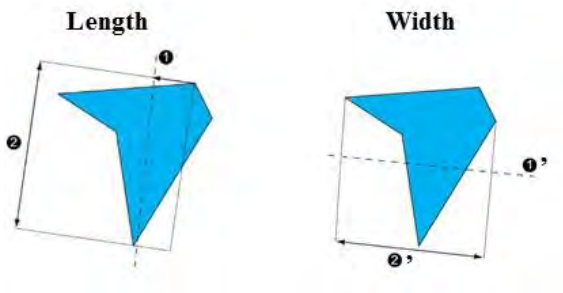

Figure II-10. Identifying the length and the width of the object.

Once major and minor axes are defined, it is possible then to determine the length and the width of a particle. The length (**2**) is the maximum distance between any two points on the perimeter of the particle projected onto the major axis. On the other hand, the width (**2'**) is the maximum distance between any two points on the perimeter of the particle projected onto the minor axis. They are, both, reported in µm.

II.3.2.2 Shape descriptors

Finally, using some equations (described below) and ratios of the abovementioned size parameters, the shape descriptors as circularity, convexity, solidity, and aspect ratio can be calculated. They can vary between 0 and 1.

Circularity

One way to measure how much an object may be close to a round shape, is quantifying its circularity. The circularity, C, is the ratio of the circular equivalent perimeter, P_E, to the actual perimeter of the object, P.

$$C = \frac{P_E}{P} = \frac{\sqrt{4\pi A}}{P} \quad \textbf{(II-14)}$$

More a particle shape becomes round and smooth, more the circularity approaches to 1. In opposition, the further away from a perfect circle a particle becomes, more the circularity tends to 0.

Convexity

The convexity, C_x, is the parameter that measures the particle edge roughness. It can be calculated dividing the convex hull perimeter, P_C, of the object by its actual perimeter, P.

$$C_x = \frac{P_C}{P} \quad \textbf{(II-15)}$$

When the surface of a particle becomes "spiky", the actual perimeter increases leading to values of the C_x close to 0. On the other hand, when the shape becomes smoother, convexity values can be expected around 1.

Solidity

Solidity, S, is the measure of the overall concavity of a particle. It is defined as the actual area, A, divided by the convex hull area, A_C.

$$S = \frac{A}{A_C} \quad \textbf{(II-16)}$$

Solidity values also range between 0 and 1. As the particle becomes more solid (filled), the real and convex hull area approach each other, resulting in a value of the solidity close to 1.

Aspect ratio

Aspect ratio (AR), as the name explains by itself, expresses a ratio of the width (W) to the length (L) of the particle. In the same way, this property also varies between 0 and 1.

$$AR = \frac{W}{L} \quad \textbf{(II-17)}$$

Another definition that can be extracted, using the aspect ratio, is the *elongation*. Such parameter is a function of the aspect ratio and may be quite useful for asymmetric or needle-like particles.

$$elongation = 1 - AR \quad \textbf{(II-18)}$$

II.3.2.3 Understanding the shape descriptors values

The **Table II-4** brings characteristics values of circularity, convexity, solidity and aspect ratio for different objects. They are usual examples of how the shape descriptors could be mainly affected by form or roughness.

If circularity and convexity values are analysed first, it can be seen that circularity is very sensitive to the overall shape of the object as well as to its roughness, while the convexity is mainly impacted by the roughness and is much less sensitive to the overall shape.

As the convexity, the solidity is highly sensitive to surface roughness, this conclusion is expected once both are related to a convex hull measurement. Throughout this work, since activated sludge flocs are not compact objects, it was either verified that solidity is equally sensitive to objects porosity.

Table II-4. Variation of the shape descriptors for several objects (adapted from (Olson, 2011).

Object	Shape description	Circularity (C)	Convexity (C_x)	Solidity (S)	Aspect Ratio (AR)
	Circle	1	1	1	1
	Touching circles	0.75	0.87	0.88	0.50
	Square	0.89	1	1	1
	Rectangle	0.71	1	1	0.25
	5-point star	0.52	0.81	0.50	0.98
	Fiber	0.14	0.89	0.10	0.20

In contrast, the aspect ratio is not affected by the roughness at all. This parameter is essentially dependent on the extension of the object, taking into account that is a function of the particle length and width. Such conclusion is even more evident when focusing on the rectangle and the fiber that roughly have equivalent aspect ratios.

In **Table II-5**, it is possible to notice the same type of comparison, however considering now activated sludge flocs. For practical reasons, the circular equivalent diameter (CED) is reported herein instead of a global shape description to label the flocs.

Then, comparing the three flocs, it can be confirmed what was previously mentioned about circularity values. This parameter is quite sensitive to the form and the roughness of the flocs, even though for the flocs presenting almost the same size (121.2 and 121.9 µm). On the other hand, convexity values seem to be exclusively sensitive to the roughness, since the first and the third floc with not similar sizes (115.0 and 121.9 µm) have a completely different form but almost the same value of convexity.

The values of solidity for the three flocs evolve similarly to the convexity values, confirming the statement that solidity strongly depends on the surface roughness of the object as well. In opposition to this behaviour, the aspect ratio values suggest any dependence in relation to the boundaries of the flocs. For example, it can be noticed the same aspect ratio for the second floc indicating a “loose” and open structure and the third one, whose the structure is relatively more regular. Finally, comparing those two flocs with the first one, it is clear that the extension of the flocs has more weight in this parameter.

Table II-5. Variation of the shape descriptors for 3 activated sludge flocs.

Floc	CED (µm)	Circularity (C)	Convexity (C_x)	Solidity (S)	Aspect Ratio (AR)
	115.0	0.30	0.38	0.78	0.87
	121.2	0.14	0.24	0.47	0.59
	121.9	0.26	0.37	0.70	0.59

II.3.3 Number, area and volume-based distributions

Particle populations can be arranged in terms of classes of a given morphological parameter. The most common way to organize them is using size classes (*CED*) as it is illustrated in the **Table II-6**. In the first size class, it is possible to find, for example, that the sum of the surfaces (areas) of all the flocs (N_1) with a size between CED_1 and CED_2 is A_1, and V_1 is found by same principle, but applied to the area and to the volume, respectively. A similar interpretation can be extended to the two other classes. This type of classification essentially enables to observe the correspondent number, area or volume fraction that a group of particles occupies in the whole particle population (N_T, A_T, V_T).

Table II-6. Size classes and their correspondent number, area and volume of particles.

Size class	Number	Area	Volume
$CED_1 - CED_2$	N_1	A_1	V_1
$CED_2 - CED_3$	N_2	A_2	V_2
$CED_3 - CED_4$	N_3	A_3	V_3
Total	N_T	A_T	V_T

Thus, the procedure to calculate the number, area and volume fraction for the first class is expressed as follows.

$$Nb_I\ (\%) = \frac{N_1}{N_T} \qquad A_I\ (\%) = \frac{A_1}{A_T} \qquad Vol_I\ (\%) = \frac{V_1}{V_T} \tag{II-19}$$

Once defined the fractions which regard each class, it is possible to represent them by frequency distributions of size (or shape). It means that those distributions can be displayed by the number area or volume of the particles. The best basis to represent each distribution will depend on the analysis aim. **Figure II-11** shows an illustrative X-population of particles under the three resolution bases.

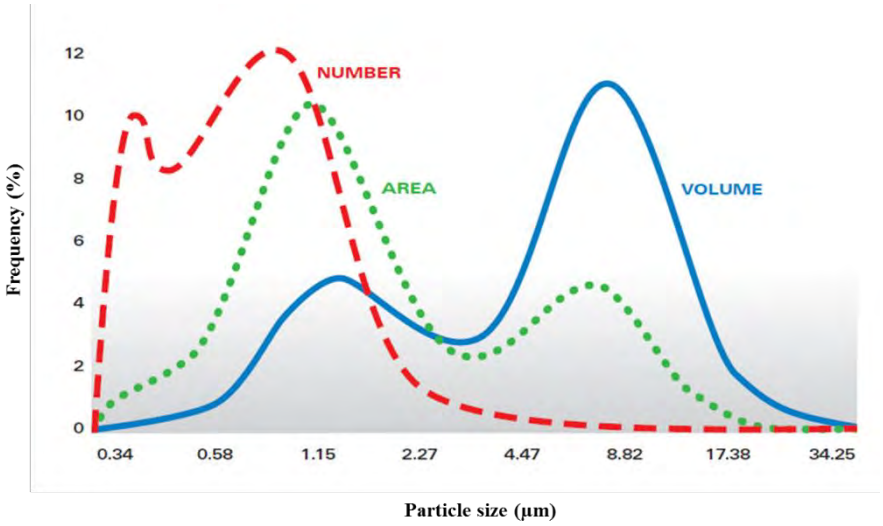

Figure II-11. Representation of a particle size distribution on number, area and volume basis (adapted from HORIBA®).

The red dashed line represents a number-based distribution. In this resolution, a very small particle has exactly the same weighting as a larger particle. This means that the contribution made by each particle to the distribution is the same.

The blue full line, in turn, is a volume-based distribution. In this basis, the contribution of each particle is proportional to its volume. As a result, the large particles dominate the distribution and the sensitivity to small particles is reduced as their volume is considerably smaller in comparison to the larger ones.

Likewise volume-based distributions, the area-based distributions capture the mostly information about the large particles, nevertheless if porous particles are being analysed, this distribution will shift even more towards right since they present a more significant surface area.

A three-dimensional representation on volume basis combining size and shape can also be considered. In this case, the numerator of the volume fraction (*Vol)* corresponds to the sum of the volume of the aggregates that have a size somewhere between d_1 and d_2 and a shape parameter (aspect ratio, circularity, solidity or convexity) somewhere between *Shape Parameter*$_1$ and *Shape Parameter*$_2$.

II.3.3.1 Mean, mode and median

In order to characterize a distribution, it is possible to determine its respective mean, mode and median. **Figure II-12** displays a non-symmetric distribution where these three parameters assume different values. It is important to know how to differ each one of these statistical parameters that are frequently misused.

Figure II-12. A non-symmetric distribution where mean, median and mode takes different values (adapted from HORIBA®).

The median value is defined as the point where half of the population resides above this number, and the other half resides below this number.

The mode is the peak of the frequency distribution, or it may be reasonable to visualize it as the highest peak observed in the distribution. The mode represents the parameter value (or parameter range) most probably found in the distribution.

The mean might be an arithmetic or geometric average of a population characteristic. There are multiples definitions of mean because this parameter is associated with the basis of the distribution calculation (number, area, volume).

A more generalized equation **(II-20)** to express mean diameters of a population introduces the moments of the density distribution as it is showed as follows:

$$D[m,\ n] = \frac{\sum_i f_i D_i^m}{\sum_i f_i D_i^n} \qquad \textbf{(II-20)}$$

Where f_i is the number fraction of particles with a diameter D_i.

Considering a number-based distribution, the mean diameter is thus identical to D[1,0]. This equation also allows to calculate important distribution moments as the D[4,3] and the D[3,2], they are respectively known as mass moment mean diameter and surface area moment mean diameter (or only Sauter diameter).

For Gaussian distributions, i.e., a symmetric one, the mean, the median and the mode have the same value.

II.3.3.2 Distribution statistics

From the distributions, it is possible to determine their respective widths *x[b, p]*. Where *x* can be any morphological parameter, *b*, any distribution basis and then can be replaced by *n* for number, *s* for area and *v* for volume basis, and *p* is the percentile reading from the distributions. The latter can be set to 0.1 to designate where 10 percent of the population lies below, 0.5 to find the median value, or 0.9 to indicate where 90 percent of the population lies below.

In **Figure II-13**, these widths are highlighted using the equivalent diameter as an illustrative example, thus the following interpretations could be drawn:

- D[v, 0.5] shows, on volume basis, where 50% of the analysed population has a size smaller than this diameter and the other 50% has a size larger than this value.
- D[v, 0.1] is the size, on volume basis, in which 10% of the particles are smaller than this diameter.
- D[v, 0.9] is the size, on volume basis, in which 90% of the particles are smaller than this diameter.

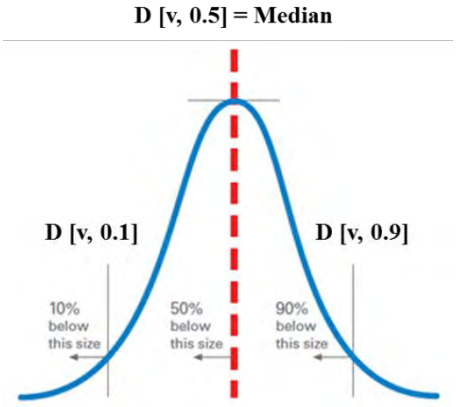

Figure II-13. Representation of the distributions widths using the diameter as morphological parameter (adapted from HORIBA®).

II.3.4 Measuring fractal dimension through image analysis

Methodologies based on image analysis are able to estimate properties for an aggregate population which has several size proportions. In a sample with particles of fractal nature, parameters such as perimeter (P), area (A) and mass of the aggregate (M) are commonly related to a characteristic length parameter l – gyration radius (R_g), equivalent diameter (CED) or maximum length (L_{max}) – in order to evaluate the fractal dimension.

For fractal dimension obtained through image analysis it is recommended an evaluation through a two-dimensional relationship such as:

$$A \propto L_{max}^{D_2} \qquad \textbf{(II-21)}$$

or

$$A \alpha P^{2/D_{pf}} \quad \textbf{(II-22)}$$

Since activated sludge flocs are noncircular aggregates, in this study, the projected area (A) was correlated to the maximum length (L_{max}) instead of the equivalent radius (r) of the flocs as it has been reported by Zhao et al. (2013) to determine D_2. In addition, projected area was correlated to perimeter (P) as well in order to estimate D_{pf} and, then, access further information. For illustration, D_2 was obtained from the slope of log-log plots of A versus L_{max} as **Figure II-14** depicts.

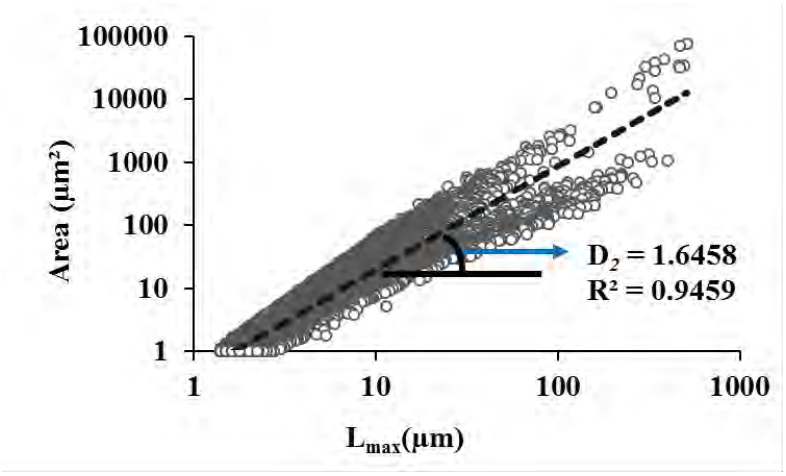

Figure II-14. Graphic determination of two-dimensional fractal dimension.

In the case of D_{pf}, defined by means of the equation **(II-22),** the slope must be divided by 2 and inverted, for its final determination. For estimating the average values of D_2 and D_{pf}, these approaches take into account all aggregates in a certain image.

II.4 Conclusion

This chapter aims at presenting the experimental set-up and the main parameters used in the next chapters.

A laboratory scale pilot was set-up, based on a typical activated sludge system, connecting a clarifier to an aerated tank in order to analyse the effect of some specific operating conditions on the morphological properties of sludge flocs. The AS pilot is fed with a synthetic wastewater. The pilot is equipped with several probes, which allow recording the temperature, the pH and the dissolved oxygen over the time. The treated effluent was assessed by measuring the chemical oxygen demand (COD) as well as the total nitrogen (TN), ammonium ($N\text{-}NH_4^+$) and nitrate ($N\text{-}NO_3^-$) concentrations. The pilot performances were evaluated through classical parameters as the total suspended solids (TSS) and the sludge volume index (SVI) measurements. During the experimental campaigns which will be described in **Chapters IV** and **V**, some of the key operating parameters were maintained constant (aerobic-anoxic periods, air flow rate, hydraulic retention time) or monitored (dissolved oxygen flow rate during the

aerobic cycles, pH and temperature), while others were varied in order to introduce perturbations on the biomass characteristics.

The morphological characterization of the activated sludge flocs can be performed by image analysis using an automated microscope to capture for each floc some basic information such as the area and the perimeter as well as the convex hull area and the convex hull perimeter of the floc. The software used may also give access to the major and minor axes, and thus to the length and the width of each floc. From all these parameters, several size descriptors (circle or sphere equivalent diameter) and shape characteristics (circularity, convexity, solidity, aspect ratio, elongation) can be defined allowing to quantify the overall shape or the surface roughness. The analysis of a great number of individual flocs can then allow determining the number, area or volume distributions of each morphological parameters. Finally, it was shown in this chapter that two fractal dimensions can also easily be extracted from image analysis, based either on the area and the perimeter of the flocs or on the area and any characteristic length parameter.

II.5 References

Eaton, A.D., and Franson, M.A.H. (2005). Standard Methods for the Examination of Water & Wastewater (American Public Health Association).

Henze, M., van Loosdrecht, M.C.M., Ekama, G.A., and Brdjanovic, D. (2008). Biological Wastewater Treatment (IWA Publishing).

Koivuranta, E., Keskitalo, J., Stoor, T., Hattuniemi, J., Sarén, M., and Niinimäki, J. (2014). A comparison between floc morphology and the effluent clarity at a full-scale activated sludge plant using optical monitoring. Environ. Technol. *35*, 1605–1610.

Mesquita, D.P., Amaral, A.L., and Ferreira, E.C. (2016). Estimation of effluent quality parameters from an activated sludge system using quantitative image analysis. Chem. Eng. J. *285*, 349–357.

Olson, E. (2011). Particle Shape Factors and Their Use in Image Analysis-Part 1: Theory. J. GXP Compliance *15*, 85.

Perez, Y.G., Leite, S.G.F., and Coelho, M. a. Z. (2006). Activated sludge morphology characterization through an image analysis procedure. Braz. J. Chem. Eng. *23*, 319–330.

Wiesmann, U., Choi, I.S., and Dombrowski, E.-M. (2007). Fundamentals of biological wastewater treatment (Weinheim: Wiley-VCH Verlag).

Wilén, B.-M., and Balmér, P. (1999). The effect of dissolved oxygen concentration on the structure, size and size distribution of activated sludge flocs. Water Res. *33*, 391–400.

Wilén, B.-M., Jin, B., and Lant, P. (2003). Impacts of structural characteristics on activated sludge floc stability. Water Res. *37*, 3632–3645.

Zhao, P., Ge, S., Chen, Z., and Li, X. (2013). Study on pore characteristics of flocs and sludge dewaterability based on fractal methods (pore characteristics of flocs and sludge dewatering). Appl. Therm. Eng. *58*, 217–223.

Chapter III. Development of a methodology to assess size and shape of activated sludge flocs

The present chapter describes the development of a methodology for morphological characterization of activated sludge aggregates using the Morphologi G3 automated microscope. The steps involved in this methodology consisted in defining some analysis settings as: sample carrier, dilution factor, magnification, threshold and total number of analyzed particles. Analyses were performed on different types of sludge in order to evaluate the methodology robustness and to put in evidence their differences in terms of morphological properties.

III.1 A Standard Operating Procedure (SOP) for characterizing activated sludge flocs

In order to establish an operating procedure for the morphological characterization of activated sludge flocs, four samples were collected from three different Wastewater Treatment Plants (WWTP) situated in the southwest of France. It must be underlined that in Cugnaux WWTP, samples were taken from two distinct processes: one sample comes from a classical activated sludge system and the other one from a pilot-scale Membrane BioReactor (MBR), then completing the four samples. The sampling was always performed in the aerated basins of each unit. For practical reasons, these samples are named according to the type of process – AS for classical activated sludge system or MBR for Membrane BioReactor – and the type of wastewater – M for Municipal, I for Industrial and G for Greywater. **Table III-1** summarizes some of the basic features about these units, which can give an idea about the nature of the samples as well as their codes.

Table III-1. Summary of the basic features of the wastewater treatment plants.

Unit	Type of process	Type of wastewater	COD_{IN} ($mg.L^{-1}$)	Sample Codes
Castanet WWTP	Activated Sludge System	Municipal and Industrial (mixed)	190 (Municipal) 2800 (Industrial)	AS-MI
Cugnaux WWTP	Activated Sludge System	Municipal	695	AS-M
	Membrane Bioreactor (Pilot-Scale)	Greywater (only)	600	MBR-G
Nailloux WWTP	Membrane Bioreactor (Full-Scale)	Municipal	750	MBR-M

The automated microscope Morphologi G3^{TM} (Malvern ®), already described in the **Chapter II**, was employed to measure the size and the shape of the activated sludge aggregates in the samples. In the moment that an operating procedure is being developed as a standard one, it is imperative to have in mind two main aspects: the accuracy and the efficiency of the image analysis protocol. For accuracy, it can be understood that the Standard Operating Procedure (SOP) must provide reproducible, repeatable and precise data. While for efficiency, it can be pointed out that consistent results must be expected, it means, coherent with what is observed in real situations in wastewater treatment plants. Moreover, the computational time to run a measurement must also be added as a key factor for an efficient SOP.

The next sections of this chapter are devoted to explain how the SOP for the morphological characterization of activated sludge flocs has been set up. They can be reasonably separated by the choice of the following five factors:

- Sample Carrier
- Dilution
- Magnification
- Threshold
- Analysis stop criterion (by number of particles or scanned area?)

Apart from the dilution factor, the other factors must be set directly on the software that commands the measurements in the Morphologi G3^{TM}. All the steps taken herein to determine the acceptable values or parameters concerning each aspect are discussed below.

III.1.1 Sample Carrier

A whole range of sample carriers are available in the Morphologi G3^{TM} instrument. It is up to the users to select the one that best suits their needs. Since the structure of the activated sludge flocs must be preserved as much as possible, drying the samples was not an option in this study. So, any carrier that would allow analysing wet dispersions was considered in priority. Another aspect that was taking into consideration, was the capability of the carrier to not break the flocs by applying pressure. Once evaluated these single aspects, the Wet Cell (**Figure III-1**) was selected as the most appropriate among the available sample carriers to run the measurements of morphological characterization.

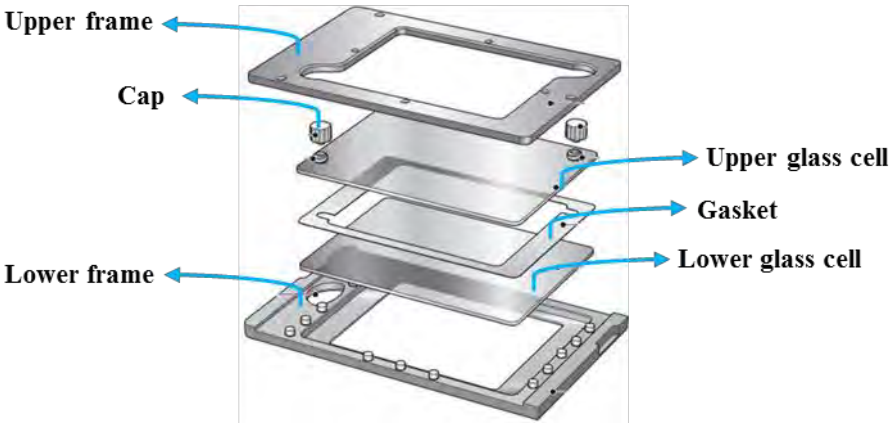

Figure III-1. Wet Cell accessory for Morphologi G3^{TM} instrument.

The Wet Cell is composed by two glass cells, two caps and a magnetically clamped metal frame, which encases the glasses. To avoid particles breakage, a gasket (≈ 1 mm) can be eventually placed between the upper and the lower glass cell, as illustrated in the **Figure III-1**. In all cases of this study, about 1 mL of sample was deposed on the lower glass cell, then the gasket was placed and finally the upper glass cell was laid covering the sample. The samples were deposed between the glass cells thanks to a Pasteur pipette sectioned (Ø 4 mm) at the end allowing any aggregate to flow down whatever its size is.

III.1.2 Determination of the Dilution Factor

Activated sludge systems are suspensions with high biomass concentration, their total suspended solids (TSS) values can normally range between 2 and 5 g.L^{-1}, achieving 10 g.L^{-1} when membrane bioreactors are used instead of classical processes. It suggests that diluting the samples is essential for a proper image acquisition and consequently to conduct an accurate morphological characterization. Otherwise, when samples are not diluted as shown in the **Figure III-2**, aggregates and filaments may appear overlapped on the images, which can lead to a misinterpretation of the objects morphology (Motta et al., 2002a; Mesquita et al., 2010a).

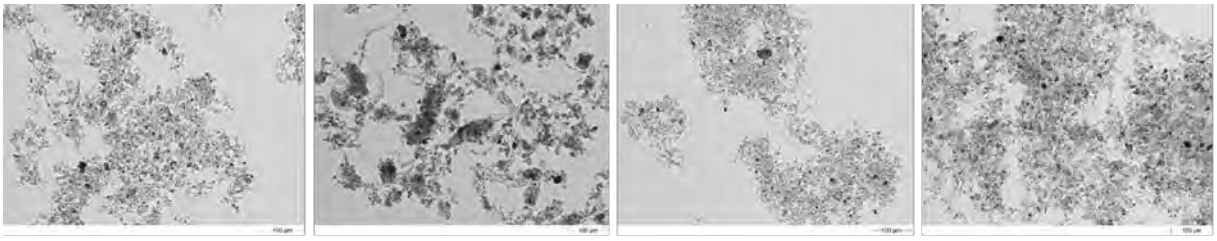

Figure III-2. Non-diluted samples from (a) AS-M, (b) AS-MI (c) MBR-G, and (d) MBR-M. The scale bar indicates 100 µm.

Therefore, new samples were prepared from each one of the four raw sludge samples and analysed in order to determine the optimal dilution factor. As it was recommended by Mesquita et al. (2013), dilutions were performed with treated effluent in order to avoid damages to floc

structure due to osmotic or ion exchange effects which can encourage defflocculation. Moreover, the time intervals between sampling and dilutions never exceeded 4 hours.

For the samples from AS-M and AS-MI, tests were run for the raw sludge and for diluted samples applying dilution factors of 1:5, 1:10, 1:20 and 1:40. In the case of MBR-G sample, measurements were run in triplicate for 1:2, 1:5, 1:10, 1:20 and 1:40 dilution factors. Due to the high suspended solids contents, the analyses with the raw sludge coming from MBR-G were not achievable. Finally, for the sample from MBR-M, measurements were performed for 1:10, 1:20 and 1:40 dilution factors.

TSS concentrations were 2.9, 5.5 and 8.6 $g.L^{-1}$ for the raw samples of AS-M, AS-MI and MBR-M, respectively, and 4.5 $g.L^{-1}$ at a 1:2 dilution, in the case of MBR-G.

III.1.2.1 Impact of dilution on the area-based size distributions

Since diluting the samples can mainly affect floc size (CED), the impact of increasing dilution factor was investigated to the four samples in which concerns their area-based size distributions. The distributions were plotted to each dilution providing a way to understand the dynamics of floc population when they are compared to the raw sludge or to initial dilutions (in the case of the MBRs). The distributions were chosen to be represented on area basis because it can enable valuable information about the screened surface of the samples **(Figure III-3)**.

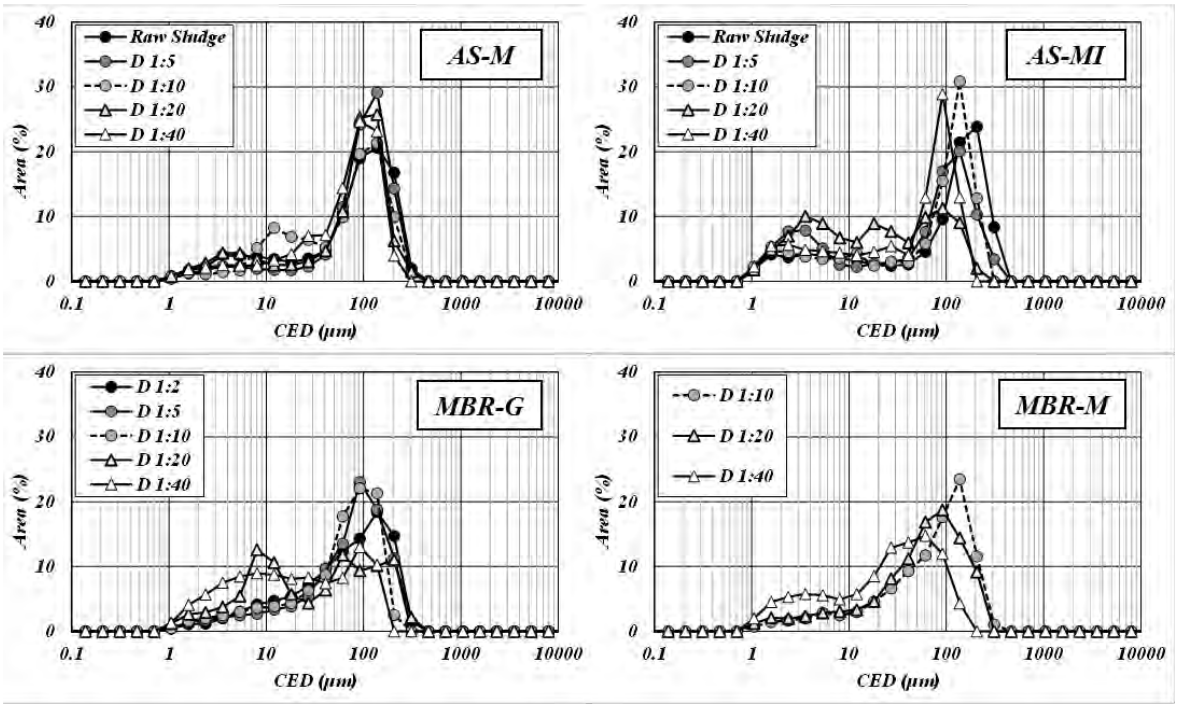

Figure III-3. Effect of dilution on area-based size distributions for the four samples: AS-M, AS-MI, MBR-G and MBR-M.

Roughly analysing the distributions, it can be stated that at least two populations of flocs exist within the samples: those with a CED upper to almost 20 µm and those with a CED lower than 20 µm. Once dilutions are performed, an interaction between these two populations is mostly noticed.

If the distributions of the raw sludge and the 1:5 dilution are compared for the samples AS-M and AS-MI, a similar behaviour can be remarked: a slight shift of the distributions to the left, which means a size reduction, and then a small increase of the area fraction of the flocs with a CED < 20 µm. The same behaviour can be identified if the distributions corresponding to 1:2 and 1:5 dilutions for MBR-G are compared as well.

When the dilution of 1:10 is performed, it is possible to detect an increase of the area fraction of the flocs with a CED around 10 µm for AS-M samples; an increase of the peak of the population with a CED > 20 µm for AS-MI and any meaningful change for MBR-G sample. In addition, MBR-M exhibited a similar profile to the one described by MBR-G at a 1:10 dilution. Modifications of the distributions for the AS samples can mainly indicate signs of flocs disclosure, which is the central aim of performing dilutions.

Since the samples were submitted to a 1:20 dilution, important modifications are noticed mainly for the curves of AS-MI, MBR-G and MBR-M. Distributions of AS-MI and MBR-G have both become tri-modal, indicating that flocs might have gone beyond disclosure and they have started to break. If a comparison is established between AS-M and AS-MI samples, then the result could endorse which has been reported by Motta et al. (2002). They have observed that samples from a WWTP fed with industrial effluent is more susceptible to size decrease, since their first dilution (at 1:5), in relation to the samples from a WWTP fed with municipal effluent.

At a dilution of 1:40, all samples distributions showed a more important deviation to the left in relation to the raw sludge or first dilutions, the deviations are even perceptible if they are compared to a dilution of 1:10, for example. In addition, a swelling of the population with a CED < 20 µm can be noticed in the four cases. For the MBR samples, a flattening of the population with a CED > 20 µm is equally observed. It can point out that flocs from MBR are probably more fragile than the ones coming from a typical activated sludge system.

III.1.2.2 Impact of dilution on the screened biomass

In order to study in-depth how dilution affects the amount of biomass screened and the dynamics of the floc populations as well, the flocs size distributions were divided in three classes (or populations) of interest:

- *Large flocs* – comprises all flocs with a CED above or equal to 200 µm.
- *Intermediate flocs* – comprises all flocs with a CED above or equal to 20 and below 200 µm.
- *Small flocs* – comprises all flocs with a circular equivalent diameter (CED) bellow 20 µm.

This strategy has been used by Mesquita et al. (2009) before and adapted to the range of sizes encountered in this study.

The area percentage of each class (III-1) for each sample was assessed in function of the dilutions factors as **Figure III-4** presents.

$$\% Area = \frac{\sum A_i}{A_T} \quad \textbf{(III-1)}$$

The area percentage expresses the contribution of each class (the sum of all floc areas A_i within the class boundaries) in relation to the overall floc population (A_T) contained in the samples.

As it can been observed in the **Figure III-4 (a)**, there is a decrease of the *Large flocs* area percentage until the dilution factor of 1:10 for, at least, three of the four tested samples. Although analyses have not been carried out for MBR-M raw sludge and its dilution at 1:5, it is almost presumable a similar behaviour for this case. Such a decrease was from 9.8% to 6.8%, 22.4% to 9.1% and 9.3% to 5.3% for AS-M, AS-MI and MBR-G, respectively. From 1:10 dilution onward, the area percentage maintains a slight decrease for all four cases, until this population has been completed vanished at 1:40 dilution in each of them. As a result of the reduction of the area percentage for this population, it might be inferred that dilution may separate each individual floc while they are overlapped or displayed in dense conditions in image analysis treatment (specious rupture) or trigger a deflocculation process (real rupture) into this class.

Regarding the *Intermediate flocs* area percentage (**Figure III-4 (b)**), it is possible to suppose, on one hand, that the type of process may depict the behaviour of the dilutions, since AS-M and AS-MI, which are both operated with a classical system, have adopted almost the same behaviour over the dilutions. In addition, the tests ran for MBR-M have exposed a coincident profile in relation to the one observed for the MBR-G sample. On the other hand, this intermediate population has globally presented an increase in its percentage area from the raw samples until 1:10 dilution, i.e., increases from 53.5% to 70.0%, 71.0% to 78.5% and 72.0 to 79.1% were noticed for AS-M, AS-MI and MBR-G, each one. This evidences perfectly suits the possible disclosure of a dense “cloud” of large flocs or, equally, possible ruptures. In overall, from the 1:10 dilution, this intermediate class has also experienced a diminution of the area percentage for each sludge, except for the AS samples, whose increase at a 1:40 dilution may be considered not important when compared to the error bar at a 1:20 dilution.

For the *Small flocs* class (**Figure III-4 (c)**), a similarity in the profiles among the dilution points depending on the process types may also be noticed. Moreover, for most of the samples, a slight increase of the area percentage between the raw sludge and the 1:10 dilution is followed by a more significant increase between 1:10 and 1:40 dilutions. This can be a result of a real or apparent rupture of large and/or intermediate flocs.

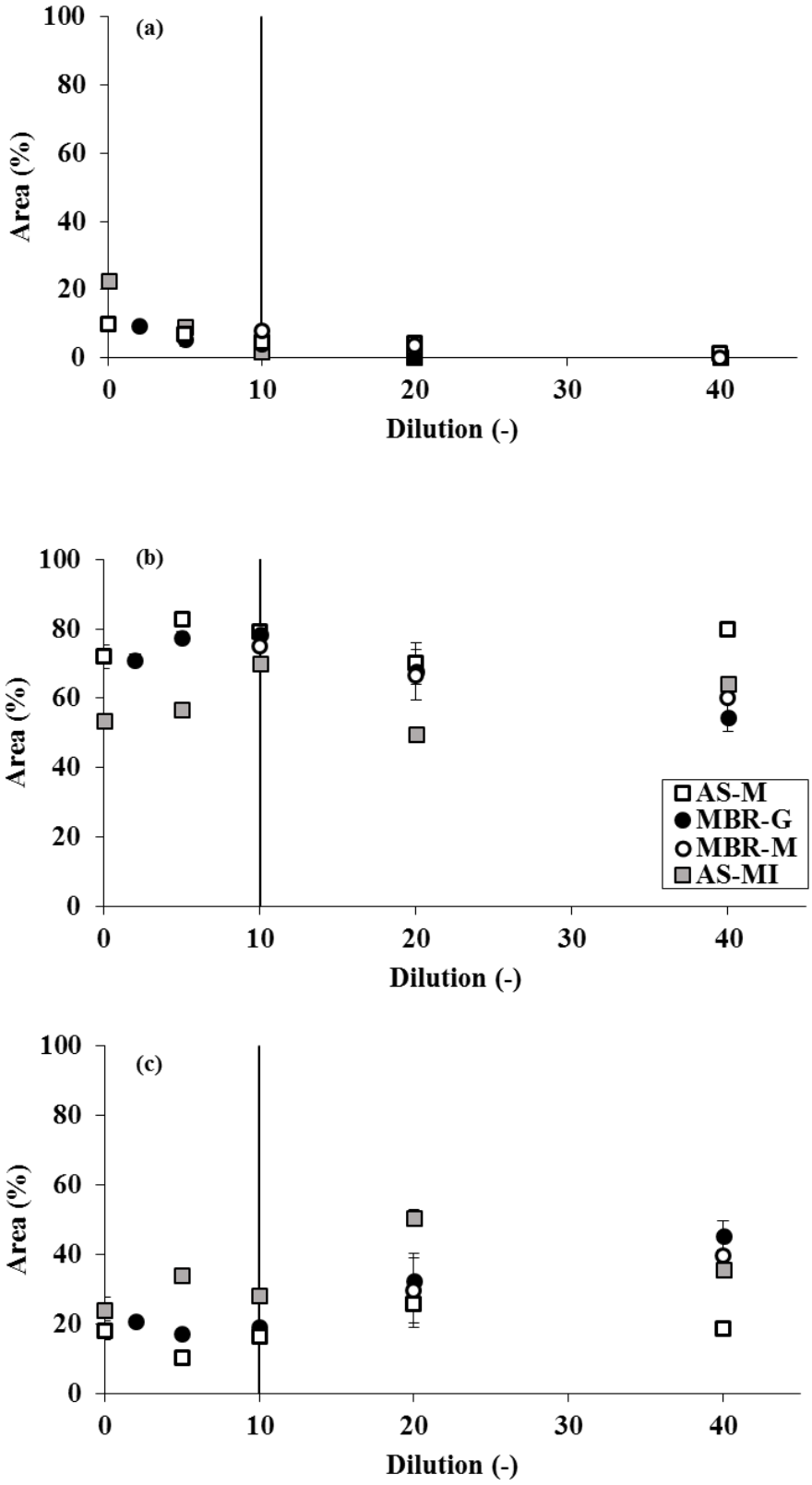

Figure III-4. Effect of dilution on each class area percentage (%Area): (a) Large flocs, (b) Intermediate flocs and (c) Small flocs for each sample.

III.1.2.3 Impact of dilution on the biomass morphological characteristics

When it comes to find the dilution factor that best suits the needs of the SOP, studies (Motta et al., 2002a; Perez et al., 2006; Mesquita et al., 2010a) are generally focused on quantifying the amount of surface available for scanning, the size and the number of particles throughout the dilutions. However, it may be also important to analyse how dilution impacts the morphological characteristics of the activated sludge flocs in which concerns their shape properties (Circularity – *C*, Convexity – C_x and Solidity – *S*).

In the **Figure III-5 (a-c)** are presented the mean values of the shape parameters calculated on area basis versus the dilution for the four types of sludge. As it can be noticed, circularity and convexity parameters seem to have some sensibility to dilution when compared to solidity, since the points drawn by the solidity mean values for each sample demonstrated less variability. The behaviour described by circularity and convexity also suggests that this sensibility is more remarkable for the flocs coming from the unit operating with an MBR process. This result may be relied to the fact that the same flocs have also presented a susceptibility to the dilution more important than the ones coming from a classical AS system. As it could be observed in the last section, there was a constant increase of the small flocs area percentages. These increases verified for circularity and convexity mean values are, then, consistent with the growth of small floc fractions, which are prone to be more circular and convex.

In this study, the optimal dilution factor was determined taking into account its capacity to satisfy the following three points together:

- The evolution of the area-based size distributions with the dilution factor;
- The lowest dilution which provides an efficient disclosure of the biomass allowing a maximum percentage of objects to be identified;
- and the minimum degree of deviation from the morphological characteristics corresponding to the raw sludge samples or initial dilutions.

Knowing this, the dilution factor of 1:10 was selected as the most suitable for the protocol. At this dilution factor, area-based size distributions started to show the first signs of interaction between the flocs populations for most of the samples. It was also possible to find a reasonable representativeness of the three groups at this dilution factor: large flocs and the area percentages of both intermediate and small flocs were globally augmented for most of the samples, which is not verified for the 1:5 dilution, for example. Finally, the analysis of the morphological properties over the dilutions revealed that at a 1:10 dilution, the points for AS-M, AS-MI and MBR-G did not present large deviation from the ones observed for the raw sludge or initial dilution (1:2).

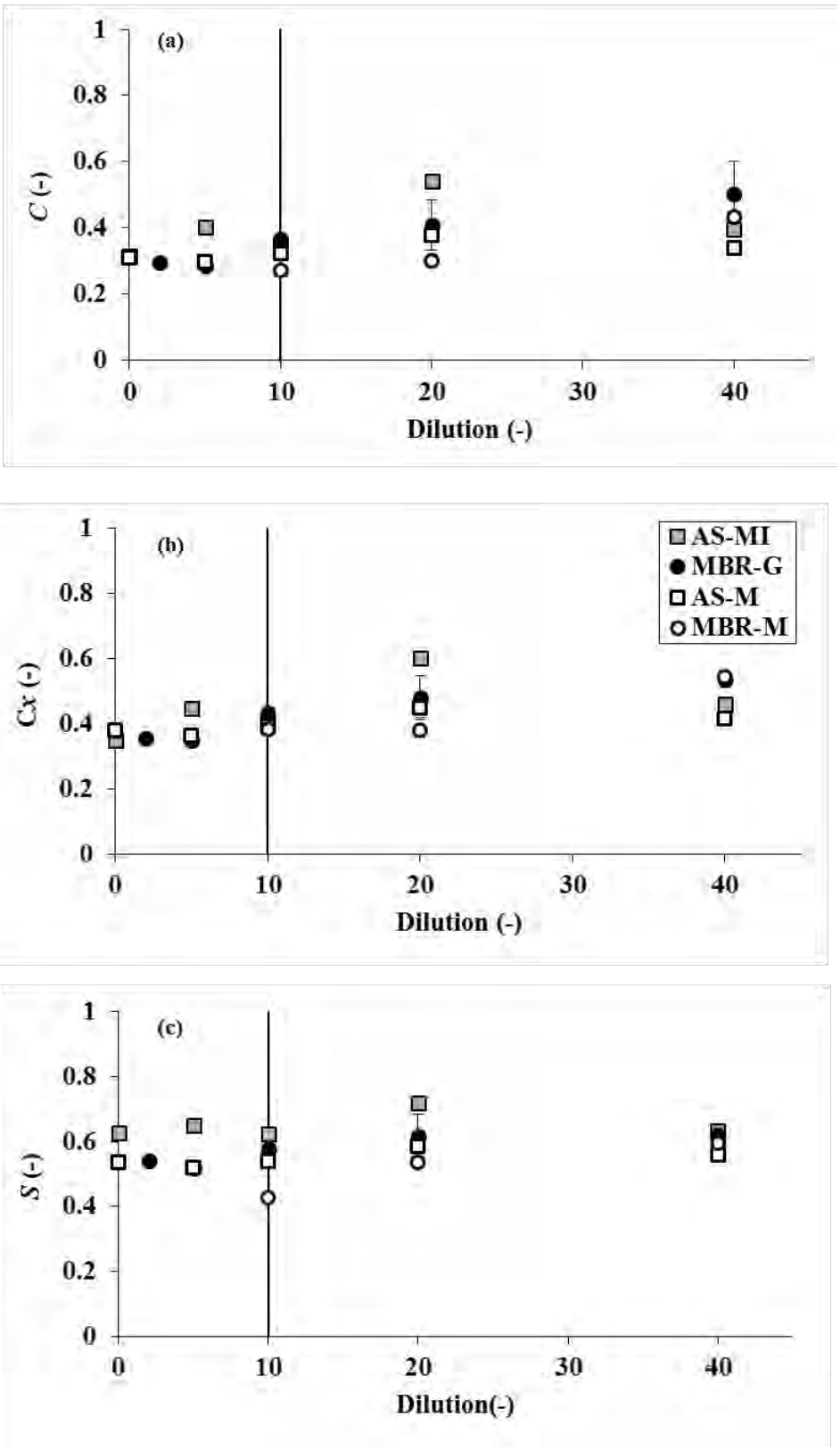

Figure III-5. Effect of dilution on the area-based mean values of (a) Circularity, (b) Convexity and (c) Solidity

III.1.3 Determination of Magnification and Analysis Stop Criterion

One of the key steps to establish a SOP is the magnification choice, in other words, that means having to select the optic lens which provides a good biomass representativeness and enables to observe several sludge flocs in detail. If the magnification can attain these two aspects, then it is possible to guarantee that accuracy will not be lost when floc morphology is measured. However, this parameter should not be determined alone in the case of the Morphologi G3 microscope. It must be determined together with the analysis stop criterion, since both factors may have an important impact on the time required to perform the measurement.

The analysis stop criterion is the parameter which defines when the analysis is stopped. It can be set, on one hand, as the Scanned Area, which means the measurement will be finished once a specific area of the wet cell has been completely screened, or, on the other hand, it can be set, on the other hand, as the Minimum Number of Particles (MNP), using this option, when a precise number of particles has been analysed, the measurement stops.

The Morphologi G3 instrument has a 5 megapixel camera and under this resolution the user can encounter the following specifications (**Table III-2**):

Table III-2. Specifications of 5x, 10x and 20x magnification available for Morphologi G3 camera.

Magnification	5x	10x	20x
Pixel size (µm)	0.56	0.28	0.14
Focal depth (µm)	24.44	6.11	3.44

Based on the reduced pixel representation and on the focal depth offered by the lens, the study was carried out only for 10x and 20x magnifications. Since one of the requirements of the SOP is to obtain a reasonable definition of the details of the floc borders, the 5x magnification option was rejected. Furthermore, regarding the analysis stop criterion, the first estimations to define the SOP were a scanned area dimension of 18 mm x 18 mm, which enables sufficient amount of biomass to be characterized and a number of particles of 50,000, which is the minimum number usually recommended to meet statistically relevant data.

Therefore, the four activated sludge samples, already presented in the last sections, were analysed in duplicate for each one of these four analysis configurations:

- Using a magnification of 10x and scanned area (18 mm x 18 mm) as analysis stopping criterion
- Using a magnification of 10x and MNP (50,000 particles) as analysis stopping criterion
- Using a magnification of 20x and scanned area (18 mm x 18 mm) as analysis stopping criterion
- Using a magnification of 20x and MNP (50,000 particles) as analysis stopping criterion

The dilution factor of 1:10, previously determined was applied for accomplishing this phase of the SOP conception. The time intervals between sampling and these tests never exceeded 1 day.

III.1.3.1 Impact of magnification and analysis stop criterion on accuracy and repeatability of the measurements.

The impact of magnification and analysis stopping criterion were investigated based on the accuracy and the repeatability of the area-based size distributions obtained after running measures on duplicate for the four samples. In order to identify first and second measures between the duplicates, they were labelled of "a" and "b", respectively. Moreover, as it can be seen in **Figure III-6**, distributions were plotted side-by-side for both magnifications and separated in two columns according to the analysis stopping criterion applied.

As first general remark, it is clearly observed a discrepancy between the flocs sizes using a 10x and 20x magnification whatever the stop criterion value. Apparently, 20x magnification shows some limitations relative to the detection of flocs with large sizes (CED > 200 µm), its distributions were always more to the left than the distributions attained using a magnification of 10x. This fact could be enough to reject the 20x magnification due its loss of accuracy. However, a more detailed explanation sample by sample is made as it follows in order to provide further evidences to this fact as well as selecting a suitable analysis stop criterion.

When AS-M sample was analysed using a 10x magnification, results have presented a good repeatability regardless of the analysis stop criterion, this can be proved by satisfactory superposition of "a" and "b" curve for both situations. On the other hand, when 20x magnification is used, repeatability is less satisfactory. Repeatability was even less satisfactory when using MNP as analysis stopping criterion in the case of 20x magnification.

For AS-MI sample, repeatability is better when using 10x magnification than 20x, when scanned area is applied as analysis stop criterion. When MNP is applied, then there is an improvement of the repeatability for 20x magnification and for 10x one, the repeatability of the curves can still be considered as good.

Regarding MBR-G sample, repeatability is less evident using scanned area than using MNP as analysis stop criterion independent on the magnification applied to run the analysis. Nevertheless, repeatability seems to be even more satisfactory if 10x is used instead of 20x magnification, in the case of MNP is set.

Finally, analyses carried out for MBR-M sample have showed a good degree of repeatability for each combination applied, being the combination scanned area an 10x magnification the best one. Repeatability could not be tested to the combination scanned area and 20x magnification due to a data that overcame more than 1 million particles and underwent software limitations.

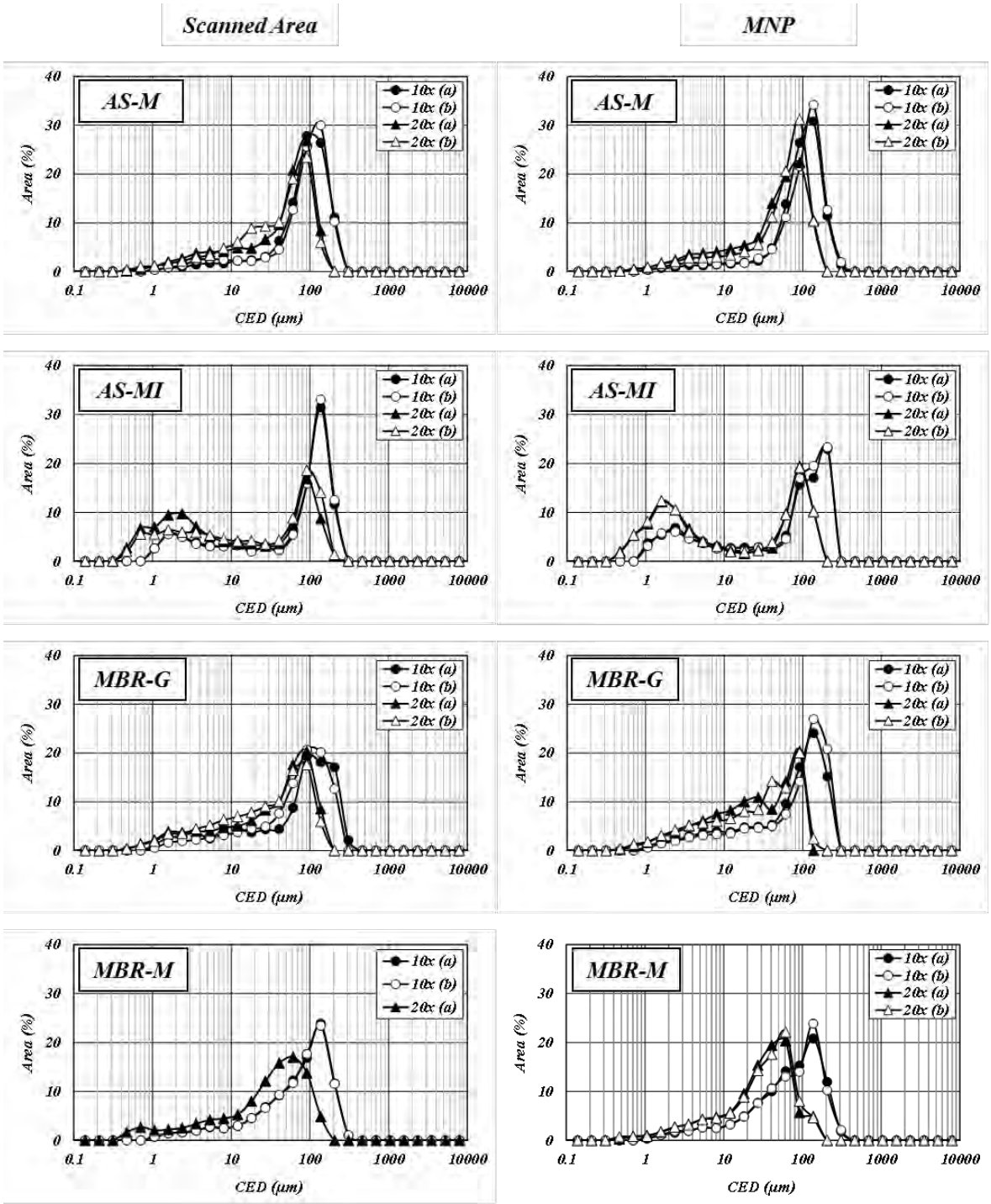

Figure III-6. Area-based size distributions on both magnifications (10x and 20x) using both analysis stopping criterion (Scanned Area and MNP) for each sample.

Based on the comments about the accuracy and repeatability of the analysis conducted for the samples, a score table (**Table III-3**) inspired in the degree of satisfaction of attain these two factors was created in order to make clear the decision for the most suitable combination.

Table III-3. Score table in terms of accuracy and repeatability of each combination for the four samples. * (+) satisfactory (-) less satisfactory

Analysis Stop Criterion	Magnification	AS-M		AS-MI		MBR-G		MBR-M	
		Accuracy	Repeatability	Accuracy	Repeatability	Accuracy	Repeatability	Accuracy	Repeatability
Scanned Area	10x	+	+	+	+	+	-	+	+
	20x	-	-	-	-	-	-	-	
MNP	10x	+	+	+	+	+	+	+	+
	20x	-	-	-	+	-	-	-	+

As **Table III-3** exposes, the combination using 10x magnification and MNP as analysis stopping criterion is the one that presents the best degree of satisfaction. It points out this combination as the potential choice for the SOP conception.

Even though the accuracy and repeatability of the data obtained through the protocol be the priority in this study, the time required to run the analysis must not be discarded. The **Table III-4** specifies how long it takes to analyse a sample using which one of the possible configurations abovementioned.

Table III-4. Comparison of the computing times for the different analysis configurations.

Analysis stop criterion	Magnification	Computing time
Scanned Area	10x	26 min
	20x	1h24 min
MNP	10x	12 min
	20x	18 min

As the integrity of the sample must be preserved, **Table III-4** reveals that using a magnification of 20x and setting the scanned area as analysis stop criterion is not feasible at all. Indeed, with such a computing time, sample might be compromised by evaporation and as consequence the results may not reflect the veracity of the sludge. Therefore, this study selected for statistical and evident reasons the configuration 10x magnification and MNP as analysis stop criterion as the most appropriate for the SOP, taking into account that the results are repeatable, all the size classes are represented and the runtime can ensure the integrity of the sample.

In addition of this conclusion, other tests were conducted to establish the minimum number of particles that should be analysed to obtain statistically reliable dataset. This next step is presented in the following section.

III.1.3.2 Minimum number of particles

By carefully choosing the number of particles that must be analysed, it is possible to achieve a relevant representativeness of the sample population. The most feasible way to set this number is running a convergence test as shown in **Figure III-7**. In this case, the evolution of the volume-based mean values for size (CED), circularity (*C*) and solidity (*S*) was plotted against the number of recorded particles. Usually, as the number of particles increases the mean values of each parameter should reach a plateau determining, then, how many particles must be included in the measure in order to acquire reliable results. Tests conducted with MBR-M sample were for mere validation purposes.

Normally, convergence tests are mostly carried out analysing the shape properties only. However, a convergence test over a size parameter as the volume-based CED was also implemented. It enabled to verify whether the number stated by the convergence test upon the shape parameters should be the true amount of particles to be taken into account in the measurements.

First of all, it can be seen that the number of particles to reach stabilization is greater for CED than for the shape parameters. For this set of samples, the results point out that the first signs of stabilization in the mean CED can be supposed when more than 80,000, 30,000, 60,000 and 50,000 flocs are analysed for AS-M, AS-MI, MBR-G and MBR-M, respectively.

For both shape parameters, the convergence seems to be rapidly attained. The first signs of stabilization can be estimated when 30,000 particles are reached for most part of the samples. Only MBR-G seemed to require more than 50,000 flocs to attain a stable plateau in the case of shape parameters.

Even though, sometimes the variability of these parameters could be considered as not substantial, minor details must be taken into account in order to make a choice. Therefore, for ensuring that any analysed sample be contained in a good degree of reliability, in which concerns their size and shape properties, 100,000 was selected as the minimum number of particles that must be analysed for carrying out the next phases of the study. Furthermore, at this amount of particles, measurements only increase about 3 minutes in the runtime.

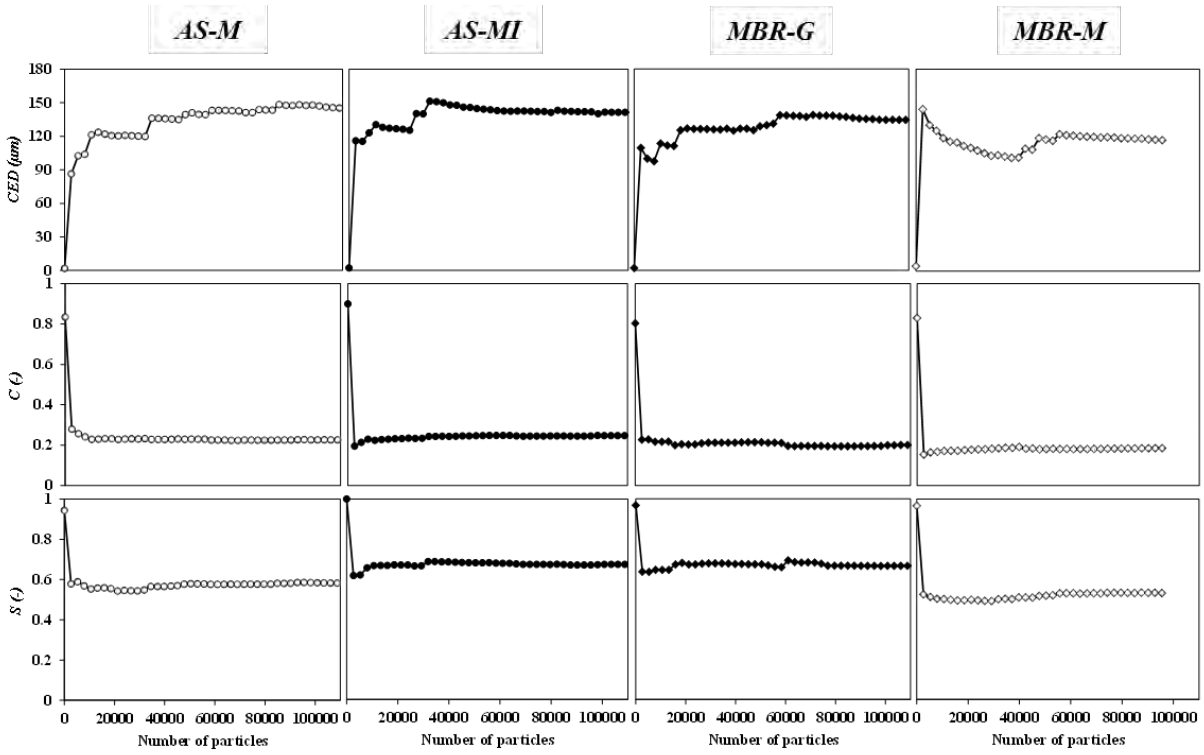

Figure III-7. Convergence test on size (CED) and shape (C and S) properties for the four samples.

These results mostly endorse that conducting a convergence test on size properties alongside shape properties can potentially enhance the quality of the results acquired during a morphological characterization. In addition, it suggests that 100 000 particles must be analysed to obtain statistically significant data.

III.1.4 Binarization

Before starting to comment about flocs segmentation, it is necessary to mention that all measurements were carried out using the same contrast conditions. In the Morphologi G3^{TM}, contrast is adjusted through an aperture diaphragm lever situated below the microscope stage. The lever is used to yield Kohler illumination, an illumination technique that provides optimum resolution and contrast in the images. In order to ensure the best resolution possible for the flocs, the measurements were always conducted with the diaphragm completely opened.

When the correct illumination allows the capture of a particle through a camera or a Charge Coupled Device (CCD), this particle is processed into pixels. Each pixel is characterized by its location and light intensity. Depending on the quality of the photographer device, the image can be displayed in colour or in black and white, known as grayscale as well. This scale generally measures the intensity of the white light from zero (no white light) to 255 (highest intensity) (Costa et al., 2013). An example of a native picture is shown in **Figure III-8 (a)**.

In order to acquire the size and the morphological parameters of the flocs, it is necessary to distinguish the pixels that are inside of those that are outside of the floc boundaries in the grey scale image, isolating them with regards to the background. This technique is generally known as the Thresholding or Binarization, when binary images are created from grayscale images.

As in most studies, the threshold established for this image analysis protocol was chosen manually, which means that is prone to human error and subjectivity. However, it should be pointed out that Morphologi G3^{TM} software is able to automatically estimate a threshold for the user needs (**Figure III-8 (b)**). This value is not the absolute value to take into account, even though it is a good first estimation towards the best threshold value.

In this study, a threshold level is aimed at correctly identifying activated sludge flocs edges and their respective pores. This should be achieved if a thin grey border completely surrounds the perimeter of the aggregate, also giving full account of the pores, exactly as it is indicated in the **Figure III-8 (c)**.

When the threshold level of 173 estimated by the software was used, the flocs were fragmented into several small flocs and it did not reflect the reality of the measure, in addition the edges were clearly eroded (**Figure III-8 (b)**). Since erosion eliminates pixels from the actual object edge, the overall effect is a tendentious data towards a floc population with smaller sizes. As a consequence, shape properties may be also affected. On the other hand, when a threshold level of 183 (**Figure III-8 (c)**), estimated manually, was used it could be considered that the aim for a thin grey border around the edge of the flocs and their complete perimeter was attained, indicating that the flocs were reasonably identified and isolated. Once the threshold of 193 (**Figure III-8 (d)**) was tested, the flocs have experienced themselves a dilatation and several small particles were created by background fading. The main effect of particle dilatation is an overestimation of its size.

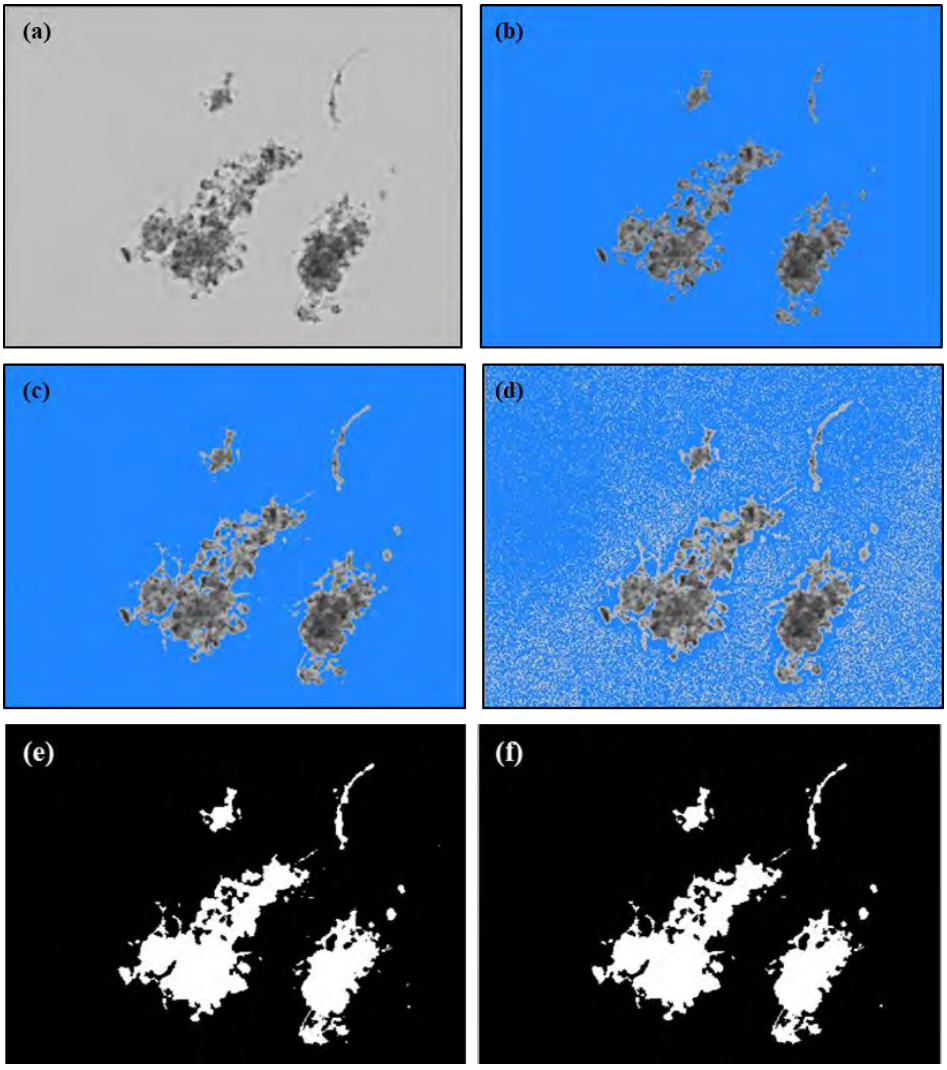

Figure III-8. Threshold levels of (a) native picture, (b) 173, (c) 183 and (d) 193 and image treatement: (e) binarization and (f) trash size filter (< 10 pixels).

Therefore, 183, within a greyscale that varies from 0 to 255, was the level of threshold adopted in this SOP to obtain a satisfactory segmentation between the activated sludge flocs and the image background. In order to complete this step and finally to have the morphology of each floc measured, the image was then binarized at this threshold level (**Figure III-8 (e)**) and a trash size filter of less than 10 pixels was applied to avoid (**Figure III-8 (f)**) any noises caused by image pixelation.

Option "Fill holes"

In all measurements, since activated sludge flocs have a porous structure, the option "Fill holes" provided by the Morphologi G3^{TM} software has not been checked. Whether not checked, any particle containing areas where the background shows voids will not be filled during the image treatment. This option has an impact on the CED, for example. A donut shaped floc has a different CED than its filled-in equivalent. Another parameter that is affected by this option is the solidity, since this shape property depends on the degree of concavities of a particle or a floc.

III.2 Application of the SOP

Once all SOP factors have been investigated and well determined, then, it is the moment of verifying its applicability. For this purpose, the four samples (AS-M, AS-MI, MBR-G and MBR-M) were submitted to a morphological characterization using the SOP exactly as it has been defined: wet cell, dilution factor of 1:10, 10x magnification, always the same contrast conditions, 100,000 as a minimum number of particles, threshold of 183 and the option "fill holes" not checked.

Since the four samples were analysed in the same conditions, SOP effectiveness was tested by comparing them in terms of their size, which means their area-based size distributions, and their shape, where the area-based circularity and solidity distributions were chosen to be represented. As a result, it is mainly expected that the SOP will be able to highlight samples particularities.

III.2.1 Comparison of the area-based size distributions

In the **Figure III-9** are displayed the area-based CED distributions corresponding to each sample.

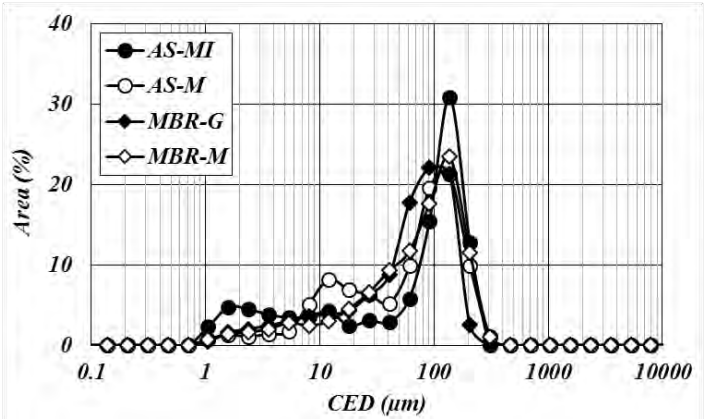

Figure III-9. Comparison of the area-based CED distributions of each sample.

As a first observation, it is possible to assume that the four sludge did not present a large variation in terms of CED mode around 150 µm. However, it seems that MBR flocs are slight smaller than the ones coming from AS samples. This fact is clearly evident in the case of the MBR fed with greywater, since the part of the curve corresponding to the largest flocs is clearly displaced on the left compared to the others. For the AS samples, the coexistence of two populations is remarked, where a contribution in area more important of the particles with a CED < 20 µm is observed in relation to the MBR samples. Moreover, the AS sample coming from the process fed with mixed wastewater, municipal and industrial, have a more pronounced contribution in area of the flocs with a CED > 20 µm than the AS process fed with municipal wastewater only. The contribution is also stronger than for the MBR samples as well. It could suggest that industrial wastewater composition might influence the flocculation ability of the aggregates.

III.2.2 Comparison of area-based circularity and solidity distributions

In the **Figure III-10** are displayed the area-based circularity (C) and solidity (S) distributions corresponding to each sample.

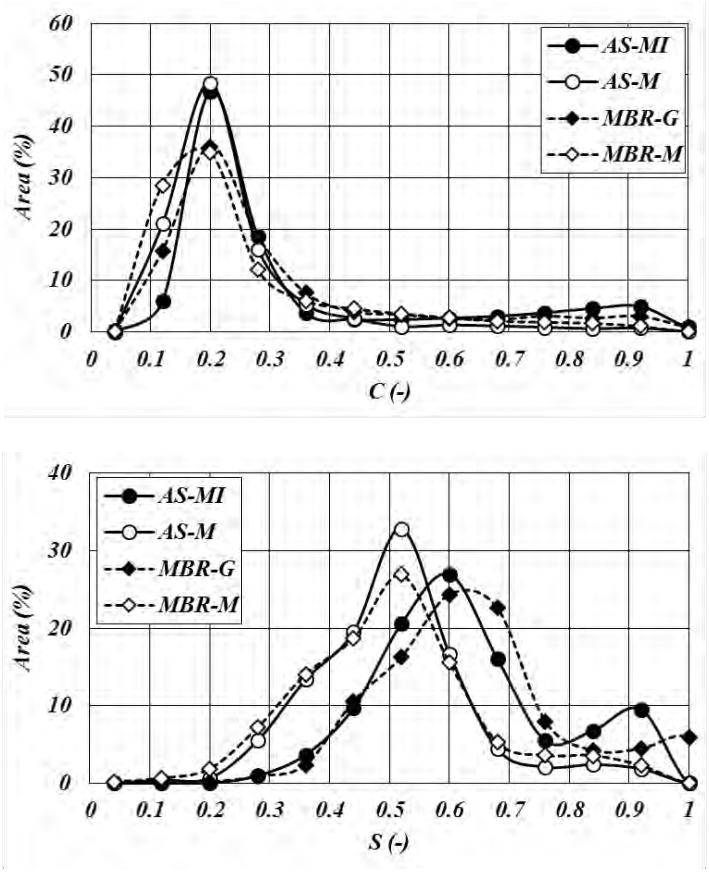

Figure III-10. Comparison of the area-based C and S distributions of each sample.

Circularity distributions suggests that sludge flocs, independent on the type of the process, present a characteristic mode value of 0.20. For the AS system cases, the distributions being more homogeneous around this mode than the MBR samples are. In addition, it must be observed that a significant portion of particles presents circularity values around 0.90, indicating that such population of flocs is quite round. This sub-population is probably constituted by the small aggregates (CED > 20 μm) which were previously noticed for AS-MI. Solidity distributions, in contrast, have revealed that the type of wastewater may have an important role on their behaviour, since for the samples coming from a process fed only with municipal wastewater, mode values were lower (0.52) than for the samples coming from a process fed with a different type of wastewater (0.60). Furthermore, the small portion of flocs of AS-MI sample, also presented high values of solidity. Taken into account that shape parameters were closer to 1 for AS-MI sample, it is then probable that industrial wastewater impacts in a certain way the aggregates flocculation.

III.3 Conclusion

The objective of this chapter was to set a Standard Operating Procedure to perform a morphological characterization of sludge flocs using the Morphologi G3. The following conclusions were drawn:

(1) A wet cell sample carrier allows obtaining a good image quality without presenting much damage to the structure of aggregates;

(2) Among the dilutions 1:5, 1:10, 1:20 and 1:40, the dilution of 1:10 provides reproducible results and enables an efficient detection of the AS flocs in the images. Moreover, at this dilution an acceptable representation of all size classes is achieved;

(3) A threshold of 183 was selected to binarize the images;

(4) Using a magnification of 10x, the level of visible details is significantly improved and the macroflocs are contained. Moreover, the image analysis of the samples is accomplished with good repeatability and in a reasonable period of time;

(5) The number of analysed particles was set to 100,000 in order to acquire a statically relevant dataset;

As a last conclusion, the fact that the SOP was established under four types of samples: from two different types of process, which treated different types of effluents, only demonstrated that the SOP herein developed has a reasonable range of applicability in which concerns morphological characterization of activated sludge flocs.

III.4 References

Costa, J.C., Mesquita, D.P., Amaral, A.L., Alves, M.M., and Ferreira, E.C. (2013). Quantitative image analysis for the characterization of microbial aggregates in biological wastewater treatment: a review. Environ. Sci. Pollut. Res. *20*, 5887–5912.

Mesquita, D.P., Dias, O., Amaral, A.L., and Ferreira, E.C. (2009). Monitoring of activated sludge settling ability through image analysis: validation on full-scale wastewater treatment plants. Bioprocess Biosyst. Eng. *32*, 361–367.

Mesquita, D.P., Dias, O., Elias, R. a. V., Amaral, A.L., and Ferreira, E.C. (2010). Dilution and Magnification Effects on Image Analysis Applications in Activated Sludge Characterization. Microsc. Microanal. *16*, 561–568.

Mesquita, D.P., Amaral, A.L., and Ferreira, E.C. (2013). Activated sludge characterization through microscopy: A review on quantitative image analysis and chemometric techniques. Anal. Chim. Acta *802*, 14–28.

Motta, M. da, Amaral, A.L., Neves, L., Araya-Kroff, P., Ferreira, E.C., Alves, M.M., Mota, M., Roche, N., Vivier, H., and Pons, M.N. (2002). Efeito da diluição na caracterização da biomassa de sistemas de tratamentos de efluentes por análise de imagem. In Proceedings of the 14th Brazilian Congress of Chemical Engineering, Natal, Brazil, p.9, CD-ROM

Perez, Y.G., Leite, S.G.F., and Coelho, M. a. Z. (2006). Activated sludge morphology characterization through an image analysis procedure. Braz. J. Chem. Eng. *23*, 319–330.

Chapter IV. Influence of sludge retention time (SRT) on activated sludge process performance and floc morphology

An Image Analysis (IA) methodology was carefully developed to aid at the lab-scale pilot oversight, mostly, in which concerns the shape and the size descriptors of the activated sludge flocs. Since the IA procedure is established, the aim is, from now on, to combine it with the classical surveys that are usually applied in full-WWTPs, which means TSS, SVI, COD and nitrogen contents monitoring. As a result, a better comprehension of the activated sludge systems behaviour under variations of operating conditions is expected. This chapter, then, introduces the first part of the experimental results that were found by subjecting the lab-scale pilot plant to different Solids Retention Times (SRTs). As it will be seen, the results mainly consisted of a follow-up of the sludge and effluent quality parameters, and of the morphological parameters which describe the activated sludge flocs.

IV.1 Variating Solids Retention Time (SRT) in the lab-scale pilot plant.

In this first experimental campaign, the lab-scale pilot plant, which was already presented in the **Chapter II**, worked during a total period of 105 days. Within this period, the influence of variating the SRT values was investigated on the process performance and on the morphological properties of the flocs. For that purpose, 3 Solids Retention Times (SRTs) were evaluated: 15, 20 and 30 days. As mentioned in **Chapter II.2.3**, the SRT is regulated by daily wasting an amount of the exceed sludge contained in the system (Q_E). The period in which the pilot plant stayed at a same SRT and the amounts of exceed sludge that should be wasted according to each SRT are detailed in the **Table IV-1**.

Table IV-1. Summary of the wasted amount of excess sludge and the duration of each period.

	Acclimation (SRT-15)	*Micronutrients addition (SRT-15)*	*SRT-20*	*SRT-30*
Q_E ($m^3.d^{-1}$)	0.002	0.002	0.0015	0.001
Period	Day 1 to 30	Day 31 to 45	Day 46 to 65	Day 66 to 105

At the beginning of the campaign, throughout the acclimation phase, the fresh activated sludge had twice the SRT of 15 days to adapt itself to the new environmental conditions. During the sludge acclimation, the feed solution contained only glucose, ammonium chloride and monobasic potassium phosphate. Since it was observed the need of adding micronutrients to the synthetic feed solution, for improving microbial activity, an additional period at a SRT of 15 days was equally respected. The composition of the full synthetic feed solution can be checked in the **Table II-1**. The composition was then kept constant during the rest of the campaign, as well as during the second campaign that will be discussed in the next chapter.

After the SRT of 15 days, the SRT was modified to 20 and then to 30 days. The general responses of the pilot-plant to the micronutrients addition and to the transitions of SRTs were then assessed. Along this first campaign, the room where the lab-scale pilot was installed passed through some maintenance interventions, making some routine measurements unfeasible.

In the following sections, *Acclimation* phase and the moment that *Micronutrients addition* took place will be clearly highlighted as well as the periods above presented by the terms: *SRT-15*, *SRT-20* and *SRT-30* for a solids retention times of 15, 20 and 30 days, respectively.

IV.2 Lab-scale pilot plant performance

IV.2.1 Monitoring of Temperature, Dissolved Oxygen (DO) and pH

Temperature, DO concentrations and pH values were continuously monitored during the whole experimental campaign. As it was sketched in the **Chapter II**, these values mostly correspond to the aerated tank environment. **Figure IV-1**, below, illustrates how such parameters have evolved over the switches of SRTs.

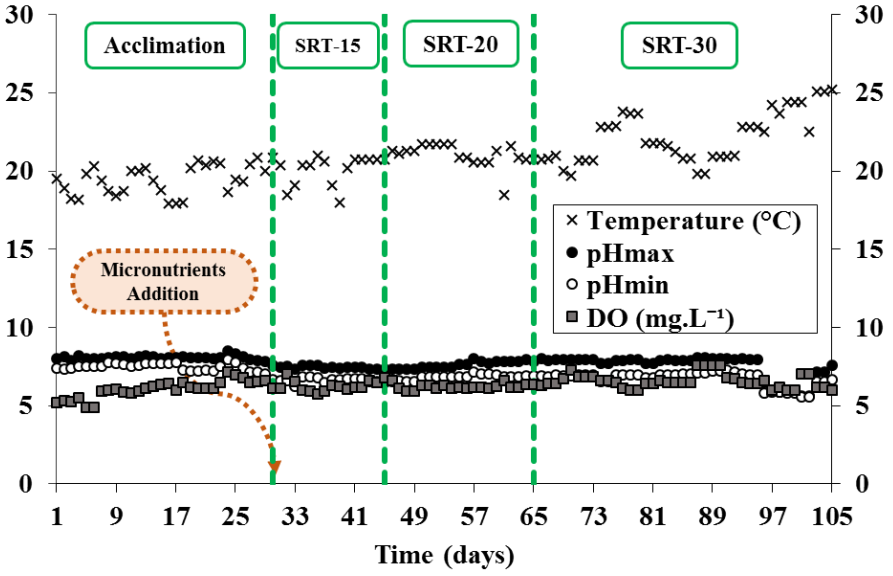

Figure IV-1. Variations of temperature, DO concentration and pH values over the switches of SRTs.

To supplement **Figure IV-1** interpretation, a statistical approach of the results is proposed in **Table IV-2**, which presents the mode (most probable value), the median (central point in the range of values) and the range values in each period for this set of physicochemical parameters.

If the temperature registers are analysed first, the fluctuations of the means over the days can be considered perfectly normal, since seasonal changes can take place exactly as it occurs in a real WWTP. For instance, a slight rise of the temperatures throughout the last two weeks could be identified due to summer season beginning. Despite this, it must be pointed out that no significant fluctuations existed during one single day and any register of a day goes beyond extreme temperatures as too cold or too warm.

Table IV-2. Statistical summary (mode, median and range of variation) for each period in the campaign regarding the temperature, pH values and DO concentration.

Acclimation			
	Mode	**Median**	**Range**
Temperature (°C)	20.0	19.5	17.9 – 20.8
pH_{max}	8.1	8.1	7.5 – 8.5
pH_{min}	7.7	7.5	6.6 – 7.9
DO ($mg.L^{-1}$)	5.8	6.1	4.9 – 7.1
SRT-15			
	Mode	**Median**	**Range**
Temperature (°C)	20.8	20.4	18.0 – 21.0
pH_{max}	7.4	7.4	7.3 – 7.6
pH_{min}	6.7	6.7	6.2 – 6.8
DO ($mg.L^{-1}$)	6.2	6.2	5.7 – 7.0
SRT-20			
	Mode	**Median**	**Range**
Temperature (°C)	21.7	21.2	18.5 – 21.7
pH_{max}	7.3	7.6	7.3 – 8.0
pH_{min}	6.8	6.8	6.5 – 7.1
DO ($mg.L^{-1}$)	6.1	6.2	5.9 – 6.6
SRT-30			
	Mode	**Median**	**Range**
Temperature (°C)	22.8	21.8	19.7 – 25.2
pH_{max}	8.0	7.9	5.5– 8.0
pH_{min}	6.9	6.9	5.5 – 7.3
DO ($mg.L^{-1}$)	6.5	6.5	6.0 – 7.6

The pH was maintained as much as possible inside the reference pH range, it means between 7.0 and 8.0. Due to aeration sequencing, pH reaches maximum values during the aerated cycle, and minimum values during the anoxic periods. Most of this difference can be explained by an efficient homogenization promoted to the mixed liquor when the aeration is turned on. No major effects owing to *Micronutrients addition* were evidenced on the pH behaviour, apart from an acceptable decrease in its values.

Nevertheless, a further decrease in both pHs (max and min) was observed in the end of the *SRT-30* period. According to Van den Broeck et al. (2012), at higher SRTs as 30 or even 50 days, the nitrification rate is increased. Since nitrification reaction is source of ions H^+, due to the oxidation of the ammonium contents, this could lead to an acidification of the medium by increasing their concentration. For confirming this statement, a lowering in the inferior limit of the pH ranges during *SRT-30* in relation to the other periods can be observed.

A critical DO level of 2 $mg.L^{-1}$ during aerated cycles is highly recommend to avoid risks as the overgrowth of filamentous bacteria (Tandoi et al., 2006). In order to satisfy this condition, the DO levels were always kept above 4 $mg.L^{-1}$. Therefore, the minimum values of the DO concentrations during aerated cycles have always met the requirement initially proposed to the pilot system.

IV.2.2 Monitoring of the sludge properties

Figure IV-2 displays the evolution of biomass concentration, expressed herein by the total suspended solids (TSS) concentration, as well as the sludge volume index (SVI) over the *Micronutrients addition* and the switches of SRT: 15, 20 and 30 days. TSS and SVI measures were daily performed during the whole experimental campaign.

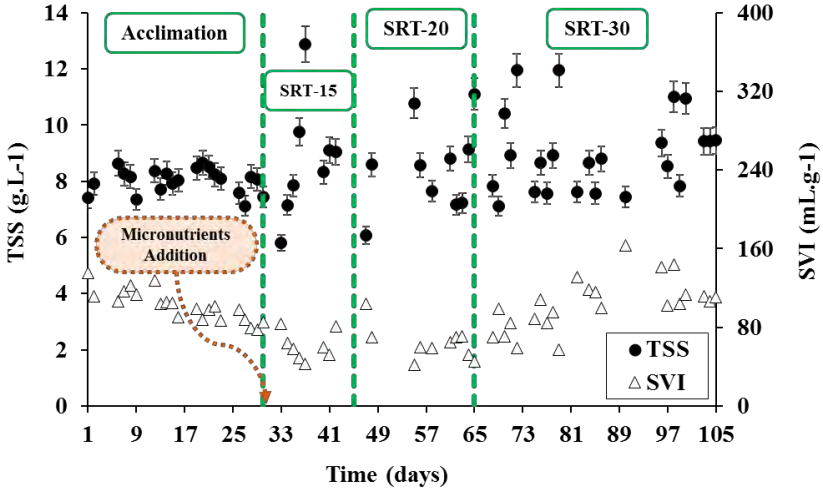

Figure IV-2. Variations of TSS and SVI over the switches of SRT.

Table IV-3 summarizes the range of values observed for TSS and SVI throughout the acclimation phase and the other periods of different SRTs.

Table IV-3. Range of values for TSS and SVI at the different periods of this experimental campaign.

	Acclimation (SRT-15)	*Micronutrients addition (SRT-15)*	*SRT-20*	*SRT-30*
TSS ($g.L^{-1}$)	7.1 – 8.6	5.7 – 12.8	6.1 – 11.1	7.1 – 11.9
SVI ($mL.g^{-1}$)	77.4 – 135.5	42.6 – 83.4	41.0 – 104.3	57.4 – 163.6

The *Acclimation* phase aims to enable the system to reach a steady-state condition by allowing the biomass to adjust itself to a new environment. Generally, stability is achieved when small variations of TSS and SVI values can be verified. Within this phase, both parameters have demonstrated some fluctuations during 1 SRT and then, tighter ones as a period of 2 SRTs is completed. Regarding the range of TSS concentration for this phase, it was considered reasonably heightened in comparison to what is normally expected (about 5 or 6 $g.L^{-1}$) for the organic load rate applied to the system. On the other hand, the values of SVI were inside the range which designates the activated sludge as presenting adequate compaction and consequently exhibiting an efficient solid-liquid separation in the clarifier (Tandoi et al., 2006).

The addition of micronutrients in the synthetic feed solution about *Day-30*, as evidenced in the **Figure IV-2**, was associated to a need of stimulating the growth of nitrifying bacteria. The particular interest in this type of bacteria will be clarified in the next sections, but for now, it is important to underline that the fact of adding micronutrients to the system have had an overall short-term effect. It mostly boosted the biomass growth until the middle of this period corresponding to *SRT-15*, which soared until to attain a concentration of 12.8 $g.L^{-1}$ and, then, it decreased again to values before noticed. SVI values for this period were even lower than the ones observed during *Acclimation* phase ensuring clarifier performance.

Throughout *SRT-20* and *SRT-30*, TSS contents have presented a profile less stable than the two previous periods. This variability is coherent with the results reported by Van den Broeck et al. (2012), which obtained larger variations in TSS concentrations as the SRT had been changed from 10 to 30 days. Bisogni and Lawrence (1971), which investigated the influence of SRT on activated sludge settling characteristics, believe that systems that are operated at high SRTs tend to increase the amounts of lost solids in the final effluent. This could mostly justify the variability of TSS values observed for the *SRT-30,* as it will be seen in the following paragraphs.

Regarding SVI values, there were no significant changes between the values of *SRT-15* and *SRT-20*. However, from *SRT-20 to SRT-30*, it is possible to notice a gradual increase of the values until the *Day-90*. In this case, it could be assumed that a less efficient bioflocculation started taking place, since a sludge that presents a SVI value over 150 $mL.g^{-1}$ might be considered as one with a not so good settleability (Grady et al., 2011). It could explain why solids were being lost during *SRT-30* and consequently why TSS have varied more in this period than in the others.

IV.2.3 Monitoring of effluent quality parameters

The pilot system was operated for degradation of organic matter and for nitrification-denitrification purposes. Therefore, the efficiencies in terms of COD and Nitrogen (TN) removal were used to evaluate the process performance.

COD and TN measurements for the synthetic feed influent, i.e. COD_{IN} and TN_{IN}, were measured at the beginning of *Acclimation* phase and after *Micronutrients addition*. COD and TN analyses at the outlet effluent, COD_{OUT} and TN_{OUT}, were performed with a frequency of once a week. NH_4^+ and NO_3^- contents were quantified as well in the outlet effluent with the same frequency. Since other forms of nitrogen exists in the outlet effluent, it could be quantified by the subtraction of the amounts of NH_4^+ and NO_3^- from the amount of TN. This difference was denominated residual nitrogen (Residual N). The evolution of effluent quality parameters is presented in the **Figure IV-3 (a-b)**.

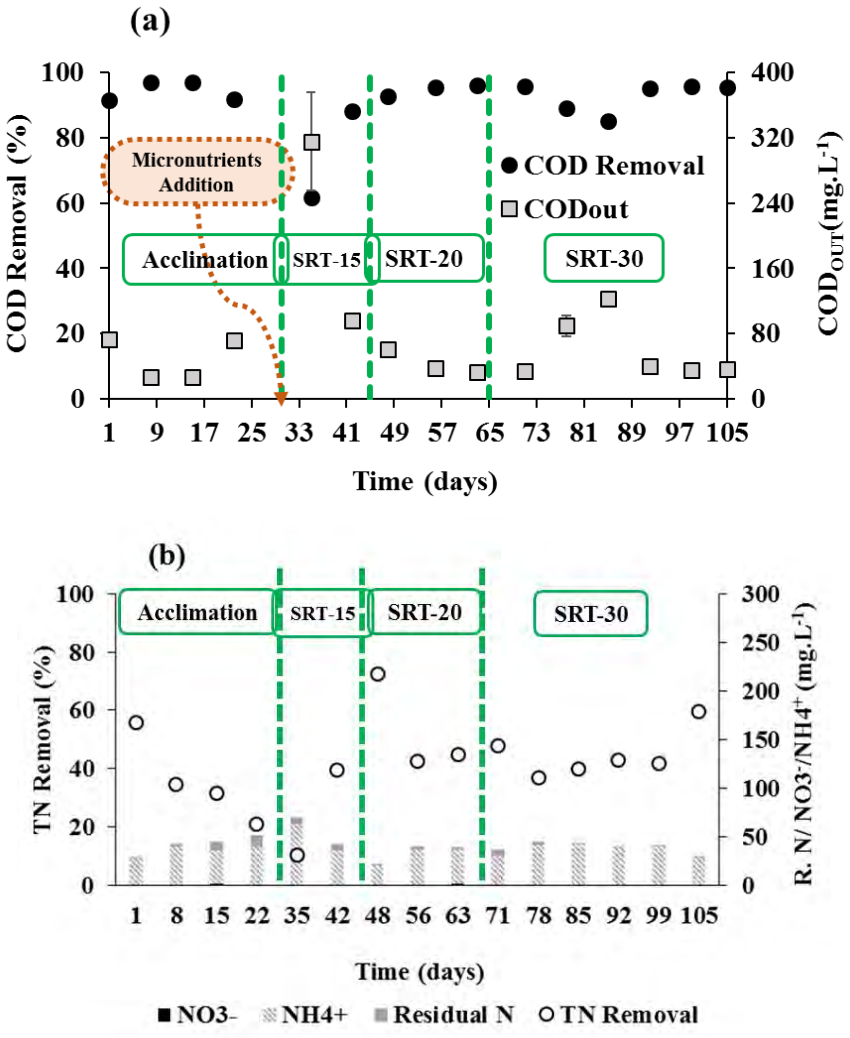

Figure IV-3. Variations of the effluent quality parameters: (a) COD and (b) TN removal over the changes of SRT.

In order to make **Figure IV-3** even more readable, **Table IV-4** shows COD_{OUT}, TN_{OUT} and the nitrogen contents at the outlet effluent in the end of the different periods of this campaign. Since

COD_{IN} and TN_{IN} for each period are also presented, it enables to check up their respective removal efficiencies.

The lab-scale pilot was able to attain excellent levels of organic removal efficiencies throughout *Acclimation* phase (**Figure IV-3 (a)**). This result is confirmed by the low concentrations of COD_{OUT} for this period, they ranged from 26.7 to 73.1 $mg.L^{-1}$ achieving a maximum COD removal of 97.0 %. On the other hand, TN removals seem to lean towards a progressive decrease during this phase (**Figure IV-3 (b)**). The efficiencies were lower than 50.0% after the first week of operation, where most part of the remaining nitrogen was still under the NH_4^+ form. Two possible explanations can be advanced: (1) an underdevelopment of the population of nitrifying bacteria to consume an important part of the nitrogen introduced into the system, or (2) the population of nitrifying bacteria had correctly developed, but the exceed quantity of existing nitrogen lead to an inhibition of their activity. Taking into account these two assumptions, the addition of micronutrients was thought as a corrective measure for improving nitrification process only, since denitrification has not demonstrated any sign of failure. That last point could be verified by the low NO_3^- concentrations remarked along the whole *Acclimation* phase.

The first COD_{OUT} measured after *Micronutrients addition* was about 320.0 $mg.L^{-1}$, a concentration reasonably higher when compared to the precedent ones from the *Acclimation* period. However, once it is observed, this measure is accompanied by large variability and the next measure at the *Day-42* (about 80.0 $mg.L^{-1}$) seems in accordance with what has been seen before. Thus, this prompt rise might reflect only the modification of the effluent properties, or it could be either interpreted as a pulse of micronutrients that were not consumed yet and then interfered with the COD measurements. Such disturbance caused by the micronutrients was less evident for TN removal efficiencies. Even though these rates were lower than the expected, at the *Day-42,* it is possible to notice some improvement mainly in relation to the consumption of NH_4^+, which is the main target of the *Micronutrients addition*.

The transition from *SRT-15* to *SRT-20* is followed by a COD_{OUT} range that remained between 33 and 38.3 $mg.L^{-1}$, which means good levels of degradation of organic matter. When working with an SRT of 20 days the pilot system has presented COD removal efficiencies equal or above 96%. This transition is either followed by a peak of TN removal of 72% right in the beginning. However, the efficiencies decreased again, this time, around 40%, one week after, maintaining at least a removal rate near to what has been previously detected at the end of the period respected for *Micronutrients addition*.

Switching from *SRT-20* to *SRT-30* produced a slight decrease of the COD removal efficiencies. A removal of about 88.0 % was observed at the *Day-85*, with a correspondent COD_{OUT} concentration of 122.7 $mg.L^{-1}$. The presence of dispersed solids in the outlet effluent could suitably explains this concentration as for this same period a small increment of SVI values were observed as well (**Figure IV-2**). Since it indicates a possible loss of the sludge settleability, the existence of solid material in the withdrawn samples is completely understandable. Nonetheless, this disturbance has no longer last and removal efficiencies stabilized again around 96%. In terms of TN removal, as compared to the rates seen at *SRT-20*, any meaningful progress could be notice. From the middle of *SRT-20* until the end of *SRT-30*, pHs values started oscillating even more among values that can be considered by Yoo et al.

(1999) as out of the optimal range (7.0 – 8.0) that favours nitrification reaction. Thus, it could be also the reason why the nitrogen contents are mostly composed by ions NH_4^+.

In general, apart from the *Day-37* and *85,* the removal efficiencies of organic matter throughout the whole campaign was always above 90 %. TN removals were maintained near to 40%, the *Micronutrients addition* presenting a short-term effect over their efficiencies. It is likely that improvements expected by this corrective measure has been supressed by the oscillations of the pH values.

Table IV-4. Lab-scale pilot plant performance in terms of COD, TN removals and concentration of nitrogen in the end of each phase at different SRTs. *M.A. = *Micronutrients Addition*

Period	COD_{IN} ($mg.L^{-1}$)	COD_{OUT} ($mg.L^{-1}$)	**COD removal (%)**	TN_{IN} ($mg.L^{-1}$)	TN_{OUT} ($mg.L^{-1}$)	**TN removal (%)**	NH_4^+ ($mg.L^{-1}$)	NO_3^- ($mg.L^{-1}$)	Residual. N ($mg.L^{-1}$)
Acclimation	875.3 ± 6.6	71.8 ± 6.2	**91.8**	64.5 ± 1.5	51.1 ± 1.3	**20.9**	39.7 ± 5.6	0.56 ± 0.06	10.8
M.A.(SRT-15)*	824.6 ± 14.5	83.3 ± 1.8	**90.1**	69.5 ± 2.0	42.2 ± 2.0	**39.4**	34.8 ± 0.4	0.05 ± 0.01	7.28
SRT-20	824.6 ± 14.5	33.8 ± 1.6	**95.9**	69.5 ± 2.0	38.3 ± 1.1	**44.9**	35.2 ± 0.5	0.77 ± 0.27	2.28
SRT-30	824.6 ± 14.5	36.6 ± 3.7	**95.6**	69.5 ± 2.0	28.2 ± 0.3	**59.5**	28.0 ± 0.2	0.15 ± 0.01	0.05

IV.3 Morphological properties of the activated sludge flocs at different SRTs

This section introduces the first results found by applying the IA procedure previously developed. The use of the IA procedure to carry out a morphological characterization over the flocs can be considered a step forward in order to obtain a better understanding of their size and shape dynamics throughout operating condition variations. Indeed, such aim constituted the core of this study, which can be mainly reached by analysing the size and shape properties alongside the process performance parameters.

The morphological characterization was mostly based on the assessment of the Circular Equivalent Diameter (CED), which was designated to characterize the size of the flocs, and the circularity, convexity and solidity, which were selected to describe them in terms of their shape properties.

IV.3.1 Sampling in the lab-scale pilot

Since the SOP was applied to carry out morphological analyses on the sludge coming from the lab-scale pilot (presented in the **Chapter II**) a supplementary step was required before carry out any morphological characterization relative to the experimental campaign: to verify if there are significant differences on the morphological characteristics of the flocs collected during the aerobic phase compared to the ones collected during the anoxic step.

As it is known, the lab-scale pilot work under an alternating aerobic-anoxic process, the presence of aeration or not could influence the results regarding the morphological characterization of the aggregates. Thus, sludge samples were collected at the end of each sequence from the bottom of the aerated tank and analysed using the SOP developed herein.

Firstly, in order to put in evidence the potential difference between the morphological properties depending on the process phase, the CED volume-based distributions corresponding to each phase were plotted side by side in the **Figure IV-4**.

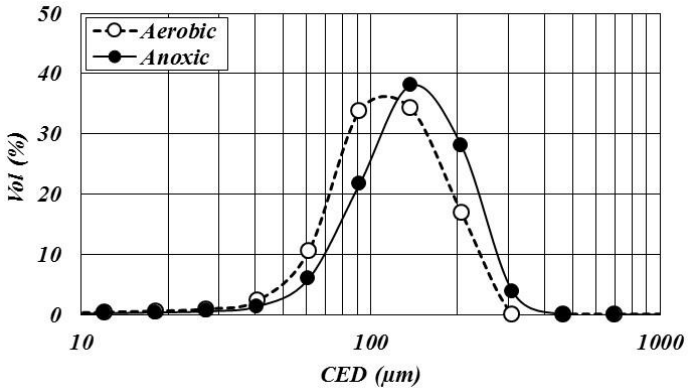

Figure IV-4. CED distributions on volume basis for the aerobic and anoxic sequencing.

Comparing the CED distributions on volume basis for these two sequences, it is possible to remark that activated sludge flocs collected when aerobic cycle was running are just slightly

smaller than the flocs coming from the anoxic sequencing. The CED modes are about 140 µm for both aerobic and anoxic sequencing. The sludge flocs may be smaller during the aerobic sequencing because they are submitted to the shear stress due to aeration, which could promote floc breakage. Although aeration be considered a key factor on floc size, it is true that other factors could also explain this slight difference between the distributions, such as CO_2 release and flocs collision resulting from agitation effects (Yuan and Farnood, 2010).

Likewise, the effect of sampling throughout aerobic or anoxic sequencing was investigated over the floc shape properties as well. For this aim, circularity (C) and solidity (S) volume-based distributions for both sequences are plotted in **Figure IV-5**.

Analysing first the circularity (C) distributions, it may be concluded that activated sludge flocs sampled during aerobic sequencing have a form slightly more round as compared to the ones collected throughout anoxic cycle, the modes are 0.21 and 0.19, respectively. Furthermore, through the aerobic sequencing distribution, it is still possible to assume that the floc population has become more homogeneous, in terms of its circularity, during this cycle.

Focusing then on the solidity (S) distributions, it is possible to observe an almost perfect overlapping of the distributions with modes at 0.60, indicating that for this case, in particular, solidity distributions have shown no difference between sampling throughout aerobic or anoxic sequencing.

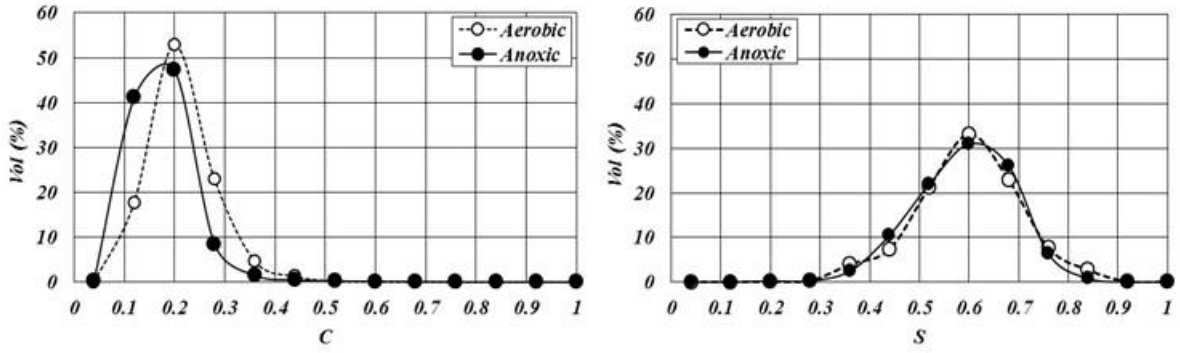

Figure IV-5. Circularity (C) and solidity (S) distributions on volume basis for the aerobic and anoxic sequencing.

In summary, a slight variability for CED and circularity distributions between the sequences has been noticed, while solidity distributions have presented almost the same behaviour in both. It may suggest that sampling during one sequence or another brings some difference between the results, not in a considerable manner, but it cannot be neglected even though. Nonetheless, activated sludge samples for morphological characterization were always taken at the end of aerobic sequencing taking into account that aeration could guarantee a good homogenization of the analysed samples

IV.3.2 Evolution of the size and shape properties distributions

An analysis of how size (CED), circularity, convexity and solidity distributions have evolved along this experimental campaign can provide another point of view in which concern the

dynamics of the floc populations throughout the changes of SRT. Likewise the mean values, volume-based distributions were determined for each one of the parameters with a frequency of once a week. Remembering that when a distribution is represented on volume basis, the large flocs are put in evidence and thus, it turns into a more feasible approach to delineate the characteristics of the whole population

In the next figures, distributions are represented by dashed lines and green colour for indicating a beginning or a transition between two periods (acclimation or *SRT*). Then, the evolution of the distributions over time is represented by a colour gradient that fills in the mark series. It changes from a dark colour to a lighter one, which always indicates the end of a period. Furthermore, each period has its own shape of mark, for example, *Acclimation phase* is characterized by a triangle. A basic principle for understanding those graphs is to pay attention to the displacement of the distributions curves as it will be commented.

IV.3.2.1 Acclimation phase

Figure IV-6 displays the evolution corresponding to the floc size (CED) distributions throughout the *Acclimation phase*.

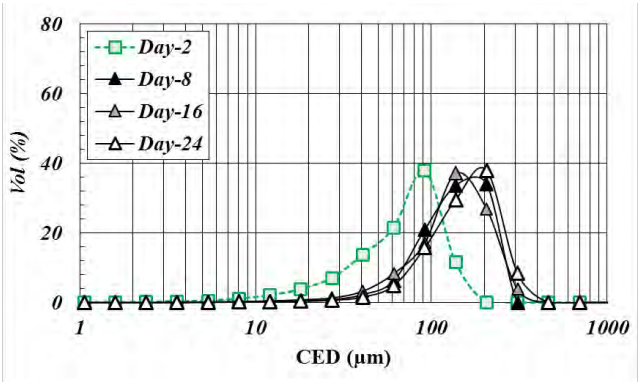

Figure IV-6. Evolution of size (CED) distributions on volume basis for *Acclimation*.

The initial size distribution (on *Day-2*), which characterizes the inoculated sludge, presented a floc population whose mode is around 90 µm. Almost a week after the beginning of the pilot system, it is possible to observe a shift of this population towards larger sizes, represented in the graph by the displacement of the distribution to the right on *Day-8*. It meant an increase of approximatively 35% of its mode (of about 140 µm). The measurements ran on *Day-16* and *24* mostly suggests a stabilization of this parameter until the end of the *Acclimation* period.

In the **Figure IV-7,** the evolution of the circularity, convexity and solidity distributions throughout the *Acclimation* is represented. The initial distributions for each one of these shapes properties evidenced the presence of a small group of flocs among the whole population that is more circular and convex (the mode of this sub-population is around 0.45 for the circularity distribution and around 0.5 for the convexity distribution). One week later, under the conditions imposed by a typical activated sludge process, it is possible to observe the reduction of this specific group. On the other hand, the population became more circular, convex and solid as well. This fact is illustrated by a slight displacement of all distributions towards the right (on

Day-8). *Day-16* and *24* are remarked by a back and forth displacement of the circularity and convexity distributions. This movement is observed for solidity distributions either, but differently from circularity and convexity distributions, it did not come back and superpose the same mode value. Hence, a difficulty for finding a stable point is noticed over the displacement of solidity distributions.

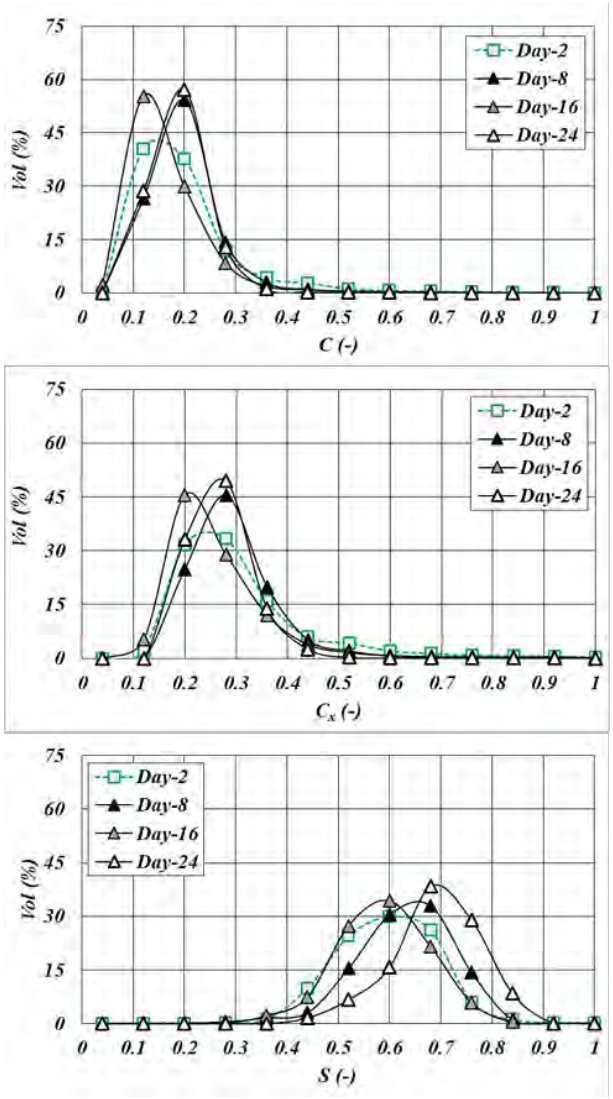

Figure IV-7. Evolution of circularity (*C*), convexity (C_x) and Solidity (*S*) distributions on volume basis for *Acclimation*.

Since the image of the flocs are registered through the measurements, **Table IV-5** enables a comparison between those flocs in the beginning and in the end of *Acclimation phase.* Unquestionably, these images are given as examples to help phenomena visualization, but they cannot represent the whole diversity of flocs.

Table IV-5. Typical flocs from the *Day-2* and *24* of the *Acclimation phase.*

Day-2	Day-24
	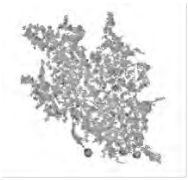
CED = 104.3 µm *C* = 0.19 C_x = 0.27 *S* = 0.62	*CED* = 134.7 µm *C* = 0.20 C_x = 0.30 *S* = 0.66

When these flocs are compared, it is obvious that there was an increase in their sizes. Nevertheless, their appearance does not seem to have changed along the *Acclimation*, it could suggest that a steady state condition for shape properties has been reached instead, even for solidity which provides an idea of the degree of concavities on the floc. Therefore, since solidity is sensitive to the overall surface of the floc, the variability that has been verified during *Acclimation phase* might be associated with a variation of floc surface rather than a change of floc shape.

IV.3.2.2 The transition from SRT-15 to SRT-20

Figure IV-8 presents how floc size (CED) distributions evolved throughout the first transition of SRT, from 15 to 20 days. The diamond mark series was highlighted in orange to represent floc characteristics after *Micronutrients addition.*

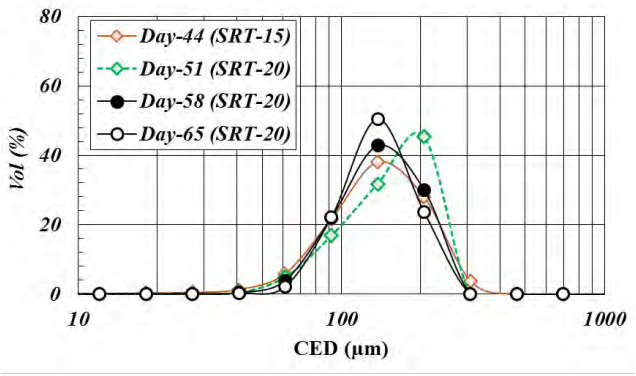

Figure IV-8. Evolution of size (CED) distributions on volume basis for *SRT-15* to *SRT-20* transition.

Floc size distribution corresponding to *Day-44* exhibited a mode value around 140 µm. It means that floc population have not presented any important change in terms of size since the beginning of the micronutrients addition. On *Day-51*, then, the first measurement equivalent to an SRT of 20 days indicated a modification of the floc size distribution: it has narrowed and the peak moved to the right. This movement can be mostly interpreted as an increase of floc size due to a population of aggregates that have become even larger after SRT transition, presenting

a mode value around 200 µm. However, this movement has a transient behaviour and distributions recovered again a mode of about 140 µm. In addition, floc population tended to a gradual homogenization since distributions (from *Day-58* and *65*) had narrowed themselves around the same mode.

Likewise size distribution, all shape properties distributions corresponding to the *Micronutrients addition* had presented an almost similar behaviour to the last ones observed for *Acclimation* (**Figure IV-9**). Then, after SRT transition, circularity distribution performed a shift towards the right indicating that floc had become more circular (a mode of 0.28), a fact that emphasizes the importance of checking out the distributions since it is less flagrant by verifying the mean values as it will be seen (section **IV.3.3**). Regarding convexity and solidity distributions, only a homogenization of floc population in terms of these two characteristics could be identified by comparing the distributions before and after SRT transition.

On *Day-58*, about two weeks after the transition, another displacement of circularity distribution was observed towards the right. At this same time, convexity and solidity distributions also performed a shift to the right, being a slighter one in the case of the convexity. By the end of *SRT-20*, circularity and solidity distributions had, one more time, their modes lying in 0.2 and 0.6, respectively, while convexity distribution stayed similar at 0.35. Although floc population seemed to become more heterogeneous in terms of solidity, since its distribution starts presenting more than one mode, it could be concluded that shifts caused on shape properties distributions, by this SRT transition, were not permanent as well.

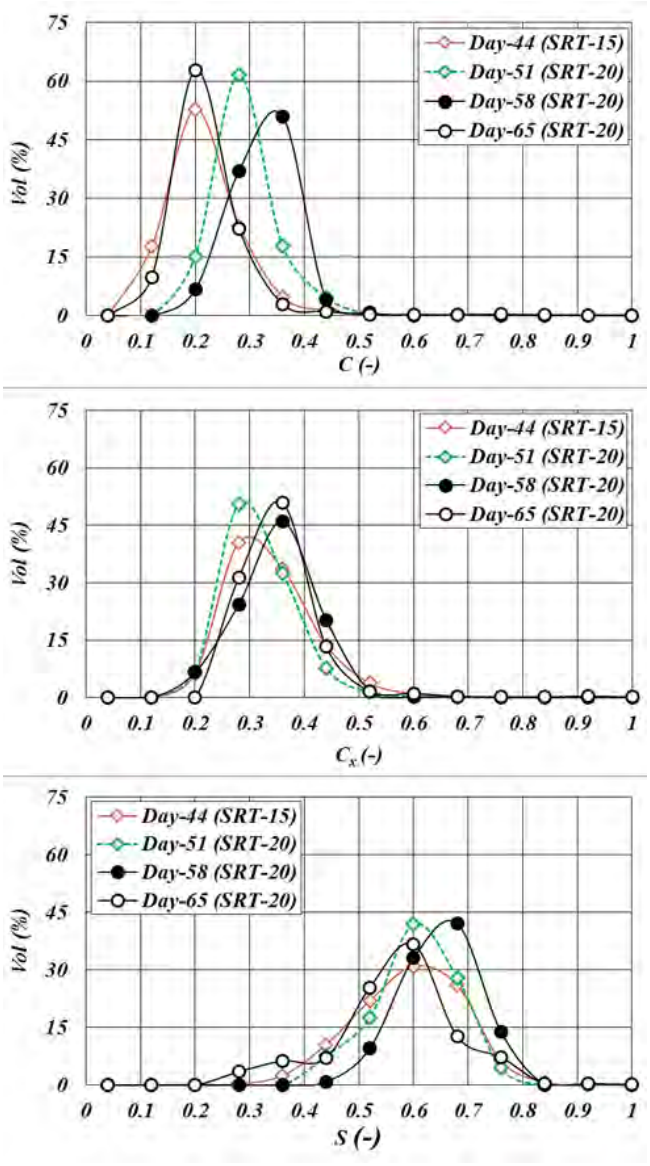

Figure IV-9. Evolution of circularity (*C*), convexity (C_x) and Solidity (*S*) distributions on volume basis for *SRT-15* to *SRT-20* transition.

Table IV-6. Typical flocs encountered on the Day-44, 51 *and* 65. from *SRT-20*.

Table IV-6. Typical flocs encountered on the *Day-44*, *51* and *65*.

Day-44	Day-51	Day-65
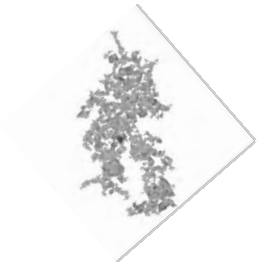	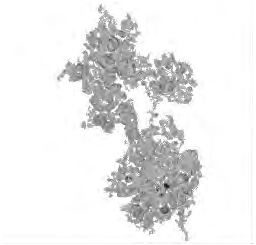	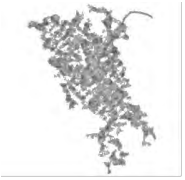
CED = 131.4 µm *C* = 0.19 C_x = 0.30 *S* = 0.60	*CED* = 166.7 µm *C* = 0.20 C_x = 0.28 *S* = 0.65	*CED* = 130.2 µm *C* = 0.19 C_x = 0.31 *S* = 0.55

Flocs from *Day-51* presented a structure that reminds a more filled package than the ones from *Day-44*. Whereas flocs from *Day-65* showed a similar structure to those ones from *Day-44*. This comparison allows illustrating how flocs have changed right after SRT transition and how they have recovered most part of their initial features in the end of *SRT*-20, even if flocs solidity were somehow lower than in the beginning of this period.

IV.3.2.3 The transition from SRT-20 to SRT-30

The evolution of floc size (CED) distributions throughout the second transition of SRT, from 20 to 30 days is presented in the **Figure IV-10** below.

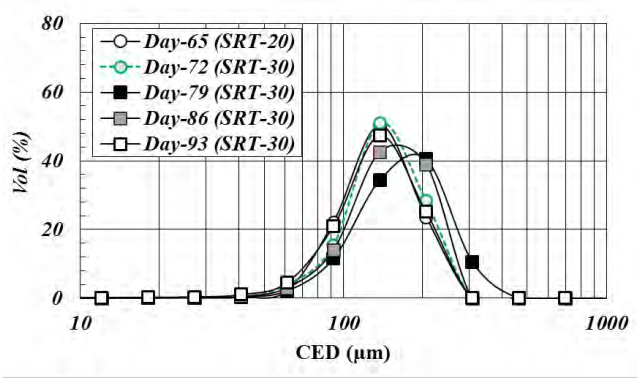

Figure IV-10. Evolution of size (CED) distributions on volume basis for *SRT-20* to *SRT-30* transition.

The first measurement after the second SRT transition, on *Day-72*, did not reveal any alteration of the floc population since the distribution had an almost perfect superposition with the one corresponding to *Day-65*. Then, two weeks after the transition, on *Day-79*, it is possible to see a similar movement to the one performed during the last SRT transition. This means a displacement that can mainly be noticed at the peaks of the distributions. Moreover, mode value for *Day-79* laid in 200 µm as well. As a pattern behaviour and despite this time it seemed to

occur more slowly, on *Day-86*, distributions start coming back to a mode of 140 µm and they finished by a homogenization of the population around this same value on *Day-93*.

A similar pattern would be also expected to the shape properties (**Figure IV-11**), however some differences were detected for circularity and solidity distributions. For example, on *Day-72*, circularity distribution shifted to the right indicating that flocs had become more circular, but not only this, the distribution also undergone a flattening, which can implicate that floc population became a few more heterogeneous. The heterogeneity of the population, about this day, can be better observed in the solidity distribution, which shows the rise of a small group with a solidity mode around 0.43. Along the next days of *SRT-30*, a progressive homogenization took place for both parameters and in the case of circularity distribution a back and forth movement is noticed as well, suggesting that SRT transition had a non-permanent effect on this parameter.

Regarding convexity distributions, any meaningful alteration could be detected, apart from a slight back and forth displacement of the modes (0.35 – 0.28 – 0.35) *on Day-72, 79* and *86*, followed by a minor heterogenization of the floc population until the end of the period.

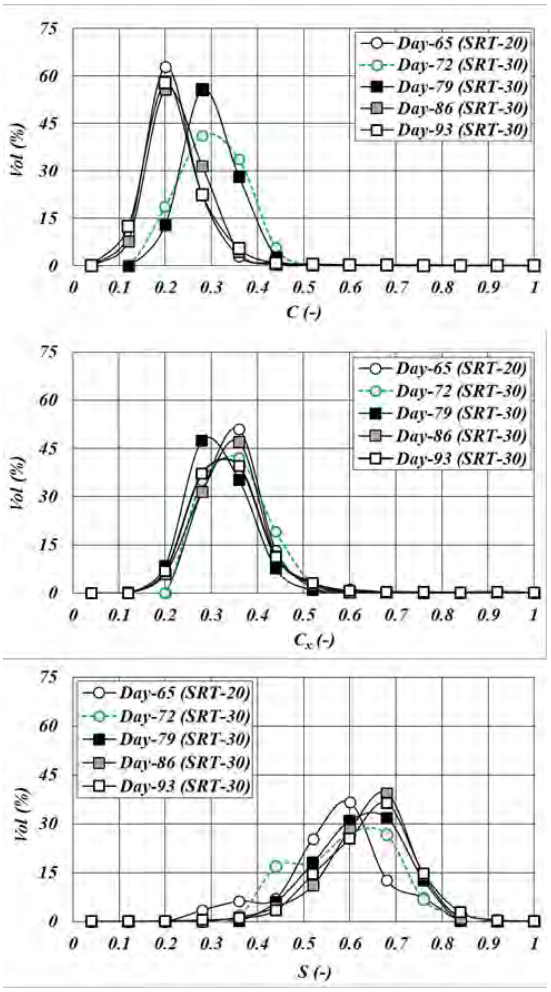

Figure IV-11. Evolution of circularity (*C*), convexity (C_x) and Solidity (*S*) distributions on volume basis for *SRT-20* to *SRT-30* transition.

Table IV-7. Typical flocs encountered on the Day-72, *79* and 93. from *SRT-30*.

Table IV-7. Typical flocs encountered on the *Day-72*, *79* and *93*.

Day-72	Day-79	Day-93
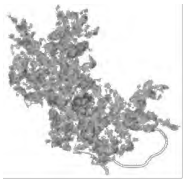		
CED = 138.1 µm *C* = 0.24 C_x = 0.34 *S* = 0.66	*CED* = 173.3 µm *C* = 0.22 C_x = 0.33 *S* = 0.68	*CED* = 136.1 µm *C* = 0.27 C_x = 0.37 *S* = 0.74

From an overall point of view, flocs throughout *SRT-30* seemed to be more robust than in the other periods, a fact that could justify the shifts to the right of circularity and solidity distributions. Nevertheless, flocs on *Day-72 and 79* have suggested a modest presence of filamentous bacteria over their surfaces. Since those days were followed by a gradual increase in the SVI values and decreases in COD removal efficiencies, the apparition of filamentous contents could suitably explain these results. On the other hand, this type of bacteria seems to be less numerous along the next days as exposes the floc on *Day-93*. The reduction in this specific population could mostly justify the back-and-forth movement described by CED, circularity and convexity distribution for this period, without mentioning the improvement observed in the SVI and COD removal rates.

It might be thought that flocs were robust even though and it could not cause the loss of pilot system performance previously commented. However, these flocs cannot be imagined as an isolated particle in the mixed liquor, they must be imagined as a complex network where they are linked to each other instead, and under this form they could definitely promote some decrease of the sludge settleability.

The reason why filamentous bacteria have grown on flocs surfaces is not completely clear, but since the transition to an SRT of 30 days produced an increase in TSS concentrations while the organic load rate was maintained constant, it could be supposed that the ratio of available food to unit of mass of microorganisms had decreased. According to Tandoi et al. (2006), substrate limitation is considered as one of the key factors that corroborates the development of filamentous bacteria.

IV.3.3 Evolution of the morphological properties of the activated sludge flocs

The mean values of the size and shape properties corresponding to each day of measurement were determined thorough their volume-based distributions. **Figure IV-12 (a-b)** presents, then, the evolution of the mean floc size (CED), solidity (S), convexity (C_x) and circularity (C) over the different periods and transitions of SRT carried out during this experimental campaign.

Focusing firstly on the profile drawn by the floc mean size, Figure IV-12 (a) enables to observe that Acclimation phase was a period remarked by the stability of this parameter. Liao et al. (2006), which were also interested in the effects of changing SRT on the sludge floc structure, have reported that at SRTs between 9 and 20 days there has been a general tendency to find this type of stability. Since Acclimation phase was conducted at an SRT of 15 days, it is possible to say that the results are in accordance with what is normally seen at usual operating conditions. The fresh sludge inoculated into the lab-scale pilot has a characteristic floc mean size of 110 µm. One week later, after the launching of the experimental campaign, flocs reached a mean CED of about 140 µm without exhibiting significant variability until the end of the *Acclimation*.

Due to an interruption for building maintenance, the room where the pilot system had been installed was isolated making the access in order to withdraw samples restricted. This fact is the reason why the period after *Micronutrients addition* is composed by only one point. However, no meaningful changes could be noticed with respect to this point as compared to the last one belonging to *Acclimation phase*. A mean CED of 140 µm was measured in the end of this period, which means that adding micronutrients had no effect on the mean size of the flocs.

Once SRT was changed from 15 to 20 days, mean CED presented a slight increase from 140 to about 180 µm. Coincidentally, TSS concentrations have also experienced an increase in almost the same day. Literature (Mesquita et al., 2016) has reported no clear correlation between CED and TSS, at least, only the CED, all by itself, is not capable to predict TSS behaviour. However, good indices of SVI were also observed for this same period, which means a similar result to the ones found by Liss et al. (2002), which reported robust flocs and satisfactory bioflocculation (as consequence satisfactory settleability as well) between SRTs of 16 and 20 days. During the next weeks in *SRT-20*, floc mean size stabilized again at 140 µm without presenting signs of large variability.

As SRT was changed from 20 to 30 days, any important modification could be noticed, right after that, in terms of mean floc size. Then, on *Day-79*, almost two weeks after SRT transition, a slight increase that attains around 180 µm occurs again. This transition was accompanied by increases of TSS concentrations, but not only, SVI values seemed to rise towards the acceptable threshold of 150 $mL.g^{-1}$ as well. If COD_{OUT} concentrations and COD removal efficiencies were taken into account in this overall balance, a small decrease of process performance will be equally observed around this same period. Thus, this time, the slight increase in the mean size of the activated sludge flocs points out to the insurgence of the filaments contents rather than a good bioflocculation.

Even though this disturbance may have been observed, it just disappeared in the course of the following weeks, which were remarked by an improvement of COD removal efficiencies, low SVI values and the stabilization of the mean CED around 140 µm one more time exactly as exposed by the distributions as well.

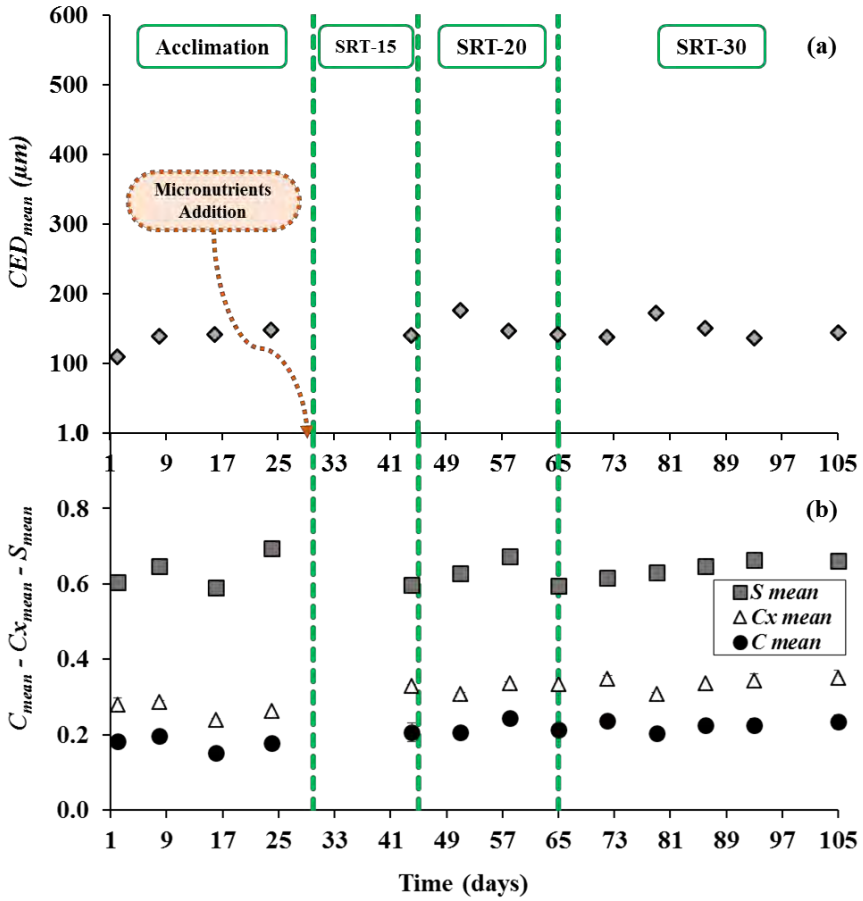

Figure IV-12. Evolution of the volume-based (a) mean floc size (CED_{mean}) and (b) mean shape properties.

Figure IV-12(b) enables to focus on the profiles drawn by the mean shape properties. In the opposite of the floc mean size, the stabilization of the mean shape properties seemed to be less evident during *Acclimation phase*, especially for the solidity values. Throughout *Acclimation,* floc mean solidity varied between 0.59 and 0.69, while their circularity and convexity varied between 0.15 – 0.20 and 0.24 – 0.28, respectively. These results could infer that for properties that depend on the floc overall surface, as the solidity does, it may be tougher to reach steady-state conditions than for properties that depend on the floc boundaries, as the circularity and the convexity do. In other words, solidity may be more sensitive to shape variations than circularity or convexity.

The fact of adding micronutrients has apparently promoted a decrease of the mean solidity and an increase of the mean circularity and convexity. Since the transition from *STR-15 to SRT-20* happened, then, it is possible to mostly identify a gradual increase in the means for circularity and solidity until *Day-58.* Although mean convexity has presented a minor decrease on *Day-51*, if a general sight is considered, it has slightly increased either until *Day-58.* Such increases in the mean shape parameters are consistent with the shifts of their distributions to the right previously noticed on this same period. Spherical and more compacted floc structure were observed before by Martins et al., (2003) for SRTs of 9, 12, 16 and 20 days. Once the pilot

system was operating with an SRT of 20 days, it could be argued that results are consistent with previous observations. It must be underlined that within this same period, not only good levels of COD removal were achieved, but the highest TN removal on *Day-48* was reached as well.

Concerning the transition from *SRT-20* to *SRT-30*, a small decrease in the means for solidity and circularity was observed right before the end of *SRT-20*, while mean convexity remained constant. Afterwards, along *SRT-30*, mean solidity presented a gradual increase until *Day-93*, whereas mean circularity and convexity were almost constant, except for the *Day-79*, when both exhibited a slight alteration in their means. Since, about this day, an upcoming disturbance was suggested through the microscopic observations, TSS, SVI and processes performance parameters together, it is probable that this suitable variation in their means may be also relied to the same fact.

A measurement was carried out on *Day-105* in order to check whether size and shape properties would not have changed after some days of the pilot system still operating at an SRT of 30 days. Then, this verification was able to prove that any other significant modification had taken place in matter of floc characteristics. In summary, observing the way that the mean values have evolved, only slight modifications are identified. As an apparent first conclusion, it can be stated that the SRT transitions had no long-term effect on floc morphology.

IV.3.4 Summarizing the transitions of SRTs

The final size (CED), circularity (C), convexity (C_x) and solidity (S) distributions corresponding to the end of each period were displayed side by side in the **Figure IV-13**. This approach can establish a comparison that enables to check if SRT transitions had an important effect on floc size and shape.

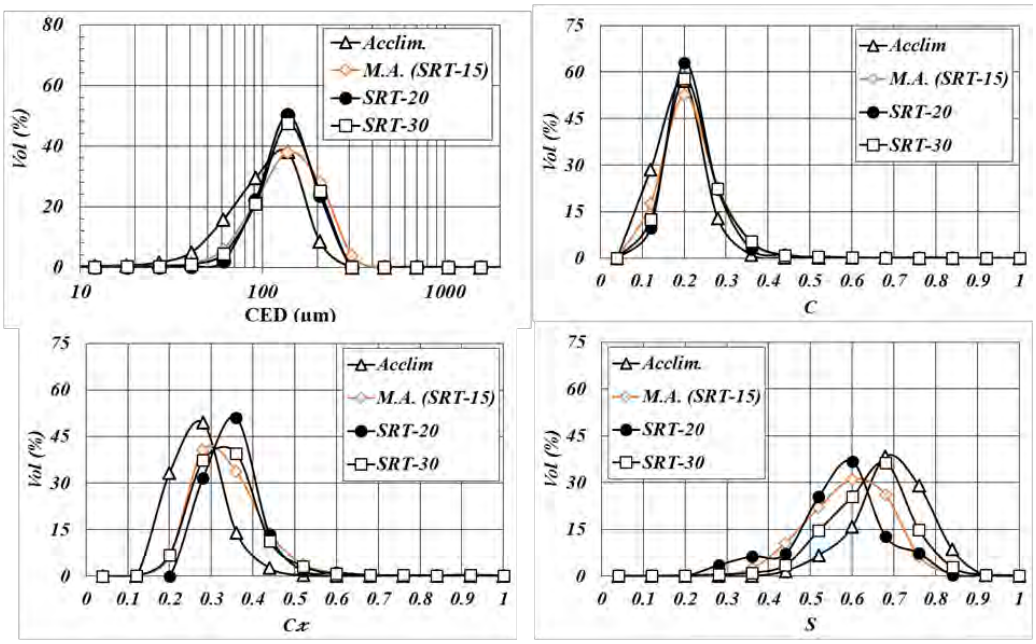

Figure IV-13. Comparison among the final CED, circularity (C), convexity (C_x) and solidity (S) distributions of each period in this campaign. - *M.A.: Micronutrients Addition*

- CED

A slight displacement of size distribution to the right has occurred after *Micronutrients addition*. Nonetheless, mode values (around 140 µm) remained constant after this corrective measure and throughout SRT transitions. A homogenization of the distributions along the campaign is observed even though.

- Circularity

By circularity distributions superposition, it could be implied that none of the perturbations imposed to the system: *Micronutrients addition* or SRT transitions have caused a meaningful impact on this floc characteristic.

- Convexity

A shift of convexity distribution to the right is observed after *Micronutrients addition*, indicating an increase of floc convexities. Anyway, SRT transitions seemed not affect this property, since the last distribution matches the one representing the *Micronutrients addition*. Furthermore, between these two periods, modes remained the same.

- Solidity

Solidity distribution undergone a shift to the left after *Micronutrients addition*, which means a decrease of the floc solidities. This parameter has equally presented more dispersed distributions, sometimes even bimodal ones. In general, solidity was more sensitive to fluctuations on floc shape as well. Anyway, throughout the SRT transitions this shape characteristic was able to recover again the values previously observed in the *Acclimation phase.*

According to the results obtained for this campaign, it can be concluded that the *Micronutrients addition* and SRT transitions had only transient impacts on floc shape and size properties. Right after a change of SRT, floc size and circularity have both presented an increase in their mean and mode values, however it always consisted of a temporary modification. In summary, with the pilot system operating continuously, no long-term effect was identified on floc morphology due to SRT transitions.

IV.4 Conclusion

The objective of this chapter was to study the associations between the morphological properties of the biological flocs and the performance of an activated sludge system according to the Solids Retention Time by the Image Analysis protocol presented in **Chapter II**. Three values of solids retention time have been experienced: 15, 20 and 30 days using the AS lab-scale pilot fed with a synthetic wastewater. The main results showed that the TSS showed some variability at a higher SRTs as 30 days and the removal efficiency was not highly sensitive to an increase of SRT. However, the SVI seems to increase, leading to a decrease of the sludge settleability in the beginning of the period with the SRT at 30 days.

Globally speaking, the removal efficiencies of organic matter throughout the whole campaign, and so regardless the SRT, was always above 90%. TN removal was near to 40%. The *Micronutrients Addition* has induced a short-term effect over these removals. Right after a change of SRT, floc size and circularity have both presented an increase of their mean and mode values, however it always consisted of a temporary modification. As a consequence, under steady-state conditions, the size and circularity distributions seem to be independent of the solids retention time in the considered range (15-30 days).

The SRT is one of the numerous operational parameters for managing WWTP, the following chapter will deal with the influence of three other operating conditions: the Organic Load Rate (OLR), the recycle rate and the COD:N ratio on the size and the shape of the biological flocs.

IV.5 References

Bisogni, J., and Lawrence, A.W. (1971). Relationships between biological solids retention time and settling characteristics of activated sludge. Water Res. *5*, 753–763.

Grady, C.P.L., Daigger, G.T., Love, N.G., and Filipe, C.D.M. (2011). Biological Wastewater Treatment (IWA Publishing - Co-Publication).

Liao, B.Q., Droppo, I.G., Leppard, G.G., and Liss, S.N. (2006). Effect of solids retention time on structure and characteristics of sludge flocs in sequencing batch reactors. Water Res. *40*, 2583–2591.

Liss, S.N., Liao, B.Q., Droppo, I.G., Allen, D.G., and Leppard, G.G. (2002). Effect of solids retention time on floc structure. Water Sci. Technol. *46*, 431–438.

Martins, A.M.P., Heijnen, J.J., and Loosdrecht, M.C.M. van (2003). Effect of dissolved oxygen concentration on sludge settleability. Appl. Microbiol. Biotechnol. *62*, 586–593.

Mesquita, D.P., Amaral, A.L., and Ferreira, E.C. (2016). Estimation of effluent quality parameters from an activated sludge system using quantitative image analysis. Chem. Eng. J. *285*, 349–357.

Tandoi, V., Jenkins, D., and Wanner, J. (2006). Activated Sludge Separation Problems (IWA Publishing).

Van den Broeck, R., Van Dierdonck, J., Nijskens, P., Dotremont, C., Krzeminski, P., van der Graaf, J.H.J.M., van Lier, J.B., Van Impe, J.F.M., and Smets, I.Y. (2012). The influence of solids retention time on activated sludge bioflocculation and membrane fouling in a membrane bioreactor (MBR). J. Membr. Sci. *401–402*, 48–55.

Yoo, H., Ahn, K.-H., Lee, H.-J., Lee, K.-H., Kwak, Y.-J., and Song, K.-G. (1999). Nitrogen removal from synthetic wastewater by simultaneous nitrification and denitrification (SND) via nitrite in an intermittently-aerated reactor. Water Res. *33*, 145–154.

Yuan, Y., and Farnood, R.R. (2010). Strength and breakage of activated sludge flocs. Powder Technol. *199*, 111–119.

Chapter V. Influence of modifying the operating conditions on activated sludge performance and floc morphology

This chapter presents the experimental results obtained while running the lab-scale pilot plant under four different operating conditions. The modified parameters are the Organic Load Rate (OLR), the recycle ratio and the ratio between the concentration of chemical oxygen demand by nitrogen in the inlet (COD:N). The changes over time of the sludge and effluent quality parameters as well as the morphological parameters and their respective distributions are presented and discussed.

V.1 Modifications of operational conditions in the lab-scale pilot

Among the classical operating conditions that can promote variations in activated sludge morphological and biological characteristics, the organic loading rate, recycle and COD:N ratios deserve a special concern. According to previous researches (Chao and Keinath, 1979; Liu and Tay, 2004; Amanatidou et al., 2015b, 2016), those parameters are strongly related to the biomass concentrations in the treatment, and hence, considerable changes with respect to the floc size and shape could take place.

The second part of the experimental campaign using the activated sludge lab-scale pilot was run from September to December 2016, corresponding to a duration of 85 days. The first period consisted of the acclimation of the sludge in the lab-scale pilot that lasted 29 days. After this first period, the pilot was respectively submitted to four operating condition variations of: (1) Organic Loading Rate (OLR), (2) Organic Loading Rate (OLR) again, (3) Recycle Ratio and (4) COD:N ratio (or C:N ratio) modification. The operating conditions set-up used during each period of this campaign are gathered in the **Table V-1**; operating conditions of the acclimation phase are the referential ones; the modifications were made by changing one of them as underlined.

Table V-1. Operating conditions modifications during the second experimental campaign.

Variables	*Acclimation*	Modifications			
		M1	*M2*	*M3*	*M4*
OLR ($kg_{COD}.m^{-3}.day^{-1}$)	1.00	3.75	1.00	1.00	1.00
COD : N Ratio	100:7	100:7	100:7	100:7	100:28
Recycle Ratio	1:1	1:1	1:1	3:1	1:1
Period	Day 1 to 28	Day 29 to 43	Day 44 to 56	Day 57 to 70	Day 71 to 85

For the acclimation phase, the synthetic wastewater composition is the one presented in Chapter II (**II.1.4.2**). The Modification 1 (*M1*), consisted of an increase in OLR without changing the Hydraulic Retention Time (HRT), the glucose concentration in the inlet solution was then set to 4000 mg.L^{-1}. It is important to emphasize that as COD:N:P ratio was maintained (100:7:1) constant during *M1*, the quantity of nitrogen and phosphorous were consequently adjusted. During Modification 2 (*M2*), the OLR was set again to the one of the acclimation phase conditions.

During the Modification 3 (*M3*) the recycle ratio varied from 1:1 to 3:1, meaning that the sludge of the clarifier was sent back to the aeration tank at a flow rate (Q_R) 3 times higher than the feed flow rate (Q_F).Finally, Modification 4 (*M4*) corresponds to a diminution of the COD:N ratio by increasing the ammonium chloride concentration in the inlet solution to 224 mg.L^{-1}.

During the 85 days of the campaign, the Solid Retention Time (SRT) was fixed to 15 days. To that end, 2.0 L of sludge was daily drained from the pilot. This amount was adjusted taking into account the sample volumes withdrawn for other analyses.

V.2 Lab-scale pilot plant performance

V.2.1 Temperature, Dissolved Oxygen (DO) and pH monitoring

Likewise part I, temperature, DO concentration and maximum and minimum values of pH were registered directly from the aerated tank. The **Figure V-1** is based on daily average values and presents the respective evolutions of these parameters over the whole campaign.

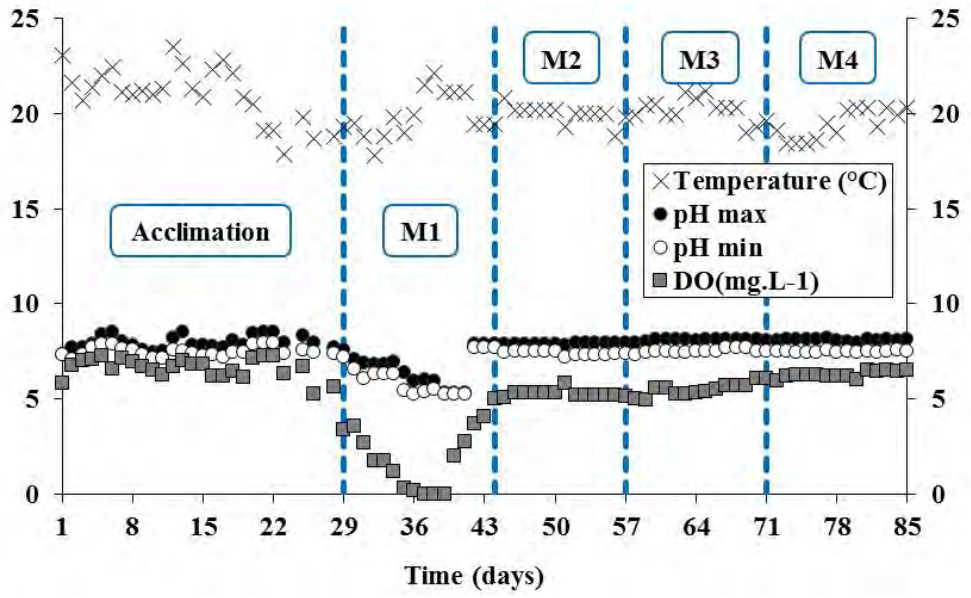

Figure V-1. Variations of temperature, DO concentration and pH values over the operating conditions modifications.

In order to provide further data, the **Table V-2** still reports the statistical characterization of each modification in terms of the mode, median and range of variation for each parameter.

Table V-2. Impact of each modification on the mode, the median and the range of values for the temperature, the pH and the DO concentration.

Acclimation			
	Mode	**Median**	**Range**
Temperature (°C)	21.0	21.0	17.9 – 23.5
pH_{max}	8.5	7.9	7.4 – 8.5
pH_{min}	7.6	7.4	7.1 – 7.9
DO ($mg.L^{-1}$)	7.3	6.7	2.4 – 7.3
M1			
	Mode	**Median**	**Range**
Temperature (°C)	21.1	19.5	17.8 – 22.1
pH_{max}	6.4	6.7	5.3 – 7.9
pH_{min}	5.3	6.1	5.3 – 7.2
DO ($mg.L^{-1}$)	0	1.7	0 – 5.0
M2			
	Mode	**Median**	**Range**
Temperature (°C)	20.2	20.0	18.8 – 20.8
pH_{max}	7.9	7.9	7.8 – 8.0
pH_{min}	7.5	7.4	7.2 – 7.5
DO ($mg.L^{-1}$)	5.3	5.2	4.9 – 5.8
M3			
	Mode	**Median**	**Range**
Temperature (°C)	20.3	19.9	18.4 – 21.5
pH_{max}	8.1	8.1	8.1 – 8.2
pH_{min}	7.5	7.5	7.5 – 7.7
DO ($mg.L^{-1}$)	5.7	5.7	5.3 – 6.3

	M4		
	Mode	**Median**	**Range**
Temperature (°C)	20.3	19.9	18.4 – 20.3
pH_{max}	8.1	8.1	8.1 – 8.2
pH_{min}	7.5	7.5	7.4 – 7.6
DO ($mg.L^{-1}$)	6.5	6.3	6.0 – 6.5

It can be observed that the temperature hardly varied during the campaign, even though some higher values were recorded during the acclimation phase with an average value of 20.8 ± 1.5 °C. These initial values registered for temperature are quite expected, considering that acclimation phase was carried out between the summer ending and the fall beginning.

The pH values were maintained between the range of 7.0 and 8.0 as much as possible. The continuous injection of the high organic load in the aerated tank during M1 led to a pH diminution that was not comprised in this specific range. The addition of 200 mL of the solution of sodium hydroxide on *Day-40* allowed to rapidly remediate this situation.

The DO measures reported in the Figure V-1 correspond to the maximum dissolved O_2 concentration reached throughout the aerobic sequences. It can be clearly seen that the levels of DO concentration were not maintained upon to the desired level (4 $mg.L^{-1}$) during *M1*.

An increase of the OLR as the one operated during M1, leads to a high quantity of soluble organic matter flowing into the aerated tank. To efficiently eliminate this organic matter, the biomass needs a greater amount of oxygen thus implying a diminution of the DO concentration. Furthermore, according to Paul et al. (1998), an increase of the OLR promotes the development of new microorganisms in the sludge environment. This bacteria growth is achieved with a consequent O_2 consumption that suggests a decrease of DO concentrations. At the *Day-40*, the DO increased again until almost reach the desired DO level at the *Day-44*, which corresponds to the switch from *M1* to *M2*. This increase may indicate the return to stable conditions.

Whatever the other modifications imposed during *M2*, *M3* or *M4*, the temperature, the pH and the DO concentration remained at their optimum level.

V.2.2 Monitoring of sludge properties

Figure V-2 displays the Total Suspended Solids (TSS) and the Sludge Volume Index (SVI) variations in the lab-scale pilot during the whole second campaign, while **Table V-3** summarizes the range of values observed for TSS and SVI in each particular period (or modification).

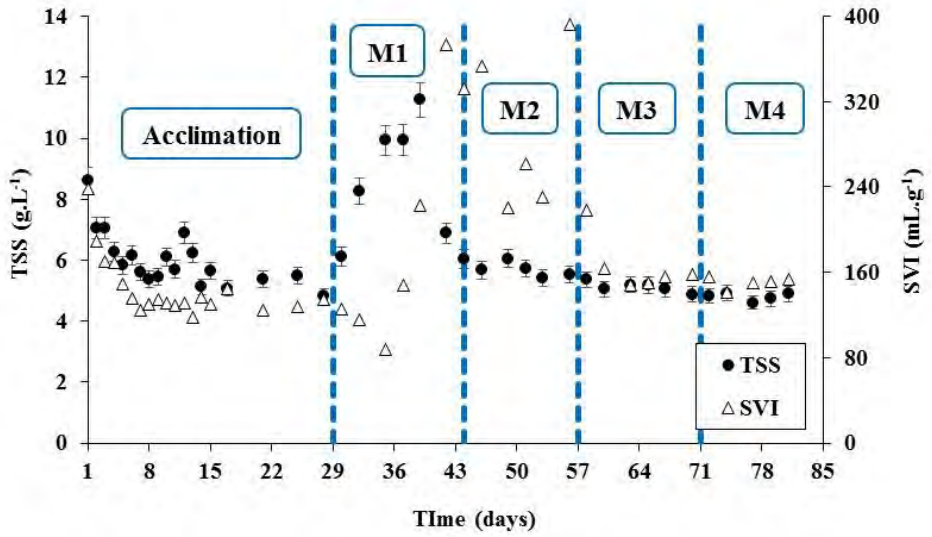

Figure V-2. Changes of TSS and SVI over the operating condition modifications.

Table V-3. Range of values of TSS and SVI over the acclimation and the four modifications.

	Acclimation	Modifications			
		M1	*M2*	*M3*	*M4*
TSS ($g.L^{-1}$)	5.1 – 8.6	6.0 – 11.2	5.0 – 6.0	4.8 – 5.1	4.6 – 4.9
SVI ($mL.g^{-1}$)	124 – 237	87 – 372	163 – 392	148 – 157	150 – 153

Overall, the *Acclimation* phase lasted almost 2 SRTs. Measurements of TSS and SVI during the *Acclimation* phase were accomplished every day for a first period that corresponded to 1 SRT (or 15 days). Then the analysis frequency was decreased to three times a week afterwards. Considering the evolutions of SVI and TSS during this period, it seems that the steady state conditions were reached after 15 days, which corresponds to the value of one SRT. Over this phase, the average values of TSS and SVI were respectively equal to 6.0 $g.L^{-1}$ and 144 $mL.g^{-1}$. However, it is important to mention that stabilised values (TSS: 5.5 $g.L^{-1}$ and SVI: 127 $mL.g^{1}$) were lower than the average ones. It may be assumed that such TSS value corresponds to the expected TSS concentration under the applied organic load of 1 $kgCOD.m^{-3}d^{-1}$ and the SVI value is within the range characterizing a sludge with good settling properties (Grady et al., 2011).

The increase of the OLR from 1.00 to 3.75 $kg_{COD}.m^{-3}d^{-1}$ (*M1)* clearly affected TSS and SVI profiles. The TSS concentrations increased dramatically, reaching a peak of 11.2 $g.L^{-1}$ on *Day-39,* suggesting a significant growth of biomass. Indeed, this fact can reasonably explain

the decrease in DO levels previously observed in the last section. According to direct observations, this was connected to suspended material that had been washed out with the treated effluent. The SVI showed a different evolution. Firstly, a diminution of the SVI was observed for almost 6 days, indicating that sludge had settled satisfactorily. Then, from *Day-37* onwards, the SVI increased strongly, attaining values up to 372 $mL.g^{-1}$. At this SVI, the sludge settled very slowly and compacted poorly, pointing out a probable separation problem, which might be the apparent correlated to the sludge washout.

The decrease in the OLR from 3.75 to 1 $kg_{COD}.m^{-3}d^{-1}$ (*M2)* showed that biomass gradually found its own balance (average TSS = 5.6 $g.L^{-1}$). On the other hand, the activated sludge presented some resistance to recovering its settleability, as demonstrated by the significant variability of the SVI values for this period.

Increasing of the recycle ratio during *M3* and the COD:N ratio during M4 seemed not to have any major impact on TSS and SVI.

V.2.3 Monitoring of effluent quality parameters

As in the first campaign of this study, COD concentration and Nitrogen contents (NH_4^+, NO_3^- and residual nitrogen – R. N) in the treated effluent were measured in order to evaluate the effluent quality and the lab-scale pilot performance. Their respective variations throughout the four operating condition modifications are presented in the **Figure V-3** as follows.

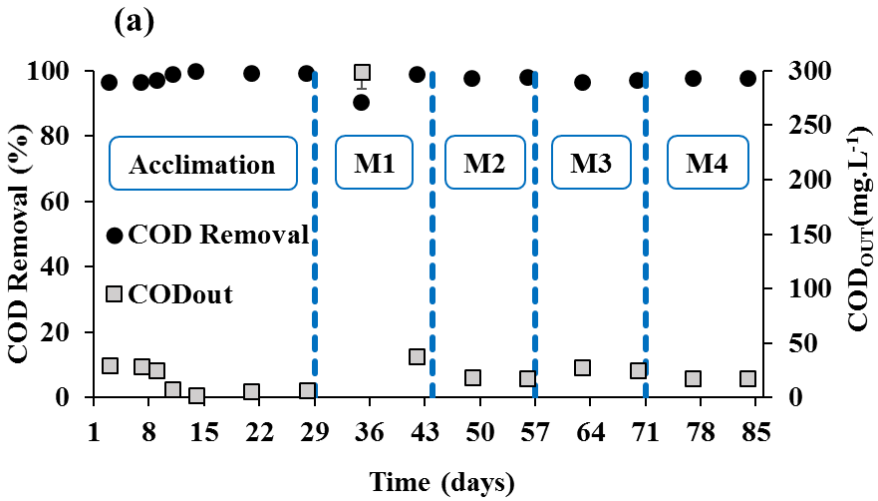

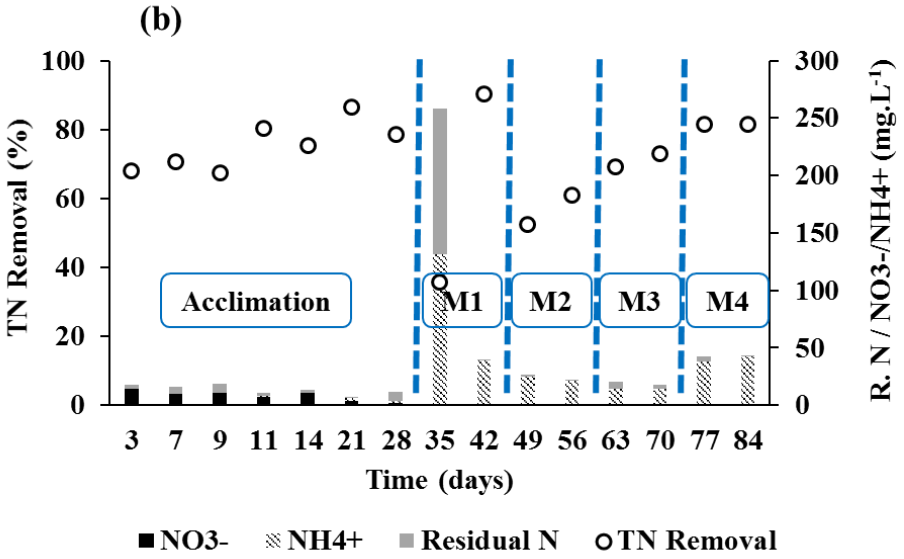

Figure V-3. Variations of effluent quality parameters over the operating conditions modifications.

To complement **Figure V-3**, more detailed values can be read in **Table V-4**. The amounts of COD_{IN} and Total Nitrogen (TN_{IN}) in the feed solution for each period are also indicated allowing an estimation of the respective removal efficiencies.

Measurements of COD_{OUT} and nitrogen contents in the *Acclimation* phase were carried out with a higher frequency right after the inoculation procedure. 5 measures were done over a period of 1 SRT. Once those parameters seemed to be stable, the frequency of sample analysis was set to once a week. During this phase, a good level of COD removal was achieved as well as a suitable level of TN removal. COD_{OUT} concentration ranged from 1.8 to 29.3 $mg.L^{-1}$ presenting a maximum removal efficiency in organic matter of 99.8%. Following an equal performance, TN contents ranged from 7.6 to 18.3 $mg.L^{-1}$ attaining a maximum removal efficiency of 86.4 %. Moreover, as it can be seen in **Figure V-3 (b)**, the nitrate (NO_3^-) levels mostly suggested an efficient nitrification-denitrification process during the *Acclimation* period.

Considering **Figure V-3 (a)**, *M1* was rapidly reflected in the effluent quality. Before the end of the modification period, where a COD_{OUT} of 37.7 ± 3.9 $mg.L^{-1}$ was measured, a pronounced increase of 298.7 ± 3.1 $mg.L^{-1}$ had been observed. Such an increase occurred because of the presence of sludge in the treated effluent for this period, as mentioned before in the analysis of TSS evolution. Although samples were filtered, it is known that a large amount of soluble material can be released during filtration if several cells are lysed. TN removal rates were also impacted by the modification of OLR: the high concentration of the Residual N in the treated effluent may also have been a result of sludge content in the analyzed samples (release of linked EPS or cells lysed). The high concentration of ammonium (NH_4^+) may be the result of increasing its inlet concentration and then, nitrification process needed adaptation through *M1*.

Despite the high values of SVI during *M2*, the decrease of the OLR from 3.75 to 1 $kg_{COD}.m^{-3}.d^{-1}$ enhanced COD removal efficiencies since at least 97.8% of the organic load received by the

system was degraded. The suction force on the activated sludge flocs applied by the recycling pump, may aid decantation in the clarifier and is not taken into account in the SVI measurements. On the other hand, TN removal efficiencies during *M2* seemed to still undergo the effect produced by the previous increase of OLR (*M1*). A decay of the TN removal rates was noticed in comparison with those of the *Acclimation* phase. From the Total Nitrogen received by the system, only 61.7% could be eliminated at the end of *M2*. A higher concentration of ammonium in the treated effluent was also confirmed. This could probably be due to the time necessary for the development of nitrifying bacteria that would have been washed out during M1.

On the other hand, TN removal efficiencies during *M2* seem to still undergo the impact caused by the increase of OLR in *M1*. A decay of the TN removal rates in *M2* could be noticed when compared to the *Acclimation* phase rates. From the total nitrogen received by the system, only 61.1% could be eliminated at the end of M*2*. In addition, through this comparison, it can be also identified a sort of inversion between the NH_4^+ and NO_3^- concentrations from one phase to another. A higher concentration of ammonium in the treated effluent can be related to an incomplete oxidation of this N species into the nitrate form. According to Rodríguez et al., (2011) a probable inhibition of the nitrifying bacteria activity could take place under high amounts of ammoniacal nitrogen such as the one observed on Day-35.

Throughout *M3*, COD_{OUT} concentrations were slightly higher than with *M2*. A few assumptions could be made to explain this modest increase in the COD_{OUT} values but, since the recirculation of the mixed liquor was increased by a factor of three during *M3*, the most likely explanation for this result would be deterioration of the bioflocs due to the pumping effects. As reported by Kim *et al.* (2001), an increase in the COD concentrations was to be expected as a result of the release of soluble organic content, which occurred after microbial floc deterioration. With respect to the TN removal, a progressive improvement was seen in *M3* and*,* by the end of this period, an efficiency of 68.2% had been achieved.

The COD removal efficiencies were not disturbed by *M4*; COD_{OUT} concentration at the end of this phase was even lower than in *M3*. Despite the TN concentration of 43.1 ± 1.3 mg.L^{-1} being greater than the admissible by the European standard for final effluent discharge (Fulazzaky et al., 2015), the TN removal efficiencies in this modification could be considered quite pronounced in relation to the amount of nitrogen (232.0 ± 5.3 mg.L^{-1}) coming into the system.

The pilot plant performance in terms of COD removal was quite satisfactory, always nearby the removal index of 94.5% usually reported in the literature (Çiçek et al., 1999). In contrast, TN removals were not often around the expected values of 88.3 %. As it was mentioned above, some factors could have contributed to compromise the nitrification-denitrification process:

- DO levels were less than 1 mg.L^{-1} during *M1*.
- A possible limitation of nitrifying bacteria due to a decrease of this specie during the sludge washout.
- The growth rate of nitrifying bacteria that is slower than the growth rate of the heterotrophic bacteria.

Table V-4. Pilot plant performance in terms of COD, TN removals and nitrogen contents at the end of each period.

Period	COD_{IN} ($mg.L^{-1}$)	COD_{OUT} ($mg.L^{-1}$)	**COD removal (%)**	TN_{IN} ($mg.L^{-1}$)	TN_{OUT} ($mg.L^{-1}$)	**TN removal (%)**	NH_4^+ ($mg.L^{-1}$)	NO_3^- ($mg.L^{-1}$)	Residual. N ($mg.L^{-1}$)
Acclimation	798.0 ± 6.0	6.4 ± 1.4	**99.2**	56.1 ± 6.0	11.9 ± 0.5	**78.7**	2.29 ± 0.03	1.81 ± 0.06	7.84
M1	4089.6 ± 25.4	37.7 ± 3.9	**99.1**	282.2 ± 5.0	38.9 ± 1.1	**86.1**	38.5 ± 1.0	0.27 ± 0.10	0.19
M2	800.6 ± 4.6	17.4 ± 0.4	**97.8**	56.9 ± 1.1	21.8 ± 1.1	**61.7**	21.0 ± 1.0	0.69 ± 0.10	0.11
M3	800.6 ± 4.6	24.8 ± 2.7	**96.8**	56.9 ± 1.1	18.1 ± 0.6	**68.2**	13.3 ± 0.6	0.73 ± 0.09	4.03
M4	785.0 ± 2.0	17.5 ± 2.3	**97.7**	232.0 ± 5.3	43.1 ± 1.3	**81.4**	41.6 ± 1.1	0.63 ± 0.02	0.77

V.3 Variations in the morphological properties of the activated sludge flocs over the campaign

This section is now focused on the morphological characterization of the aggregates over the modifications. The image analysis procedure to conduct a morphological characterization of the flocs was used as key-tool to better understand the variability on the activated sludge process, constituting hence the core of this study.

The Circular Equivalent Diameter (CED) was selected in order to characterize the size of the aggregates, while their shape was described in terms of the circularity, convexity, solidity and sometimes the aspect ratio.

V.3.1 Evolution of the mean morphological parameters of the activated sludge flocs

The evolution of the mean floc size (CED), solidity (S), convexity (C_x) and circularity (C) over the operating condition modifications is shown in **Figure V-4**. The mean morphological parameters were obtained from the calculation of their volume-based distributions. For information only, an analysis of those distributions will be accomplished on the following sections, allowing thus to complement which is herein seen.

Regarding the size of the AS flocs (**Figure V-4 (a)**), the mean CEDs observed during the *Acclimation* phase are consistent with the data from previous studies (Mesquita et al., 2011; Wilén and Balmér, 1999) on a AS process functioning under normal conditions. The first mean floc size during this phase (118.9 ± 56.2 µm) was smaller than the others and corresponded to the inoculated activated sludge supplied by Nailloux WWTP. After one week, the mean floc size increased until it stabilized around 225 µm. Throughout the next 3 weeks, only small variations were noticed in the size of aggregates, similarly to what was observed before in TSS and SVI profiles for this same period.

As OLR changed from 1.00 to 3.75 $kg_{COD}.m^{-3}.d^{-1}$ (*M1*), the size of the biological aggregates increased drastically. Twenty-four hours after OLR modification, the floc size had almost doubled, the mean volume-based CED passing from about 220 to 400 µm. Then, it continued to increase slowly reaching a value around 500 µm on *Day-35*. It should be added that SVI values, and COD_{OUT} and NH_4^+ concentrations were proportionally higher at this moment. Such an exponential increase in the mean CED values can lead to the supposition that flocs became larger but not compact, since the analyses of sludge and effluent quality parameters revealed a worsening of the pilot performance. Furthermore, the end of *M1* and the beginning of *M2* were marked by a significant decrease in the size of the aggregates, which seemed to be correlated with the decrease of the TSS and the washout of large aggregates.

A decrease in the mean CED from 491.6 to 362.3 µm was noticed after the transition from *M1* to *M2*. During the modification, the size of the aggregates stabilized around 370 µm. As a sludge washout was identified at the end of *M1*, it seemed likely that the decrease in the floc mean size was associated with this incident rather than with the OLR diminution. Considering that the OLR in *M2* and in the *Acclimation* phase were the same, it could be concluded that floc characteristics (such as the size) were not only dependent on the current operating conditions but also on the changes brought by the previous conditions.

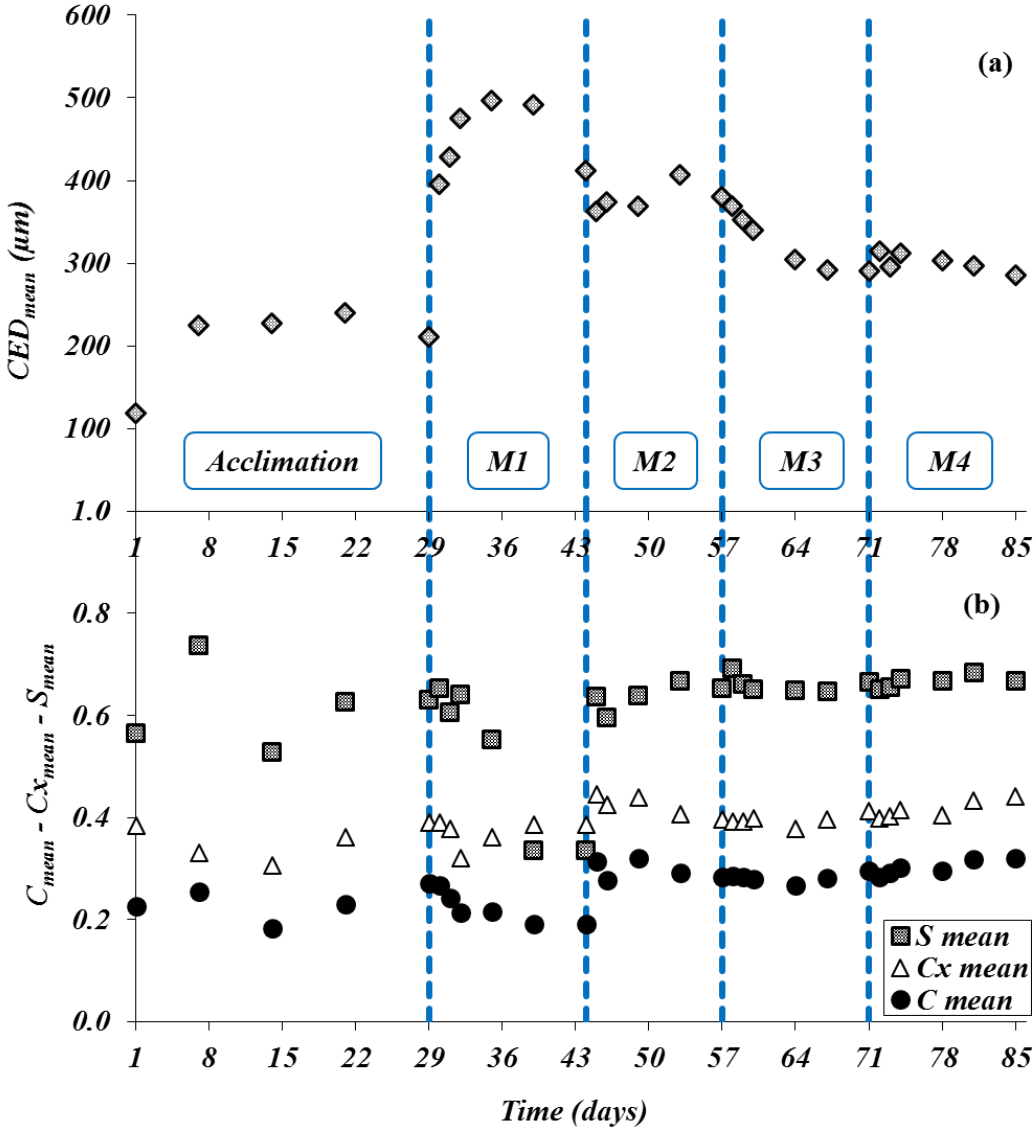

Figure V-4. Evolution of the volume-based (a) mean floc size (CED mean) and (b) mean shape properties.

Despite the increment in shear stress due to the increase of the recycle ratio during *M3*, the floc size did not present a meaningful decrease. The mean floc sizes were 380.9 µm and 304.2 µm at the beginning and at the end of the modification, respectively. Nevertheless, this result can imply that floc deterioration clearly occurred, confirming the assumption about the release of soluble organic material that slightly increased the COD_{OUT} concentrations in this period.

The modification to a lower COD:N ratio (*M4)* resulted in a small decrease of the mean floc size (285.7 µm) as compared to the beginning of *M4* (303.3 µm). This trend was similar to the one described by Amanatidou *et al.* (2015) who observed that, at low COD:N ratios, the amount of denitrification gases (N_2) increased inside the aggregates, leading to floc breakage.

In this study, the evolution of the floc shape properties was assessed over all four modifications.

In **Figure V-4(b)**, the evolution of the mean solidity expresses the variations regarding the existence of concavities on the floc surface. Considerable fluctuations in this shape property can be seen throughout the *Acclimation* period. During *M1*, floc solidity decreased slightly until Day-36 and a drop in the values (S = 0.29) was observed immediately afterwards. This evidence, added to the other symptoms, suggests a separation problem since a higher degree of concavities can indicate poor floc compaction. On the other hand, once *M2* started, solidity values quickly recovered their initial range without showing large variations during *M3* or *M4*.

Apart from *M1*, it can be seen that circularity and convexity mean values evolved in a similar manner during the *Acclimation* and the other modifications. Compared to the solidity, floc circularity and convexity during *Acclimation* were quite stable (around 0.21 and 0.30, respectively). During *M1*, similarly to the solidity, circularity and convexity underwent a small decrease in their mean values until *Day-36* of *M1*. This means that aggregates became less and less circular and even rougher. Afterwards, mean circularity did not present any meaningful evolution and convexity values remained constant. Microscopic observations for this period confirmed the growth of filamentous bacteria after Day-36, which could clarify the circularity and convexity behaviour from this day onwards. The presence of filaments on the floc surface promoted a global shape closer to a circle and caused simultaneous variation of both the actual and the convex hull perimeter, making convexity less sensitive in this type of situation.

In *M2*, circularity and convexity values did not recover their acclimation characteristics as was observed for solidity. In contrast, these parameters maintained a monotonous increase until the end of *M4*. Since *M3* and *M4* both promoted a decrease of the aggregate size, circularity and convexity behaviors may be related to a size reduction. Usually, small flocs are more regular (i.e., circular and smoother) than the larger ones (Xu and Gao, 2012).

Overall, it can be considered that the evolution of these three shape properties was mostly affected by the development of filamentous bacteria due to the increase of OLR during *M1*.

V.3.2 Evolution of size and shape properties distributions

The evolution of the size (CED), circularity, convexity and solidity distributions were followed along this second campaign, at a frequency of once a week for acclimation phase, and then, at a higher frequency for evaluating the impact of operating condition modifications. This increase in the frequency of morphological measurements is mainly due to the fact that throughout the first part of experiments (**Chapter IV**), some flagrant moments could have been missed with a measurement frequency of once a week. Considering that statement, the morphological parameters of the activated sludge flocs were daily measured during the first week, and then, twice a week in the second week of modification.

The distributions presented in the following sub-sections are displayed on volume basis, if there is an exception it will be ahead specified.

In the next figures, the initial distributions corresponding to the beginning (or transition) of each period (acclimation or modification) are represented by dashed lines and blue colour. The evolution of the distributions over time is represented by a colour gradient that fills the mark

series. It varies from a dark colour to a light one, which always indicates the end of the period. The basic principle for understanding these graphs is focused on observing the displacement of curves distributions, as it was demonstrated in the previous chapter.

V.3.2.1 Acclimation phase

The **Figure V-5** shows the behaviour of size (CED), circularity (C), convexity (C_x) and solidity (S) distributions during the *Acclimation* phase, which lasted about 2 SRTs. All distributions are represented on a volume-based resolution.

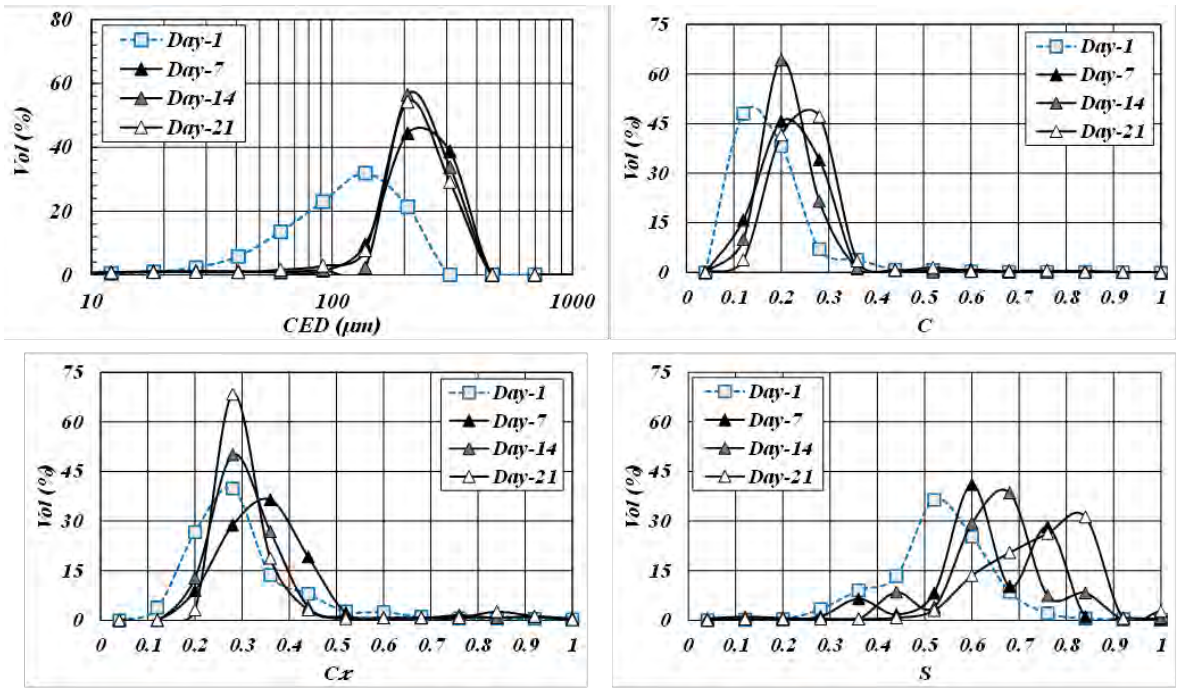

Figure V-5. Evolution of the size (CED), circularity (C), convexity (C_x) and solidity (S) distributions on volume basis for *Acclimation* phase.

As it has been commented, distributions on *Day-1* correspond to the inoculated sludge, i.e., they essentially reflect the morphological features that could be found in the activated sludge flocs of Nailloux WWTP or in the modifications due to transportation. The mode of the size distribution is about 150 µm and the range of sizes is between 30 and 300 µm. The inoculum presents low circularity values around 0.15 indicating that bioflocs are far from being circular. The convexity values, on the other hand, cover a wide range from 0.05 to 0.5 revealing that the surface of aggregates is not smooth at all. The solidity distribution is also quite large, indicating the presence of large concavities at the surface of flocs.

After one week (*Day-7*), all parameters (size, circularity, convexity and solidity) distributions shifted towards the right. The increase of floc size indicates that a biomass growth took place during this first week of acclimation. On a morphological point of view, the circularity, convexity as well as solidity increased. Flocs are more circular and their surface roughness seems to have decreased. After a period of 1 SRT (*Day-14*), the first signs of the steady-state

conditions could be detected on size (CED) and convexity distributions, whose modes are about 200 µm and 0.3, respectively. The circularity and solidity distributions maintain the evolution.

By the *Day-21*, CED distribution did not present a significant variation in comparison to the *Day-14*, while circularity and solidity distributions still showed an evolution. The results emphasize that the steady-state conditions are more remarkable depending on the type of parameter. For instance, signs of stabilization seem to be more easily recognized in the size than in the shape properties.

To better visualize these size and morphological variations over the acclimation phase, some recorded flocs have been selected and reported in **Table V-5.** Microscopic observations between the inoculated samples (*Day-1*) and the samples from the third week of the *Acclimation* phase (*Day-21*) highlight the comparison of the profiles previously described.

Table V-5. Microscopic observations in *Day-1* and *21* of *Acclimation* phase.

Day-1	Day-21
	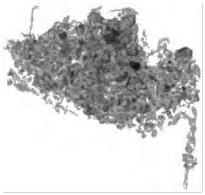
CED = 120.5 µm *C* = 0.17 C_x = 0.27 *S* = 0.56	*CED* = 176.2 µm *C* = 0.23 C_x = 0.33 *S* = 0.67

Flocs presented a broadly irregular structure on the first day, in opposition to the floc that can be observed by the end of the *Acclimation* phase (*Day-21*), when they seem denser and even more circular. As previously seen in the **Chapter III**, a couple of factors could be the origin of such a difference: one is the type of the biological process (MBR or traditional activated sludge system) used in the treatment, and the other one is the nature of the effluent which is feeding the system. Since the pilot is fed with a synthetic wasterwater, while inoculum sludge came from a municipal WWTP, changes in sludge floc characteristics are not surprising and in accordance with the results obtained in **Figure V-13**

V.3.2.2 Modification M1

The **Figure V-6** shows the curves for size (CED), circularity (C), convexity (C_x) and solidity (S) distributions during the modification *M1*, which consisted of increasing OLR from 1 to 3.75 $kg_{COD}.m^{-3}.d^{-1}$. All distributions are represented on a volume-based resolution.

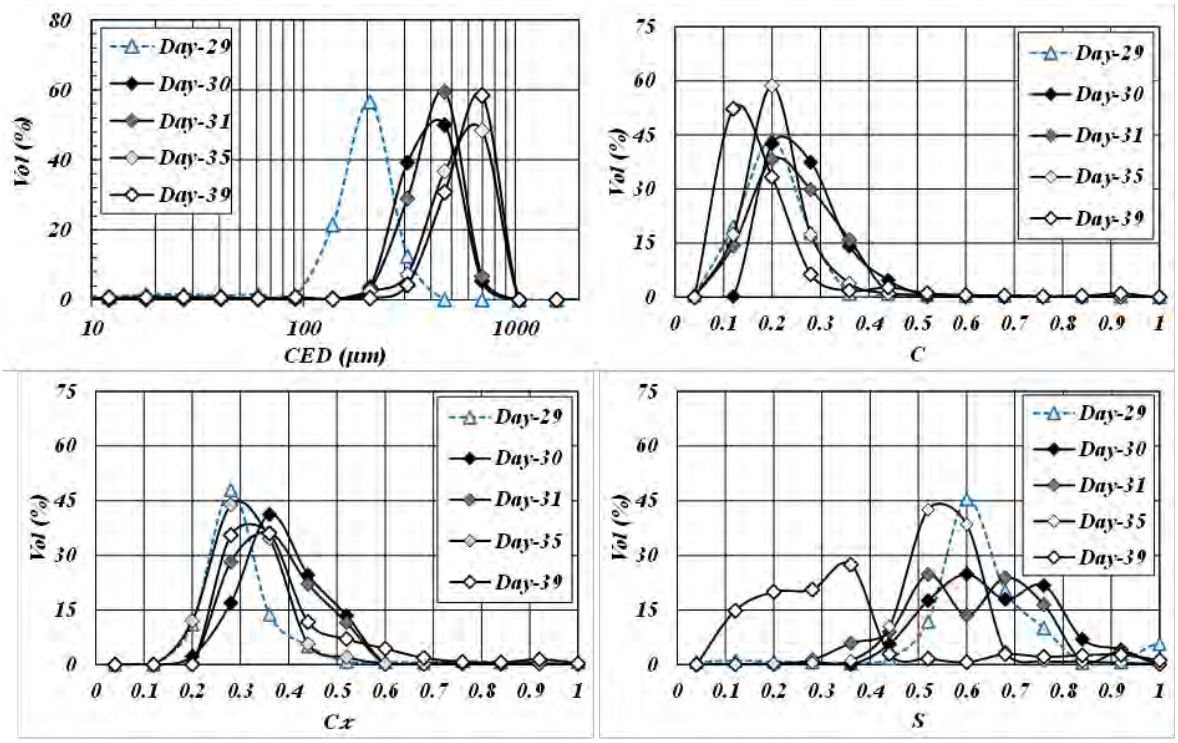

Figure V-6. Evolution of the size (CED), circularity (C), convexity (C_x) and solidity (S) distributions on volume basis for *M1*.

Once the CED distributions are analysed, it becomes clear the progress of the floc size towards the right side of the graph confirming the increase of the aggregates dimension previously observed during the evolution of the mean CED values (**Figure V-4 (a)**). The distribution modes increased from 200 to 460 µm from *Day-29* to *30*, and then, from 460 to 700 µm from *Day-31* to *35*. This last mode remained constant until *Day-39*. Increasing the OLR led to more considerable concentrations of suspended solids in the system due to biomass growth. Therefore, it could be assumed that this significant increase of the floc size is directly associated with the increase of the OLR.

Circularity distributions have not hugely evolved during the first days of *M1*, the mode of the distribution lying around 0.2. The modification of OLR has promoted a slight increase in the circularity of some aggregates. Between the *Day-29* and *31* a fraction of aggregates with a circularity of 0.2-0.5 is noticed. Afterwards, a significant evolution of circularity between *Day-35* and *39* is noticed when the mode of the distribution shifted to lower values, almost 0.1, indicating that flocs were less and less circular.

On the other hand, flocs convexity (C_x) has globally increased since the final distribution (*Day-39*) was slightly higher than the initial one (*Day-29*). During *M1,* convexity distributions became bimodal. Indeed, a sub-population characterized by higher convexities than the major one seems to have appeared. This is probably due to the presence of a considerable portion of small flocs, more convex than the larger ones. Thus, the increase in the mean convexity over *M1* shown in **Figure V-4 (b)** can be explained by this part of the flocs population.

Finally, it is possible to observe solidity distribution shifting towards lower values between the first (*Day-29*) and the last (*Day-39*). The solidity modes have decreased from 0.6 to about 0.3, implying an increase of large concavities (or even porosity) on the surface of the activated sludge flocs.

Since high contents of filamentous bacteria was identified through microscope observations (**Table V-6**), it can diagnose the sludge separation problem as a filamentous bulking condition. It can certainly explain the increase in the mean CED values and the low values of the median circularity and solidity by the end of *M1*. According to prior investigations (Barbusiński and Kościelniak, 1995; Meng et al., 2006), flocs with a great number of associated filaments are prone to present a large dimension with an irregular (open and loose) structure and poor settleability as well.

Table V-6. Microscopic observations in *Day-29*, *31*, *35* and *39* from *M1*.

Day-29	Day-31	Day-35	Day-39
	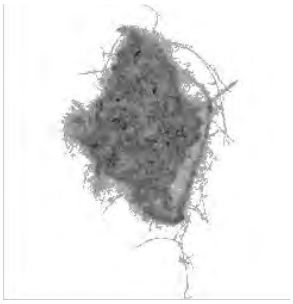	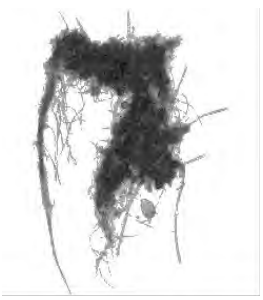	
CED = 170.2 µm *C* = 0.25 C_x = 0.34 *S* = 0.66	*CED* = 402.0 µm *C* = 0.20 C_x = 0.28 *S* = 0.68	*CED* = 556.5 µm *C* = 0.15 C_x = 0.23 *S* = 0.51	*CED* = 471.0µm *C* = 0.17 C_x = 0.40 *S* = 0.37

V.3.2.3 Modification M2

The **Figure V-7** shows the behaviour of size (CED), circularity (C), convexity (C_x) and solidity (S) distributions during the modification *M2* (OLR = 1 $kg_{COD}.m^{-3}.d^{-1}$). All distributions are represented on a volume-based resolution.

Focusing on CED distributions, a significant displacement towards the left occurs at the beginning of *M2*, the mode decreasing from 700 to 460 µm seemed to be connected to the sludge that was washed out with the treated effluent rather than the OLR decrease. In opposition, any other meaningful size evolution was noticed until the end of *M2*, which is already a first indication that the conditions encountered at the end of the *Acclimation* phase were not recovered.

Regarding circularity (C) and convexity (C_x) distributions, they firstly showed an increase in their modes assuming values of 0.28 and 0.36, respectively. Then, around *Day-45* and *46* both become bimodal.

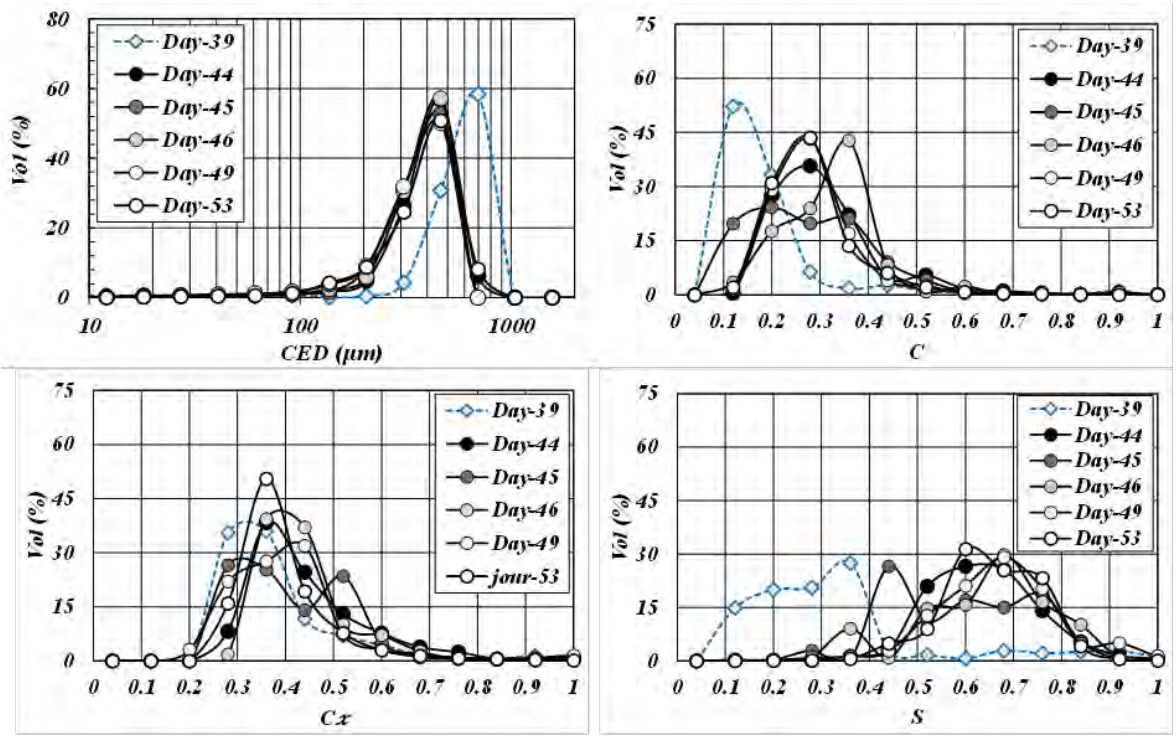

Figure V-7. Evolution of the size (CED), circularity (C) and convexity (C_x) distributions on volume basis

From the *Day-39* to *44*, the solidity (S) distributions moved to the right, indicating an increase of the floc solidities exactly as it could be previously seen when looking at the evolution of the mean values. This evidence suggests that a sudden distribution movement is either related to the sludge washout event, when most of the flocs plagued by filaments (the ones with low solidities) have probably left the clarifier with the floating sludge. From the *Day-44* until the end of the modification, solidity distributions become even more heterogeneous.

Searching for more details about the existence of this sub-population of flocs, it was decided that the distributions regarding the floc aspect ratios should be analysed since it could give an idea of the aggregates elongation. When aspect ratio distributions were analysed on number basis, remembering that on a number-based resolution, small particles are mainly highlighted, it was possible to confirm an expressive amount of small free filaments among the activated sludge flocs population (**Figure V-8**).

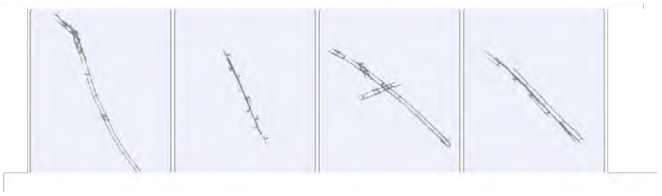

CED = 7.39 µm
C = 0.350
C_x = 0.964
S = 0.747
AR = 0.125

Figure V-8. Population of small free filaments identified during *M2.*

An inversion of the distribution towards low aspect ratios (in terms of their modes from 0.7 to 0.3) is the clearest evidence that the population of small aggregates had become more elongated due to a possible detachment of the filaments from the bioflocs (**Figure V-9**).

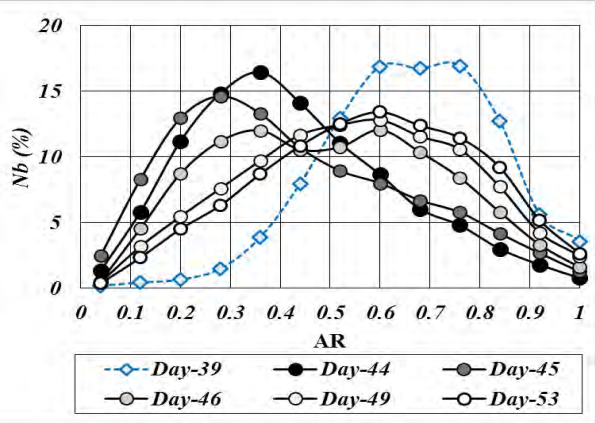

Figure V-9. Evolution of the aspect ratio (AR) on number basis for *M2*.

Other microscopic observations between the beginning (*Day-45*) and the end of *M2* (*Day-53*) can be seen in **Table V-7**.

Table V-7. Microscopic observations in *Day-45*, *46*, *49* and *53* from *M2*

Day-45	Day-46	Day-49	Day-53
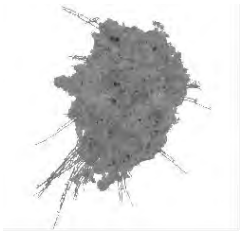	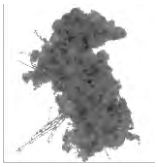	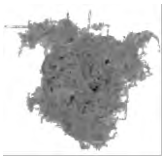	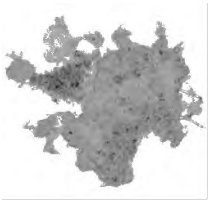
CED = 397.6 µm *C* = 0.23 C_x = 0.34 *S* = 0.51	*CED* = 357.7 µm *C* = 0.29 C_x = 0.39 *S* = 0.63	*CED* = 355 µm *C* = 0.34 C_x = 0.43 *S* = 0.74	*CED* = 377.7 µm *C* = 0.29 C_x = 0.37 *S* = 0.71

Those observations revealed that, at the beginning of *M2,* activated sludge flocs were still plagued by bacteria in a filamentous form as a consequence of the bulking situation verified over *M1*. Moreover, the gradual disappearance of the filaments from the flocs surface can likely explain the SVI variability underlined in **Figure V-2** and the rise of a sub-population constituted in most part by them, throughout *M2*.

Analysis of the 3D-distributions in M1 and M2

As seen in the previous sections, the modifications of OLR brought several variations regarding both the size and shape of the AS flocs. The previous analysis was conducted for the floc size on the one hand and for the shape properties on the other. However, to reach a deeper

understanding of the changes caused by the modifications, it is indispensable to cross the morphological parameters. To that end, three-dimensional (3D) distributions were plotted.

This approach is illustrated for the Solidity-CED and Circularity-CED pairs on some specific days of *M1* (*Day-29,35 and 39*) and *M2* (*Day-44, 49 and 53*), which could reasonably represent the beginning, the middle and the end of both modifications. Circularity and Solidity were selected to be represented alongside the CED because of their responses during OLR modifications. In the 3D-distributions, the Z-axis and the colour gradient (from a cold colour to a warmer one) shows layers representing percentages of the volume.

Analysing, firstly, *M1* (**Figure V-10**) from *Day-29* to *Day-35*, it is possible to observe that:

- the S-CED distribution peak becomes wider and a portion of small particles with high solidity values (CED < 50 µm and $S > 0.4$) appears,
- the C-CED distribution reveals that some large and quite circular flocs (CED > 100 µm and $C > 0.6$) disappear at the same time.

This means that, after almost one week of the modification, flocs increased in size and deviated from a regular shape. From *Day-35* to *Day-39*, distributions S-CED and C-CED suffered shifts towards lower values of solidity and circularity, respectively, this modification being more pronounced in the case of the pair S-CED than C-CED. The S modes decreased from 0.6 to 0.3 whereas C modes ranged from 0.2 to 0.1. This implies an increase in the degree of concavities (or porosity) for an even less circular population of AS flocs, which were concentrated in a group of large aggregates. In summary, it can be supposed that the AS flocs increased in size, acquiring an irregular structure after OLR increase. This finding is in accordance with the microscopic observations indicating filamentous bulking for this period, which attributed to the flocs poor settling properties (SVI > 150 $ml.g^{-1}$).

Comparing the 3D-distributions corresponding to *Day-39* and *Day-44* (**Figure V-11**) during *M2,* the distribution corresponding to the pair S-CED shows a sudden shift to the left, mainly indicating an increase in the floc solidities. Such an abrupt displacement is coherent with the ones observed for the distributions in 2D for both parameters, and which can be identified in a concomitantly way thanks to the 3D-distributions. The 3D-distributions also highlight the stability of the floc size while circularity and solidity parameters gradually evolve in opposite directions.

A gradual homogenization of the 3D-distributions observed along *M2* endorses the detachment of filaments from the flocs verified between *Day-45* and *Day-46*, which was highlighted by the inversions of the aspect ratios distributions on number basis exposed in the **Figure V-9**.

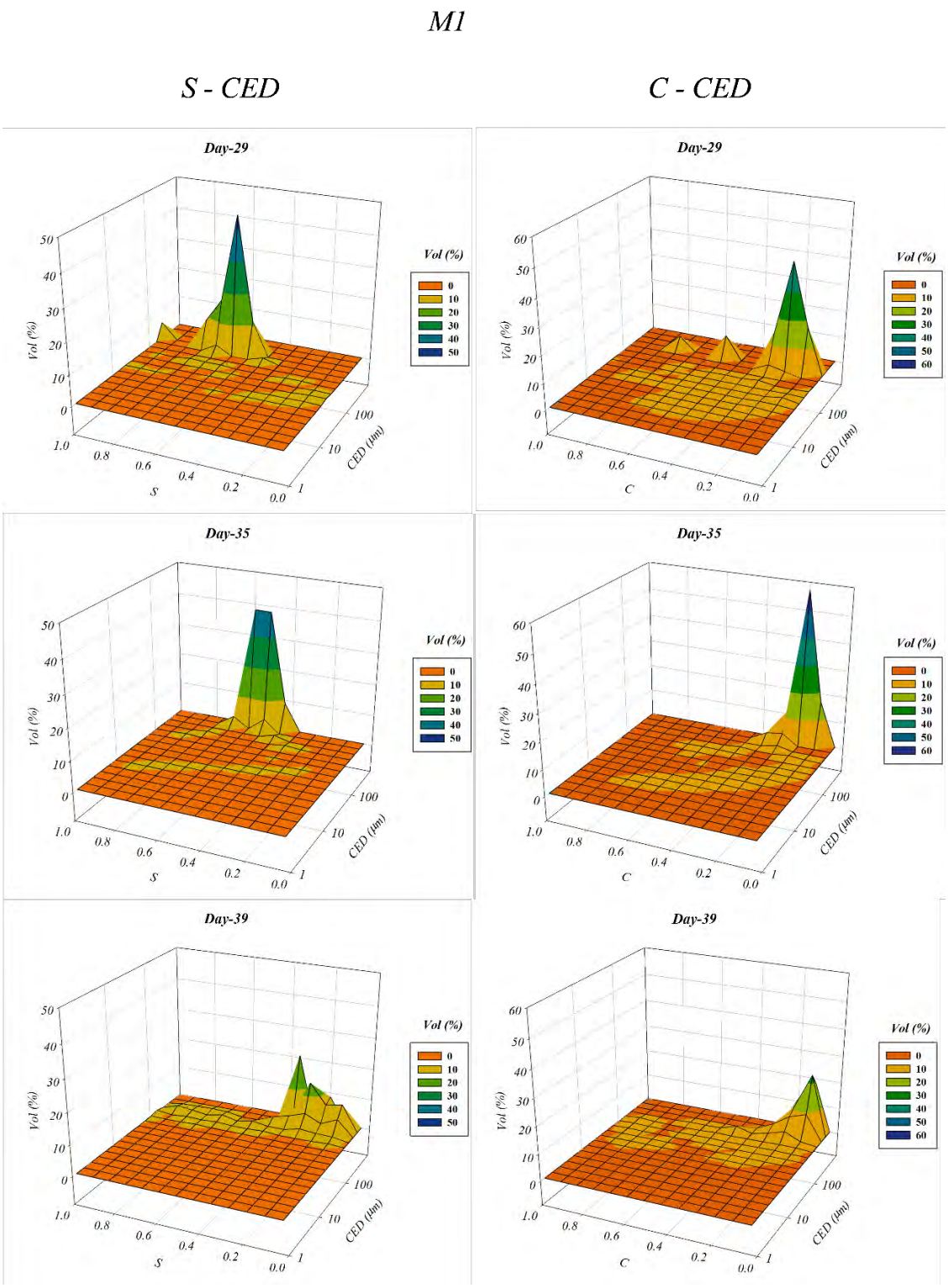

Figure V-10. Volume-based 3D-distributions of the pairs S-CED and C-CED for Days 29, 35 and 39 from *M1*.

M2

S - CED *C - CED*

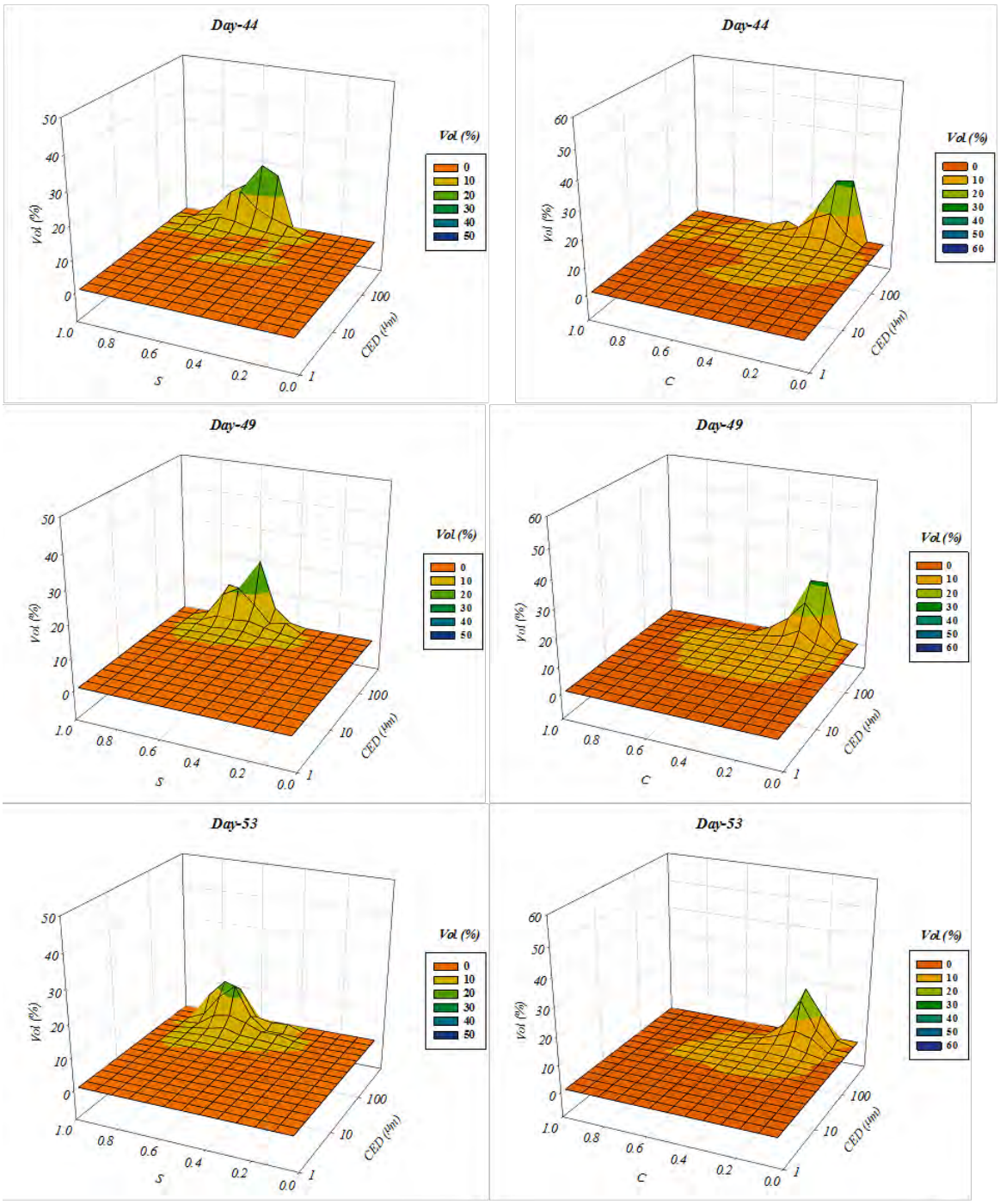

Figure V-11. Volume-based 3D-distributions of the pairs S-CED and C-CED for Days 44, 49 and 53 from *M2*.

V.3.2.4 Modification M3

The **Figure V-12** presents the curves for size (CED), circularity (C), convexity (C_x) and solidity (S) distributions during the modification *M3*, which consisted of increasing the recycle ratio from 1:1 to 3:1. All distributions are represented on a volume-based resolution.

Through an analysis of the size (CED) distributions, it is possible to state that increasing the recycle ratio has led to a decrease of the floc size, the mode of the distributions decreasing from 460 to 300 µm, confirming which was previously noticed during the evolution of the mean CED values (**Figure V-4**). The distributions have slightly moved to the left becoming broader than the one on *Day-57* or *58*, which means that floc population became more heterogeneous as well. It can be assumed that increasing the recycle ratio makes the sludge flocs more susceptible to the hydrodynamic shear stress that is mainly generated by the recycle pump. The breakage of the flocs into smaller ones might then occurs.

Contrary to the size distributions, the modification of the recycle ratio have had no meaningful impact on the shape parameters. Observing circularity (C), convexity (C_x) and solidity (S) distributions, altogether, it is possible to notice a similar behaviour among them. They did not present a significant displacement of their respective distributions after the recycle ratio had been increased. However, a slight shift of their tails could be verified, circularity and convexity to the right, while solidity moved to the left. This observation indicates that a new population of large flocs were relatively more circular, less rough and with more concavities either.

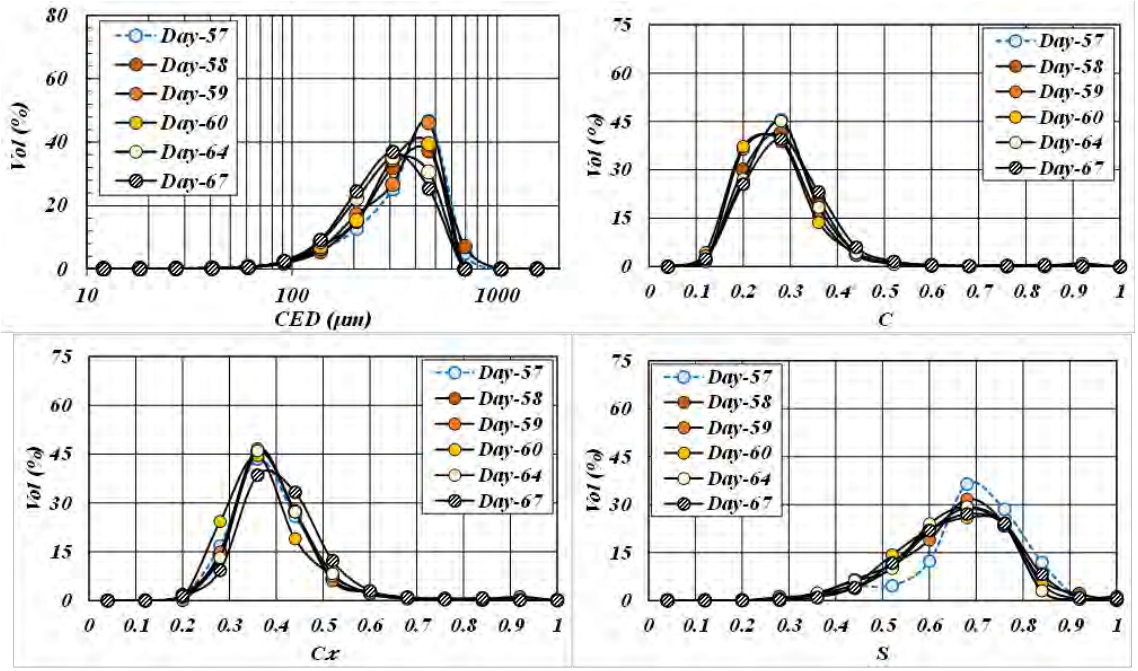

Figure V-12. Evolution of the size (CED), circularity (C), convexity (C_x) and solidity (S) distributions on volume basis for *M3*.

Trends in this modification could be confirmed by the microscopic inspection showed in **Table V-8**, as follows.

Table V-8. Microscopic observations in *Day-58*, *60*, *64* and *67* from *M3*

Day-58	Day-60	Day-64	Day-67
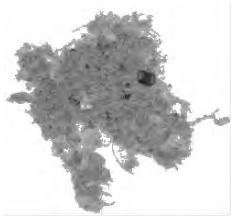	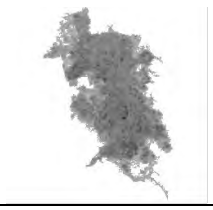	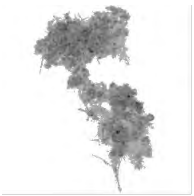	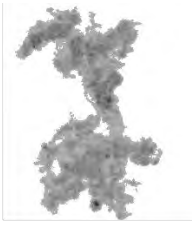
CED = 373.4 µm *C* = 0.32 C_x = 0.40 *S* = 0.73	*CED* = 350.5 µm *C* = 0.30 C_x = 0.40 *S* = 0.71	*CED* = 293.6 µm *C* = 0.23 C_x = 0.34 *S* = 0.62	*CED* = 297.8 µm *C* = 0.25 C_x = 0.36 *S* = 0.60

Along the modification, the evidence that activated sludge flocs were fragmented by recycle ratio increase was progressively noticed since the aggregates seemed to detach from each other by the *Day-64* and *67*.

V.3.2.5 Modification M4

Figure V-13 shows the curves for size (CED), circularity (C), convexity (C_x) and solidity (S) distributions throughout the modification *M4*, which consisted of decreasing the C:N ratio from 100:7 to 100:28. All distributions are represented on a volume-based resolution.

Evaluating the size (CED) distributions, no meaningful change was perceived at the distribution curves until *Day-72*. About *Day-73*, size distribution has become wider than before around the same mode. Based on literature studies, it might indicate another decrease of floc size. This time, flocs were broken up as a consequence of decreasing COD:N ratio. Possible hypotheses to explain this floc rupture were listed below:

- According to Ye et al. (2011), low COD:N ratio means a considerable concentration of nitrogen in relation to carbon in the feed. When microorganisms are submitted to such conditions they stop producing extracellular polysaccharides and start stocking carbon to maintain their activities. As EPS are known to be essential to aggregate cohesion, their diminution can increase flocs fragility and thus a slight modification of the size distributions may occur.

- Furthermore, Amanatidou et al. (2016) have reported that at low COD:N ratio, the quantity of denitrification gases increases. Therefore, the N_2 trapped into the flocs can exert a pressure coming from inside that favours floc breakage.

At the end of *M4* (*Day-85*), a distribution narrowing was observed, suggesting that a fraction of the large aggregates from *Day-81* was broken generating flocs of smaller sizes. The population reaching a better homogeneity than at the beginning of the phase.

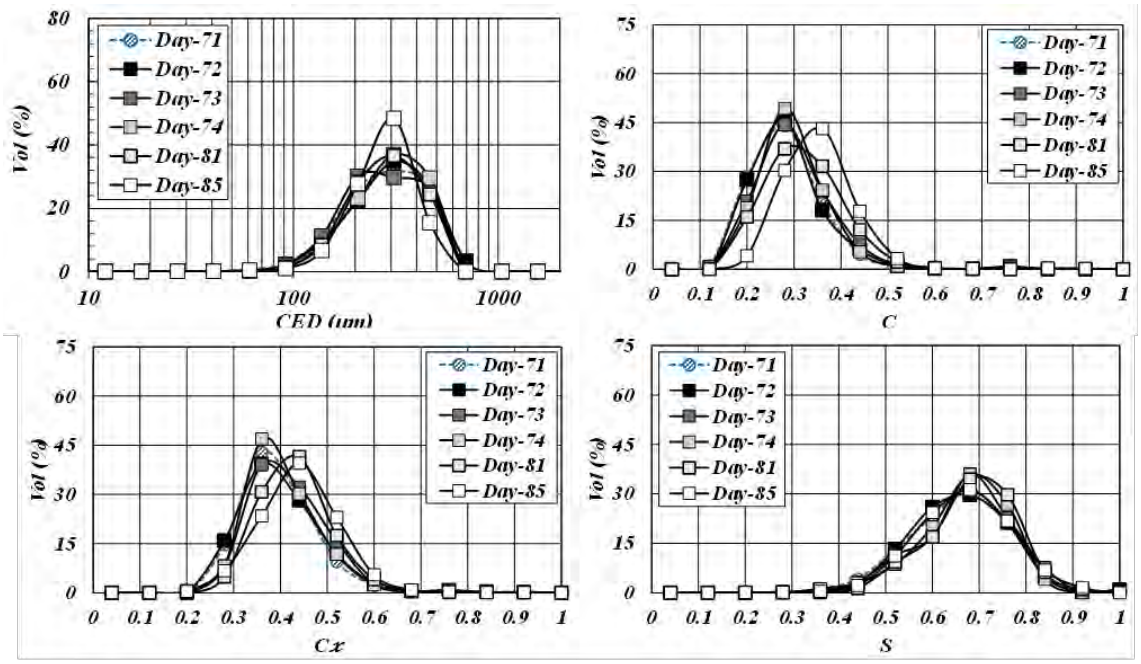

Figure V-13. Evolution of the size (CED), circularity (C), convexity (C_x) and solidity (S) distributions on volume basis for *M4.*

Evaluating the distributions of circularity (C) and convexity (C_x), it is possible to see that distributions have shifted towards the right throughout the last days (*Day-82* and *85*), indicating that flocs shape was closer to a circle and less rough than in the previous case. The modes increased from 0.28 to 0.36 for circularity and 0.36 to 0.44 for convexity. As enlightened before this type of behaviour can be explained by the decrease of aggregate size through this modification since smaller flocs tend to present higher values of circularity and convexity.

For solidity (S) distributions, any difference on floc behaviour related to this shape descriptor was noticed between the end of *M3* and the whole *M4*, suggesting that both modifications have a similar effect on the values of activated sludge flocs solidity.

By means of the microscopic observations, as it is shown in **Table V-9**, floc morphological characteristics were not so different from those splitting apart at the end of *M3*. As circularity and convexity values have increased, this fact is more evident in the images when compared to solidity behaviour, which was quite constant.

Table V-9. Microscopic observations in *Day-72*, *74*, *81* and *85* from *M4*.

Day-72	Day-74	Day-81	Day-85
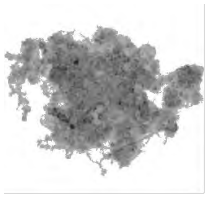	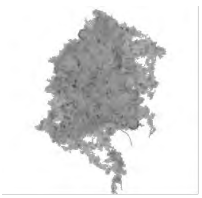	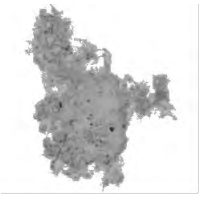	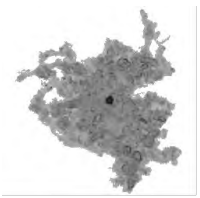
CED = 305.3 µm *C* = 0.35 C_x = 0.42 *S* = 0.80	*CED* = 307.0 µm *C* = 0.37 C_x = 0.46 *S* = 0.78	*CED* = 298.7 µm *C* = 0.36 C_x = 0.47 *S* = 0.73	*CED* = 302.2 µm *C* = 0.35 C_x = 0.45 *S* = 0.73

V.3.3 Summarizing the modifications effects on the activated sludge flocs morphology

The size (CED), circularity (C), convexity (C_x) and solidity (S) distributions at the end of each phase were placed side by side in order to identify the main effects promoted by the modifications (*M1, M2, M3* and *M4)* on activated sludge flocs morphology (**Figure V-14**). All distributions are represented on a volume-based resolution.

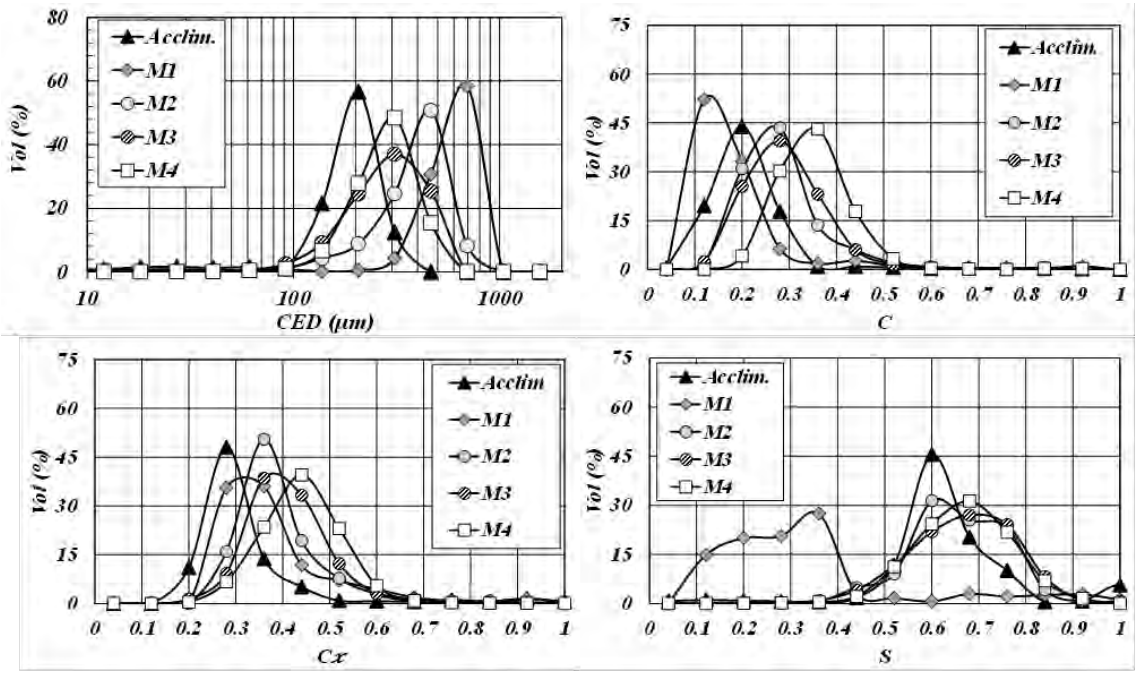

Figure V-14. Comparison among the final distributions of each period (*Acclimation, M1, M2, M3 and M4)* during this campaign.

- *Acclimation* → *M1*:

The size of the flocs has increased greatly presenting low circularities and high surface roughness. In addition, the values of solidity showed high sensitivity to this modification.

Such morphological characteristics are coherent with the filamentous bulking that was detected during *M1*.

- *M1* → *M2*:

Once acclimation conditions were restored, the flocs have decreased their sizes showing an apparently more circular and smoother structure. Moreover, solidity values similar to those from the *Acclimation* phase could be noticed. However, these morphological changes seem to be more related to the fact that sludge has been washed out with the treated effluent at the end of *M1* than to the fact that OLR was decreased. The morphological characteristics of bioflocs at the end of *M2* were highly different from the ones at the end of the *Acclimation* indicating that the impacts caused by *M1* were not completely reversible, at least within 15 days.

- *M2* → *M3*:

Changing recycle ratio from 1:1 to 3:1 promoted floc rupture triggered by a higher shear stress. This phenomenon is well represented by the size distribution that shifted to the left. At the same time, the shape descriptors (circularity, convexity and solidity) slightly increased.

- *M3* → *M4*:

The size distribution has narrowed during *M4*. Since floc size has decreased, their circularity and convexity have once again increased. No significant effect of this modification on solidity distribution was observed.

V.3.4 Evolution of fractal dimensions (D_{pf} and D_2) over modifications

As mentioned in **Chapter II**, while D_{pf} is obtained from the slope of log-log plots of *A versus P* ($A \propto P^{2/D_{pf}}$), D_2 is determined through a similar method, where L_{max} is used instead of *P*. According to these fractal approaches, densely packed and rather circular aggregates are prone to present D_{pf} and D_2 next to 1 and 2, respectively. On the other hand, if flocs are highly branched or show a rather loose conformation, then D_2 tends towards 1 while D_{pf} can assume values beyond 1. **Figure V-15** illustrates the evolution of both, D_{pf} and D_2, over the modifications.

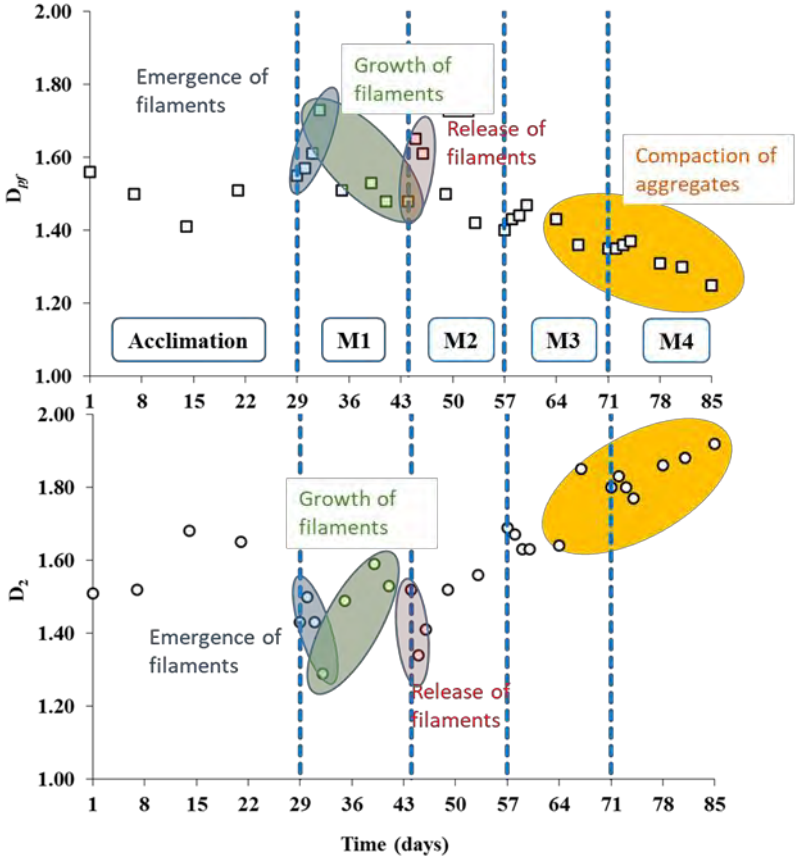

Figure V-15. Variations of D_2 and D_{pf} over the operating condition modifications.

The variations of both fractal dimensions can be explained by the evolution of number or volume-based distributions of Perimeter (P), Area (A) and Maximum Length (L_{max}). For the sake of the clarity, only some specific days distributions are reported in the following paragraphs, nevertheless all the distributions can be consulted in the **Annex II** of the manuscript.

During the first two weeks of the Acclimation step (Day-*1* to *14*), the modes of the number distributions of the perimeter *P* (**Figure V-16 (a)**), the area *A* (**Figure V-16 (c)**), and the maximum length of flocs (L_{max}) (**Figure V-16(e)**) seem to not evolve significantly, indicating that the smallest aggregates (emphasized more on number distributions than on surface or volume distributions), which are also the most numerous do not show significant evolution, either in terms of size nor of shape.

If large aggregates are considered analysing volume distributions, it can be seen that the mode of volume-based perimeter *P* distribution (**Figure V-16 (b)**) decreases from 3300 µm to 1200 while the mode of the volume-based area *A* distribution (**Figure V-16 (d)**) also decreases from 40 000µm² to 18 000µm² and both distributions spread over a larger range. Thus, the area and perimeter of flocs simultaneously decrease, and since the perimeter decreases faster, D_{pf} also

tends to decrease from 1,56 on the *Day-1* to 1.41 on the *Day-14*. It seems that the flocs are more spherical and denser. D_2 also changes but following a slightly different way which may be explained by the change of L_{max} over the period (**Figure V-16 (f)**). Indeed, between *Day-1* to *Day-7*, L_{max} increases similarly to the floc area in a volume base, and thus D_2 does not change meaningfully. The evolution of L_{max} is much more noticeable between *Day-7* and *Day-14*, when a significant decrease of the mode of the distribution of L_{max} and a spread of the distribution may also be observed, leading to an increase of D_2 over the period from 1.52 the *Day-7* to 1.68 the *Day-14*.

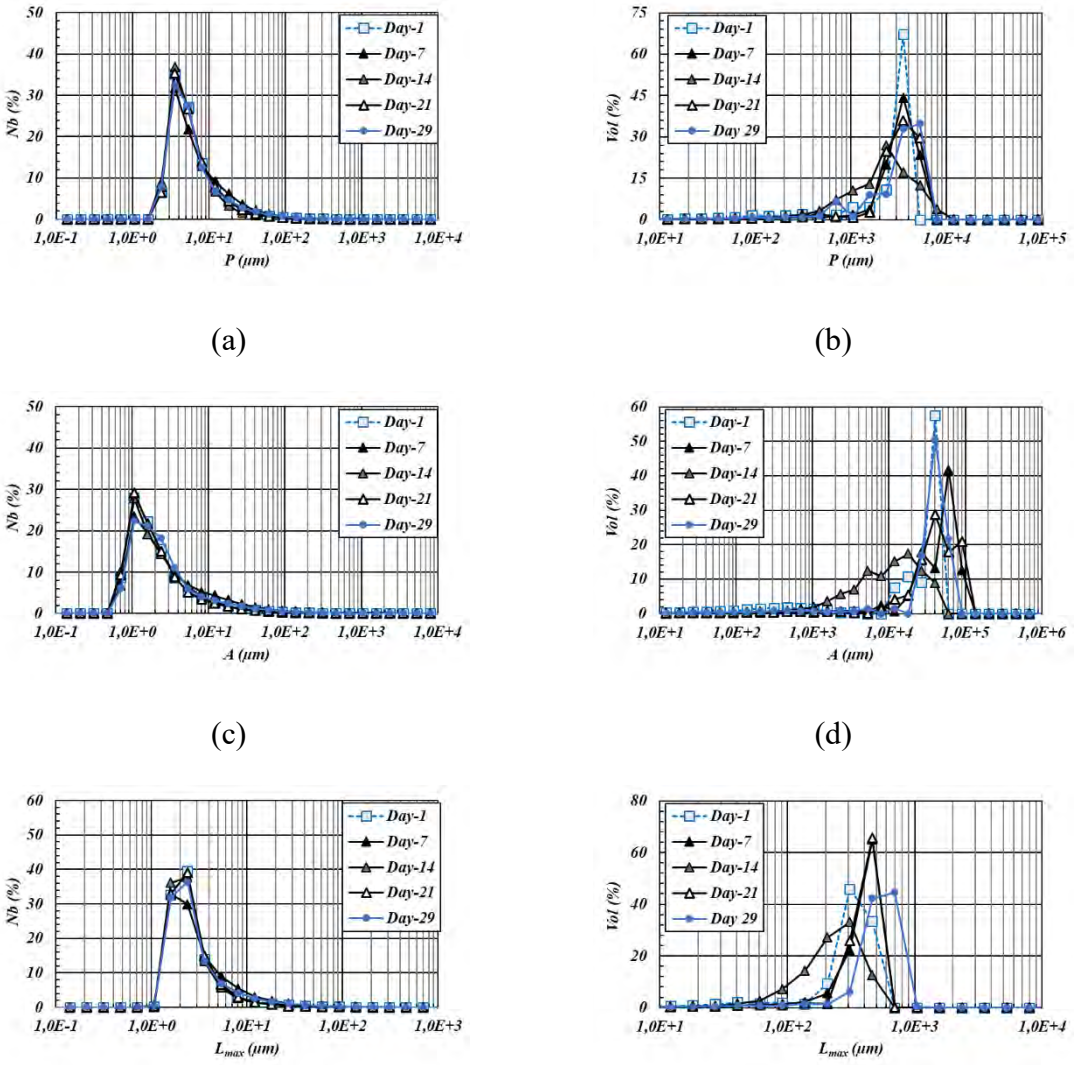

Figure V-16. Perimeter, Area and Maximum length distributions on number and volume basis during *Acclimation*.

Over the last part of the Acclimation phase (*Day-21* to *Day-29*), the number and volume distributions of the area and perimeter tend to stabilize around values close to the ones found in the first day, and so does D_{pf}, whose value is stable around 1.55. Concerning L_{max}, the distributions do not evolve expressively between *Day-14* to *Day-21*, and since the area slightly

increases during this period, D_2 also slightly decreases from 1.68 on the *Day-14* to 1.65 the *Day-21*. In the opposite, between *Day-21* and *Day-29*, L_{max}, considered on a volume basis, notably increases while the area is nearly constant, leading to a decrease of D_2 indicating that the large aggregates become less spherical and present more open structures with D_2 close to 1.43 at the end of the *Acclimation phase*.

Over *M1* modification, a strong increase of D_{pf} and an equivalent decrease of D_2 are observed during the increase of the loading rate. Along *M1*, the morphological properties of the whole population of flocs seem to evolve as it can be concluded observing the number and volume distributions of the different size parameters shown in **Figure V-17**.

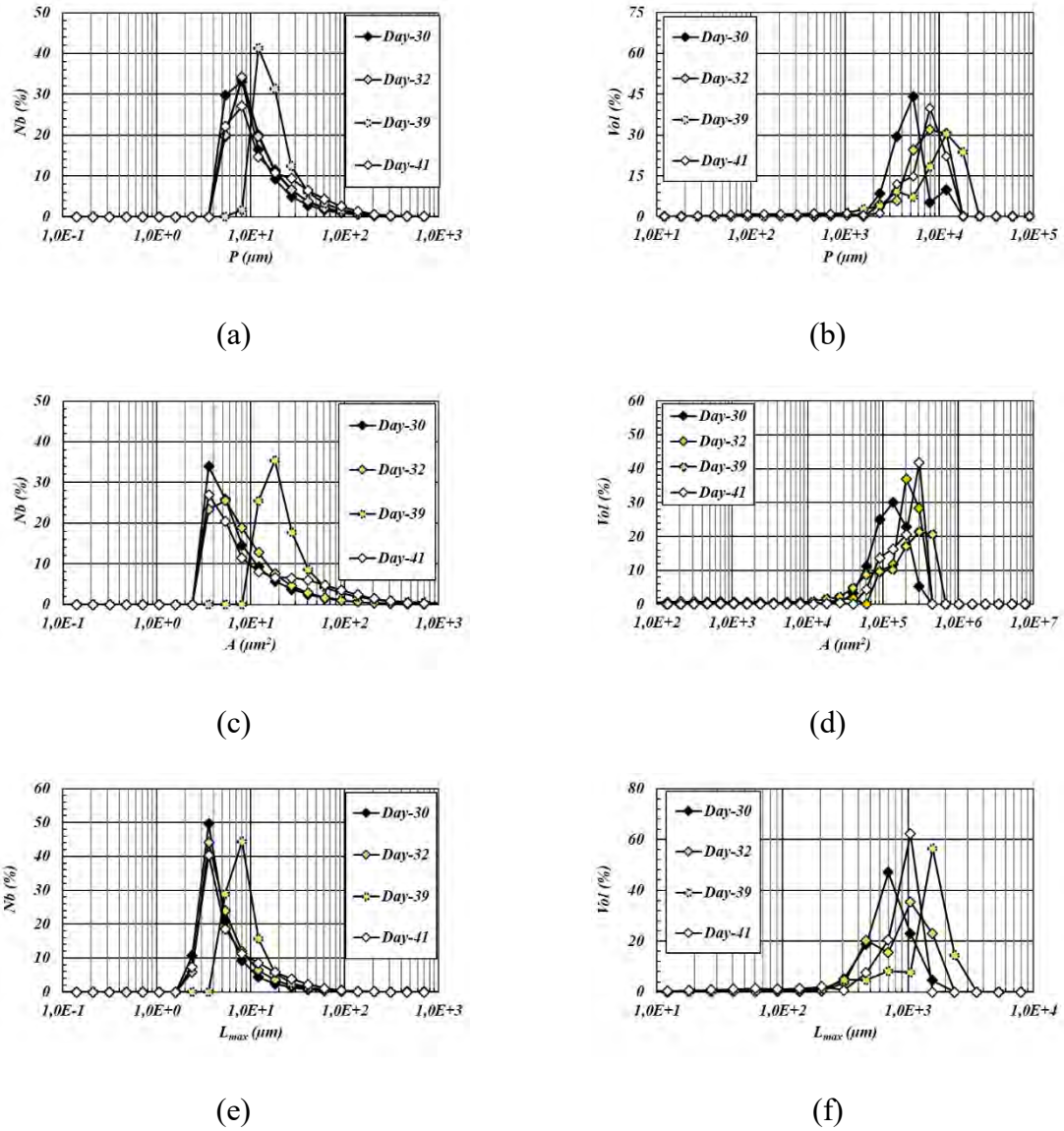

Figure V-17. Perimeter, Area and Maximum length distributions on number and volume basis over *M1*.

Between *Day-30* and *Day-32* of *M1* modification, the emergence of filamentous bacteria induces an increase of the perimeter and the maximum length of flocs, while the area does not vary much as it can be seen on the number and volume distributions. A simplified scheme is proposed (**Figure V-18**) to illustrate this evolution. The appearance of small filaments on the outer edge of flocs is identified as an increase of the surface roughness, expressed by an increase of D_{pf} from 1.57 on the *Day-30* to 1.73 on the *Day-32* and a decrease of D_2 from 1.50 on the *Day-30* to 1.28 on the *Day-32*. The shape of aggregates being less and less spherical, their compactness decreases.

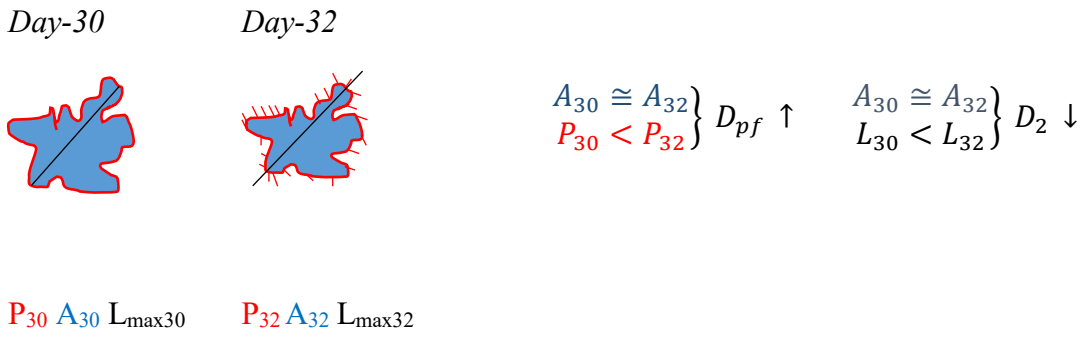

Figure V-18. Scheme illustrating how floc area and perimeter variations between Day-30 and 32 may impact both fractal dimensions.

The growth of filaments continues until about *Day-39*, producing aggregates with a great number of filaments at their outer edge. Between *Day-32* and *Day-39*, a strong increase of the area is observed on the number distribution and a smaller one is detected on the volume-based area distribution. The perimeter distribution, both on a number or volume base, for this part, stays relatively unchanged during that period. These contrasted evolutions may be explained by the way that images are analysed. Indeed, when the filaments become long and numerous, the software is not more able to individualize the filaments and link this packs of filaments to portions of the aggregates, as it is suggested in the scheme below (**Figure V-19**).

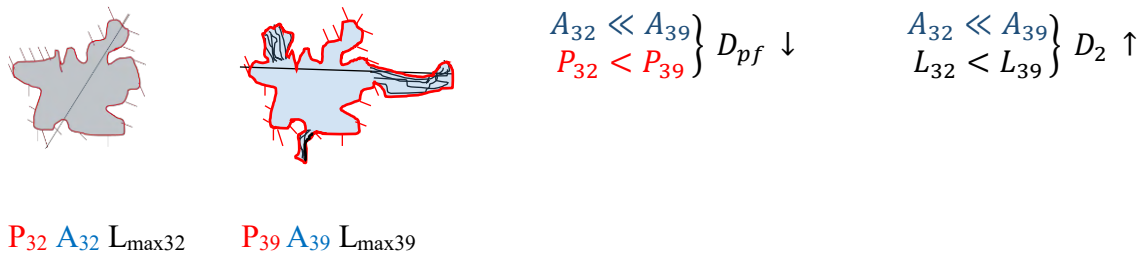

Figure V-19. Scheme illustrating how floc area and perimeter variations between Day-32 and 39 may affect both fractal dimensions.

Thus, the strong development of filaments is interpreted by image analysis as an important decrease of D_{pf} from 1.61 on the *Day-32* to 1.53 on the *Day-39* and respectively an increase of

D_2 (from 1.29 on the *Day-32* to 1.59 on the *Day-39*), suggesting a "fake" compaction and densification of the flocs. Indeed, as it was mentioned in the previous sections, the growth of filaments implied a decrease of the morphological parameters (circularity and solidity) and a strong increase of SVI values which are characteristic of aggregates poorly compacted and with highly irregular shapes.

From the *Day-41* to *Day-45*, the area, the perimeter and the maximum length of the large aggregates decrease while those of the smaller ones slightly increase as it is respectively suggested by the volume and number distributions (**Figure V-20**).

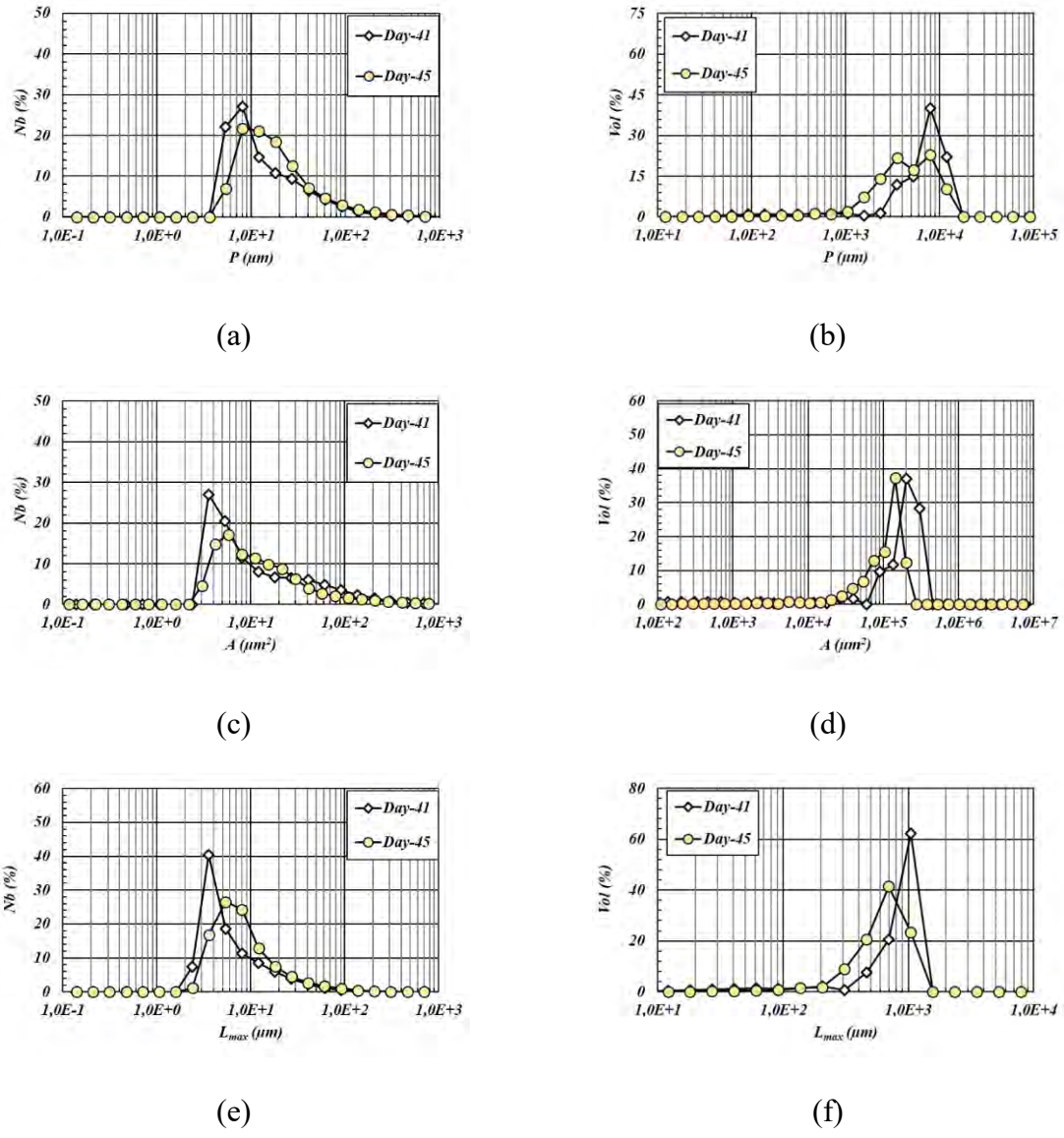

Figure V-20. Perimeter, Area and Maximum length distributions on number and volume basis from Day-41 to 45.

This trend is directly related to the release of the filaments. Indeed, when the filaments are detached from the aggregates, the number of small fragments strongly increases. Moreover,

these filaments are elongated, so the mean perimeter and the maximum length of the small objects obviously increase. Concerning the large aggregates, losing their filaments, their area decreases, as well as their perimeter and maximum length as suggested by the **Figure V-21**. Since the fractal dimensions are based on number calculations, the emergence of a new population of highly elongated filaments leads to the increase of D_{pf} from 1.48 on the *Day-41* to 1.65 on the *Day-45* and a respective decrease of D_2 from 1.53 to 1.34.

Day-41 *Day-45*

Figure V-21. Representation of filaments detachment between Day-41 and 45.

From *Day-45* until the end of *M2*, it can be noticed that the area (number distribution) is fairly constant as shown in **Figure V-22**. The perimeter and the maximum length slightly decrease leading to a decrease of D_{pf} from 1.65 on the *Day-45* to 1.40 on the *Day-57* and an increase of D_2 from 1.34 on the *Day-45* to 1.69 on the *Day-57*, characterizing a progressive compaction of the aggregates.

The *M3* modification corresponds to an increase of the recycle ratio, which induced during the first days a slight decrease of the area (volume base distribution) probably linked to the aggregate size reduction (**Figure V-23**). Indeed, increasing the recycle ratio, the aggregates are more likely to be broken by the increase of the frequency of the mechanical stress. During the four first days, the perimeter and the maximum length are nearly not impacted, thus leading to an increase of D_{pf} from 1.40 the *Day-57* to 1.47 to Day-60 and a slight decrease of D_2 from 1.69 to 1.63.

Finally, during M4, the change of the ratio DCO:N induced a slight decrease of the perimeter and of the maximum length while the area was nearly constant (**Figure V-24**). Thus, it led to a regular decrease of D_{pf} from 1.35 on the *Day-71* to 1.25 on the *Day-85* (respectively a progressive increase of D_2 from 1.80 to 1.92) suggesting a compaction of the aggregates as it was already assumed observing the other morphological parameters.

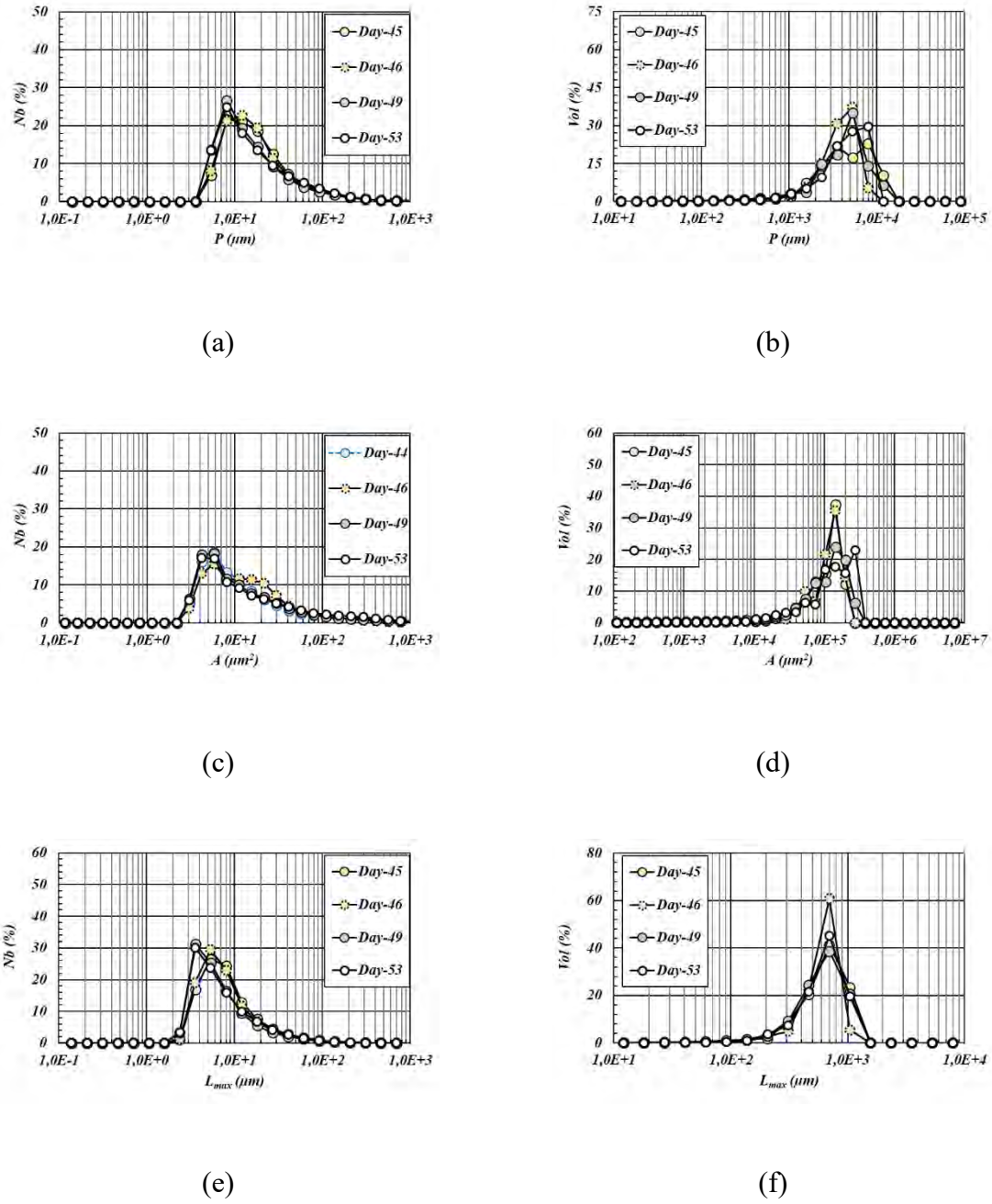

Figure V-22. Perimeter, Area and Maximum length distributions on number and volume basis over *M2*.

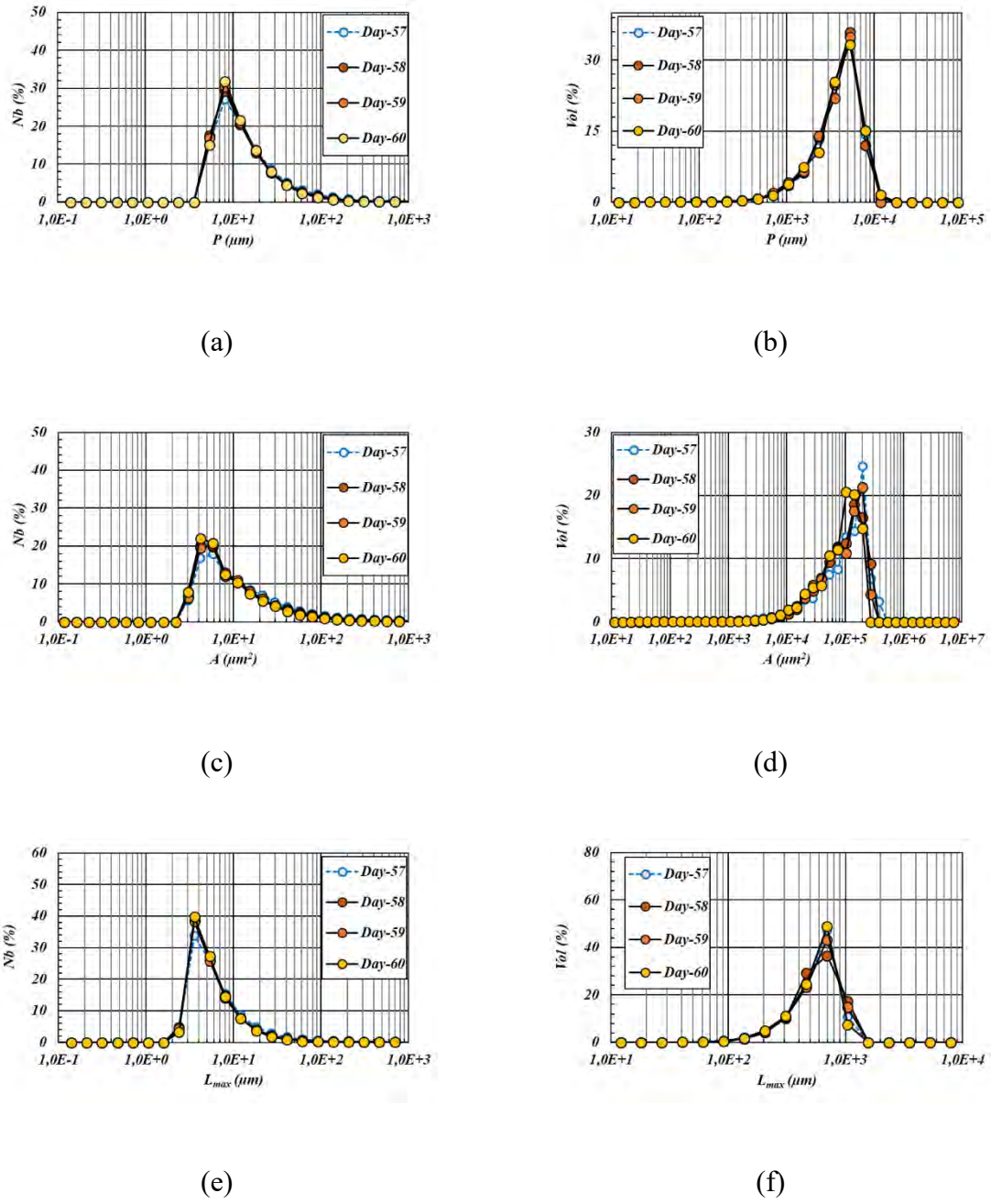

Figure V-23. Perimeter, Area and Maximum length distributions on number and volume basis over the beginning of *M3*.

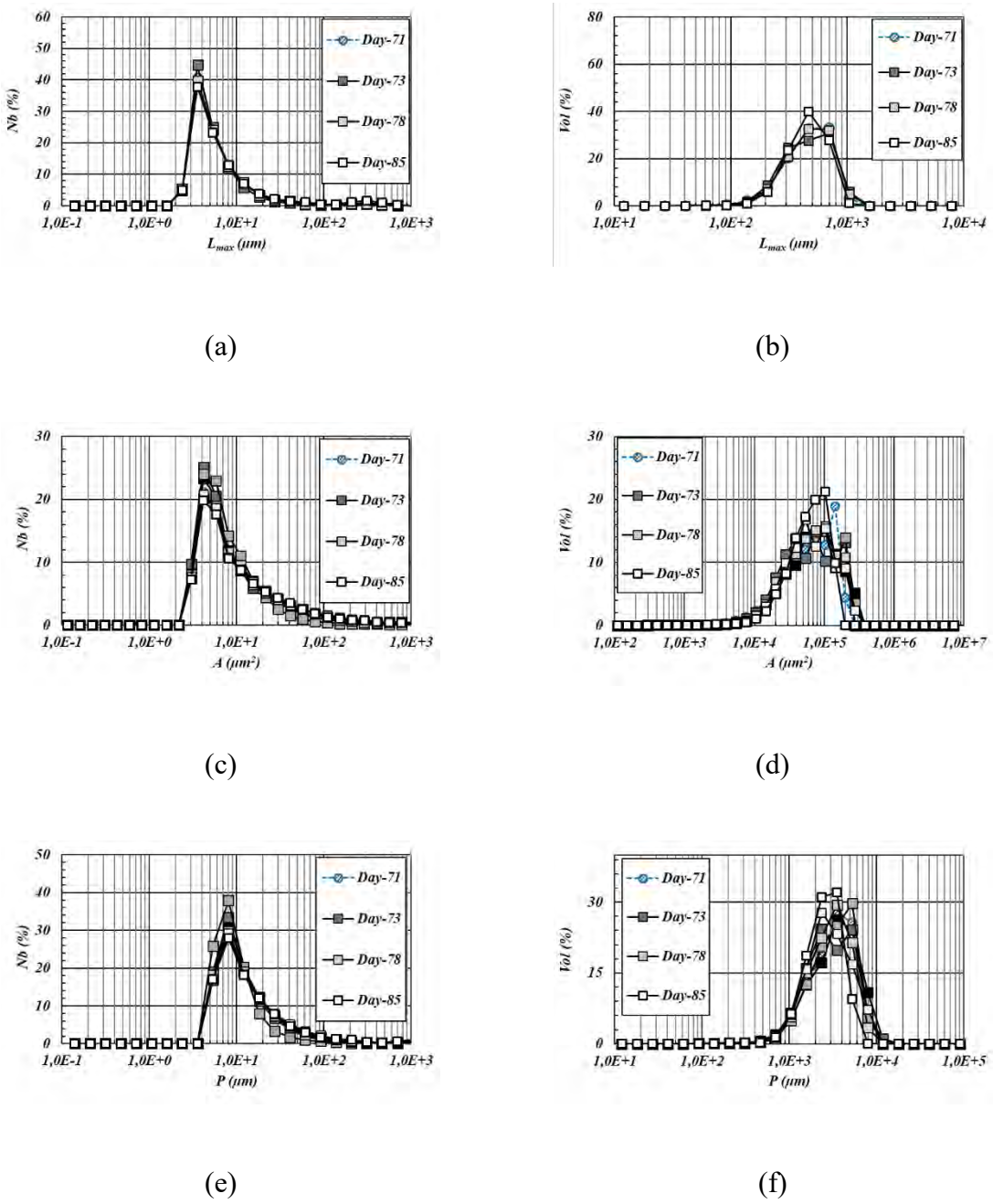

Figure V-24. Perimeter, Area and Maximum length distributions on number and volume basis over the beginning of *M4*.

In summary, assessing fractal dimension can be a valuable tool to support a well-based morphological characterization of activated sludge flocs. It allows not only the detection of process disturbances as the growth of filamentous bacteria but also to identify patterns in activated sludge system behaviour as the release of filament contents or the evolution of the aggregates towards a better compaction.

V.4 Conclusion

In this chapter, the pilot performance was evaluated under various operating conditions. After an acclimation period the pilot has been submitted to OLR, COD:N and recycle ratio modifications. The sludge and effluent quality parameters have been put in relation with the morphological properties of flocs, determined through the Image Analysis protocol presented in **Chapter III** The main following conclusions can be drawn:

- The *Acclimation* period was marked by the stability of the sludge quality parameters as TSS or SVI after almost 1 SRTs. The values of effluent quality parameters also reveal an adequate performance of the AS lab-scale pilot within this phase. In parallel, it was noticed that the floc CED also became stable after about 1 SRT, while the morphological parameters, solidity, circularity and convexity continued to evolve over about 2 SRTs.

- Increasing the OLR (*M1*) of the system lead to an increase in TSS concentrations and SVI values over the maximum acceptable limit (150 mL.g-1). The COD and nitrogen removal were both impacted as well. Microscope observations exposed a filamentous bulking event characterized by large flocs and a drop in the mean solidity values (from 0.6 to 0.35). It is clear that the development of filamentous bacteria, known to have a negative impact on wastewater treatment performance can be easily seen on size and shape properties, notably on the solidity parameter that is highly sensitive to the presence of large concavities. These variations are even more evident after examining the 3D-distributions for the pair S-CED.

- Because of the bulking event, sludge plagued by filaments has been washed out at the end of *M1* and beginning of *M2*. It mainly explains the stabilization of TSS and the variability of SVI values during *M2*. The sludge washed out also had an impact on the mean CED since the large flocs with a loosely structure were removed. The solidity also drastically increased since much less concave flocs still remained in the clarifier. At the same time, the number-based distributions of the aspect ratio changed a lot putting in evidence the release of the small filaments.

- During the increase of recycle ratio (*M3*) and the decreased of C:N ratio (*M4*), no meaningful variations were observed in the evolutions of TSS, SVI and solidity values. COD concentrations were slightly higher in *M3* because of a probable release of soluble organic material after floc breakage. On the other hand, nitrogen removal has been compromised as shown by the high concentrations of ions $NH4^+$ in the treated effluent over both modifications. Since *M3* and *M4* provoked a decreased in the mean floc size, the flocs have gradually presented a more regular shape.

- Finally, the evolution of two fractal dimensions (D_{pf} and D_2) have been presented over the whole second campaign. Their variations have been discussed and related to the changes of the number and volume-based distributions of area (*A)*, Perimeter (*P)* and maximum length (L_{max}). The results reveal that the rise and the release of filaments can be expressed by a prompt increase of D_{pf} and a rapid increase of D_2, whereas the growth of filaments generated a fast diminution of D_{pf} and a slight increase of D_2. The monitoring of a fractal dimension seemed thus able to detect the apparition of filamentous bulking.

From these results, it is clear that the size and shape floc properties, in particular the CED and solidity or circularity values are dependent to each other. The shape parameters being more sensitive to sludge modifications, especially in relation to the development of filamentous bacteria or the release of the filaments.

V.5 References

Amanatidou, E., Samiotis, G., Bellos, D., Pekridis, G., and Trikoilidou, E. (2015a). Net biomass production under complete solids retention in high organic load activated sludge process. Bioresour. Technol. *182*, 193–199.

Amanatidou, E., Samiotis, G., Trikoilidou, E., Pekridis, G., and Taousanidis, N. (2015b). Evaluating sedimentation problems in activated sludge treatment plants operating at complete sludge retention time. Water Res. *69*, 20–29.

Amanatidou, E., Samiotis, G., Trikoilidou, E., Tzelios, D., and Michailidis, A. (2016). Influence of wastewater treatment plants' operational conditions on activated sludge microbiological and morphological characteristics. Environ. Technol. *37*, 265–278.

Barbusiński, K., and Kościelniak, H. (1995). Influence of substrate loading intensity on floc size in activated sludge process. Water Res. *29*, 1703–1710.

Chao, A.C., and Keinath, T.M. (1979). Influence of process loading intensity on sludge clarification and thickening characteristics. Water Res. *13*, 1213–1223.

Çiçek, N., Franco, J.P., Suidan, M.T., Urbain, V., and Manem, J. (1999). Characterization and Comparison of a Membrane Bioreactor and a Conventional Activated-Sludge System in the Treatment of Wastewater Containing High-Molecular-Weight Compounds. Water Environ. Res. *71*, 64–70.

Fulazzaky, M.A., Abdullah, N.H., Mohd Yusoff, A.R., and Paul, E. (2015). Conditioning the alternating aerobic–anoxic process to enhance the removal of inorganic nitrogen pollution from a municipal wastewater in France. J. Clean. Prod. *100*, 195–201.

Grady, C.P.L., Daigger, G.T., Love, N.G., and Filipe, C.D.M. (2011). Biological Wastewater Treatment (IWA Publishing - Co-Publication).

Kim, J.-S., Lee, C.-H., and Chang, I.-S. (2001). Effect of pump shear on the performance of a crossflow membrane bioreactor. Water Res. *35*, 2137–2144.

Liu, Y., and Tay, J.-H. (2004). State of the art of biogranulation technology for wastewater treatment. Biotechnol. Adv. *22*, 533–563.

Meng, F., Yang, F., Xiao, J., Zhang, H., and Gong, Z. (2006). A new insight into membrane fouling mechanism during membrane filtration of bulking and normal sludge suspension. J. Membr. Sci. *285*, 159–165.

Mesquita, D.P., Amaral, A.L., and Ferreira, E.C. (2011). Characterization of activated sludge abnormalities by image analysis and chemometric techniques. Anal. Chim. Acta *705*, 235–242.

Paul, E., Plisson-Saune, S., Mauret, M., and Cantet, J. (1998). Process state evaluation of alternating oxic-anoxic activated sludge using ORP, pH and DO. Water Sci. Technol. *38*, 299–306.

Rodríguez, D.C., Pino, N., and Peñuela, G. (2011). Monitoring the removal of nitrogen by applying a nitrification–denitrification process in a Sequencing Batch Reactor (SBR). Bioresour. Technol. *102*, 2316–2321.

Wilén, B.-M., and Balmér, P. (1999). The effect of dissolved oxygen concentration on the structure, size and size distribution of activated sludge flocs. Water Res. *33*, 391–400.

Xu, W., and Gao, B. (2012). Effect of shear conditions on floc properties and membrane fouling in coagulation/ultrafiltration hybrid process—The significance of Alb species. J. Membr. Sci. *415*, 153–160.

Ye, F., Ye, Y., and Li, Y. (2011). Effect of C/N ratio on extracellular polymeric substances (EPS) and physicochemical properties of activated sludge flocs. J. Hazard. Mater. *188*, 37–43.

Conclusions et perspectives

A l'heure actuelle, les procédés à boues activées représentent la voie de traitement biologique la plus largement utilisée, en raison notamment de son faible coût *d'investissement* et de sa facilité d'exploitation. Ces procédés font intervenir un ensemble de microorganismes agglomérés sous la forme de flocs biologiques dont le principal rôle est de dégrader la pollution. Ce procédé est constitué d'un réacteur biologique au sein duquel les eaux résiduaires sont mélangées avec de la biomasse (flocs biologiques) maintenue en suspension et d'un décanteur. La pollution présente dans les eaux à épurer sert de substrat pour le développement des micro-organismes contenus dans la biomasse. Cette dernière est ensuite séparée par décantation au sein d'un clarificateur et une partie de la biomasse est recyclée dans le réacteur. Les propriétés morphologiques des agrégats qui jouent un rôle primordiale sur l'efficacité du procédé, particulièrement sur la décantation, elles sont fortement influencées par les conditions opératoires.

Dans ce contexte, ce travail de thèse a eu pour objectif principal d'apporter un nouvel éclairage sur cette relation entre les paramètres opératoires, les propriétés morphologiques des flocs et les performances du procédé, en se centrant sur les propriétés de taille et de forme des flocs de boues. Par ce biais, nous souhaitions aussi apporter une meilleure compréhension des perturbations qui peuvent avoir lieu au sein des procédés par boues activées et voir dans quelle mesure il était possible de les anticiper.

Pour ce faire, la mise au point d'un protocole d'analyse d'images a, tout d'abord, été réalisée en utilisant le microscope automatique Morphologi G3^{TM} sur des échantillons de boues activées réelles provenant de différentes stations d'épuration. La mise au point du protocole a consisté en la détermination des paramètres permettant d'assurer une caractérisation morphologique précise, fiable et statistiquement significative des flocs des boues activées. Ainsi, les principaux résultats sont les suivants :

- Le choix d'une cellule en voie humide permet de limiter l'endommagement des agrégats.

- Le facteur de dilution 1:10 permet d'obtenir une répartition spatiale des agrégats au sein de la cellule en voie humide de manière assez satisfaisante, résultant d'un arbitrage entre le recouvrement des agrégats et la modification de leur taille ou leur structure.

- Des essais dédiés à la répétabilité et la précision des mesures ont mis en évidence que le grossissement 10x et le nombre minimum de particules en tant que critère d'arrêt de l'analyse représentent le meilleur compromis afin de conserver l'intégralité de échantillon et garantir la véracité des résultats tout en conservant une durée d'acquisition et de traitement des données acceptable.

- Les tests de convergence réalisés sur les paramètres de taille aussi bien que de forme ont montré que la convergence statistique pour l'ensemble des paramètres est atteinte pour environ 100 000 flocs.

- L'acquisition des images doit toujours être réalisée dans les mêmes conditions de contraste maximal, le seuil de binarisation mis en œuvre lors du traitement des images a été défini à 183.

Une installation expérimentale a ensuite été conçue sur la base d'un système à boues activées classique. La première campagne expérimentale a eu pour objectif d'étudier l'influence du temps de séjour (SRT de 15, 20 ou 30 jours) sur les propriétés morphologiques des agrégats et l'efficacité du procédé qui a été évaluée en termes de MES dans le bassin, IB, DCO soluble, concentration en azote souble total, et en ammonium et nitrate. Un ajout de nutriments à la composition initiale de l'effluent synthétique a également été mis en place pendant cette campagne et conservé pour la suite. Son impact sur le fonctionnement du procédé et les caractéristiques des flocs est donc également discuté.

Les résultats de cette première campagne ont mis en évidence les résultats suivants :

- Le suivi de paramètres de qualité de l'effluent a prouvé le bon fonctionnement de l'installation pilote. Globalement, les pourcentages observés pour le taux d'abattement de la DCO étaient de bonne qualité car supérieurs à 90% sur l'ensemble de la campagne. D'autre part l'élimination d'azote total a été de moins bonne qualité pendant cette première campagne, aux alentours de 40%. L'ajout de micronutriments qui avait pour but l'amélioration des niveaux d'élimination d'azote n'a eu un effet curatif probablement trop tardif.

- Le suivi des Matières En Suspension et de l'Indice de Boue a montré que la concentration de la biomasse a varié fortement pour un âge de boue important. Pour cet âge de boues de 30 jours l'IB a légèrement augmenté, impliquant de ce fait une légère diminution de la capacité de sédimentation des flocs de boues.

- Le suivi des paramètres de taille et de forme des agrégats a été effectué non seulement sur les valeurs moyennes mais aussi sur les distributions. Il en ressort qu'en régime stationnaire ces propriétés morphologiques semblent indépendantes de l'âge de boue. Ainsi, toute modification de l'âge de boues, dans la gamme 15-30 jours, n'a qu'un effet transitoire sur la taille et la forme des agrégats.

La deuxième campagne expérimentale a été réalisée sur des types de modifications opératoires plus variés, à savoir le changement de la charge volumique (*OLR*), du taux de recirculation et du rapport COD:N.

Les principales conclusions sont rappelées ci-dessous :

- Une augmentation des MES et de l'IB est observée lorsque une forte charge volumique est imposée au système. De façon concomitante, les analyses réalisées sur l'effluent de sortie ont montré une diminution de l'efficacité du procédé vis-à-vis de l'abattement de la DCO et de l'azote total. A leur tour, les caractéristiques morphologiques des flocs ont fortement évolué et se sont traduites par une augmentation significative de la taille et une diminution des paramètres de forme tels que la circularité et la solidité, suggérant l'apparition significative de concavités à la surface des flocs. Bien que l'augmentation de l'IB soit un bon indicateur d'une perturbation du système, il ne permet pas à lui seul

d'identifier la cause du problème. Par contre, couplé aux mesures morphologiques il a permis de confirmer le développement d'un foisonnement filamenteux lors de l'augmentation de la charge volumique.

- Le couplage des analyses classiques avec les caractérisations morphologiques a ensuite permis d'identifier un phénomène de lessivage de boues. En effet, l'évacuation de boues par la surverse du décanteur est caractérisée par une diminution de la concentration de biomasse (MES) et de fortes valeurs d'IB suivies par une diminution de la taille des flocs et une augmentation brusque de la solidité.

- La diminution de la charge organique a par la suite entraîné le relargage de filaments. Les analyses classiques ont été moins sensibles à l'apparition de ce phénomène étant donné que les valeurs de MES, DCO et azote total n'ont que peu varié pendant cette période. Les paramètres morphologiques, que ce soit en termes de valeurs globales (moyennes) ou de distributions ont été nettement plus impactés par ce phénomène qui s'est matérialisé par une diminution du rapport d'aspect des flocs et l'apparition de la bimodalité des distributions en volume de la circularité et de la convexité.

- Les modifications de taux de recirculation et de rapport DCO:N ont présenté peu d'impact sur la performance, laquelle est restée globalement conforme à ce qui est généralement observé dans des stations d'épuration réelles et ce, jusqu'à la fin de cette campagne. L'impact de ces modifications a été plus évident pour les paramètres de taille et forme des flocs. Pendant ces deux modifications, une diminution de la taille des flocs a été observée avec une homogénéisation de leur forme, cette dernière représentée par une progressive augmentation de la circularité et de la convexité.

- Enfin, la représentation tridimensionnelle des distributions couplant les données de taille et de forme s'est révélée être un outil prometteur, permettant de mieux visualiser la dynamique de ces changements des propriétés morphologiques et ainsi de mieux comprendre les mécanismes responsables de l'évolution des boues. Une autre approche intéressante permettant de mieux suivre les évolutions du procédé a été introduite basée sur l'évaluation de deux dimensions fractales reliant l'aire et le périmètre des flocs (D_{pf}) ou l'aire et la longueur maximale (D_2). De brusques variations de D_{pf} et D_2 ont ainsi permis d'identifier les différentes phases du foisonnement filamenteux (apparition, croissance, et relargage des filaments) tandis qu'une évolution graduelle de ces deux grandeurs a été corrélée à l'augmentation de la compacité des flocs provoquée par les changements de taux de recirculation et du rapport COD:N.

Les conclusions apportées par ce travail de thèse suggèrent de nombreuses perspectives, tant sur un plan expérimental que sur un plan de traitement des données et de modélisation des phénomènes. Quelques pistes sont données ci-dessous :

Perspectives

Au plan expérimental, l'analyse et le traitement d'images réalisés dans ce travail devrait être étendus au suivi d'une station d'épuration fonctionnant avec une alimentation en effluent réel afin d'en mesurer la robustesse. En effet, il est difficile d'anticiper comment les variations sur la nature et la composition des effluents pourraient, et avec quelle dynamique, engendrer des perturbations sur les propriétés morphologiques des flocs.

De plus, dans ce travail, les indicateurs de performance classiquement utilisés dans les stations d'épuration (MES, IB, dosages chimiques, ..) ont été utilisés. Néanmoins pour relier de manière plus concrète les propriétés morphologiques des flocs aux performances du procédé, des mesures plus précises de décantation dans des conditions hydrodynamiques maîtrisées comparables à celle des décanteurs industriels pourraient être réalisées. De même, il pourrait s'avérer intéressant de mesurer les propriétés rhéologiques des boues et de relier ces données aux propriétés morphologiques. Ces données couplées pourraient ainsi aider à la modélisation du comportement rhéologique des boues activées.

A plus long terme probablement, il serait sans doute intéressant de pouvoir intégrer à des approches d'analyse d'images des informations sur la microbiologie des flocs de boues. Ceci, afin de mieux comprendre comment les interactions avec l'environnement (abondance ou pénurie en nutriments, contraintes hydrodynamiques liées à l'aération et au recyclage des boues, etc.) induisent des modifications au niveau des populations des micro-organismes présents dans la biomasse. En effet, les paramètres morphologiques ou la dimension fractale des flocs ne sont qu'une forme d'expression des réponses de la biomasse à ces stimulations.

Enfin, en ce qui concerne le traitement des jeux de données issues de l'analyse d'image, une autre approche serait de recourir à des méthodes de la statistique multi-variable, comme cela a pu être réalisé dans la littérature, lesquelles pourraient apporter un éclairage nouveau sur ces résultats.

ANNEXES

Annexes

Annex I

Evolution of the volume-based 3D-distributions of the pairs AR-CED for *Modification M2*. It consists of an alternative way to verify the detachment of the filaments.

M2

AR - CED

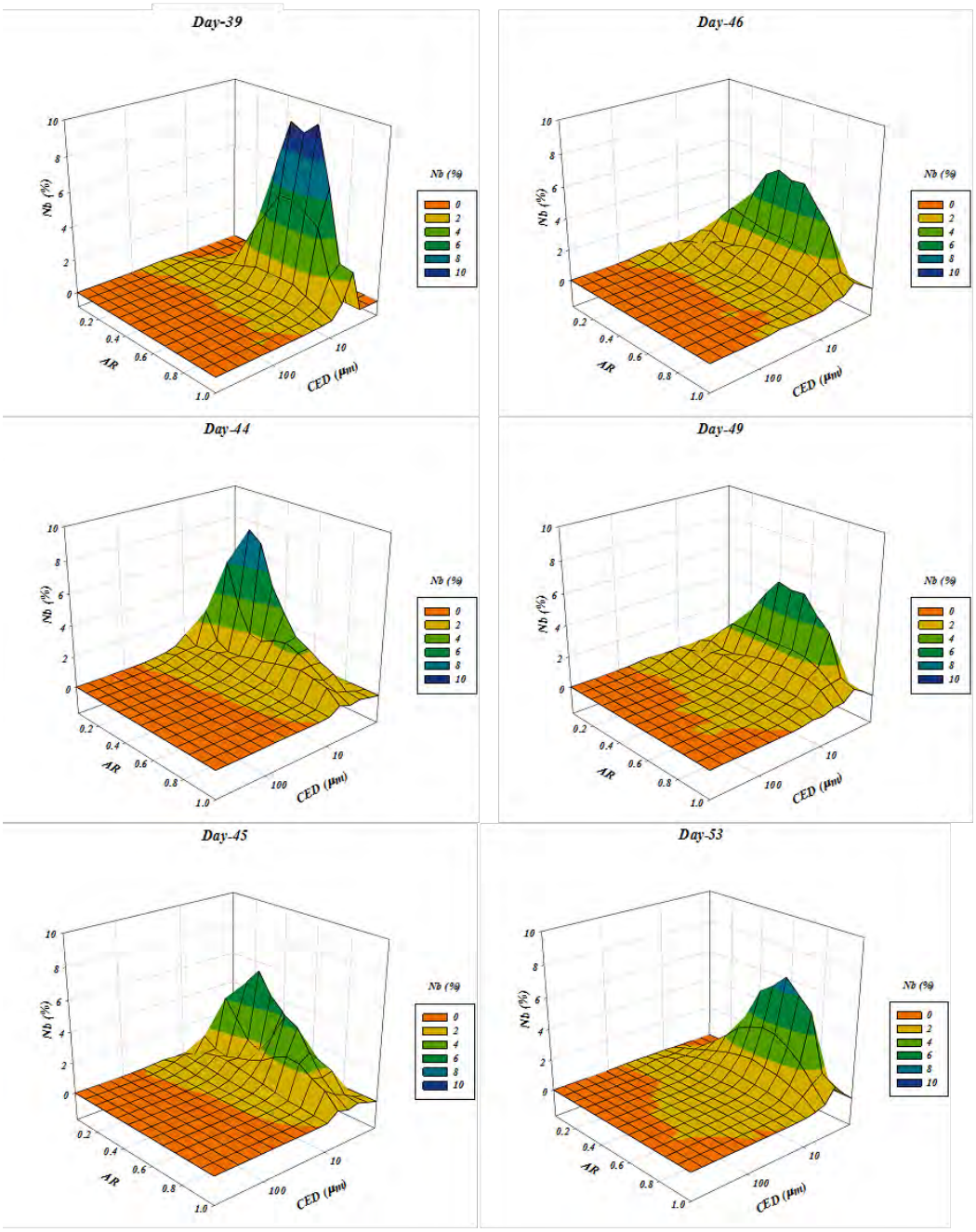

Annex II

Perimeter, Area and Maximum length distributions on number and volume basis during *M1*.

M1

Number basis *Volume basis*

Perimeter

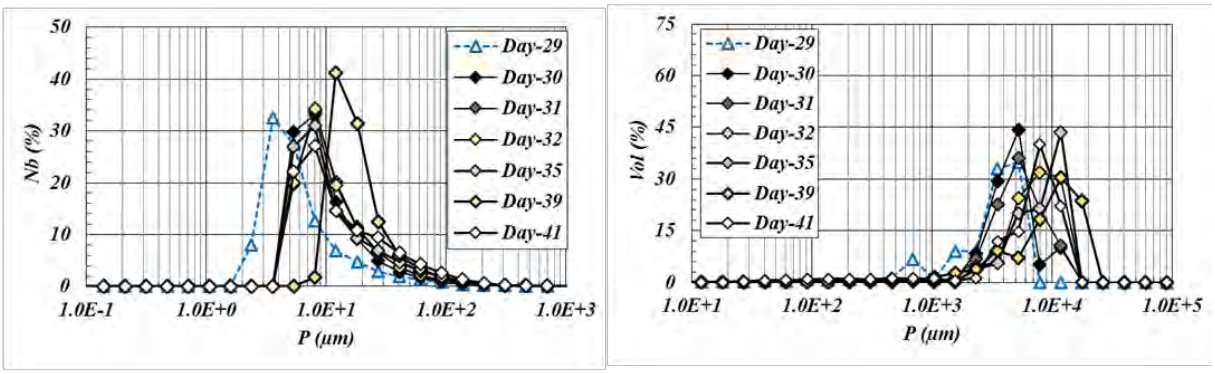

Area

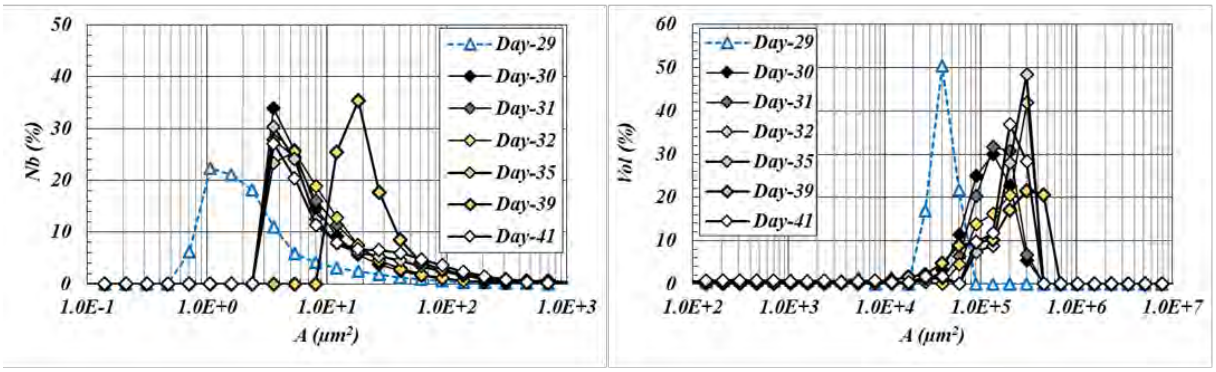

Maximum length

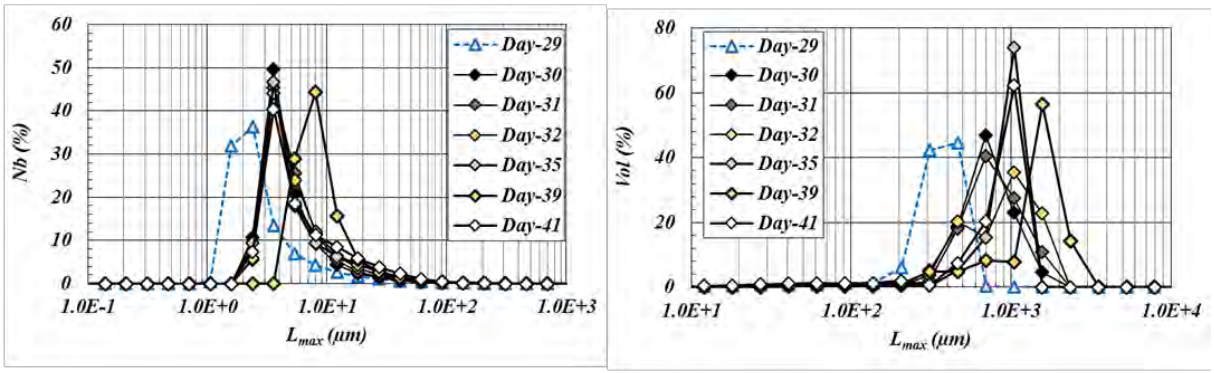

Perimeter, Area and Maximum length distributions on number and volume basis during *M2*.

M2

Number basis *Volume basis*

Perimeter

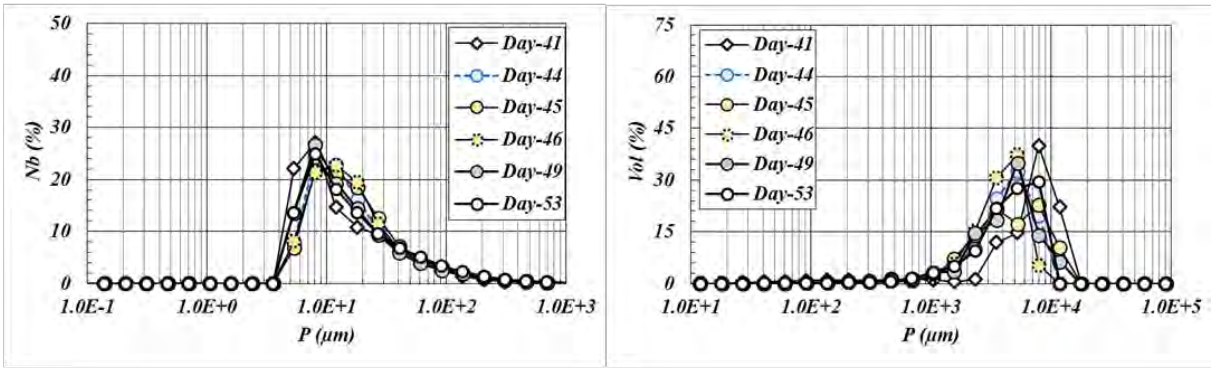

Area

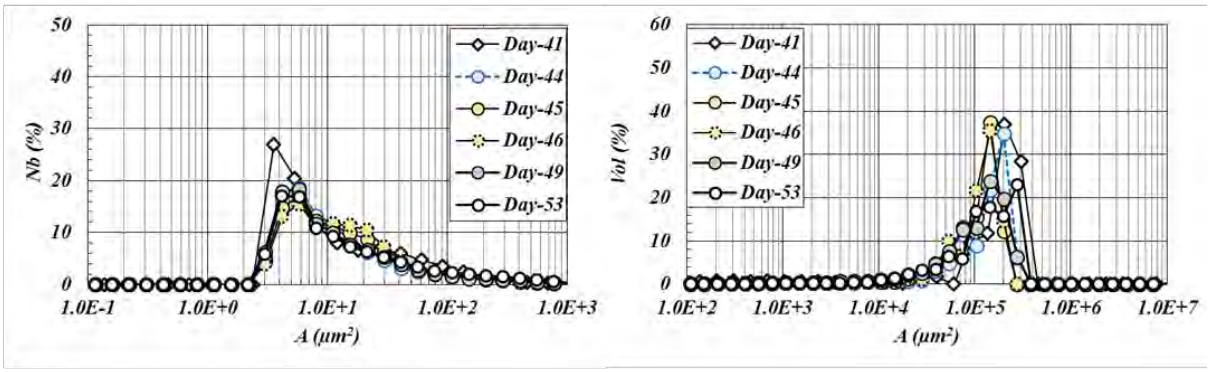

Maximum length

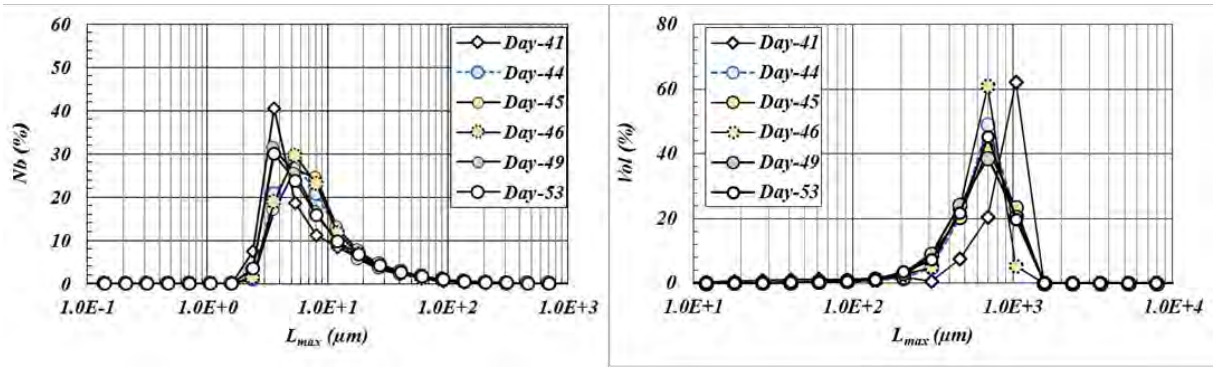

Perimeter, Area and Maximum length distributions on number and volume basis during *M4*.

M4

Number basis *Volume basis*

Perimeter

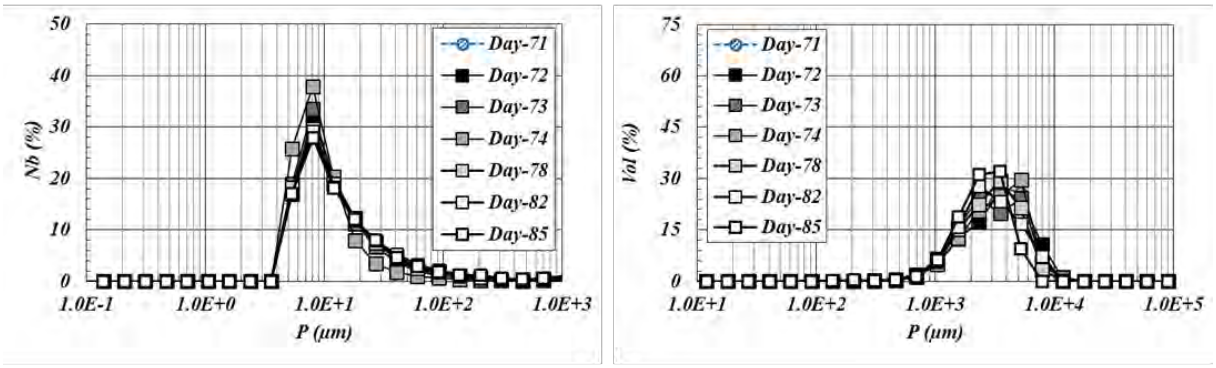

Area

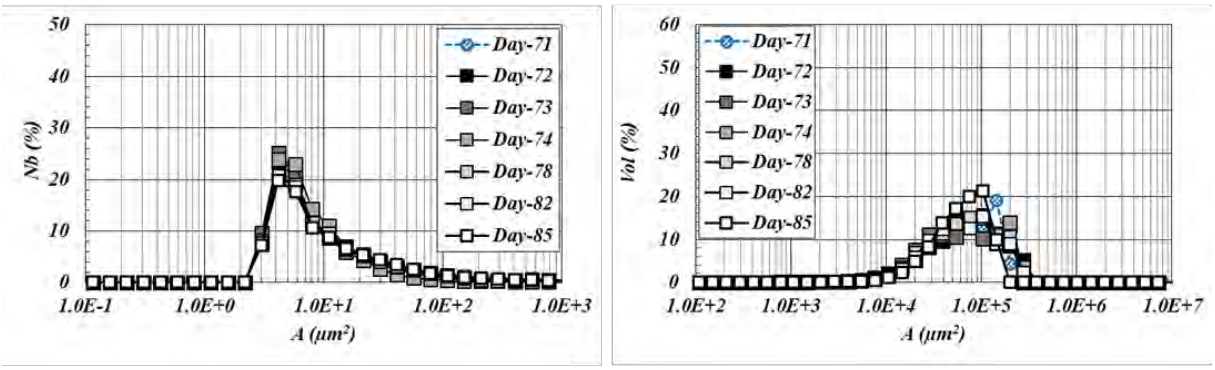

Maximum length

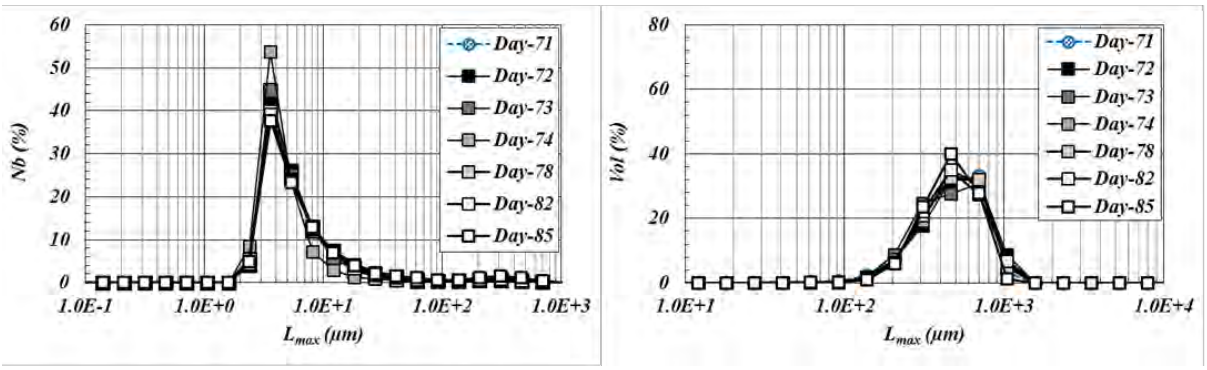

Résumé :

Les Procédés par Boues Activées sont utilisés dans le traitement biologique des effluents. L'impact des conditions opératoires sur l'efficacité du procédé est supposé dû en partie à la variation des propriétés des boues. Notre objectif est d'apporter un nouvel éclairage sur cette relation triangulaire en considérant les propriétés morphologiques des flocs de boues. Une méthodologie fiable de caractérisation des flocs par analyses d'images a été développée. Deux campagnes expérimentales utilisant un système à l'échelle pilote alimenté par un effluent synthétique ont permis d'analyser l'effet de paramètres opératoires, tels que l'âge de boue, la charge organique, le taux de recirculation et le rapport DCO:N. Alors qu'un changement d'âge de boue n'a qu'un effet temporaire sur la taille et la circularité, la croissance de bactéries filamenteuses, induite par une charge organique élevée, impacte fortement la taille, la solidité et la dimension fractale des flocs.

Mots-clés : Flocs - Boues activées - Morphologie - Traitement des eaux usées - Analyse d'image - Distribution de taille

Abstract:

Activated Sludge Processes are applied in the biological treatment of wastewater. The impact of the operational parameters on process efficiency is presumably relied to the properties of the sludge. Our aim is to bring new insights into this relationship by characterizing the size and the shape of sludge flocs and linking them to the operating conditions and the process performance. A reliable methodology was developed for the characterization of flocs by image analysis. Two experimental campaigns were then performed with a lab-scale activated sludge system fed with synthetic wastewater, allowing to analyse the effect of some parameters, such as the solids retention time, the organic load rate, the recycle rate and the COD:N ratio. While a change of the solids retention time only has a temporary effect on the floc size and circularity, the development of filamentous bacteria, promoted by a high organic load rate, highly impacts the size, solidity and fractal dimension of flocs.

Keywords: Flocs - Activated sludge - Morphology - Wastewater treatment - Image analysis - Particle size distribution